Commonwealth of Kentucky

Transportation Cabinet
Frankfort, Kentucky 40622

Fred N. Mudge
Secretary of Transportation

Paul E. Patton
Governor

August 14, 1996

Mr. Paul Toussaint
Division Administrator
Federal Highway Administration
330 West Broadway
Frankfort, KY 40602

Dear Mr. Toussaint:

Subject: IMPLEMENTATION STATEMENT
KYHPR 94-155, *Evaluation and Analysis of Innovative Concepts for Bridge Seismic Retrofit*

This report is the first of three reports for the above referenced study. The objective of this study was to develop earthquake time histories for use in the design of transportation facilities throughout the commonwealth. In order to achieve this objective, the following tasks were defined:

1. definition and evaluation of earthquakes in seismic zones that have the potential to generate damaging ground motions in Kentucky,

2. specification of the source characteristics, accounting for the spreading and attenuation of the ground motions to the top-of-the-bedrock at sites in Kentucky, and

3. determination of seismic zoning maps for the commonwealth based on peak-particle accelerations, response spectra, and time histories.

These tasks have been addressed in the report entitled *Source Zones, Recurrence Rates, and Time Histories for Earthquakes Affecting Kentucky* (KTC-96-4). Seismic input data (time histories, response spectra, and surface accelerations) were generated for all counties in
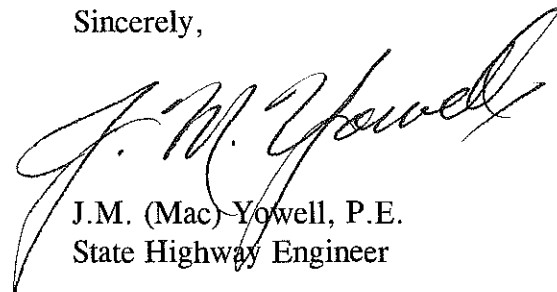
Kentucky and have been included in this report. It should be noted that the seismic data is generated at the county seat and not at the county centroid.

Time histories of hypothetical earthquakes, along with their peak-particle accelerations, and 0 and 5 percent damped response spectra are developed as guidelines for the seismic design of highway structures and bridges within Kentucky. The time histories are derived through the use of random vibration analyses, and take into consideration the probability of earthquakes from nearby seismic zones, the attenuation of ground motions with distance in the Central United States, and the possibility of a random event occurring outside of the generally recognized zones of seismicity in the area. Suggested peak-particle accelerations, time histories, and response spectra are intended for use at sites where the structure is assumed to be situated at the top of a bedrock foundation. For sites underlain by soils, and in particular for those sites underlain by poorly consolidated soils, it is recommended that site specific investigations be conducted by qualified professionals in order to determine the possibilities of frequency-dependent amplification (including resonance), damping, and soil failure when subjected to the suggested time histories.

In addition to above referenced report, two additional reports will be generated in the near future. By October 31, 1996, the first draft of a report entitled *Seismic Evaluation of Highway Bridges in Kentucky* will be submitted. This report will outline the steps for conducting seismic evaluations of existing bridges. A design procedure for seismic retrofits, complete with detailed examples, will also be outlined.

The first draft of the second additional report, entitled *Notes on Seismic Evaluation and Retrofit of Highway Bridges in Kentucky*, will be submitted by November 30, 1996. This report will provide the material necessary for a training course in seismic evaluation and retrofit measures.

Sincerely,

J.M. (Mac) Yowell, P.E.
State Highway Engineer

Research Report
KTC-96-4

Source Zones, Recurrence Rates, and Time Histories for Earthquakes Affecting Kentucky

by

Ron Street
Associate Professor, Department of Geological Sciences

Zhenming Wang
Research Assistant, Department of Geological Sciences

Issam E. Harik
Professor of Civil Engineering and Head, Structures Section,
Kentucky Transportation Center

David L. Allen
Chief Research Engineer

and

James J. Griffin
Research Assistant

Kentucky Transportation Center
College of Engineering, University of Kentucky

in cooperation with

Transportation Cabinet
Commonwealth of Kentucky

and

Federal Highway Administration
U.S. Department of Transportation

March 1996

1. Report No. KTC-96-4	2. Government Accession No.	3. Recipient's Catalog No.
4. Title and Subtitle **SOURCE ZONES, RECURRENCE RATES, AND TIME HISTORIES FOR EARTHQUAKES AFFECTING KENTUCKY**		5. Report Date March 1996
		6. Performing Organization Code
7. Author(s) R. Street, Z. Wang, I.E. Harik, D.L. Allen, and J.J. Griffin		8. Performing Organization Report No. KTC-96-4
9. Performing Organization Name and Address Kentucky Transportation Center College of Engineering University of Kentucky Lexington, Kentucky 40506-0281		10. Work Unit No. (TRAIS)
		11. Contract or Grant No. KYHPR-94-155
12. Sponsoring Agency Name and Address Kentucky Transportation Cabinet State Office Building Frankfort, Kentucky 40622		13. Type of Report and Period Covered Final
		14. Sponsoring Agency Code

15. Supplementary Notes
Prepared in cooperation with the Kentucky Transportation Cabinet and the U.S. Department of Transportation, Federal Highway Administration

16. Abstract
Time histories of hypothetical earthquakes, along with their peak-particle accelerations, and 0 and 5 percent damped response spectra are developed as guidelines for the seismic design of highway structures and bridges within Kentucky. The time histories are derived through the use of random vibration analyses, and take into consideration the probability of earthquakes from nearby seismic zones, the attenuation of ground motions with distance in the Central United States, and the possibility of a random event occurring outside of the generally recognized zones of seismicity in the area. Suggested peak-particle accelerations, time histories, and response spectra are intended for use at sites where the structure is assumed to be situated at the top of a bedrock foundation. For sites underlain by soils, and in particular for those sites underlain by poorly consolidated soils, it is recommended that site specific investigations be conducted by qualified professionals in order to determine the possibilities of frequency-dependent amplification (including resonance), damping, and soil failure when subjected to the suggested time histories. It should be noted that the seismic data is generated at the county seat and not at the county centroid.

17. Key Words Peak-Particle Accelerations Response Spectra Time Histories	18. Distribution Statement Unlimited with approval of Kentucky Transportation Cabinet		
19. Security Classif. (of this report) Unclassified	20. Security Classif. (of this page) Unclassified	21. No. of Pages 194	22. Price

FormDOT 1700.7 (8-72)   Reproduction of Completed Page Authorized

EXECUTIVE SUMMARY

The peak-particle accelerations, time histories, and response spectra derived in this report are based on the historical seismicity, published attenuation of ground motions with distance study for the Central United States, and the seismic moment-stress drop relationship suggested by Torro, et al., (1992). It is believed that the greatest uncertainties with the results in this study have to do with the seismic moment-stress drop relationship suggested by Torro, et al., (1992), and the maximum magnitude of the 50- and 500-year events in the Northeastern Kentucky region. For a variety of reasons, there are very few earthquakes in the Central United States for which there exists well defined stress drop values. In addition, because of the lack of an earthquake greater than 5.2 $m_{b,Lg}$ in the Central United States since 1975, when digital data first became available, there are no instrumentally derived stress drops for larger magnitude events.

The uncertainty with the 50- and 500-year maximum magnitude events in Northeastern Kentucky is primarily due to the lack of instrumentation in the area prior to the 1980 Sharpsburg, Kentucky, earthquake, when a single seismograph station was installed near Sharpsburg. In 1989, as a result of the 4.6 $m_{b,Lg}$ earthquake near Judy, Kentucky, on September 7, 1988, a tripartite array of seismometers was installed in Northeastern Kentucky. Since the installation of a tripartite array of seismometers, several small earthquakes ($<$ 3.5 $m_{b,Lg}$) have been detected and located in Northeastern Kentucky and the adjacent areas of Ohio and West Virginia. Most likely prior to 1989, and almost certainly prior to 1980, few, if any of these events would have been reported. To date, however, the seismicity in the area has not exhibited a pattern (such as that which has been found in the New Madrid Seismic Zone), and the time frame of detection and location of the seismicity is too short to make any definitive statements about its rate.

SCOPE OF STUDY

The objective of this study is to develop earthquake time-histories for use in the design of transportation facilities throughout the commonwealth. To achieve this objective, the scope of the work was divided into the following tasks: definition and evaluation of earthquakes in seismic zones that have the potential to generate damaging ground motions in Kentucky, specification of the source characteristics of the earthquakes, accounting for the spreading and attenuation of the ground motions to the top-of-the-bedrock at sites in Kentucky, and determination of seismic zoning maps for the commonwealth based on peak-particle accelerations, response spectra, and time histories.

RECOMMENDATIONS

Time histories of hypothetical earthquakes, along with their peak-particle accelerations, and 0 and 5 percent damped response spectra are developed as guidelines for the seismic design of highway structures and bridges within Kentucky. The time histories are derived through the use of random vibration analyses, and take into consideration the probability of earthquakes from nearby seismic zones, the attenuation of ground motions with distance in the Central United States, and the possibility of a random event occurring outside of the generally recognized zones of seismicity in the area. Suggested peak-particle accelerations, time histories, and response spectra are intended for use at sites where the structure is assumed to be situated at the top of a bedrock foundation. For sites underlain by soils, and in particular for those sites underlain by poorly consolidated soils, it is recommended that site specific investigations be conducted by qualified professionals in order to determine the possibilities of frequency-dependent amplification (including resonance), damping, and soil failure when subjected to the suggested time histories.

CREDITS

TABLE OF CONTENTS

1. Seismicity in the Central and Eastern United States

1.1 Definitions

The symbol $m_{b,Lg}$ is used throughout this paper to denote the body-wave magnitude of an earthquake as determined from the vertical-component 1-s Lg waves recorded at seismic stations in Eastern North America (Nuttli, 1973b). The formulas used to compute the $m_{b,Lg}$ of an earthquake are:

$$m_{b,Lg} = 3.75 + 0.90\,(\log_{10} D) + \log_{10}\left(\frac{A}{T}\right) \qquad 0.5^o \le D \le 4^o \qquad (1.1)$$

$$m_{b,Lg} = 3.30 + 1.66\,(\log_{10} D) + \log_{10}\left(\frac{A}{T}\right) \qquad 4^o \le D \le 30^o \qquad (1.2)$$

where D is a distance in degrees, A is the amplitude of the vertical component of approximately 1-s Lg waves in microns, T is the period, and the ratio A/T is expressed in microns per second (zero-to-peak amplitude).

A Modified Mercalli Intensity Scale (MMI) is the intensity scale currently used in the United States as modified by Wood and Neumann (1931). The scale consists of twelve intensity levels ranging from I to XII, where an increase in intensity describes a more severe effect on people, structures, and the landscape. At Modified Mercalli intensity I (MMI) few, if any people feel the earthquake. At MMI VII everyone feels it (those inside buildings run outside), some chimneys are damaged, and, depending upon the quality of construction and design, building damage ranges from negligible to considerable. At MMI XII, damage is total and the landscape may be permanently altered.

1.2 History of Seismic Activity in Kentucky

The largest historic earthquakes in the Central or Eastern United States are the great earthquakes of 1811-1812 in what is present-day Northeastern Arkansas and Southeastern Missouri (Nuttli, 1973a; Street and Nuttli, 1990). Street (1982) estimated body-wave magnitudes ($m_{b,Lg}$) of 7.2, 7.0, 7.1, and 7.3 for the largest earthquakes in the

sequence. The first two events occurred on December 16, 1811, at 3 and 6 a.m. local time, the third event occurred on January 23, 1812, at 8 a.m. local time, and the fourth event occurred on February 7, 1812, at 2 a.m. local time. Figure A.1 in Appendix A illustrates the isoseismal for the best documented earthquake of the 1811-1812 sequence, the 3 a.m. December 16, 1811, event. Newspaper articles described the effects of the earthquake in Kentucky:

> *Frankfort, KY.* "About two o'clock on Sunday night was felt in this place a violent shock of an Earthquake. It continued for several minutes and produced a considerable vibration of houses. Some bricks are said to have fell from the top of the court house chimney" (The American Republic, Frankfort, KY).

> *Henderson, KY.* "A severe shock of an earthquake was felt at this place on the 16th inst. at half past 2 o'clock, A.M. - many chimneys were cracked by the motion; - and at sun-rise another shock threw down most of the chimneys so injured" (The Weekly Register-Chronicle, Washington, D.C.).

> *Lexington, KY.* "About half after two o'clock, yesterday morning, a severe shock of an Earthquake was felt at this place: the earth vibrated two or three times in a second, which continued for several minutes, and so great was the shaking that the windows were agitated equal to what they would have been in a hard gust of wind" (Kentucky Gazette, Lexington, KY).

> *Louisville, KY.* "On Monday morning the 16th instant, this place was visited by a most alarming Earthquake. . ., we are induced to believe, the continuation was from 4 to 6 minutes, though some say it was not so long; - about an hour afterwards, another shock was felt; and a little after sunrise, a third, which broke off several chimneys, and injured some houses otherwise." (Poulson's American Daily Advertiser, Philadelphia, PA).

> *Washington and Maysville, KY.* "On Monday morning, a very severe shock of an earthquake was experienced at this place (i.e., Washington) and Maysville, but much more severely and oftener at the latter place, from whence two or three families have removed" (American Statesman & Columbian, Lexington, KY).

These and other accounts of the earthquake, indicate that nearly all of Kentucky experienced Modified Mercalli (MM) intensity VII or greater effects. An exception might be the part of Kentucky east of what is now Mount Sterling. Kentucky was only sparsely settled at the time of the earthquakes, and with the exception of a few communities along the Ohio River in Northeastern Kentucky, Eastern Kentucky was not settled. In addition, the few structures that did exist in Eastern Kentucky were typically one-story log cabins, which most likely did not sustain any damages since they were particularly well suited to

withstanding shaking from an earthquake (Berry, 1908).

The 1811-1812 earthquakes occurred in what is now referred to as the New Madrid Seismic Zone (NMSZ), which is best described as the tightly clustered pattern of earthquake epicenters in Northeastern Arkansas, Northwestern Tennessee, and Southeastern Missouri in Figure A.2. Figure A.3 illustrates the epicentral locations of the four great earthquakes that occurred in the NMSZ during the winter of 1811-1812, and compares them to the present-day pattern of seismicity. In addition to the four great earthquakes, hundreds of aftershocks were reported by the early settlers. From the newspaper accounts, Street and Nuttli (1990) concluded that between December 16, 1811, when the first earthquake occurred, and March 15, 1812, that at least six aftershocks of magnitude 6.2 to 7.0 $m_{b,Lg}$ and 197 aftershocks of magnitude 5.2 to 6.2 $m_{b,Lg}$ occurred.

The New Madrid earthquakes of 1811-1812 were unique in the annals of seismicity in that four great events occurred geographically very close to one another, and all within a period of two months. They caused ground failure (i.e., sandblows, slumping, landslides, and fissures) over a 48,000-square-kilometer area, and were felt throughout most of North America east of the Rocky Mountains (Street and Nuttli, 1990). They are, however, not the only damaging earthquakes to have occurred in the Central or Eastern United States. Figure A.4 illustrates the historical seismicity in the Central and Eastern United States, along with the names of generally accepted seismic zones (Bollinger, et al., 1992). Of the seismic zones shown in Figure A.4, only the New Madrid, Wabash Valley (which in Figure A.4 is included in the Upper Mississippi Seismic Zone), Giles County, Virginia, and Eastern Tennessee are believed to be capable of producing damaging ground motions in Kentucky. These seismic zones, along with Northeastern Kentucky, which experienced damaging earthquakes in 1980 and 1988, are discussed below.

1.3   Seismic Source Zones

Numerous studies have been undertaken to quantify, by means of seismic zonation, the seismic hazard in the Central United States. Notable among these are the studies by Nuttli and Herrmann (1978), Barstow, et al., (1981), Algermissen, et al., (1982), EPRI (1986), Bernreuter, et al., (1988), and Johnston and Nava (1990). Differences in zonation are a function of the accuracy of historical seismicity in predicting future events (interpreted differently by different researchers), and the significance they attach to the influence that known geologic features have on the seismicity. For example, Nuttli and Herrmann (1978) emphasized the spatial distribution of the historical seismicity and only loosely correlated their choices of seismic zones with tectonic features. In contrast, Johnston and Nava (1990) argued that if only larger events are considered, there is a good correlation of earthquakes with tectonic structures.

The seismic source zones in this study are primarily based on the historical seismicity. Major geologic and geophysical features are used to constrain the location or extent of the seismic zones in some instances.

1.3.1 New Madrid Seismic Zone

The New Madrid Seismic Zone (NMSZ) is the best understood seismic zone in the Central and Eastern United States. As shown in Figure A.2, the major trends of the contemporary seismicity of the NMSZ have been well documented over the past 20 years. Focal mechanism studies of earthquakes in the Southeastern trend of seismicity have demonstrated that the predominant sense of motion along the trend is right-lateral strike-slip fault. Focal mechanism studies of earthquakes along the Northwestern trend of seismicity have shown that they are associated with a dip-slip fault trending approximately N22°W, with a dip of 31° at the Northwestern end and 48° at the Southeastern end of the trend (Chiu, et al., 1992).

Earthquakes in the NMSZ are believed to be caused by stresses (compression) resulting from motion between the North American and European plates. The principal axis of compression within the seismic zone is N80°E (Zoback and Zoback, 1981). With few exceptions, focal depths of the well-located earthquakes within the major trends of seismicity are concentrated between 5 and 14 km in depth (Chiu, et al., 1992). The maximum magnitude earthquake for the New Madrid Seismic Zone has been estimated by Nuttli (1981) as being comparable to the February 7, 1812 New Madrid earthquake described above. His estimate is based on an analysis in which he deleted the largest historical earthquakes and their aftershocks (i.e., the 1811-1812 sequence), determined a magnitude-recurrence relation for the remaining catalog of events, and then extrapolated a magnitude-recurrence relation to a recurrence interval of 1,000 years. The magnitude associated with the 1,000-year event was in good agreement with the magnitude that has independently been determined for the February 7, 1812, earthquake.

1.3.2 Wabash Valley Seismic Zone

Isoseismals of the two largest earthquakes in the Wabash Valley Seismic Zone, the September 27, 1891, and November 9, 1968, events, are shown in Figures A.5 and A.6, respectively. Street (1980) calculated an $m_{b,Lg}$ of 5.5 to 5.8 for the September 27, 1891, event, which was centered near Mount Vernon, Ill., where several chimneys were shaken down and a church was damaged. The November 9, 1968, earthquake was more damaging than the September 27, 1891, earthquake, but since the 1968 earthquake occurred nearly eight decades later, the area about the epicenter of the 1968 event was much more densely settled and, hence, more vulnerable to damage. Stover and Coffman (1993) estimated the $m_{b,Lg}$ magnitudes of the two events as being 5.2 and 5.5, respectively.

In more recent times, the most significant earthquake to have occurred in the Wabash Valley Seismic Zone is the event of June 10, 1987. Taylor, et al., (1988) estimated the $m_{b,Lg}$ magnitude of this event at 5.2, and described it as a predominantly strike-slip event with a focal depth of 10 km. Hamburger and Rupp (1988) argued that the event could be related to the Northwest-trending LaSalle Anticlinal Belt, whereas Taylor, et al., (1988) suggested that the earthquake could be related to the reactivation of Northeasterly trending basement graben faults such as those seen by Sexton, et al., (1986) in seismic reflection and potential field profiles 50 km to the south of the main shock epicenter. Figure A.7 illustrates the isoseismal for the June 10, 1987, earthquake.

Nuttli and Herrmann (1978) estimated a maximum credible earthquake of 6.6 $m_{b,Lg}$ for the Wabash Valley Seismic Zone. More recently, Obermeier, et al., (1992) found evidence of one or more strong earthquakes centered near Vincennes, IN. Based on the areal extent of liquefaction features (dikes), Obermeier, et al., (1992) concluded that if all the dikes are from a single event, the level of shaking would have been on the order of 6.7 $m_{b,Lg}$, a magnitude that is in close agreement with Nuttli and Herrmann's (1978) maximum credible earthquake.

A recent finding that has an impact on the boundaries of the Wabash Valley Seismic Zone is that of Heigold and Kolata (1993). Heigold and Kolata concluded from seismic reflection and potential field data that a major Proterozoic crustal boundary separates the Wabash Valley Fault System from the Reelfoot Rift and New Madrid Seismic Zone (Figure A.8). The findings suggested that the structural development of the two areas is quite dissimilar, and there appears to be some justification for separating the two seismic zones on the basis of something more than the rate and pattern of historical seismicity. Heigold and Kolata's (1993) crustal boundary would truncate the southern extent of the Wabash Valley Seismic Zone.

Another study that has some bearing on the boundaries of the Wabash Valley Seismic Zone is the one by Hass, et al., (1992) regarding the completeness of the existing seismicity catalogs. The statistical analysis of the existing earthquake catalogs conducted by Hass, et al., led to the conclusion that the earthquakes in the part of West-central Kentucky included in Nuttli and Herrmann's (1978) definition of the Wabash Valley Seismic Zone were most likely blasts associated with strip mining. This observation agrees with data from the University of Kentucky, which has operated seismic stations in West-central Kentucky since 1982, and recorded only one earthquake in the area, a 2.6 $m_{b,Lg}$ event, near Greenville, KY, on January 8, 1995.

In summary, the southern boundary of the Wabash Valley Seismic Zone as drawn by Nuttli and Herrmann (1978) appears to extend too far to the south and include too much of Western Kentucky. This study assumes that the southern boundary of the Wabash Valley Seismic Zone is better represented by the northern boundary of the Proterozoic

crustal boundary discussed by Heigold and Kolata (1993). Figure A.9 illustrates the boundaries of the Wabash Valley Seismic Zone as assumed in this study.

1.3.3 Giles County, Virginia, Seismic Zone

The Giles County Seismic Zone has not been as intensely studied as the New Madrid and Charleston, South Carolina, Seismic Zones, since it is in a sparsely populated area and the largest earthquake known to have occurred in it was the 5.8 m_b magnitude event of May 31, 1987, whose isoseismal is shown in Figure A.10. Figure A.11, taken from Bollinger, et al., (1992), illustrates their perception of the Giles County Seismic Zone. They viewed the earthquakes within the dashed rectangular area as belonging to the zone proper, and the earthquakes outside the rectangular area but within the circular area as being "halo" events. Based on the earthquakes within the rectangular area and a variety of techniques for estimating the maximum magnitude earthquake for a seismic zone, Bollinger, et al., (1992) concluded that the most likely maximum magnitude for the Giles County Seismic Zone is 6.3 m_b. Wheeler (1995) argued that the Giles County Seismic Zone is best explained by compressional reactivation of Iapetan faults.

1.3.4 Eastern Tennessee Seismic Zone

The largest known earthquake in the Eastern Tennessee Seismic Zone is the Waynesville, North Carolina, earthquake of 1916, whose isoseismal is shown in Figure A.12. The majority of the seismicity in the seismic zone is located in what Powell, et al., (1994) describe as a 300-km-long by 50-km-wide evolving seismic zone in which slip on north- and east-striking surfaces is slowly coalescing into a Northeast-trending zone. Most of the instrumentally located epicenters in the seismic zone lie close to but east of the New York-Alabama aeromagnetic lineament and west of the Clingman aeromagnetic lineament between the latitudes of 34.3° and 35.5°N (Figure A.13). Wheeler (1995) felt that because the structural position of the Eastern Tennessee Seismic Zone and focal mechanisms of the earthquakes within it are similar to those in the Giles County Seismic Zone, the earthquakes in the Eastern Tennessee Seismic Zone are also caused by compressional reactivation of Iapetan faults. Bollinger (1992) and Bollinger, et al., (1992) considered the Eastern Tennessee Seismic Zone as a potential source of a large earthquake, similar in magnitude to the 6.3 $m_{b,Lg}$ estimated for the Giles County Seismic Zone.

1.4 Recommended Seismic Source Zones and Their 50- and 500-Year Maximum Magnitude Events

1.4.1 Seismic Source Zones

In summary, four seismic zones are close enough to Kentucky to be capable of

producing earthquakes large enough to cause damage within the commonwealth. Figure A.14 illustrates the boundaries of the four seismic zones as assumed in this study, while Table 1.1 gives the coordinates of the boundaries.

The boundary for the New Madrid Seismic Zone is well constrained for the Southwest- and Northwest-trending portions of the seismic zone by the contemporary earthquake activity. The extension of the New Madrid Seismic Zone in the northeast direction into Western Kentucky is not well constrained by contemporary earthquake activity; in fact, such an extension has recently been questioned by Hildenbrand, et al., (1994). From magnetic and gravity data, Hildenbrand, et al., (1994) interpreted a series Northwest-trending faults and a zone of igneous intrusions, forming what is referred to as the Paducah Gravity Lineament (PGL); this precludes a northeast extension of the New Madrid Seismic Zone, shown in Figure A.15. This study assumed that the New Madrid Seismic Zone does not extend northward into Western Kentucky; in particular, it was assumed that a major earthquake, such as those in 1811-1812, could only occur in the Southwest- or Northwest-trending portions of the seismic zone.

The boundary of the Wabash Valley Seismic Zone as shown in Figure A.14 is close to what was suggested by Nuttli and Herrmann (1978), with the exception of the southern boundary. The southern boundary of the Wabash Valley Seismic Zone as shown in the figure was chosen to coincide with the northern boundary of Heigold and Kolata's (1993) magnetic lineament, which they noted also coincides with a well-defined zone of sparse seismicity.

The boundary of the Eastern Tennessee Seismic Zone as shown in Figure A.14 is based on the historical and instrumental seismicity for the area, as is the boundary for the Northeastern Kentucky area. The boundary for the Giles County Seismic Zone is the one suggested by Bollinger, et al., (1992).

1.4.2   50- and 500-Year Maximum-Magnitude Earthquakes

Nuttli and Herrmann (1978) and Nuttli (1981) concluded that the 7.3 $m_{b,Lg}$ earthquake of February 7, 1812, represents the maximum-magnitude earthquake in the New Madrid Seismic Zone. Nuttli and Herrmann (1978) also concluded that the maximum-magnitude event for the Wabash Valley Seismic Zone is a 6.6 $m_{b,Lg}$ event. In both instances, the maximum-magnitude earthquake is a 1,000-year event. Using a very different approach, Johnston and Nava (1990) concluded that what they referred to as the "Wabash Lobe" of their seismic zone B is capable of a maximum-magnitude 6.5 $m_{b,Lg}$ event.

Table 1.1:   Seismic Source Zone Configuration[1].

Seismic Zone	Latitude (°N)	Longitude (°W)
Eastern Tennessee	34.50	85.00
	35.00	85.50
	35.50	85.50
	36.50	84.00
	36.00	83.00
Giles County, Virginia	39.50	85.00
	41.50	85.00
	41.50	83.00
	39.50	83.00
New Madrid	35.25	90.72
	35.45	90.93
	36.35	89.75
	36.60	90.10
	37.00	89.50[2]
	36.70	89.10[2]
	36.47	89.40
	36.00	88.85
	35.75	89.20
	36.05	89.60
Wabash Valley	37.50	89.50
	39.00	88.00
	39.60	87.50
	39.60	86.50
	38.50	87.00
	37.00	88.00

1.   The polygonal source zones are described by specifying their corner periods in terms of latitude (°N) and longitude (°W) pairs. For consistency, these corners are ordered such that each successive pair is the next corner, progressing clockwise about the source region.

2.   As discussed in the text, the northeast-trending extension of the New Madrid Seismic Zone has been called into question by the work of Hildenbrand, et al., (1994). These two sets of coordinates correspond with the southern boundary of Hildenbrand, et al.'s, (1994) magnetic anomaly.

In the Giles County Seismic Zone the largest earthquake known to have occurred is the 5.8 $m_{b,Lg}$ Giles County earthquake of May 31, 1897 (Street, 1979; Bollinger and Wheeler, 1988), but Bollinger (1992) argued that the seismic zone is capable of a 6.3 $m_{b,Lg}$ earthquake. Bollinger (1992) and Bollinger, et al., (1992) also argued that the Eastern Tennessee Seismic Zone is capable of a 6.3 $m_{b,Lg}$ earthquake, even though the largest documented event for the seismic zone is the 5.1 $m_{b,Lg}$ earthquake of February 21, 1916.

Nuttli's (1981) maximum-magnitude earthquake of 7.3 $m_{b,Lg}$ for the New Madrid Seismic Zone, and Nuttli and Herrmann's (1978) maximum-magnitude earthquake of 6.6 $m_{b,Lg}$ for the Wabash Valley Seismic Zone have been accepted for this study. Likewise, Bollinger's (1992) estimate of the maximum-magnitude earthquake for the Giles County Seismic Zone (i.e., a 6.3 $m_{b,Lg}$ event), and Bollinger et al's. (1992) 6.3 $m_{b,Lg}$ magnitude event for the Eastern Tennessee Seismic Zone have been accepted.

This study also accepts, in general, the suggested rate of seismicity for each of the seismic zone, despite the fact that the boundaries of some of the seismic zones have been slightly changed to accommodate recent findings. Figures A.16 through A.19 illustrate the means of the suggested rate of occurrences for the four seismic zones ($\pm$ one standard deviation). Superimposed on the plots are solid squares representing the magnitudes for the 50- and 500-year events of the seismic zones included in this study, which are:

Seismic Zone	50-year event	500-year event
New Madrid	6.3	7.0
Wabash Valley	5.5	6.3
Eastern Tennessee	4.7	6.2
Giles County, Virginia	4.3	6.2

In general, the 50- and 500-year events used in this study for the calculation of ground motions fall within one standard deviation of the rate of occurrence suggested by the means in Figures A.16 through A.19. Exceptions are the 50-year events for the Wabash Valley and Eastern Tennessee Seismic Zones. The reasons for increasing the magnitude of the 50-year event in the Wabash Valley Seismic Zone are (1) our lack of knowledge of the seismic zone, (2) the uncertainty associated with the magnitudes of many of the larger earthquakes in the seismic zone in the nineteenth century, and (3) the proximity of parts of Northwestern Kentucky to the seismic zone. The reason for accepting a lower magnitude for the 50-year event in the Eastern Tennessee Seismic zone is that the largest earthquake ever instrumentally recorded in the seismic zone is the 4.7 $m_{b,Lg}$ event on November 30, 1973, near Maryville, Tennessee, and the absence of magnitude greater than 4.0 $m_{b,Lg}$ in or even near Kentucky; the bulk of the seismicity in the seismic zone occurs south of Knoxville, Tennessee.

1.5 Background Seismicity (i.e., Local Events)

1.5.1 Background Seismicity

For areas with no known significant seismicity or known geologic/tectonic features capable of significant earthquakes, but in which the data are too poor to confidently exclude the existence of earthquakes, a random event is customarily assumed that is capable of occurring anywhere within the area (Johnston and Nava, 1990). With the exception of the Northeastern Kentucky area (discussed below) and those areas along the peripheral edges of the commonwealth that are associated with the New Madrid, Wabash Valley, and Eastern Tennessee Seismic Zones, Kentucky has experienced very few earthquakes. The largest event outside of those areas within one of the seismic zones outlined above is the Central Kentucky event of February 28, 1854, whose isoseismal is shown in Figure A.20. Street and Green (1984) gave coordinates of the epicenter of the 1854 earthquake of 37.6°/84.0°W, and assigned it a maximum MM intensity of V and a magnitude of 4.0 $m_{b,Lg}$. Towns in Kentucky whose newspapers reported the earthquake was felt there included Barbourville, Bardstown, Cynthiana, Danville, Georgetown, Harrodsburg, Hustonville, Lebanon, Lexington, Paris, and Richmond. The most severe effects of the earthquake were reported in Lebanon, where dishes and windows were rattled, and in Lexington where it "shook houses sensibly" (Lebanon Post, Lebanon, KY).

Since 1982, the Seismic Lab at the University of Kentucky has operated permanent seismic stations throughout the commonwealth. Since that time, several small (i.e., $m_{b,Lg}$ < 3.0) earthquakes within Kentucky have been located outside the boundaries of the seismic zones described above. These events are defined as background seismicity; their epicenters are scattered, and they do not appear to be spatially related to any known tectonic feature.

Figure A.21 illustrates the background seismicity for the commonwealth in terms of the suggested maximum local event for each county. With the exception of the 28 highlighted counties, the predicted magnitude of the local event is 4.5 $m_{b,Lg}$ at an epicentral distance of 20 km. This prediction is derived by adding 0.5 to the magnitude of the February 28, 1854, event discussed above.

1.5.2 Northeastern Kentucky

The largest earthquake known to have occurred within Kentucky is the July 27, 1980, event near Sharpsburg. Figure A.22 illustrates the isoseismal for this earthquake. It was a 5.2 $m_{b,Lg}$ event, had a maximum MM intensity of VII, and caused approximately $4 million damage in Bath, Bourbon, Fleming, Mason, Montgomery, Nicholas, and Rowan Counties (Street, 1982). On September 7, 1988, a 4.6 $m_{b,Lg}$ earthquake occurred 11 kilometers southeast of the 1980 event. Street, et al., (1993) estimated the maximum

MM intensity of the 1988 earthquake to be V to VI; within the epicentral area of the earthquake, brick veneer and basement walls were cracked, plaster fell off walls, small objects were knocked off tables, and the contents of cupboards were shaken to the floor.

As shown in Figure A.23, several other minor earthquakes are known to have occurred in Northeastern Kentucky and the adjacent areas of Ohio and West Virginia (Street, et al., 1993). The largest of the more recent earthquakes in the area was a 3.8 $m_{b,Lg}$ event that occurred on February 19, 1995, in Highland County, Ohio (Figure A.21). Because of the two damaging events in the 1980's, as well as the continuing earthquake activity in the area, it was assumed that Northeastern Kentucky has a slightly higher seismic risk than those areas that have been historically aseismic. It is recommended that the maximum magnitude of the local event in Northeastern Kentucky (Bracken, Robertson, Mason, Nicolas, Fleming, Bath, Montgomery, Menilee, Rowan, Lewis, Carter, Greenup, and Boyd Counties) be 5.3 $m_{b,Lg}$, which is 0.1 unit larger than the 1980 earthquake near Sharpsburg, Kentucky, for the 50-year event, and a 5.5 $m_{b,Lg}$ for the 500-year event. These counties are shaded in Figure A.21.

1.5.3 Southeastern Kentucky

The five Southeastern Kentucky counties (Whitley, Know, Bell, Harlan, and Letcher) highlighted in Figure A.21 have periodically experienced moderate (≤ 4.0 $m_{b,Lg}$) seismic events. MM intensity VI earthquakes, centered near Middlesboro and Barbourville, KY, in 1954 and 1976, respectively, are the largest events known to have occurred in the five county area. Stover and Coffman (1993) gave $m_{b,Lg}$ magnitudes of 4.3 for the 1954 event and 4.0 for the 1976 event. More recently, Bell County experienced a 3.1 $m_{b,Lg}$ earthquake on August 28, 1983, and Harlan County experienced a 3.6 $m_{b,Lg}$ earthquake on August 17, 1990.

Because of the magnitude of the 1954 event and the occurrence of the other events in the area, it is recommended that the maximum magnitude of the local event for the five Southeastern Kentucky counties be 4.75 $m_{b,Lg}$.

1.5.4 Western Kentucky

The predicted maximum magnitude of a local seismic event for the eight counties in Western Kentucky (Fulton, Hickman, Carlisle, Ballard, McCracken, Graves, Marshall, and Livingston) shaded in Figure A.21 is 5.3 $m_{b,Lg}$. This magnitude is based on the counties' proximity to the New Madrid and Wabash Valley Seismic Zones, moderate size historical events, and occasional events within the counties which have been detected by the University of Kentucky Seismic Network. Within the eight-county in 1994, for example, earthquakes measuring 2.0 $m_{b,Lg}$ in McCracken County on June 4, 3.6 $m_{b,Lg}$ in Ballard County on September 26, and 2.7 and 2.5 $m_{b,Lg}$ in Fulton County on November

20 and 27, respectively, were recorded. Historically, the largest earthquake to have occurred in the eight county area is the MM intensity VI, 4.6 $m_{b,Lg}$ event of November 1, 1883, (Stover and Coffman, 1993).

A 5.3 $m_{b,Lg}$ local event is also the maximum predicted for Henderson and Daviess Counties, as shown in Figure A.21. Historically, the largest earthquake to have occurred in the Henderson and Daviess County area is the MM intensity VI, 4.6 $m_{b,Lg}$ event of September 2, 1925 (Stover and Coffman, 1993).

2. SEISMIC RISK ANALYSIS

In developing a seismic risk map for an area, the seismic waves generated by an earthquake at its source, and the manner by which these seismic waves propagate away from the source to a site, are extremely important considerations. Unfortunately, estimates of ground motions based on direct regression of strong-motion data from an area such as Southern California should only be used for that area itself, unless source characteristics, travel paths, and local site factors can be shown to be similar (Reiter, 1990). Attenuation of seismic waves in the Central and Eastern United States is known to be quite different from attenuation in California, where many of the strong-motion data in the United States have been collected. The attenuation of seismic waves in the Central United States is much lower than for waves in California (Nuttli, 1973b).

2.1 Source Characteristics of Earthquakes in the Central United States

The source characteristics of an earthquake can have a marked effect on the resulting ground motions generated by the event. A simplistic, but commonly used earthquake source model is one suggested by Brune (1970, 1971). Brune's model consists of a circular fault of radius, r, that ruptures over the whole area at the same time. Of course, actual earthquakes do not consist of circular fault planes, and the rupturing process is not instantaneous. However, for many purposes, including this study, the Brune model gives reasonable results. The principal parameters of the Brune model that are referred to in this study are:

a. *Corner frequency* - the frequency at which the Fourier amplitude spectrum of the ground motion displacement for shear waves changes from a relatively constant level at lower frequencies to a decreasing level at higher frequencies; it is proportional to the reciprocal of the source size, or

$$f_o = 0.37 \frac{V_s}{r} \qquad (2.1)$$

where V_s is the shear-wave velocity (km/s), and r (km) is the radius of circular area equal in size to the actual rupture area.

b. *Stress drop* - the difference between the stress along the fault just before the

earthquake and the dynamic frictional stress between the two sides of the fault, which resists motion, or

$$\Delta\sigma = 8.5\, M_o \left(\frac{f_o}{V_s} \right)^3 \qquad (2.2)$$

where M_o (dyne-cm) is the seismic moment. The seismic moment is defined as:

$$M_o = \mu\, A\, D \qquad (2.3)$$

where μ (dyne-cm^2) is the rigidity modulus, A (cm^2) is the fault rupture area, and D (cm) is the average relative movement (slip) between the opposite sides of the fault.

Figure 2.1 illustrates the idealized Brune model for two earthquakes having the same seismic moments, but different stress drops, which results in different corner frequencies and rupture radii. The flat part of the model, which is the Fourier amplitude spectrum of the shear-wave (displacement) ground motion, is used in determining the seismic moment of the events. That portion of the displacement spectra with a slope of ω^{-2} corresponds to a constant acceleration. Superimposed on the plot is a hatched area indicating the frequency range over which $m_{b,Lg}$ is measured. In general, the larger the magnitude of the earthquake, the larger the rupture area, the lower the corner frequency, and the larger the seismic moment.

The stress drop of earthquakes in the Central and Eastern United States has not been well established. This is due to the lack of instrumented earthquakes, and disagreements on how to best model an earthquake at its source. This study used the $m_{b,Lg}$ - M_o model employed by Torro, et al., (1992), shown in Figure 2.2, which is based on their estimates of stress drops for Central United States earthquakes.

Other source characteristics that can affect ground motions at a site include radiation pattern, fault type, directivity, and focal depth. The radiation pattern of an earthquake refers to the relative strength of a given wave in different directions (azimuths) with respect to the fault rupture orientation. For example, the radiation pattern of S-waves from a strike-slip fault is strongest in directions parallel to and perpendicular to the fault plane. In contrast, these are the directions of the weakest P-waves.

The 1994 Northridge, California, earthquake is a good example of how the fault type affects ground motions. Strong-motion records from near the epicenter of the 1994 event show that the vertical ground motions generated by the earthquake were larger than

had been generally prepared for in the area building codes. The 1994 Northridge earthquake was a dip-slip event, which typically results in larger vertical ground motions than the strike-slip mechanism that was believed to be the major source of risk for the area prior to the 1994 earthquake.

The directivity effect, which occurs because the source of seismic waves is moving along a fault at a finite rupture velocity, is another source characteristic that can affect an earthquake's ground motions. In general, if a fault rupture propagates toward a particular site, the ground motion at the site will be greater than if a fault rupture propagates away from it. Strong-motion data from the 1994 Northridge earthquake indicate a northward directivity effect; that is, maximum horizontal ground motions to the north of the epicenter of the event were, in general, greater than those to the south of the epicenter of the event (Stewart, et al., 1995).

The importance of the final parameter, focal depth, is best illustrated by two earthquakes in Southern Illinois: the 3.8 $m_{b,Lg}$ event of August 14, 1965, and the 5.5 $m_{b,Lg}$ event of November 9, 1968 (Figure A.6). Both earthquakes caused MM intensity VII damages, even though their magnitudes were appreciably different. The August 14, 1965, Southern Illinois earthquake caused extensive MM intensity VII damages in Cairo, Ill., where the earthquake was centered, but little damage outside the immediate epicentral region. The November 9, 1968, South-central Illinois earthquake caused widespread MM intensity VII damages, including extensive masonry damage in Henderson, KY, 80 km east-southeast of the epicenter (Stover and Coffman, 1993). The MM intensity VII damages resulting from the two earthquakes, despite the large difference in their magnitudes, are a direct result of the differences in focal depths. Herrmann (1979) found the focal depth for the 1965 earthquake to be 1.5 km, whereas Stauder and Nuttli (1970) reported a focal depth of 20 km for the 1968 event.

In this study, these parameters have been averaged. For example, the RMS (root-mean-square) value of the radiation pattern is used, earthquakes are considered to be point sources (thereby avoiding the problem of directivity), and the focal depths of all earthquakes are assumed to be 10 km.

2.2   Attenuation of Ground Motions in the Central United States

Nuttli and Herrmann (1984) suggested the following attenuation of acceleration with distance relationship for the peak acceleration for the Central United States:

$$\log_{10} a_h = 0.57 + 0.50\, m_{b,Lb} - 0.83\, \log_{10} \sqrt{(R^2 + h^2)} - 0.00069\, R \qquad (2.4)$$

where R is the epicentral distance (km), h is the focal depth (km), and a_h is the arithmetic average of the peak accelerations of the two orthogonal horizontal accelerations (cm/s^2). This relationship was derived by Nuttli and Herrmann (1984) from theoretical calculations utilizing source scaling and absorption for earthquakes in the Central United States, and calibrated using available strong-motion data. Reiter (1990) referred to this as a semi-theoretical approach of relating magnitude to peak-particle motion.

In this study, as discussed below, random vibrations in the frequency domain were used to simulate ground motions, and account for the attenuation of the ground motions from the source to the site through the use of a frequency-dependent quality factor (Q), as suggested by Shin and Herrmann (1987). Peak-particle accelerations are therefore a function of the source characteristics (as discussed above) and the attenuation. Peak-particle accelerations obtained through random vibrations were then scaled to be within reasonable agreement with those obtained by Nuttli and Herrmann (1984). The + signs in Figure 2.3 illustrate the peak-particle accelerations as a function of distance for a hypothetical 6.3 $m_{b,Lg}$ "distant" earthquake obtained using Equation 2.1, while the solid line indicates the attenuation of the peak-particle acceleration with distance used in this study. Figure 2.4 illustrates the peak-particle accelerations obtained using random vibration analyses, as outlined above (solid line) for a hypothetical 4.75 $m_{b,Lg}$ "local" event, and the peak-particle accelerations obtained using the attenuation of acceleration as a function of distance relationship suggested by Nuttli and Herrmann (1984).

2.3 The Deterministic and Probabilistic Approaches to Seismic Hazard Analysis

Seismic hazard analyses used in the Central United States are based either on a *deterministic* or a *probabilistic* approach. The deterministic analysis makes use of discrete, singled-valued events or models to arrive at the required description of the earthquake hazard at a site. The analysis consists of four basic elements (Reiter, 1990):

(1) The earthquake source or sources;
(2) The selected controlling earthquake(s) - which could be the maximum earthquake, the maximum credible earthquake, or some other earthquake, depending on the criterion chosen;
(3) The earthquake effect at the site, such as the intensity; and
(4) The seismic hazard at the site in terms of peak acceleration, velocity, or some other agreed-upon measure.

A probabilistic seismic hazard analysis allows the use of a multi-valued or continuous event. It can include competing models, taking into account their uncertainties, and output an estimate of the likelihood of earthquake ground motion (or some other

damage measure) occurring at the location of interest (Reiter, 1990). An advantage of the probabilistic analysis is that it permits a quantitative comparison between different options, such as competing seismic zonation models.

The steps used in the analysis for this study are most similar to those outlined by Reiter (1990) for a deterministic study. Earthquake source zones are identified and controlling earthquakes (50- and 500-year events) chosen, local events are considered, and the seismic hazard is determined for sites throughout the commonwealth in terms of peak acceleration, time histories, and damped response spectra.
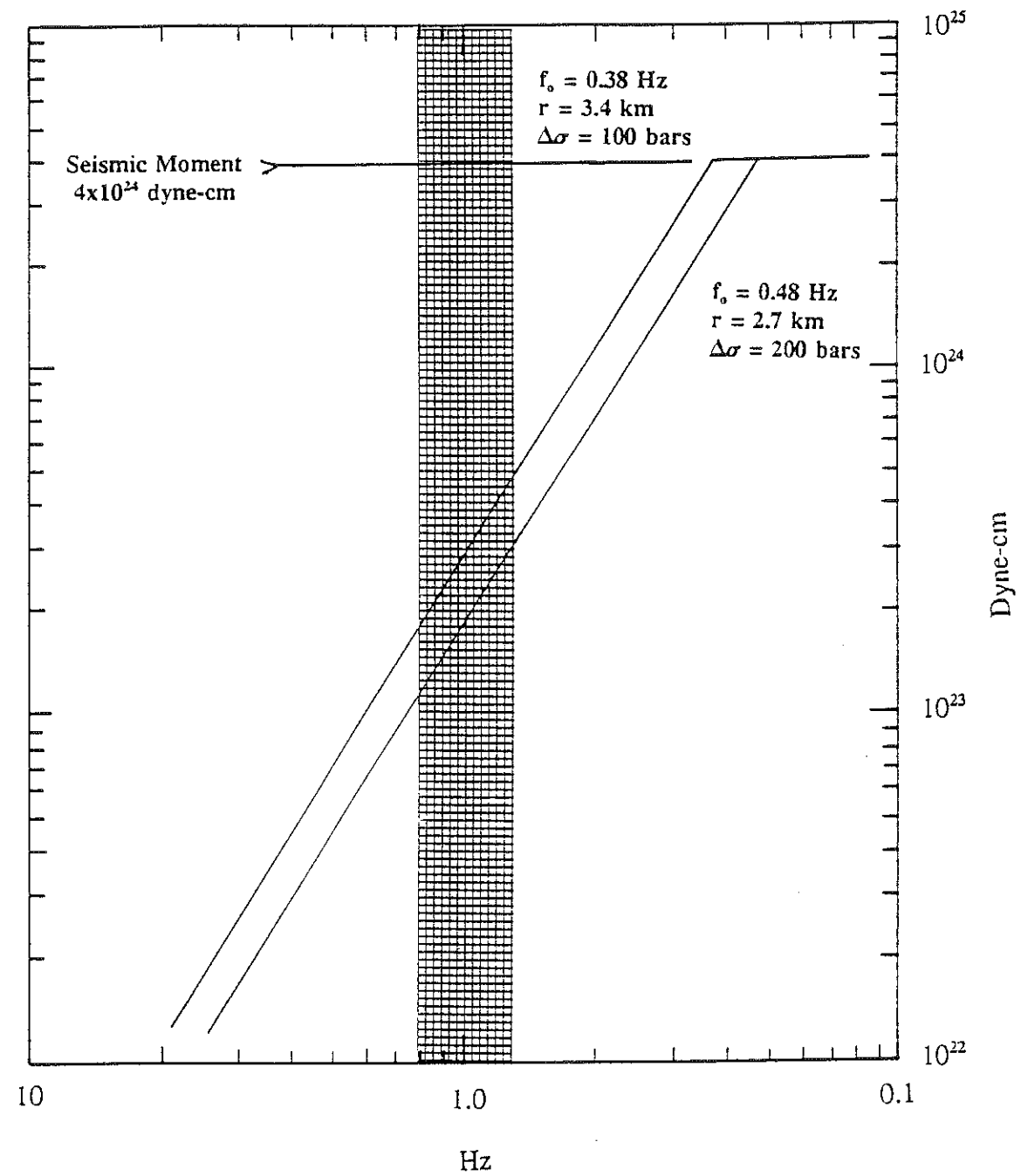
Figure 2.1. Brune model for displacement spectra of two hypothetical earthquakes, having the same seismic moment, but different stress drops. Hatched area on graph indicates the frequency range over the amplitudes of the Lg-wave are used in calculating $m_{b,Lg}$ in the central United States.
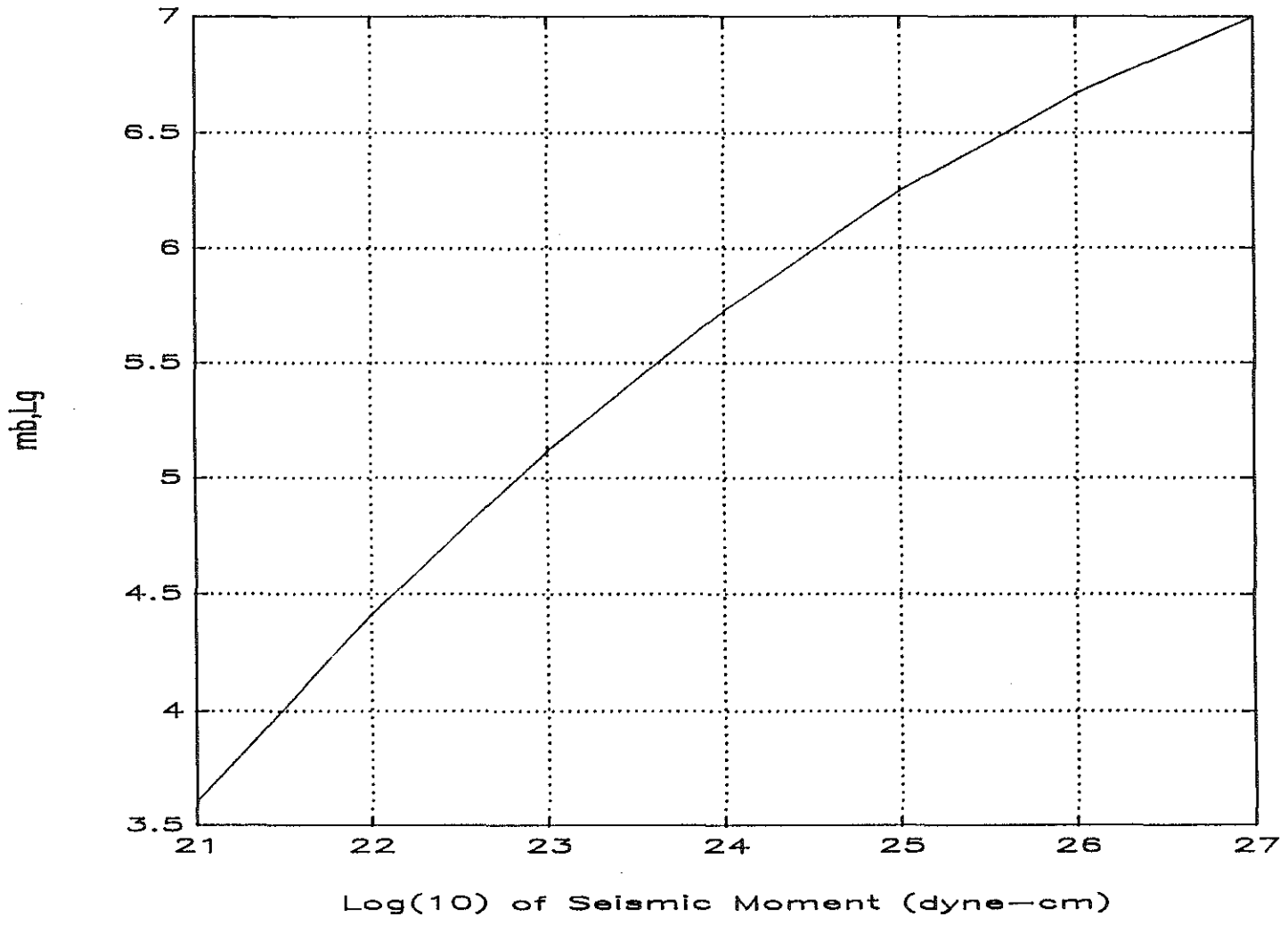
Figure 2.2.   Seismic Moment (M_o) - $m_{b,Lg}$ Relationship (Taken from Torro, et. al., 1992).
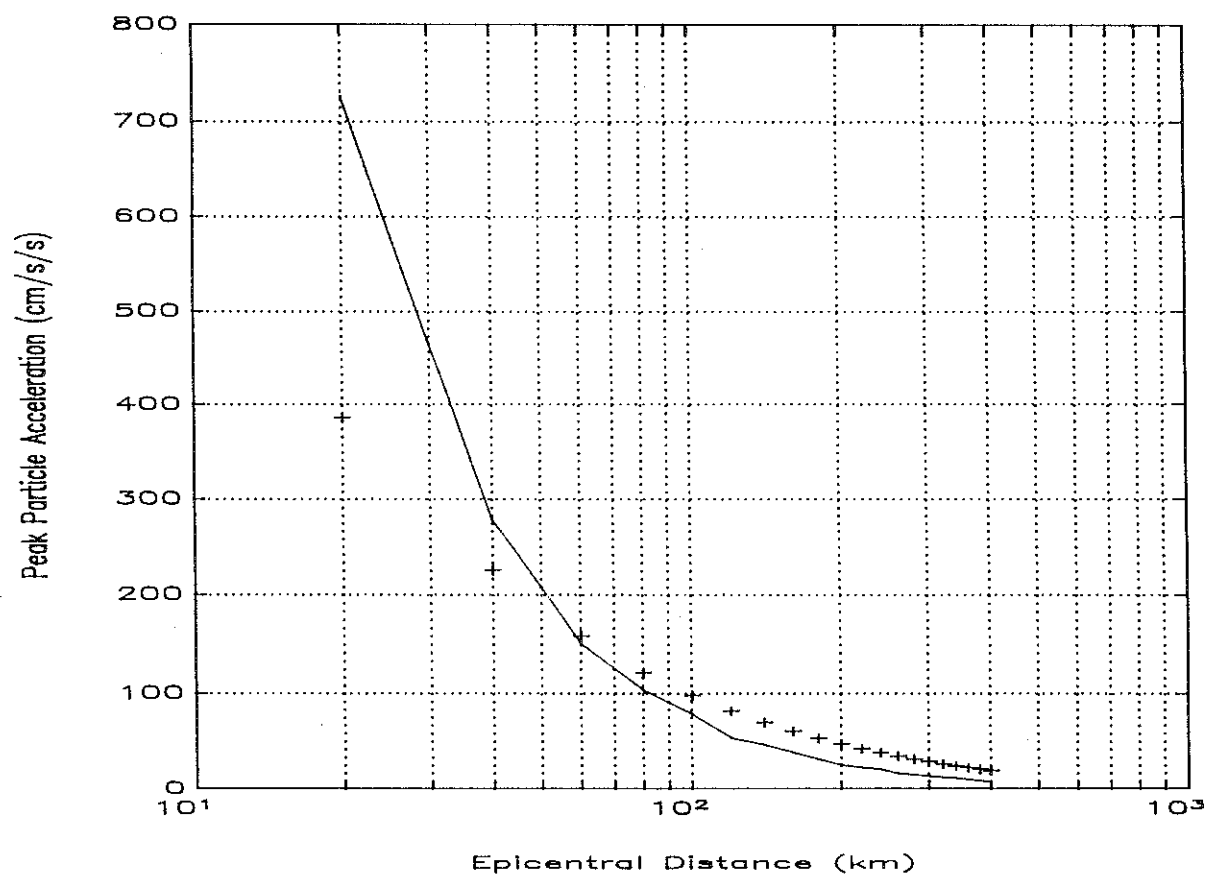
Figure 2.3. The solid line shows the peak-particle acceleration - distance scaling used in this study for a 6.3 m $_{b,Lg}$ event as compared to the Nuttli and Herrmann (1984) given in Equation 2.4 of text. Peak-particle accelerations predicted by Equation 2.4 are indicated by the + symbols. As used in this study, the epicentral range of greatest interest is for an event of this magnitude, is in excess of a few tens of km.
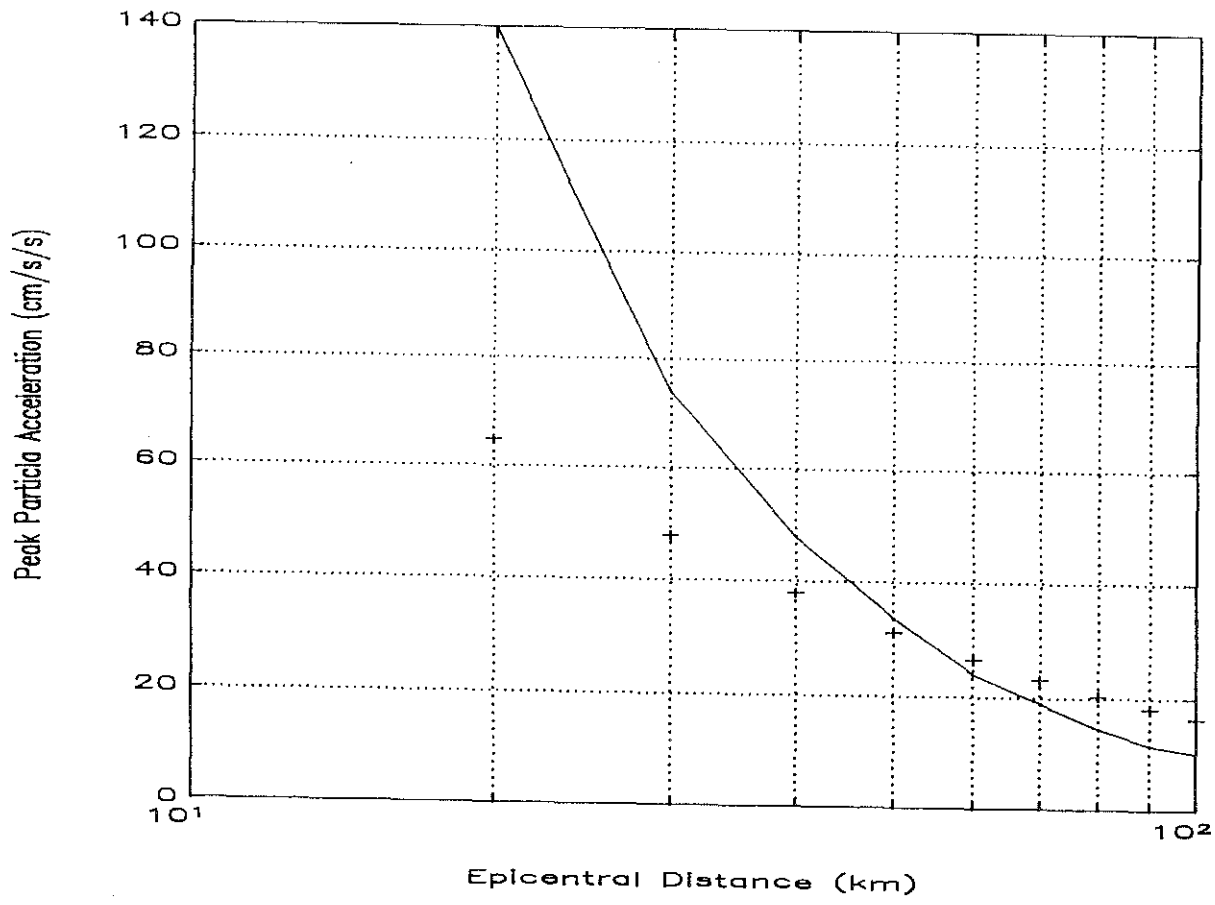
Figure 2.4.   The solid line shows the peak-particle acceleration - distance scaling used in this study for a 4.75 $m_{b,Lg}$ event as compared to the Nuttli and Herrmann (1984) given in Equation 2.4 of text. Peak-particle accelerations predicted by Equation 2.4 are indicated by the + symbols. As used in this study, the epicentral range of greatest interest is for an event of this magnitude, is in the range of 20 to a few tens of km.

3. SITE EFFECTS

The presence of soils can dramatically alter the ground motions at a site through the mechanisms of amplification, deamplification, frequency modulation, and duration. This has been well demonstrated by the Armenian (1985), Michoacan (1980), Loma Prieta (1989), Northridge (1994), and Hanshin (1995) earthquakes. Amplification is caused by the need for conservation of energy across impedance boundaries; deamplification is primarily caused by damping; frequency modulation is the result of selective filtering (including resonance); while duration is caused by such mechanisms as resonance and basin-generated surface waves resulting from the conversion of S-waves to surface-waves (Street, et al., 1995). Site effects can be roughly grouped into two types: those due to ground failure such as liquefaction, landslides, and ground rupture, and those that result in enhanced ground shaking. While the former effects are dramatic and attract most of the public and scientific interest, the latter effects can be of much greater consequence.

Holzer (1994) estimated the losses due to site effects resulting from the 1989 Loma Prieta, California, earthquake. Of the $5.9 billion in damages to property, transportation systems, communications, and utilities, 98 percent ($5.8 billion) was directly attributed to shaking. Of this amount, only 2 percent ($131 million) of the damages was attributed to liquefaction, landslides, and ground rupture, while 70 percent ($4.2 billion) was attributed to enhanced ground shaking resulting from the presence of soils overlying bedrock. As noted by Holzer (1994), the consequences from other earthquakes would not necessarily follow the same pattern of damages; however this example does point out the relative importance of site effects.

The determination of site effects at specific sites throughout Kentucky is beyond the scope of this study. Areas in Kentucky where site effects are of particular concern include the Jackson Purchase area and sites along the Ohio River such as Henderson, Owensboro, Louisville, and Maysville that are underlain by thick deposits of geologically young floodplain, estuarine, and lacustrine sediments. Ground-motion values suggested for sites in this study underlain by soils should be divided by two (assuming a vertically propagating wave) to correct for the free-surface effect, and propagated to the surface using an appropriate technique, such as SHAKE91 (Idriss and Sun, 1992).

4. RECOMMENDED TIME HISTORIES AND RESPONSE SPECTRA FOR USE AT THE TOP OF BEDROCK

4.1 Random Vibration Model Used for Generating Ground Motions

For the purpose of deriving recommended time histories for characteristic earthquakes in the various seismic zones, the stochastic simulation model proposed by Boore (1983), and recommended by Reiter (1990), was used.

Adopting the mathematical representation of O'Connor and Ellingwood (1992), the spectral density of strong motions derived from the Boore model, $S_a(\omega)$, can be derived by the equation:

$$S_a(\omega) = C \, M_o \, S(\omega,\omega_c) \, P(\omega,\omega_m) \, (1/R) \, e^{-\omega R/2 Q \beta} \tag{4.1}$$

where

$$
\begin{aligned}
C &= \text{a constant related to the source parameters,} \\
S(\omega,\omega_c) &= \text{spectral density of the energy released at the source,} \\
M_o &= \text{seismic moment (dyne-cm),} \\
P(\omega,\omega_m) &= \text{high-cut filter with a cutoff of } \omega_m, \\
R &= \text{epicentral distance,} \\
Q &= \text{specific quality factor (which is inversely related to attenuation),} \\
\beta &= \text{shear-wave velocity (km/s),} \\
\omega &= \text{circular frequency,} \\
\omega_c &= \text{corner frequency exhibited by the shear wave spectral density, and} \\
\omega_m &= \text{maximum circular frequency.}
\end{aligned}
$$

The attenuation factor, $1/R$, in Equation 4.1 is assumed to be R^{-1} for epicentral distances less than 100 km, and $R^{-1/2}$ for epicentral distances equal to or greater than 100 km (Herrmann, 1985). The constant, C, is related to the source parameters by:

$$C = \frac{RP \, (FS)(RF)}{4 \pi \omega \beta^3} \tag{4.2}$$

where RP is the radiation pattern, FS is the amplification due to the free-surface boundary

condition, and RF is a reduction factor to account for the partitioning of the seismic energy into horizontal components.

The source parameters, seismic moment, M_o, and spectral corner frequency, $f_o = \omega_c/2\pi$, are related by the equation:

$$f_c = 4.9 \times 10^6 \beta \left(\frac{\Delta \sigma}{M_o} \right)^{\frac{1}{3}} \tag{4.3}$$

where f_c is in Hertz, $\Delta\sigma$ is the stress drop in bars, and M is in dyne-cm (Brune 1970, 1971). As a practical matter, peak-particle accelerations are associated with frequencies greater or equal to the corner frequency, whereas peak-particle displacements are associated with frequencies less than or equal to the corner frequency.

The seismic moment and stress drop are related to the $m_{b,Lg}$ magnitude scale (used in the Central United States) by the relationship shown in Figure 2.2 (Torro, et al., 1992). This relationship assumes a moderately increasing stress drop with seismic moment, which is similar to that suggested by Nuttli, et al., (1989), except that for lower magnitude (≤ 5.5 $m_{b,Lg}$) events, the stress drop is held constant at 100 bars. For great earthquakes ($m_{b,Lg} \geq 7.0$; i.e., $M_o \geq 10^{27}$ dyne-cm), the stress drop is 250 bars.

4.2 Recommended Peak-Particle Accelerations, Time Histories, and Response Spectra

Using the random-vibration modeling described above, time histories and response spectra for the local, 50-, and 500-year events were calculated for all of the county seats in Kentucky. The epicentral distances between the local events and county seats were everywhere defined to be 20 km. The epicentral distances between the 50- and 500-year events associated with the four seismic zones considered in this study and the county seats were based on the geographical coordinates of the county seats and the following epicentral locations:

Eastern Tennessee Seismic Zone	36.5°N	84.0°W
Giles County, Virginia, Seismic Zone	37.2°N	81.2°W
New Madrid Seismic Zone	36.65°N	89.52°W
Wabash Valley Seismic Zone	37.7°N	88.5°W

Epicenters for the hypothetical events in the Eastern Tennessee and Giles County, VA, Seismic Zones were chosen to be a point within the seismic zone close to the Kentucky border. The epicenter for the hypothetical event in the New Madrid Seismic Zone is New

Madrid, Missouri, the approximate location of the 7.3 $m_{b,Lg}$ February 7, 1812, earthquake. The epicenter for the hypothetical event in the Wabash Valley Seismic Zone is the same as the epicenter of the 5.5 $m_{b,Lg}$ November 9, 1968, earthquake, which is near the southern end of the seismic zone and fairly close to the Kentucky border.

Table 4.1 gives the peak-particle accelerations determined in this study for each of the county seats in Kentucky for a 50-year time period. Five time histories for each county seat were generated: one for the local event, and one for each of the four seismic zones, assuming a hypothetical 50-year event. The peak-particle accelerations given in Table 4.1 are the largest peak-particle accelerations obtained for the county seats indicated from the five time histories. Table 4.2 was derived in a similar manner, except that peak-particle accelerations are the largest values estimated for the county seats, as determined from local events and the hypothetical 500-year events in each of the four seismic zones. Figures 4.1 and 4.2 illustrate the distribution of the peak-particle accelerations given in Tables 4.1 and 4.2, respectively.

Many of the peak-particle accelerations given in the tables are due to the local events. As noted by Naeim and Anderson (1993), such peak accelerations more often than not correspond to high frequencies that are out of the range of the natural frequency of most structures, and large peak-acceleration values alone can seldom initiate either resonance in the elastic range, or be responsible for large-scale damage in the elastic range of a structure. For structures susceptible to repeated loading, the longer duration of the ground motions at a site due to the hypothetical 50- or 500-year events could result in far greater damages than the high-frequency, short-duration, peak-particle acceleration associated with the local event. In practice, it is recommended that all of the hypothetical time histories and response spectra applicable to a given site be used in evaluating the seismic vulnerability of a structure, rather than relying upon a single parameter, such as the peak-particle acceleration.

Time histories and associated 0 and 5 percent damped response spectra for the local, 50-, and 500-year events are derived for locations throughout Kentucky. Appendix B contains the rsponse spectra for the 50-year event, while Appendix C has the response spectra for the 500-year event. Figures 4.3 and 4.4 illustrate the recommended seismic zonation for the 50- and 500-year events in Kentucky. Boundaries of the zones in the two figures coincide with county lines. The zones are based on peak particle acceleration, and the envelopes of the 5 percent damped response spectra for that particular zone. For example, in Figure 4.3 there are four zones having a peak acceleration of 0.15g, designated by 0.15g-1 through 0.15g-4. While the four zones all have a peak particle acceleration of 0.15g, which is typically a high-frequency characteristic in an accelerogram, the response spectra for the zones differ at the longer periods because of differences in peak particle velocities and the duration of ground motions resulting from differences in epicentral distances from the hypothesized earthquakes.

Figure 4.1. Map of horizontal peak-particle acceleration by county, at the top of rock, and with a 90 percent probability of not being exceeded in 50 years.
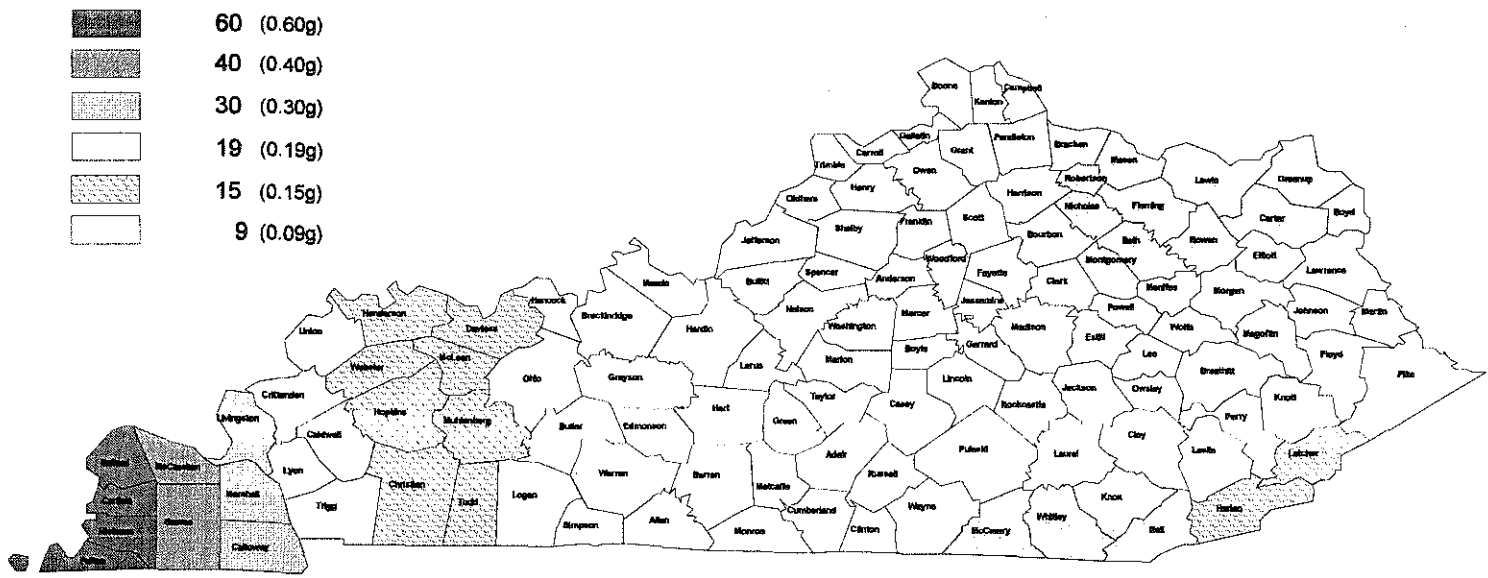
Figure 4.2. Map of horizontal peak-particle acceleration by county, at the top of rock, and with a 90 percent probability of not being exceeded in 500 years.

Figure 4.3. Map of recommended zones in Kentucky for a 50-year event, based on the time histories and response spectra given in Appendix A.
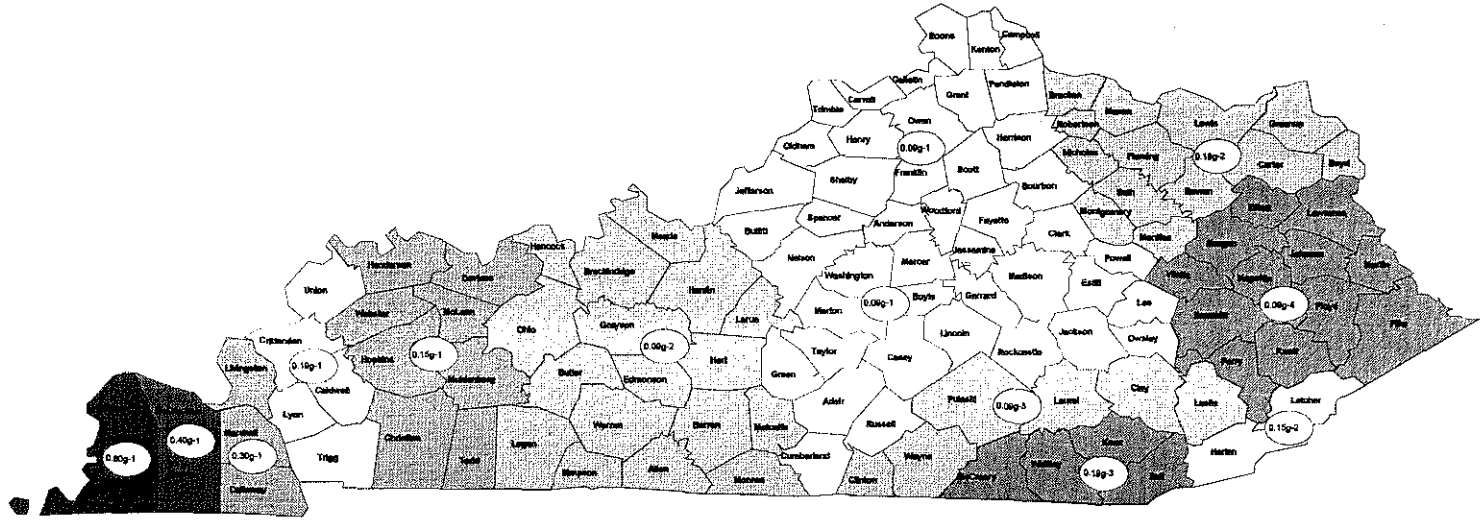
Figure 4.4. Map of recommended zones in Kentucky for a 500-year event, based on the time histories and response spectra given in Appendix B.

Table 4.1:   Peak-Particle Acceleration Corresponding to 50-Year Event.

County	County Seat	Acceleration	
		Percent of Gravity	cm/s^2
ADAIR	Columbia	8.7	85.3
ALLEN	Scottsville	9.1	89.3
ANDERSON	Lawrenceburg	9.5	93.2
BALLARD	Wickliffe	26.6	260.9
BARREN	Glasgow	8.2	80.4
BATH	Owingsville	13.5	132.2
BELL	Pineville	12.9	126.5
BOONE	Burlington	9.4	92.2
BOURBON	Paris	8.9	87.3
BOYD	Ashland	13.5	132.2
BOYLE	Danville	9.2	90.3
BRACKEN	Brooksville	14.7	144.2
BREATHITT	Jackson	9.3	91.2
BRECKINRIDGE	Hardinsburg	9.4	92.2
BULLITT	Shepherdsville	8.7	85.3
BUTLER	Morgantown	9.5	93.2
CALDWELL	Princeton	8.8	86.3
CALLOWAY	Murray	8.3	81.4
CAMPBELL	Alexandria	8.5	83.4
CARLISLE	Bardwell	26.2	257.0
CARROLL	Carrollton	9.3	91.2
CARTER	Grayson	14.7	143.9
CASEY	Liberty	9.0	88.3

Table 4.1: Peak-Particle Acceleration Corresponding to 50-Year Event (cont'd).

County	County Seat	Acceleration	
		Percent of Gravity	cm/s²
CHRISTIAN	Hopkinsville	9.4	92.2
CLARK	Winchester	8.7	85.3
CLAY	Manchester	8.6	84.4
CLINTON	Albany	8.2	80.4
CRITTENDEN	Marion	8.3	81.4
CUMBERLAND	Burkesville	9.1	89.3
DAVIESS	Owensboro	14.4	141.3
EDMONSON	Brownsville	9.3	91.2
ELLIOTT	Sandyhook	9.6	94.6
ESTILL	Irvine	8.5	83.4
FAYETTE	Lexington	8.4	82.4
FLEMING	Flemingsburg	13.6	133.2
FLOYD	Prestonburg	9.4	92.2
FRANKLIN	Frankfort	9.4	92.2
FULTON	Hickman	26.8	262.9
GALLATIN	Warsaw	8.9	87.3
GARRARD	Lancaster	9.9	97.1
GRANT	Williamstown	8.8	86.3
GRAVES	Mayfield	14.5	142.2
GRAYSON	Leitchfield	8.9	87.3
GREEN	Greensburg	8.6	84.4
GREENUP	Greenup	13.9	136.3
HANCOCK	Hawesville	8.3	81.4

Table 4.1:   Peak-Particle Acceleration Corresponding to 50-Year Event (cont'd).

County	County Seat	Acceleration	
		Percent of Gravity	cm/s²
HARDIN	Elizabethtown	9.5	93.2
HARLAN	Harlan	13.3	130.5
HARRISON	Cynthiana	9.5	93.2
HART	Munfordville	8.9	87.3
HENDERSON	Henderson	13.9	136.4
HENRY	Newcastle	9.8	96.1
HICKMAN	Clinton	30.8	302.1
HOPKINS	Madisonville	9.0	88.3
JACKSON	McKee	9.0	88.3
JEFFERSON	Louisville	9.4	92.2
JESSAMINE	Nicholasville	8.6	84.4
JOHNSON	Paintsville	8.4	82.4
KENTON	Independence	9.0	88.3
KNOTT	Hindman	9.1	89.3
KNOX	Barbourville	13.1	128.5
LARUE	Hodgenville	9.6	94.2
LAUREL	London	8.9	87.3
LAWRENCE	Louisa	10.2	100.0
LEE	Beattyville	9.0	88.3
LESLIE	Hyden	9.1	89.3
LETCHER	Whitesburg	12.5	122.6
LEWIS	Vanceburg	12.7	124.6
LINCOLN	Stanford	8.5	83.4

Table 4.1: Peak-Particle Acceleration Corresponding to 50-Year Event (cont'd).

County	County Seat	Acceleration	
		Percent of Gravity	cm/s²
LIVINGSTON	Smithland	12.5	122.6
LOGAN	Russellville	9.1	89.3
LYON	Eddyville	8.6	84.4
MADISON	Richmond	8.8	86.3
MAGOFFIN	Salyersville	8.1	79.5
MARION	Lebanon	9.2	90.3
MARSHALL	Benton	14.1	138.3
MARTIN	Inez	9.1	89.3
MASON	Maysville	13.1	128.6
McCRACKEN	Paducah	13.4	131.5
McCREARY	Whitley City	8.6	84.4
McLEAN	Calhoun	8.9	87.3
MEADE	Brandenburg	8.4	82.4
MENIFEE	Frenchburg	13.5	132.7
MERCER	Harrodsburg	9.3	91.2
METCALFE	Edmonton	9.3	91.2
MONROE	Tompkinsville	8.7	85.3
MONTGOMERY	Mount Sterling	12.7	125.0
MORGAN	West Liberty	9.9	96.7
MUHLENBERG	Greenville	9.4	92.2
NELSON	Bardstown	8.4	82.4
NICHOLAS	Carlisle	14.4	141.6
OHIO	Hartford	9.4	92.2

Table 4.1: Peak-Particle Acceleration Corresponding to 50-Year Event (cont'd).

County	County Seat	Acceleration	
		Percent of Gravity	cm/s²
OLDHAM	Lagrange	8.8	86.3
OWEN	Owenton	8.6	84.4
OWSLEY	Booneville	9.1	89.3
PENDLETON	Falmouth	9.4	92.2
PERRY	Hazard	9.0	88.3
PIKE	Pikeville	8.8	86.3
POWELL	Stanton	8.6	84.4
PULASKI	Somerset	8.5	83.4
ROBERTSON	Mount Olivet	12.7	124.3
ROCKCASTLE	Mount Vernon	9.0	88.3
ROWAN	Morehead	13.0	127.3
RUSSELL	Jamestown	9.3	91.2
SCOTT	Georgetown	9.1	89.3
SHELBY	Shelbyville	8.6	84.4
SIMPSON	Franklin	8.8	86.3
SPENCER	Taylorsville	8.3	81.4
TAYLOR	Campbellsville	9.0	88.3
TODD	Elkton	9.1	89.3
TRIGG	Cadiz	8.9	87.3
TRIMBLE	Bedford	8.8	86.3
UNION	Morganfield	9.4	92.2
WARREN	Bowling Green	9.0	88.3
WASHINGTON	Springfield	8.3	81.4

Table 4.1: Peak-Particle Acceleration Corresponding to 50-Year Event (cont'd).

County	County Seat	Acceleration	
		Percent of Gravity	cm/s^2
WAYNE	Monticello	9.6	94.2
WEBSTER	Dixon	8.6	84.4
WHITNEY	Williamsburg	12.6	123.6
WOLFE	Campton	9.6	94.2
WOODFORD	Versailles	9.4	92.2

Table 4.2:   Peak-Particle Acceleration Corresponding to 500-Year Event.

County	County Seat	Acceleration	
		Percent of Gravity	cm/s²
ADAIR	Columbia	8.7	85.3
ALLEN	Scottsville	9.1	89.3
ANDERSON	Lawrenceburg	9.5	93.2
BALLARD	Wickliffe	63.2	620
BARREN	Glasgow	8.2	80.4
BATH	Owingsville	16.9	165.8
BELL	Pineville	17.8	174.6
BOONE	Burlington	9.4	92.2
BOURBON	Paris	8.9	87.3
BOYD	Ashland	16.7	163.8
BOYLE	Danville	9.2	90.3
BRACKEN	Brooksville	18.6	182.5
BREATHITT	Jackson	9.3	91.2
BRECKINRIDGE	Hardinsburg	9.4	92.2
BULLITT	Shepherdsville	8.7	85.3
BUTLER	Morgantown	9.5	93.2
CALDWELL	Princeton	17.8	174.6
CALLOWAY	Murray	27.1	265.9
CAMPBELL	Alexandria	8.5	83.4
CARLISLE	Bardwell	60.8	596.4
CARROLL	Carrollton	9.3	91.2
CARTER	Grayson	18.3	179.5
CASEY	Liberty	9	88.3
CHRISTIAN	Hopkinsville	14.4	141.3

Table 4.2:   Peak-Particle Acceleration Corresponding to 500-Year Event (cont'd).

County	County Seat	Acceleration	
		Percent of Gravity	cm/s²
CLARK	Winchester	8.7	85.3
CLAY	Manchester	8.6	84.4
CLINTON	Albany	8.2	80.4
CRITTENDEN	Marion	17.9	175.6
CUMBERLAND	Burkesville	9.1	89.3
DAVIESS	Owensboro	14.4	141.3
EDMONSON	Brownsville	9.3	91.2
ELLIOTT	Sandyhook	9.6	94.6
ESTILL	Irvine	8.5	83.4
FAYETTE	Lexington	8.4	82.4
FLEMING	Flemingsburg	17.1	167.8
FLOYD	Prestonburg	9.4	92.2
FRANKLIN	Frankfort	9.4	92.2
FULTON	Hickman	58.7	575.8
GALLATIN	Warsaw	8.9	87.3
GARRARD	Lancaster	9.9	97.1
GRANT	Williamstown	8.8	86.3
GRAVES	Mayfield	41.3	405.2
GRAYSON	Leitchfield	8.9	87.3
GREEN	Greensburg	8.6	84.4
GREENUP	Greenup	17.5	171.7
HANCOCK	Hawesville	8.3	81.4
HARDIN	Elizabethtown	9.5	93.2
HARLAN	Harlan	13.3	130.5

Table 4.2: Peak-Particle Acceleration Corresponding to 500-Year Event (cont'd).

County	County Seat	Acceleration	
		Percent of Gravity	cm/s^2
HARRISON	Cynthiana	9.5	93.2
HART	Munfordville	8.9	87.3
HENDERSON	Henderson	13.9	136.4
HENRY	Newcastle	9.8	96.1
HICKMAN	Clinton	60.5	593.5
HOPKINS	Madisonville	13.2	129.5
JACKSON	McKee	9	88.3
JEFFERSON	Louisville	9.4	92.2
JESSAMINE	Nicholasville	8.6	84.4
JOHNSON	Paintsville	8.4	82.4
KENTON	Independence	9	88.3
KNOTT	Hindman	9.1	89.3
KNOX	Barbourville	17.9	175.6
LARUE	Hodgenville	9.6	94.2
LAUREL	London	8.9	87.3
LAWRENCE	Louisa	10.2	100
LEE	Beattyville	9	88.3
LESLIE	Hyden	9.1	89.3
LETCHER	Whitesburg	12.5	122.6
LEWIS	Vanceburg	15.9	156
LINCOLN	Stanford	8.5	83.4
LIVINGSTON	Smithland	25.4	249.2
LOGAN	Russellville	9.7	95.2
LYON	Eddyville	20.1	197.2

Table 4.2:   Peak-Particle Acceleration Corresponding to 500-Year Event (cont'd).

County	County Seat	Acceleration	
		Percent of Gravity	cm/s²
MADISON	Richmond	8.8	86.3
MAGOFFIN	Salyersville	8.1	79.5
MARION	Lebanon	9.2	90.3
MARSHALL	Benton	27.2	266.8
MARTIN	Inez	9.1	89.3
MASON	Maysville	16.6	162.8
McCRACKEN	Paducah	30.9	303.1
McCREARY	Whitley City	14.7	144.2
McLEAN	Calhoun	10.7	108
MEADE	Brandenburg	8.4	82.4
MENIFEE	Frenchburg	17.1	167.8
MERCER	Harrodsburg	9.3	91.2
METCALFE	Edmonton	9.3	91.2
MONROE	Tompkinsville	8.7	85.3
MONTGOMERY	Mount Sterling	15.9	156
MORGAN	West Liberty	9.9	96.7
MUHLENBERG	Greenville	10.9	106.9
NELSON	Bardstown	8.4	82.4
NICHOLAS	Carlisle	17.8	174.6
OHIO	Hartford	9.4	92.2
OLDHAM	Lagrange	8.8	86.3
OWEN	Owenton	8.6	84.4
OWSLEY	Booneville	9.1	89.3
PENDLETON	Falmouth	9.4	92.2

Table 4.2:   Peak-Particle Acceleration Corresponding to 500-Year Event (cont'd).

County	County Seat	Acceleration	
		Percent of Gravity	cm/s^2
PERRY	Hazard	9	88.3
PIKE	Pikeville	8.8	86.3
POWELL	Stanton	8.6	84.4
PULASKI	Somerset	8.5	83.4
ROBERTSON	Mount Olivet	16.1	157.9
ROCKCASTLE	Mount Vernon	9	88.3
ROWAN	Morehead	16.3	159.9
RUSSELL	Jamestown	9.3	91.2
SCOTT	Georgetown	9.1	89.3
SHELBY	Shelbyville	8.6	84.4
SIMPSON	Franklin	8.8	86.3
SPENCER	Taylorsville	8.3	81.4
TAYLOR	Campbellsville	9	88.3
TODD	Elkton	11.1	108.9
TRIGG	Cadiz	17.1	167.8
TRIMBLE	Bedford	8.8	86.3
UNION	Morganfield	14.2	139.3
WARREN	Bowling Green	9	88.3
WASHINGTON	Springfield	8.3	81.4
WAYNE	Monticello	9.6	94.2
WEBSTER	Dixon	13.2	129.5
WHITNEY	Williamsburg	23.9	234.5
WOLFE	Campton	9.6	94.2
WOODFORD	Versailles	9.4	92.2

5. Conclusions and Recommendations

The peak-particle accelerations, time histories, and response spectra derived for this report are based on the historical seismicity, published attenuation of ground motions with distance study for the central United States, and the seismic moment-stress drop relationship suggested by Torro, et al., (1992). It is believed that the greatest uncertainties with the results in this study have to do with the seismic moment-stress drop relationship suggested by Torro, et al., (1992), and the maximum magnitude of the 50- and 500-year events in the northeastern Kentucky region. For a variety of reasons, there are very few earthquakes in the Central United States for which there exists well defined stress drop values. In addition, because of the lack of an earthquake greater than 5.2 $m_{b,Lg}$ in the Central United States since 1975 when digital data first became available, there are no instrumentally derived stress drops for larger magnitude events.

Time histories of hypothetical earthquakes, along with their peak-particle accelerations, and 0 and 5 percent damped response spectra are developed as guidelines for the seismic design of highway structures and bridges within Kentucky. The time histories are derived through the use of random vibration analyses, and take into consideration the probability of earthquakes from nearby seismic zones, the attenuation of ground motions with distance in the Central United States, and the possibility of a random event occurring outside of the generally recognized zones of seismicity in the area. Suggested peak-particle accelerations, time histories, and response spectra are intended for use at sites where the structure is assumed to be situated at the top of a bedrock foundation. For sites underlain by soils, and in particular for those sites underlain by poorly consolidated soils, it is recommended that site specific investigations be conducted by qualified professionals in order to determine the possibilities of frequency-dependent amplification (including resonance), damping, and soil failure when subjected to the suggested time histories.

ACKNOWLEDGEMENTS

APPENDIX A:
FIGURES FOR CHAPTER 1
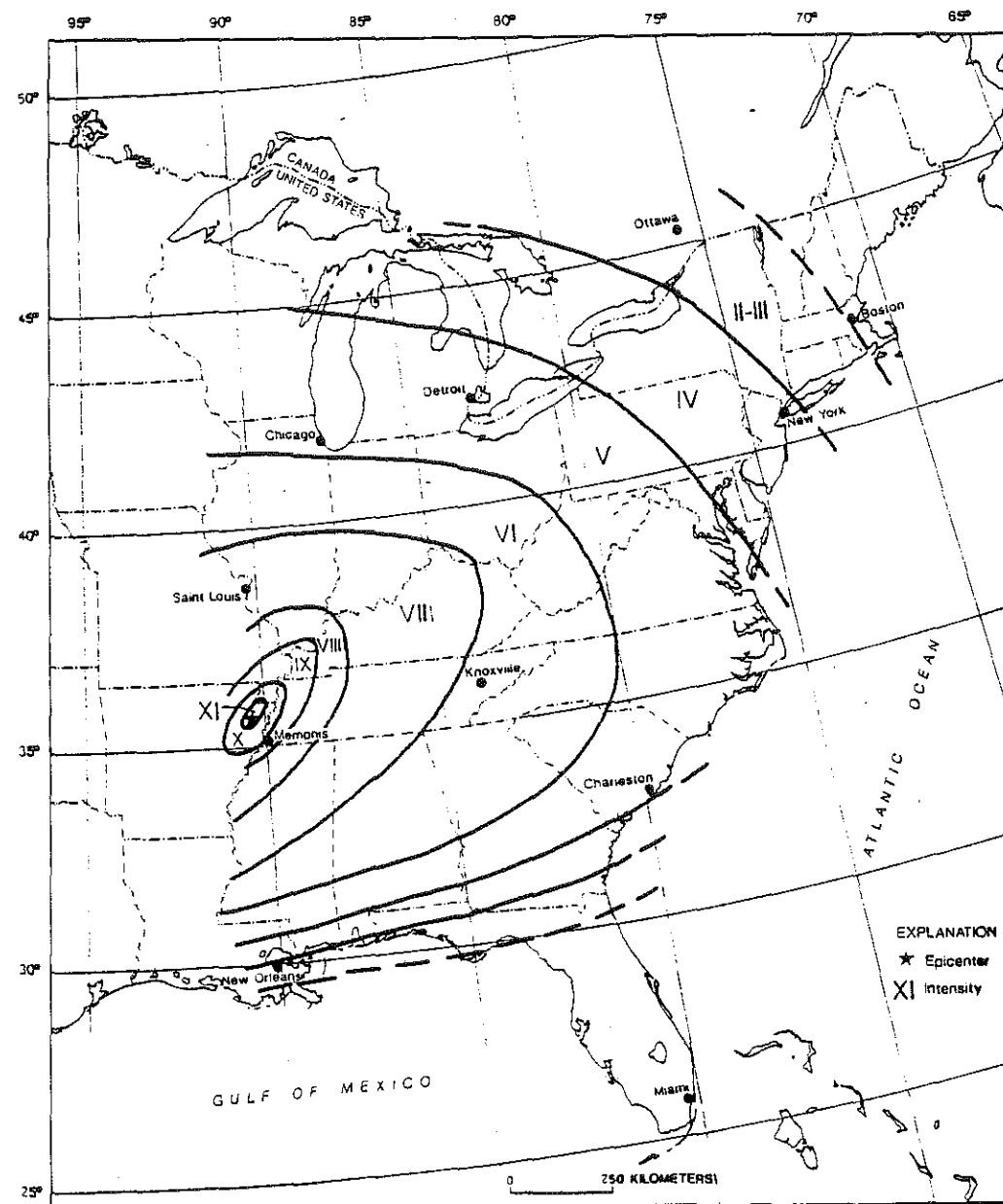
Figure A.1. Isoseismal map for the Arkansas earthquake of December 16, 1811, 08:15 UTC (first of the 1811-1812 New Madrid series). This map is a simplified version of Nuttli (1973a). Figure is taken from Stover and Coffman (1993).
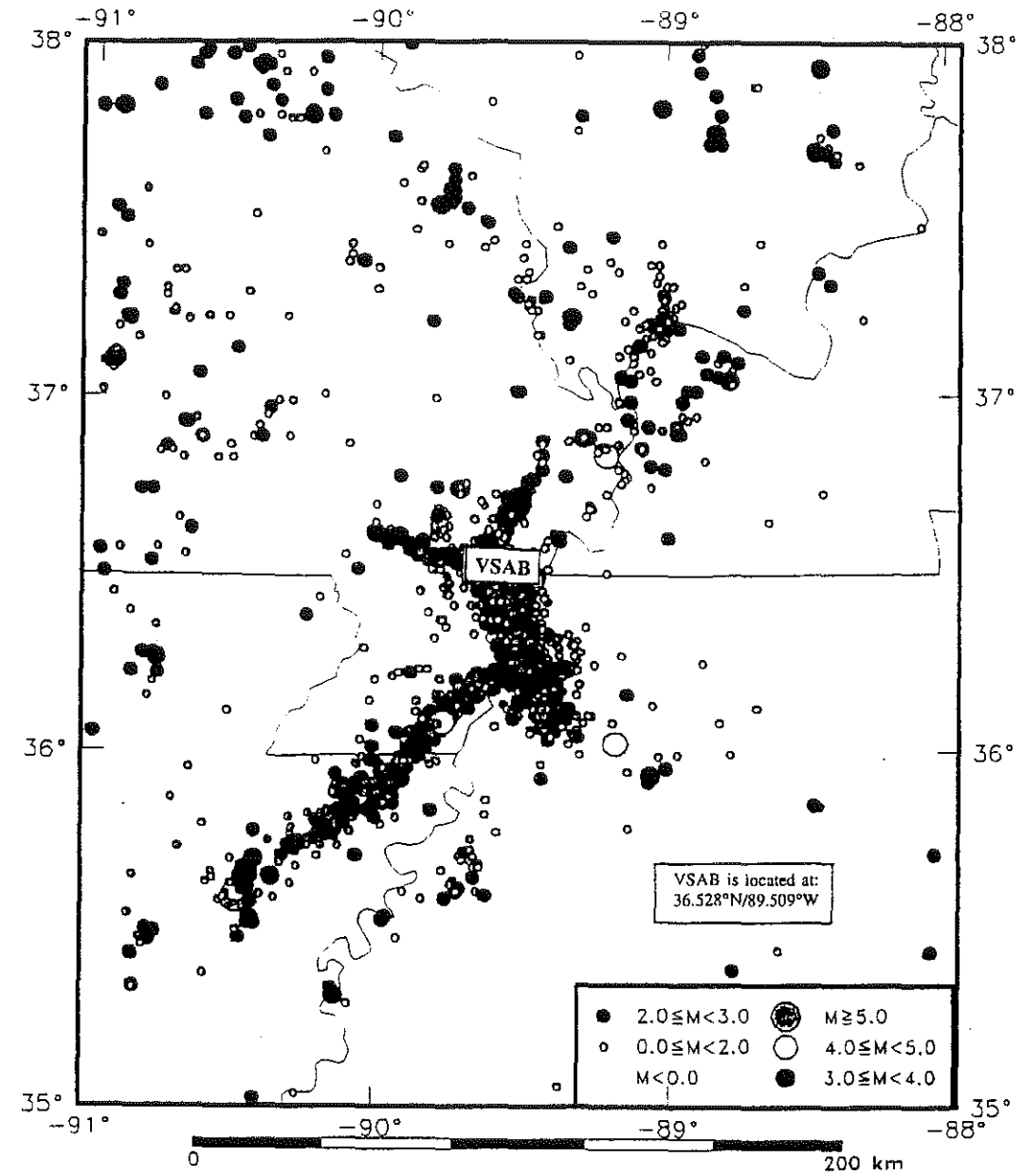
Figure A.2. Instrumentally located seismicity in the New Madrid Seismic Zone between the years of 1974 and 1989 (provided by Center for Earthquake Research and Information, University of Memphis).
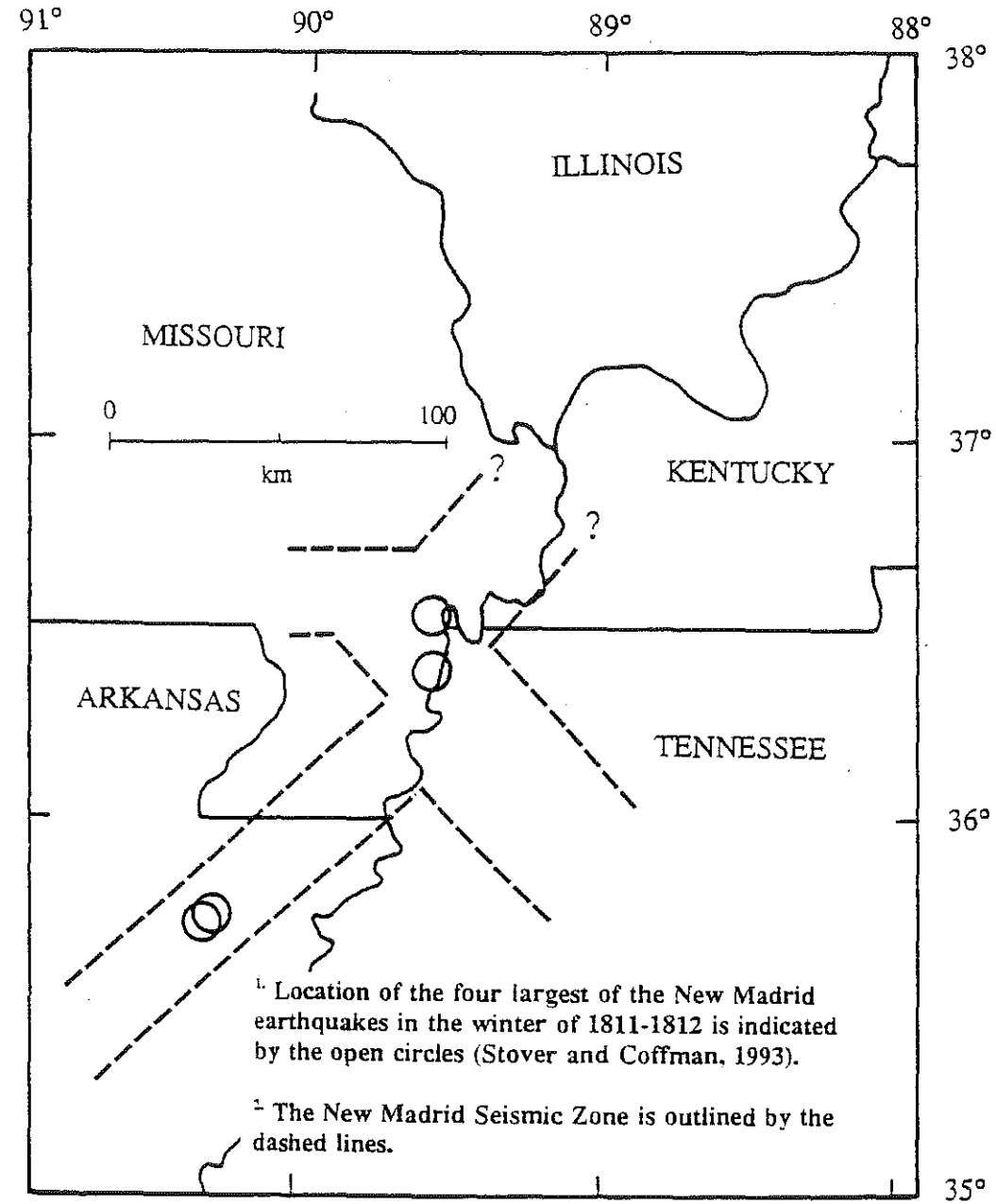
Figure A.3. Epicenters of the four largest 1811-1812 New Madrid earthquakes with respect to the boundaries of the major trends of the instrumental seismicity shown in Figure A.2.

Map labels and annotations:

91° 90° 89° 88° 38°

ILLINOIS

MISSOURI

0 100
km

37°

KENTUCKY

ARKANSAS

TENNESSEE

36°

¹· Location of the four largest of the New Madrid earthquakes in the winter of 1811-1812 is indicated by the open circles (Stover and Coffman, 1993).

²· The New Madrid Seismic Zone is outlined by the dashed lines.

35°
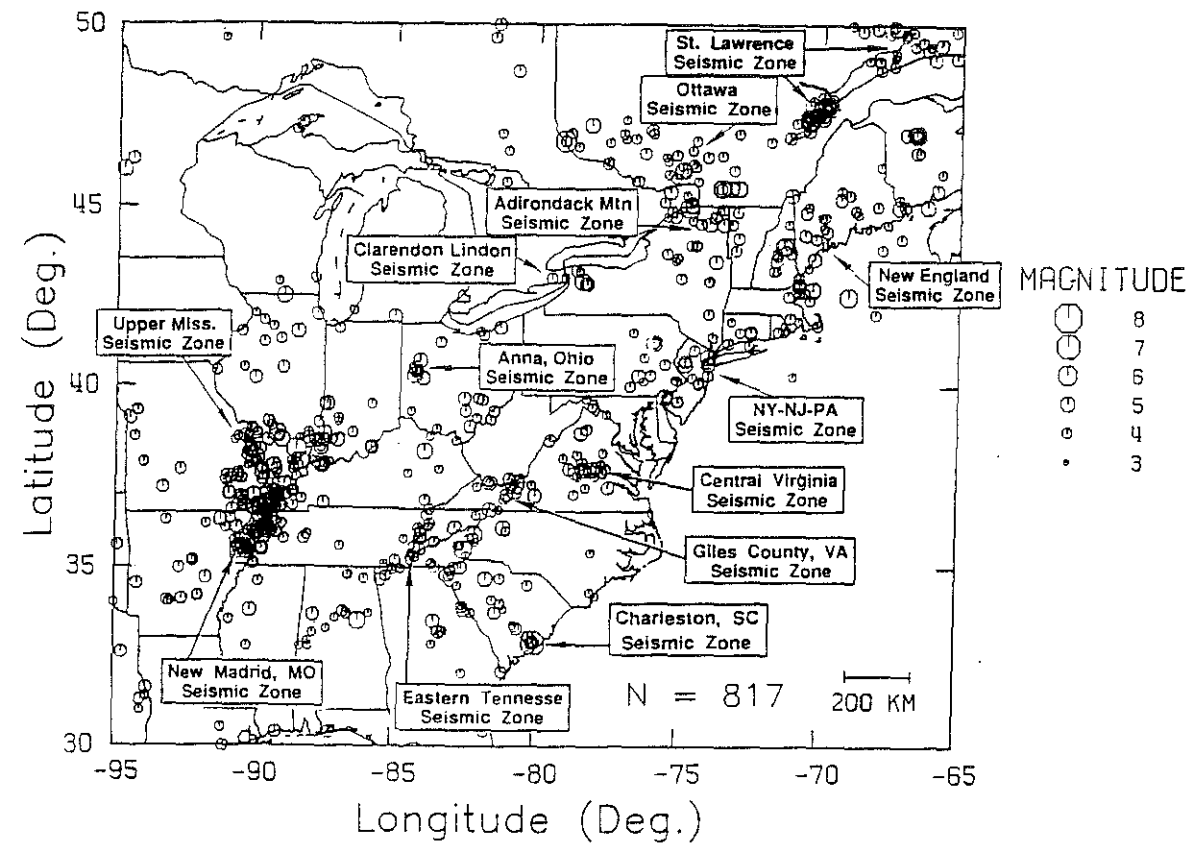
Figure A.4. Seismicity map for central and eastern North America (1568-1987) with some of the principal seismic zones identified. N is the number of epicenters plotted. (Taken from Bollinger, 1992).
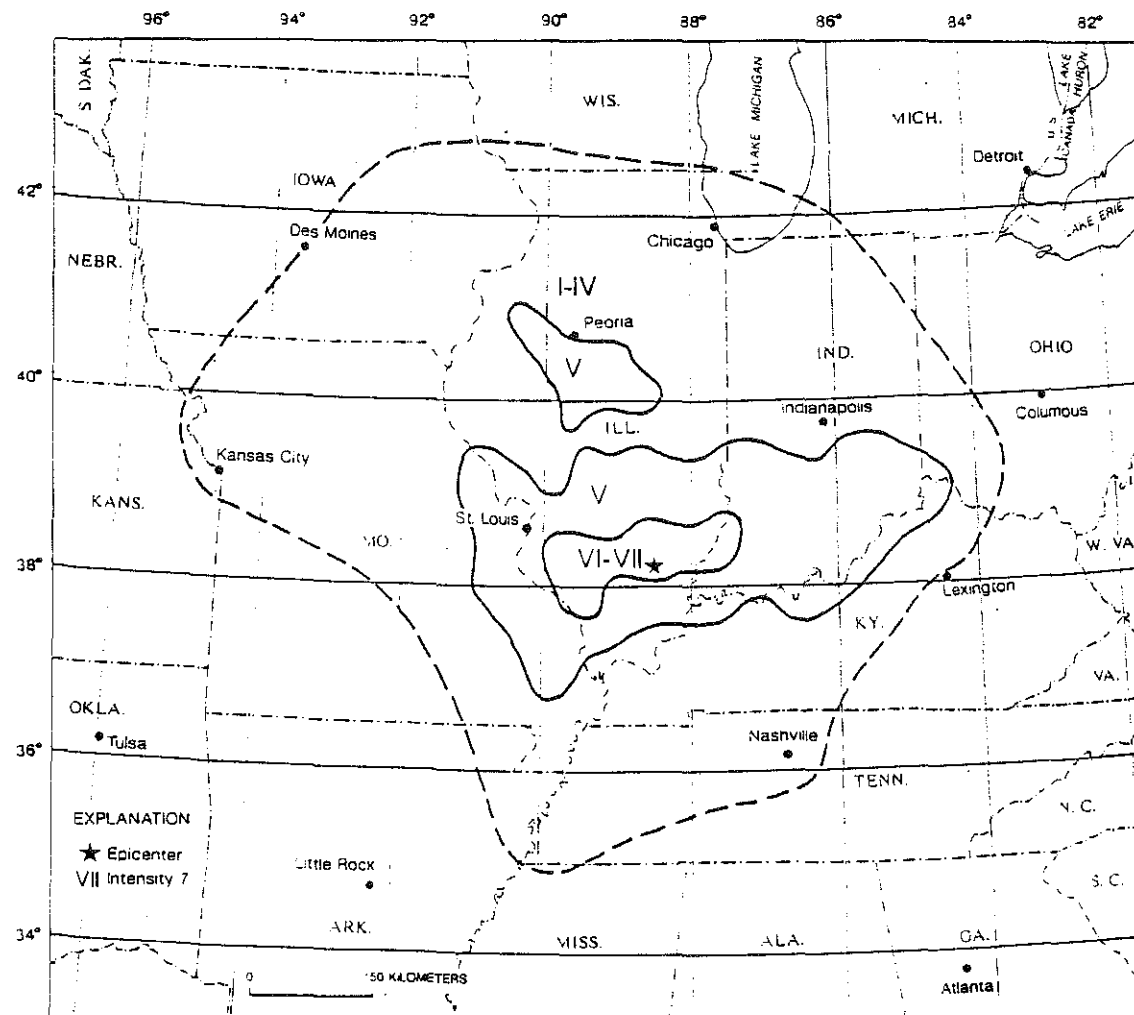
Figure A.5. Isoseismal map for the southern Illinois earthquake of September 27, 1891. (Taken from Stover and Coffman, 1993).
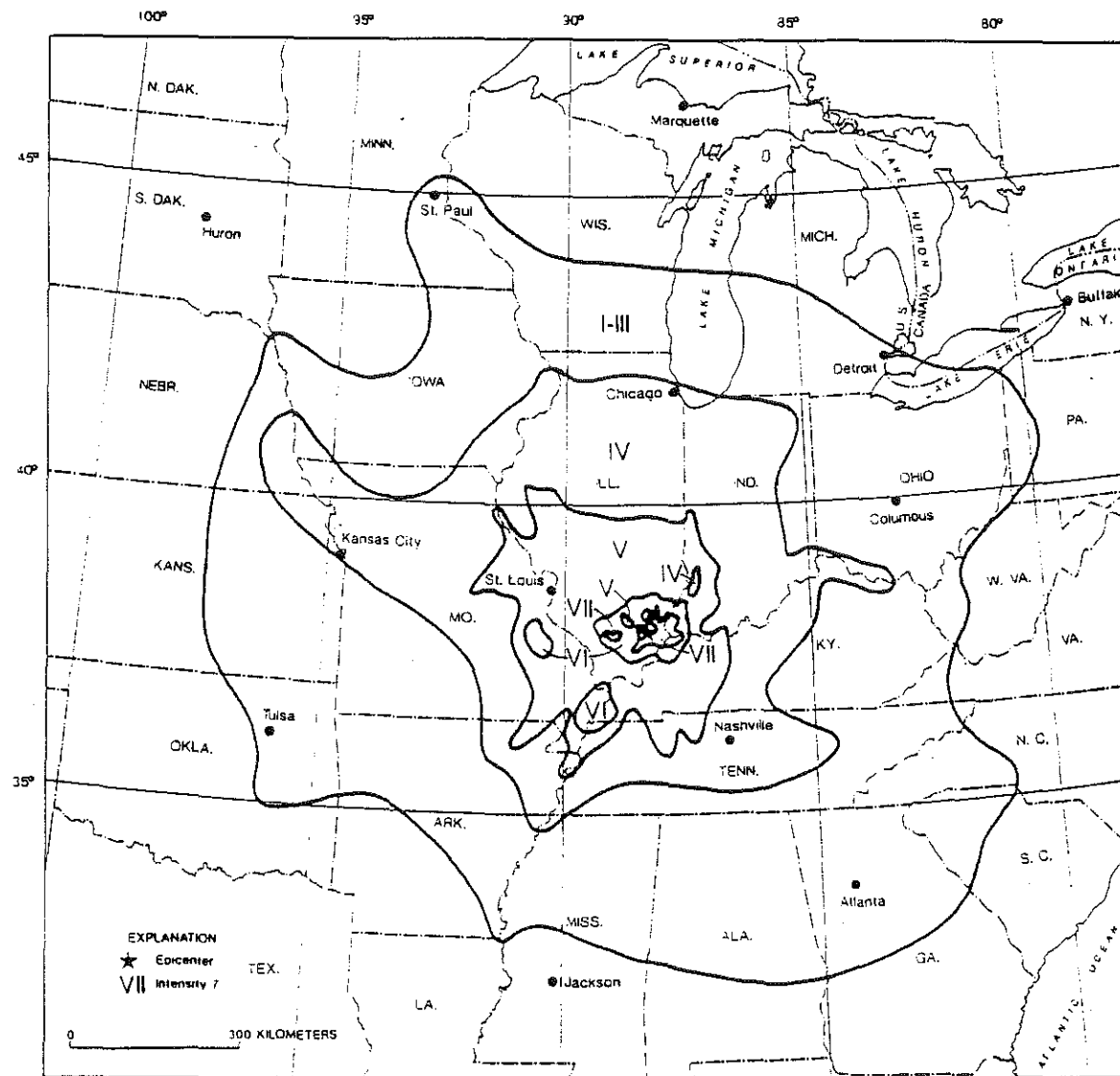
Figure A.6. Isoseimal map for the southern Illinois earthquake of November 9, 1968. (Taken from Stover and Coffman, 1993).
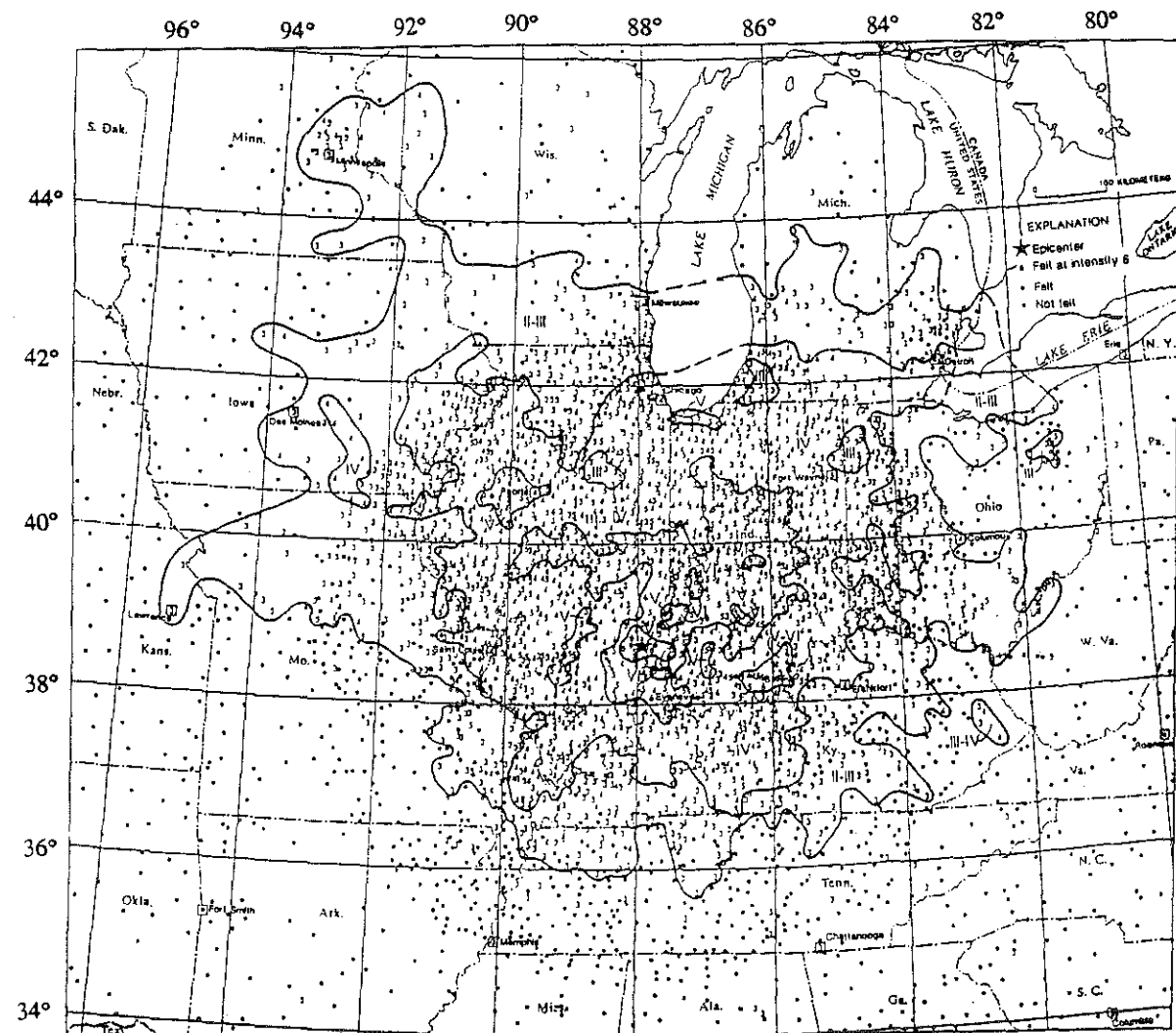
Figure A.7. Isoseismal map for the southern Illinois earthquake of June 10, 1987. Roman numerals represent Modified Mercalli intensities between isoseismals; Arabic numerals, open circles, and blackened circles represent effects in specific communities; squares denote labeled cities and towns. (Provided by the U.S. Geological Survey, unpublished).
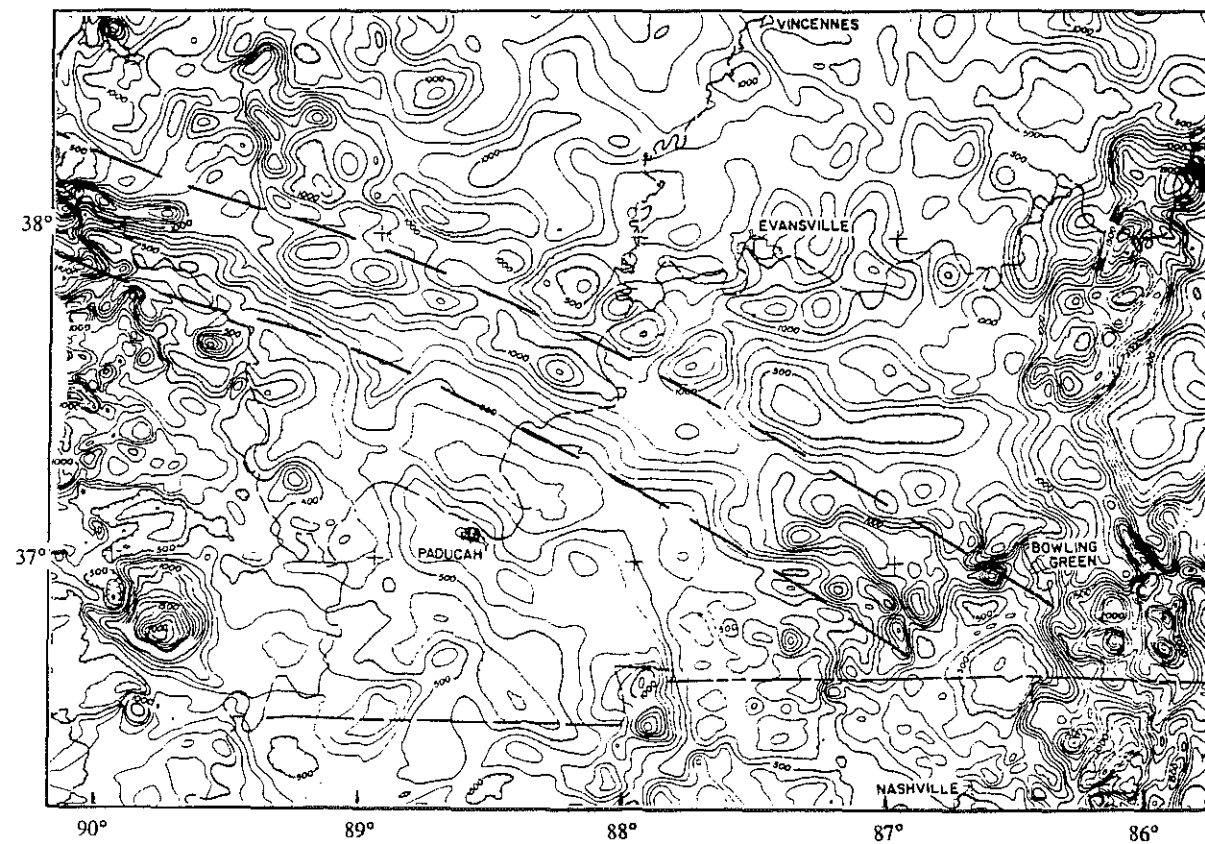
Figure A.8. Aeromagnetic map of the east-central mid-continent region (dashed lines delineate the South-Central Magnetic Lineament). Contour interval = 100 nT. The magnetic lineament marks the position of the crustal boundary. (Taken from Heigold and Kolata, 1993).
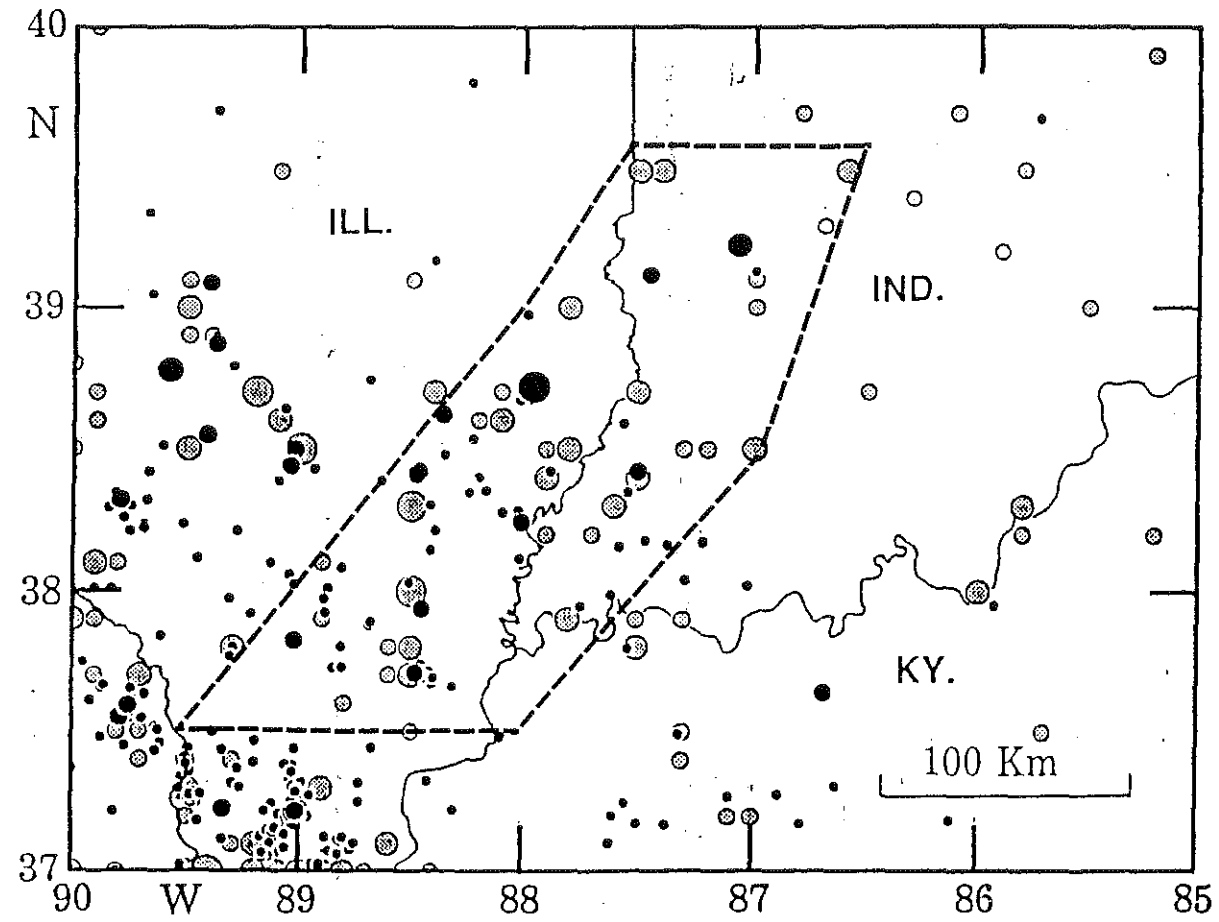
Figure A.9. Seismicity of southern Illinois and Indiana. Historical earthquake locations are shown by shaded circles, instrumentally recorded earthquakes are shown by filled circles. (Taken from Hamburger, M.W., and J.A. Rupp, 1988).
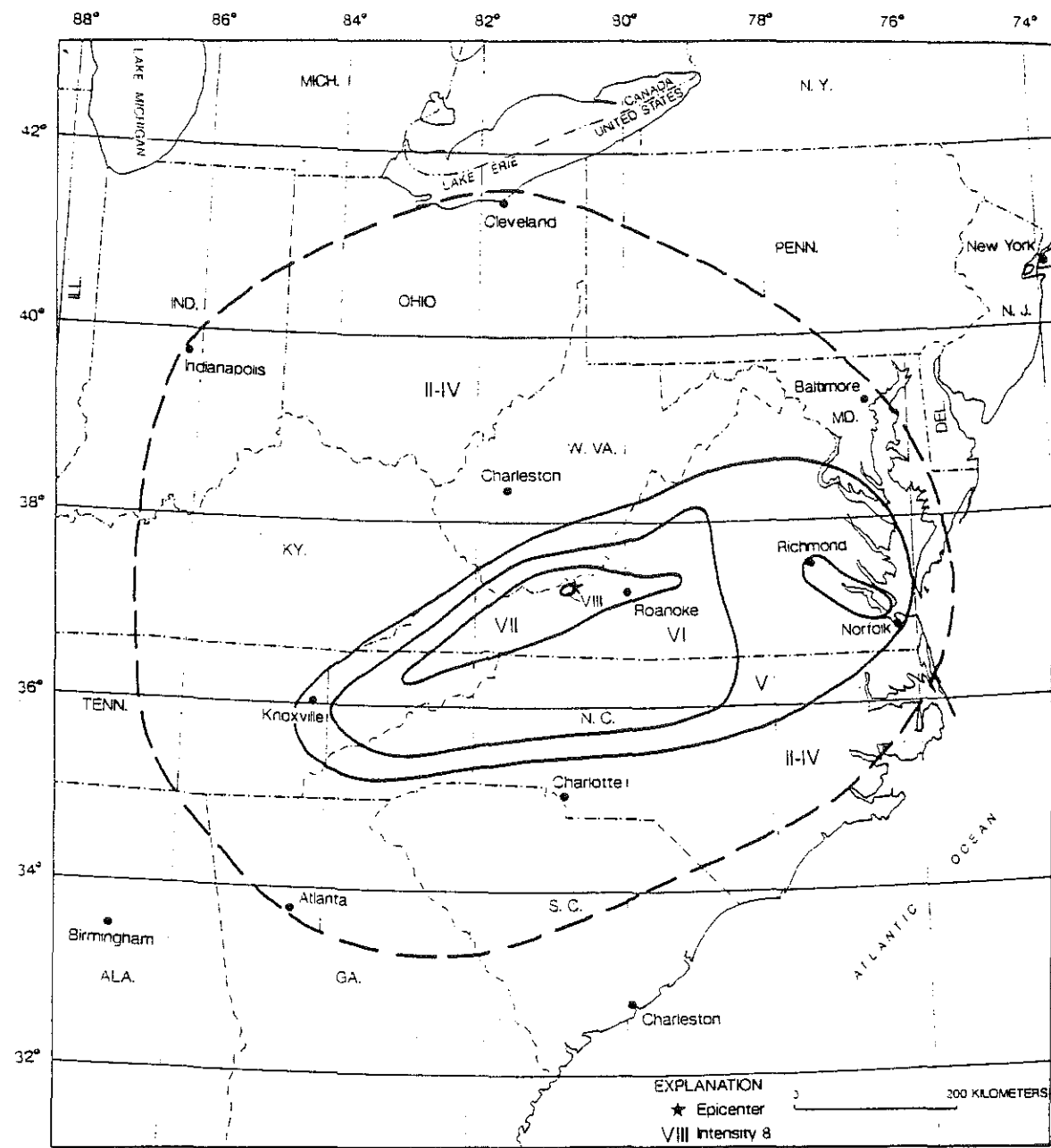
Figure A.10. Isoseismal map for the Giles County, Virginia, earthquake of May 31, 1897. (Taken from Stover and Coffman, 1993).
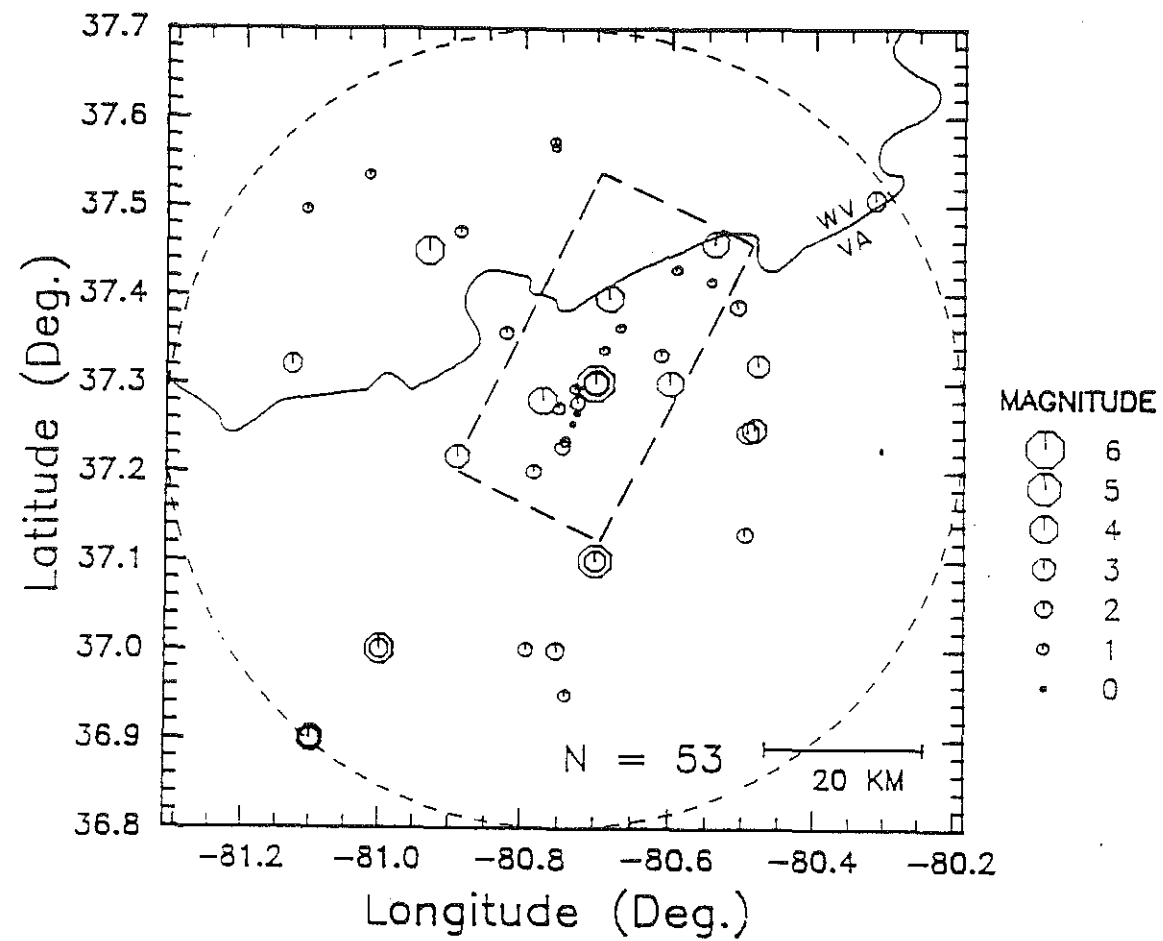
Figure A.11. Seismicity map for the Giles County, Virginia, seismic zone - 1876 through 1987, showing all the epicenters (octagon symbols) and the circular and rectangular definitions of the zone. The circular definition is a general one and includes the off-zone 'halo' events. The rectangular definition is for the zone proper and includes only those earthquakes thought to have originated within the principal seismogenic structure. (Taken from Bollinger, et al., 1992).
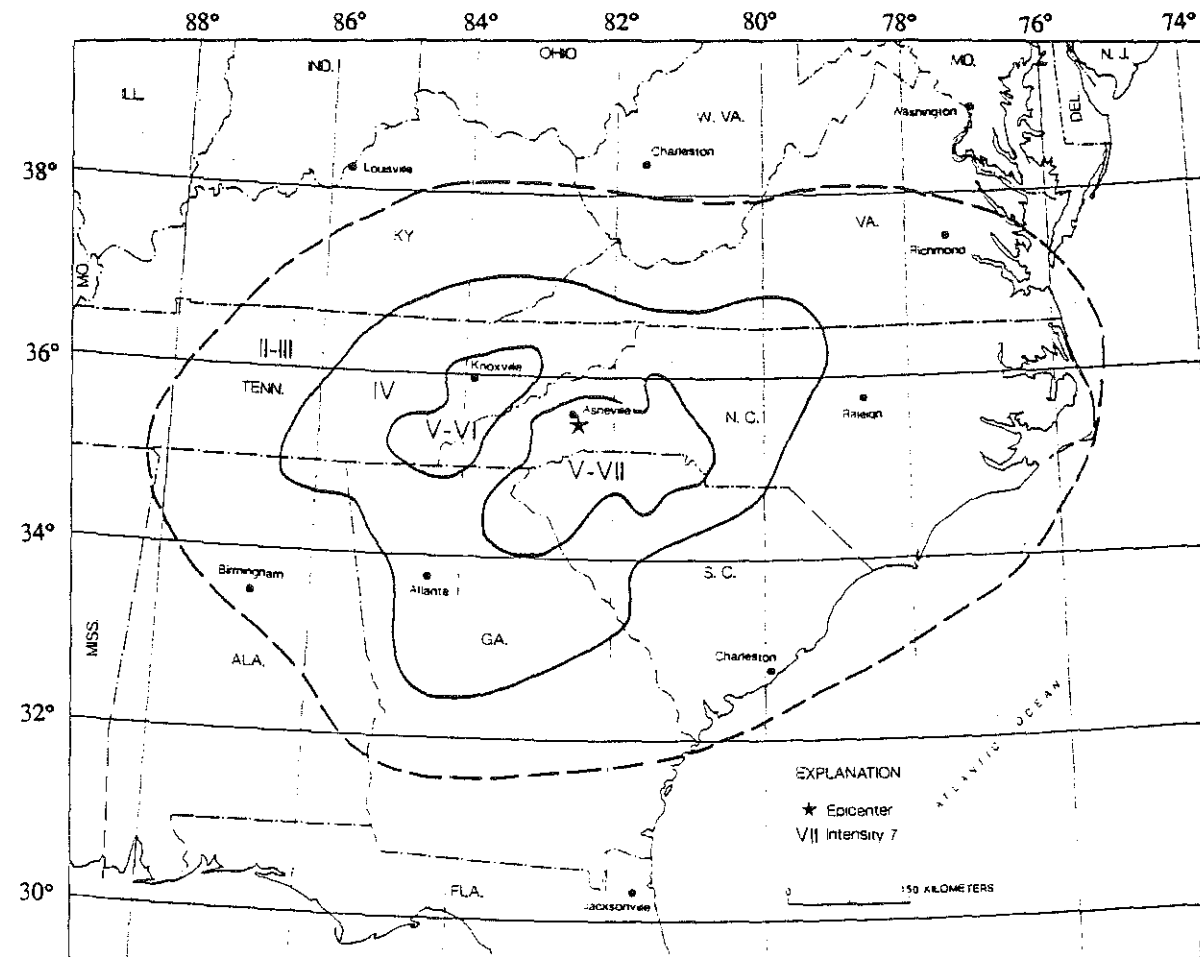
Figure A.12. Isoseismal map for the Waynesville, North Carolina, earthquake of
February 21, 1916. (Taken from Stover and Coffman, 1993).
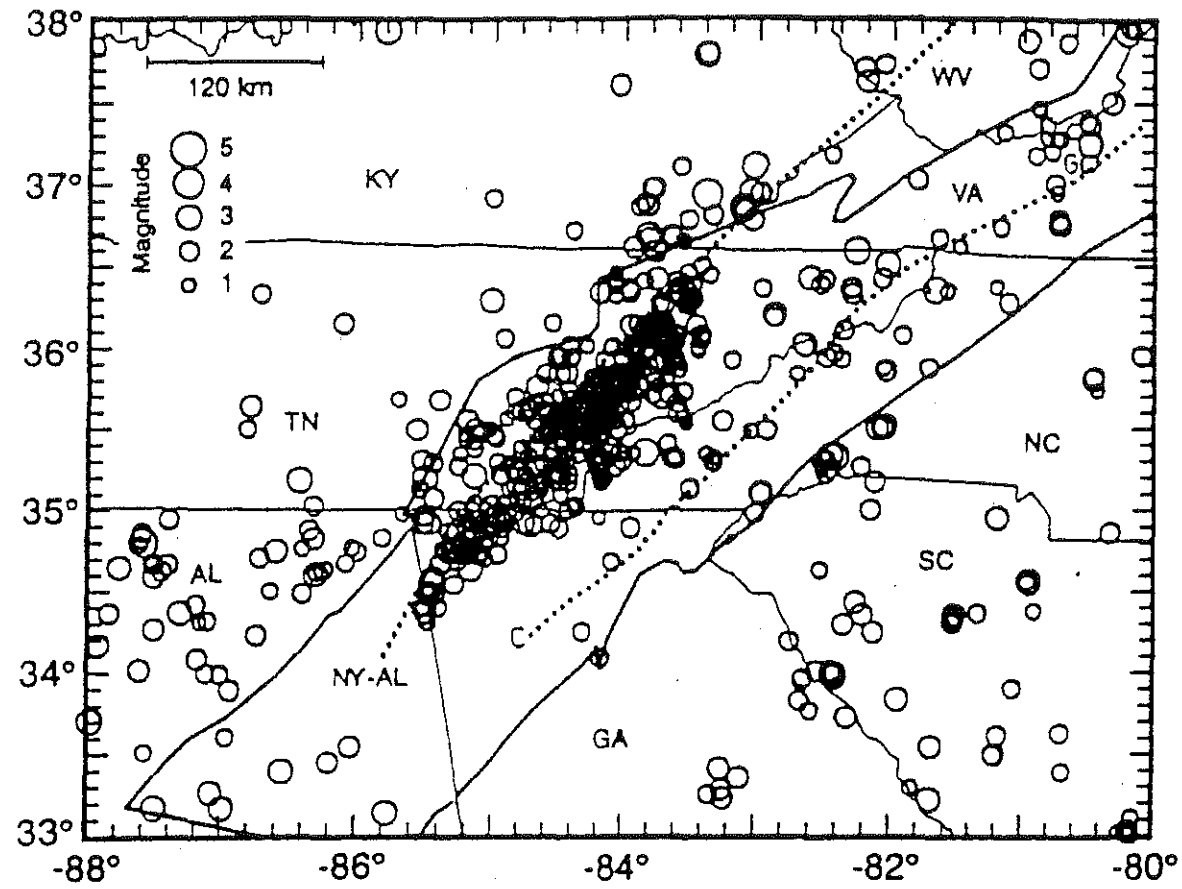
Figure A.13. Seismicity in the Eastern Tennessee Seismic Zone (ETSZ) and
surrounding regions for 1981-1992. The dotted lines indicate the New
York-Clingman (NY-AL) and Clingman (C) magnetic lineaments. The
location of the Giles County, Virginia, Seismic Zone is indicated by the
letter G. (Taken from Powell, et al., 1994).
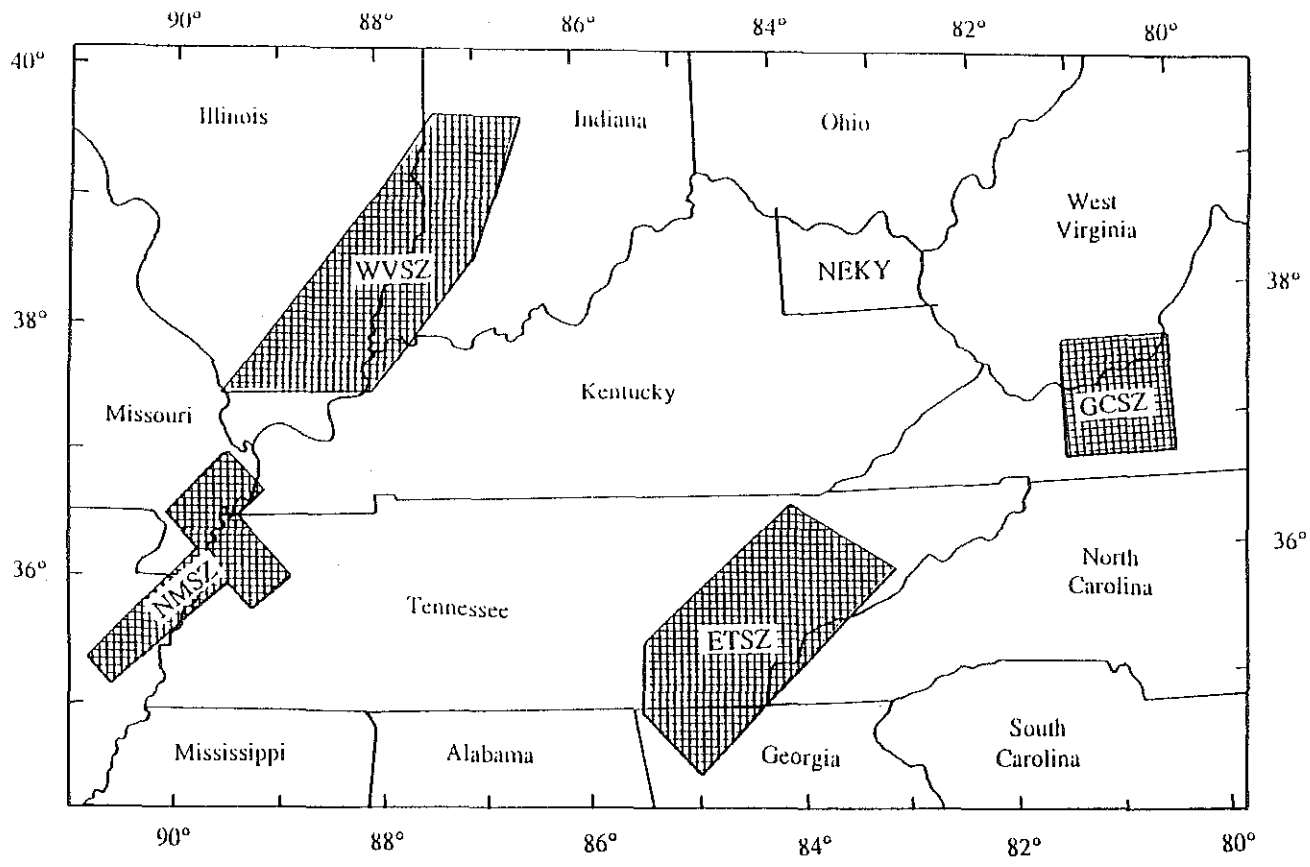
Figure A.14. Seismic zones considered in this study are indicated by the hatched areas. ETSZ = Eastern Tennessee Seismic Zone; GCSZ = Giles County, Virginia, Seismic Zone; NMSZ = New Madrid Seismic Zone; and WVSZ = Wabash Valley Seismic Zone. As indicated in the text, northeastern Kentucky area (NEKY) is not considered to be a seismic zone, at this time, but it is given special attention because of the ongoing seismicity in the area and the damaging earthquakes that occurred in Bath County, Kentucky, in 1989 and 1988.
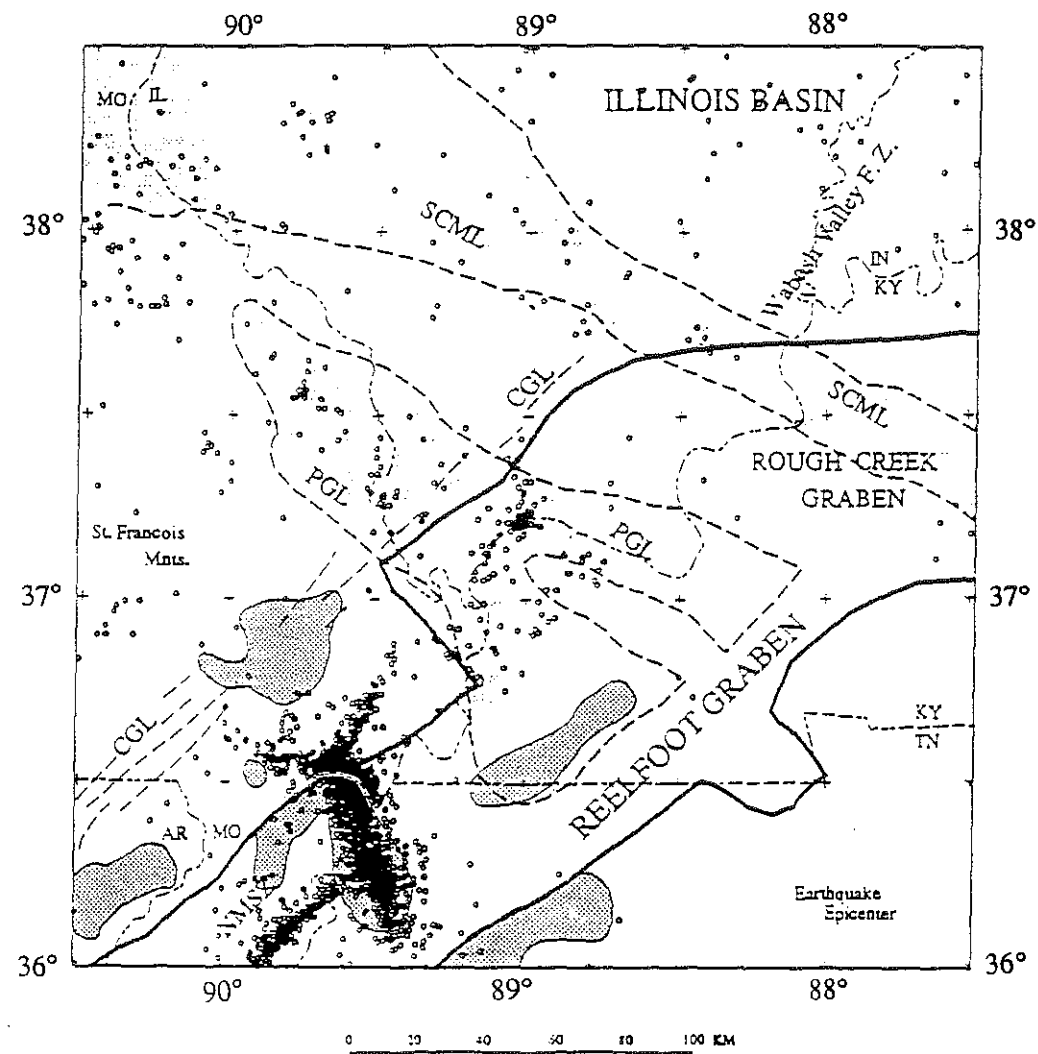
Figure A.15. Regional geological features expressed in the potential-field data of the southern Illinois and northern Reelfoot rift region. Heavy solid lines show the interpreted margins of the Reelfoot and Rough Creek grabens. Light shaded areas labeled PGL and SCML depict two prominent geophysical features, the Paducah gravity lineament and south-central magnetic lineament, respectively. Darker shaded areas represent subsurface igneous intrusions associated with the Reelfoot rift. NE-trending dashed lines depict linear gravity and magnetic features that form the Commerce geophysical lineament (CGL). Small circles are locations of earthquake epicenters detected by the Missouri Valley regional seismic network from 1975 to 1991. (Taken from Hildenbrand, et al., 1994).
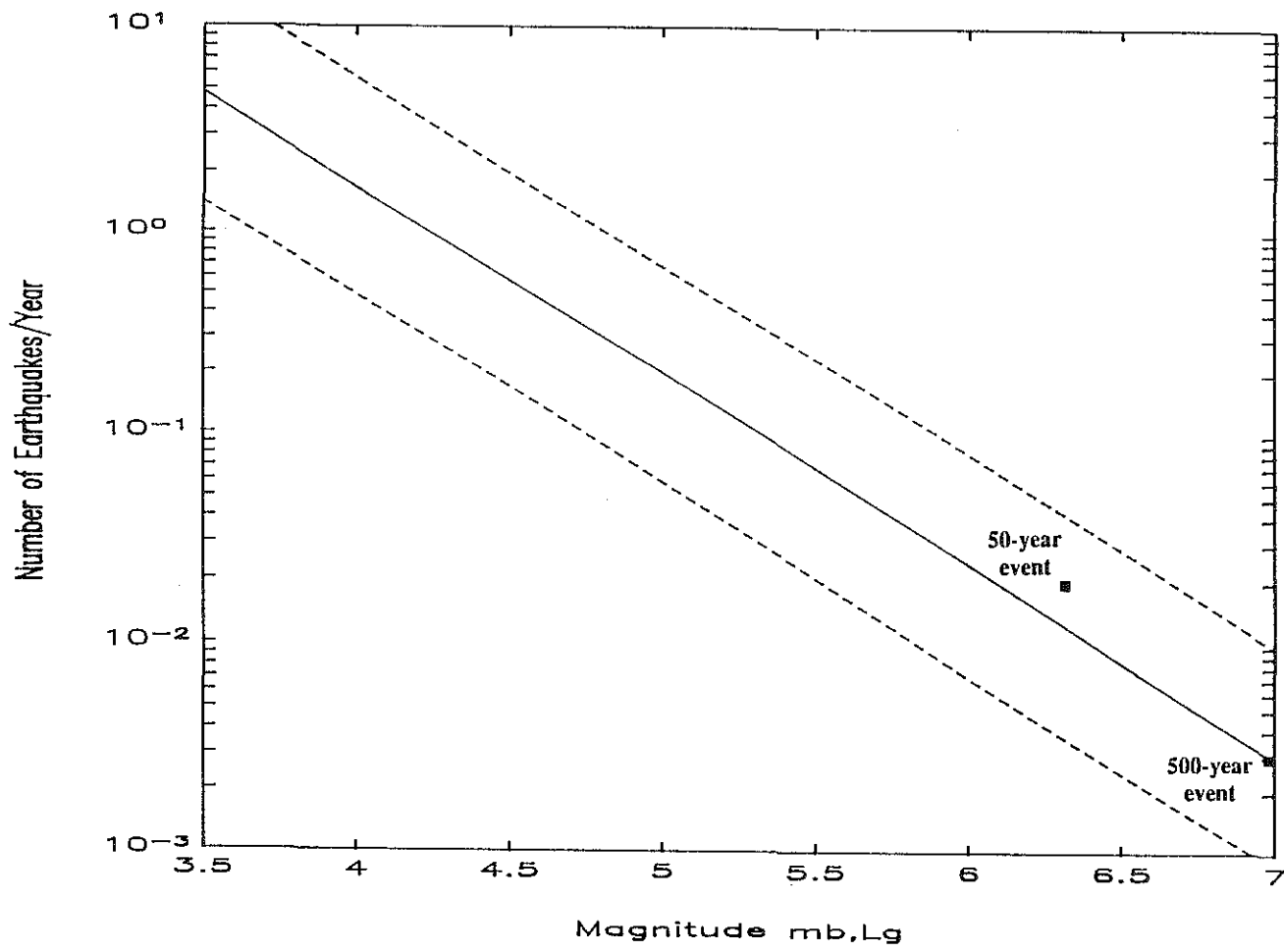
Figure A.16. Cumulative magnitude-recurrence curve (± 1 σ) for the New Madrid Seismic Zone (from Nuttli and Herrmann, 1978). The 50- and 500-year events used in this study are superimposed on the plot for comparison.
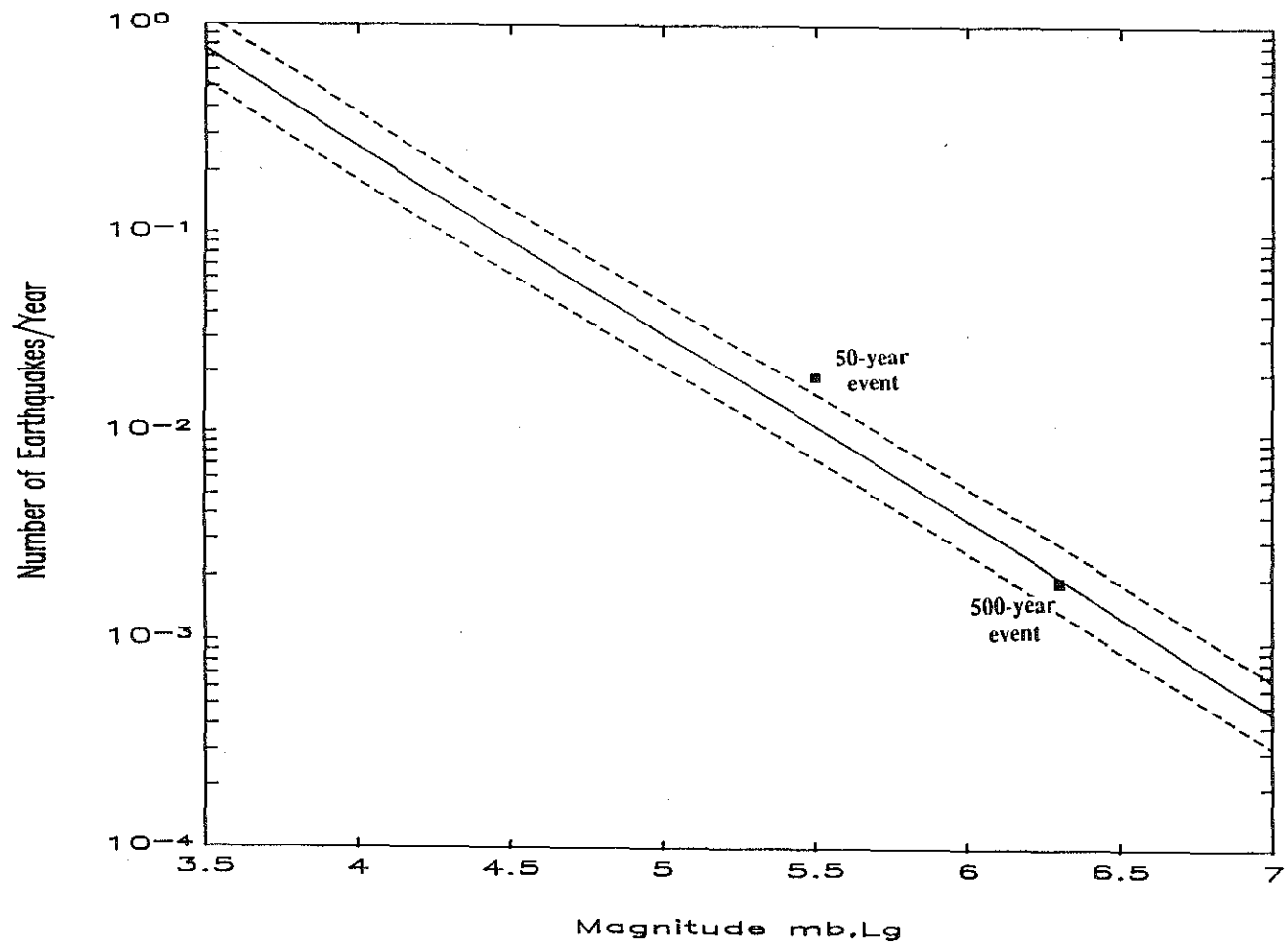
Figure A.17. Cumulative magnitude-recurrence curve (± 1 σ) for the Wabash Valley Seismic Zone (from Nuttli and Herrmann, 1978). The 50- and 500-year events used in this study are superimposed on the plot for comparison.
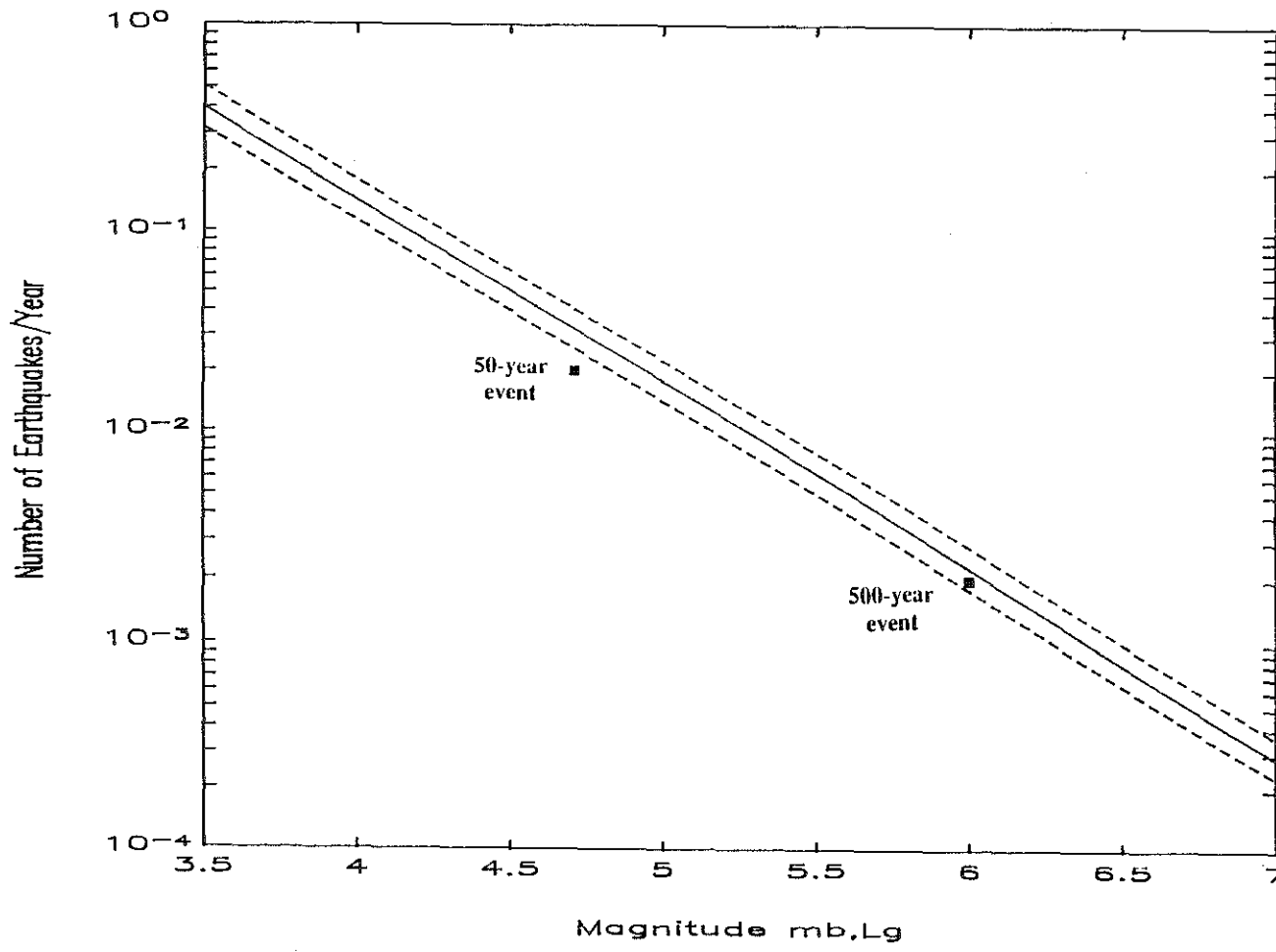
Figure A.18. Cumulative magnitude-recurrence curve (± 1 σ) for the Eastern Tennessee Seismic Zone (from Bollinger, et al., 1989). The 50- and 500-year events used in this study are superimposed on the plot for comparison.
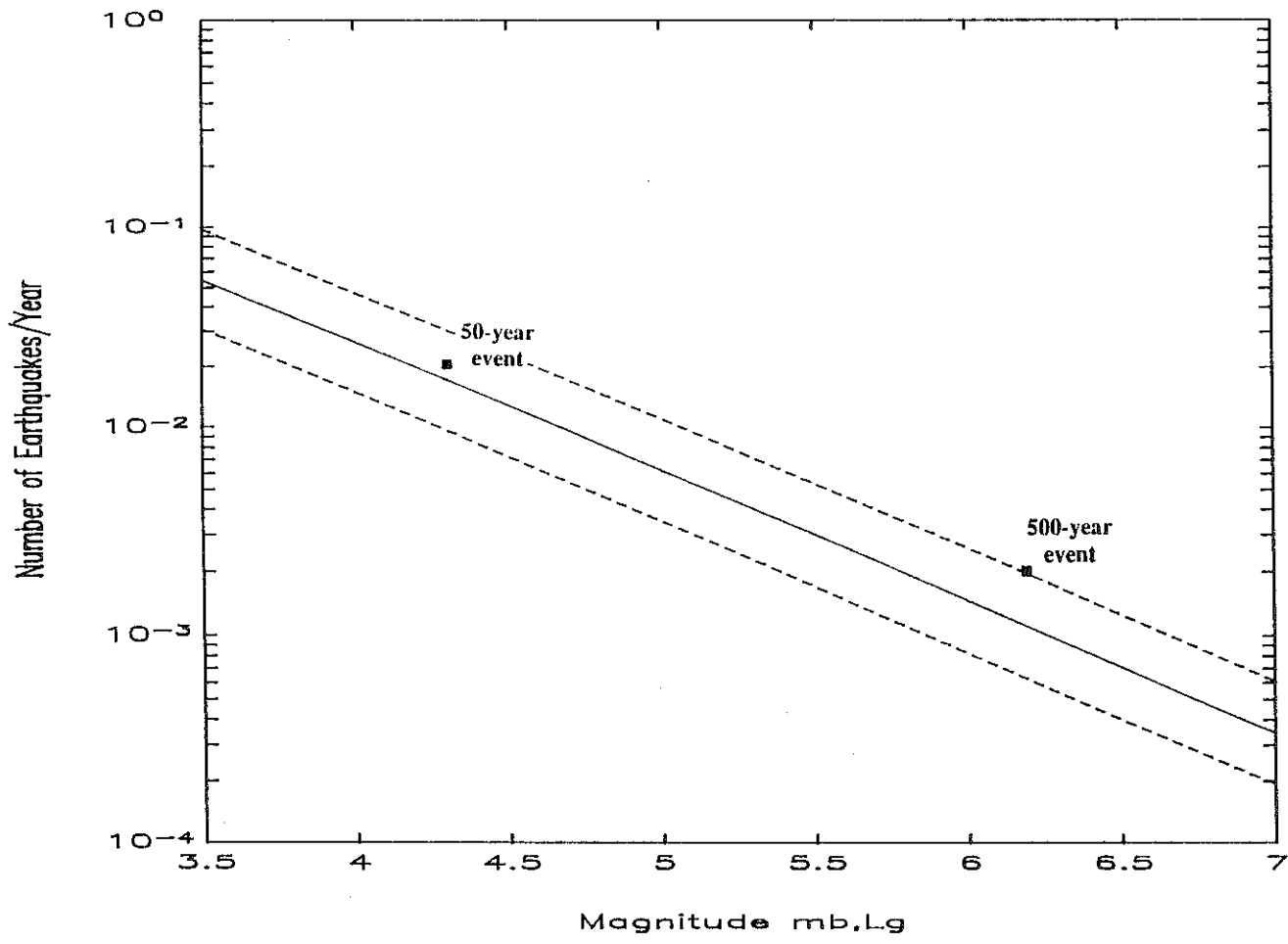
Figure A.19. Cumulative magnitude-recurrence curve (±1 σ) for the Giles County, Virginia, Seismic Zone (from Bollinger, et al., 1989). The 50- and 500-year events used in this study are superimposed on the plot for comparison.
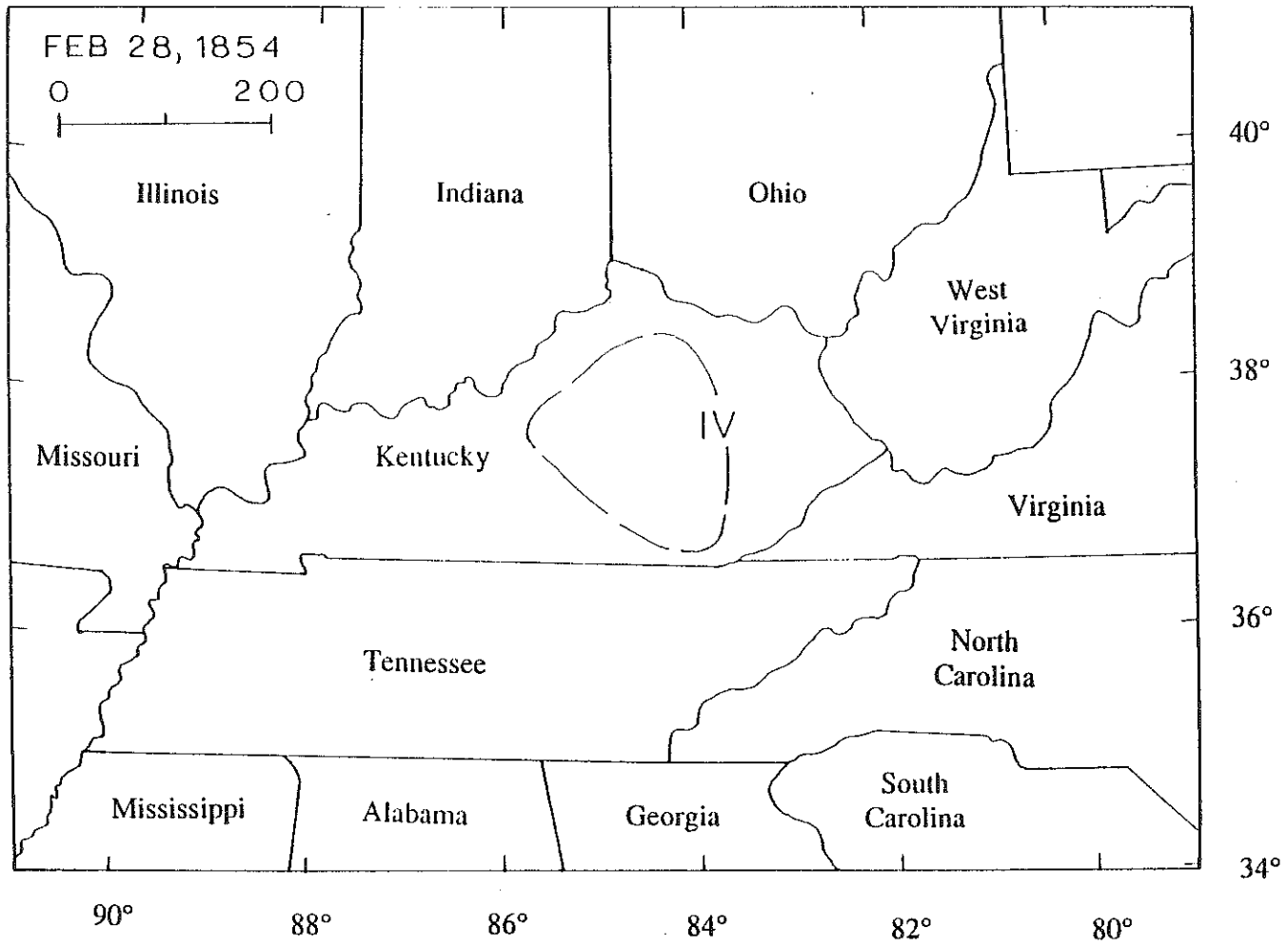
Figure A.20. Isoseismal for the central Kentucky earthquake of February 28, 1854. (Taken from Street and Green, 1984).

Figure A.21. Magnitudes ($m_{b,Lg}$) of the "local events" suggested for Kentucky by this study.
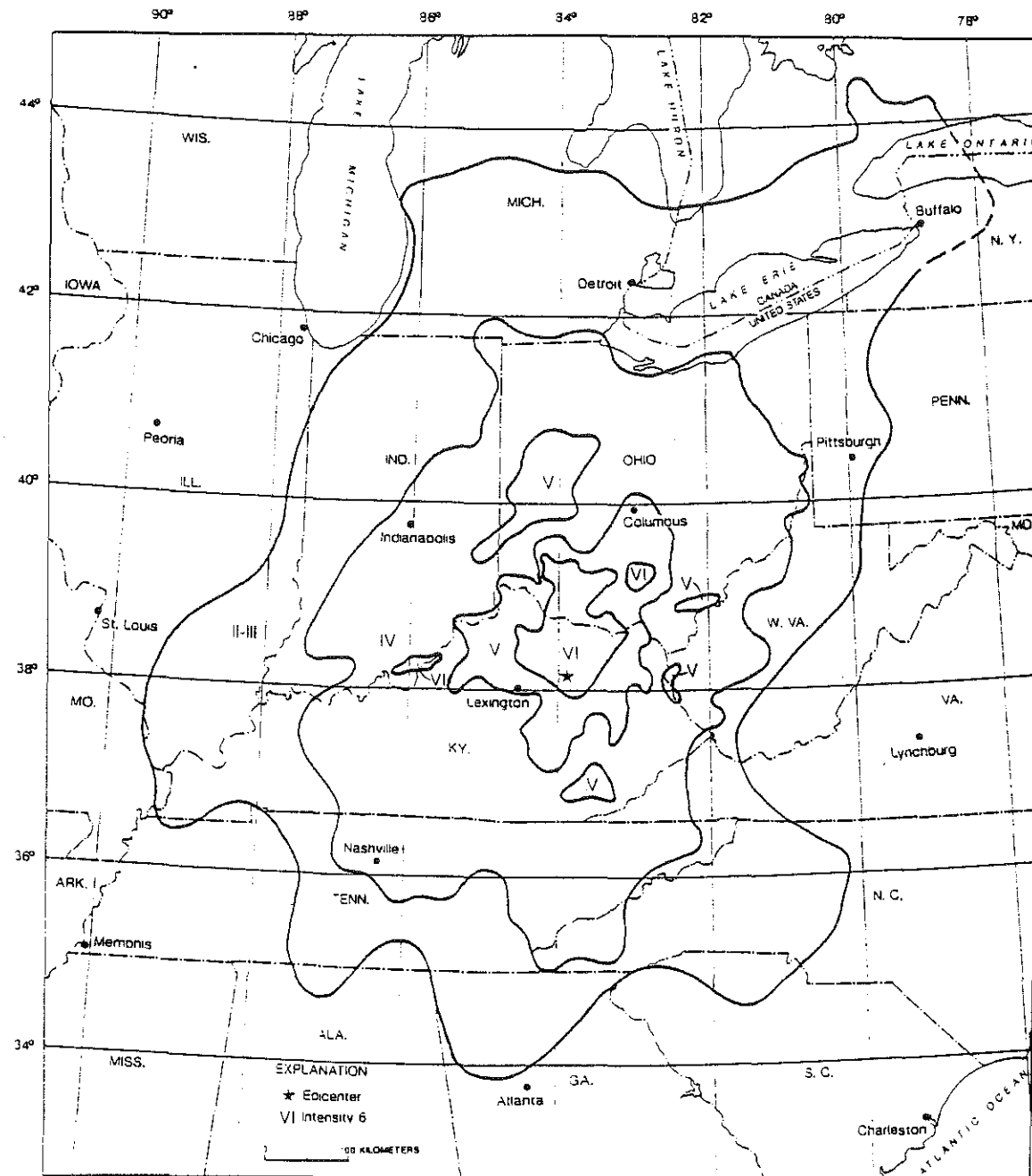
Figure A.22. Isoseismal map for the northern Kentucky earthquake of July 27, 1980. (Taken from Stover and Coffman, 1993).
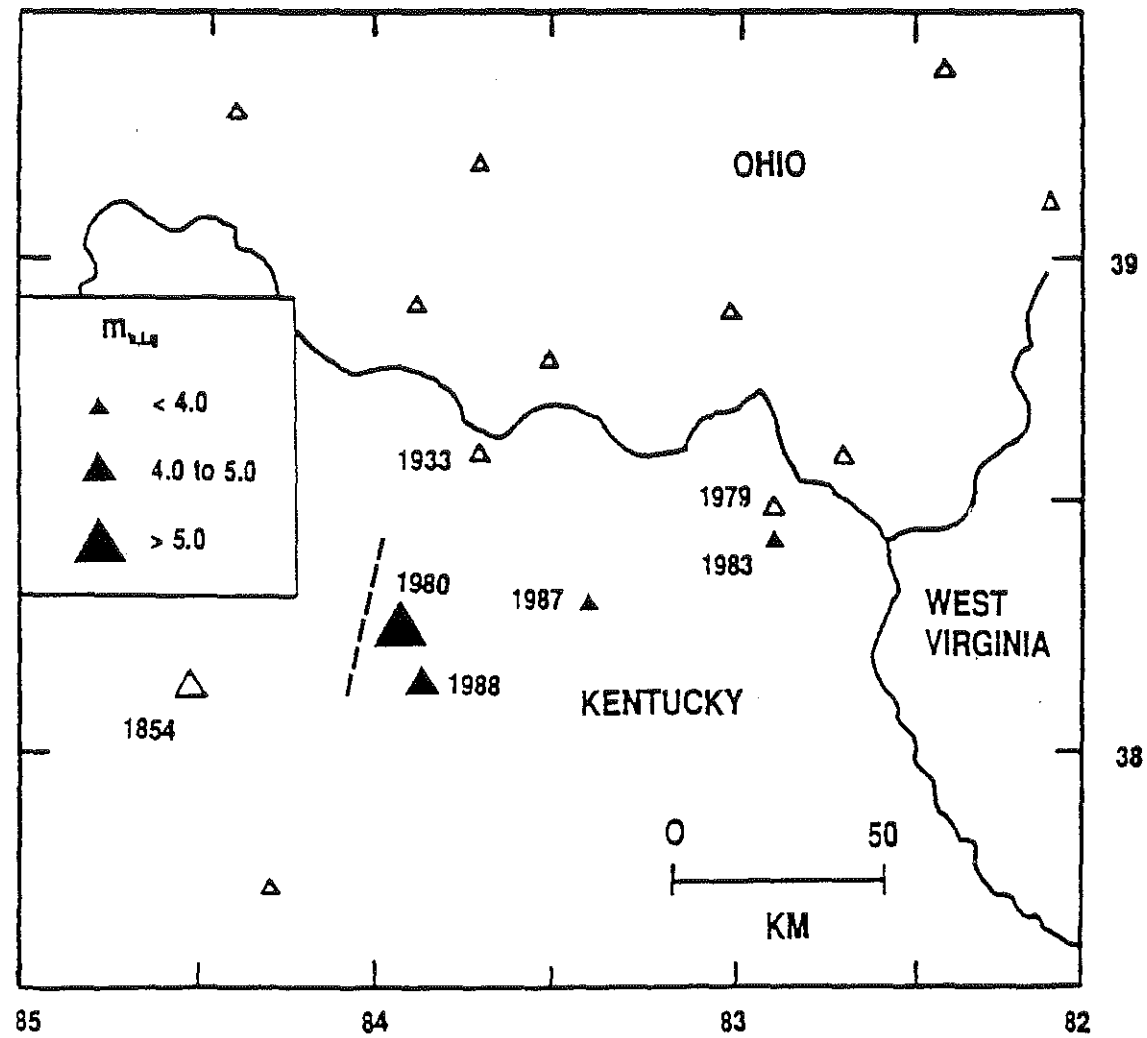
Figure A.23. Epicenters of earthquakes in the northeastern Kentucky area. Open triangles indicate epicentral locations of events that occurred prior to 1980 when the first high-gain seismographs were installed in the region; solid triangles indicate instrumentally located events from 1980 through 1988. The dashed line indicates the approximate location of a lateral velocity discontinuity in the crust that is believed to represent the western border of the seismicity. (Taken from Street, et al., 1993).

APPENDIX B:
TIME HISTORIES AND RESPONSE SPECTRA
FOR 50-YEAR EVENT
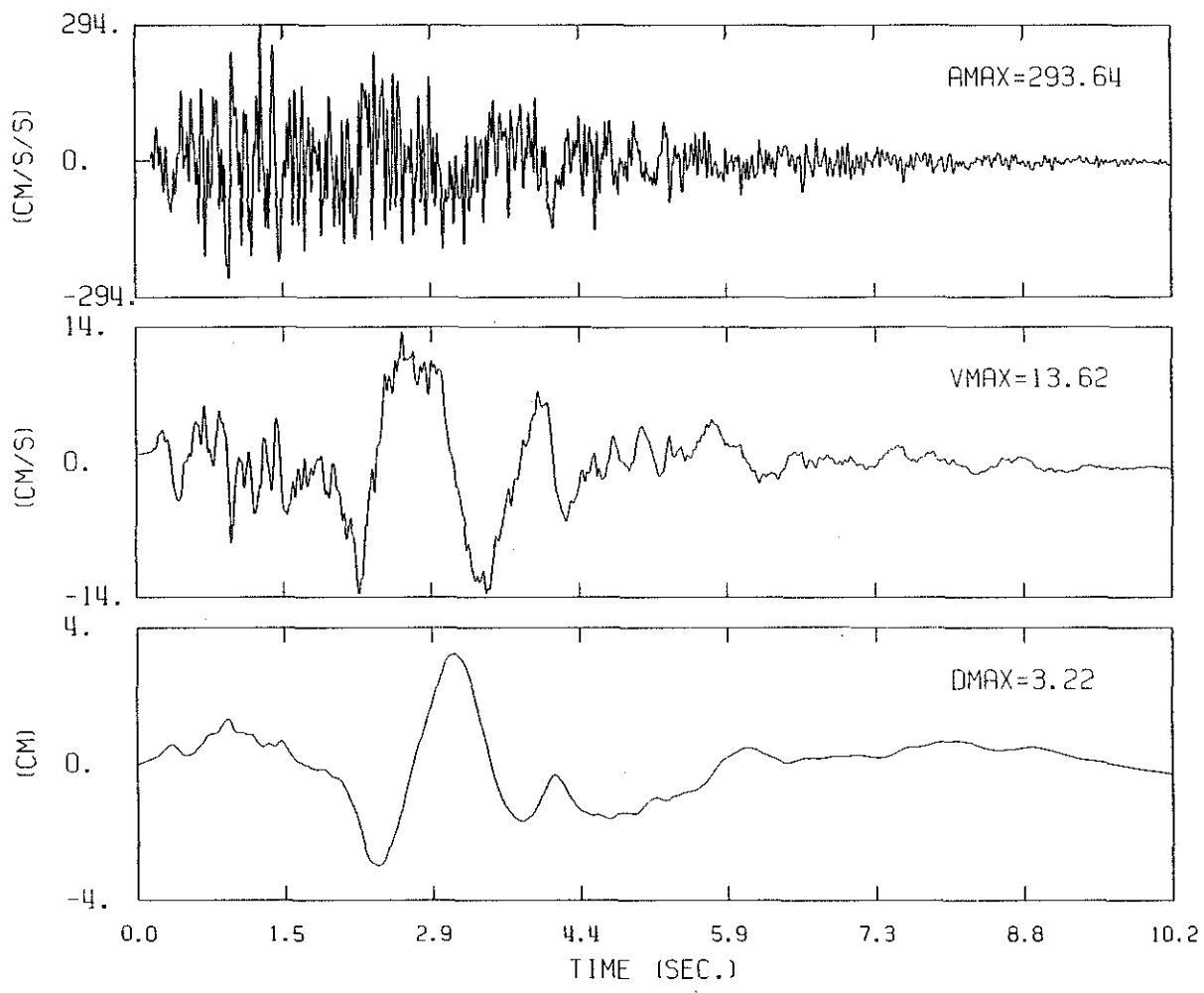
Figure B.1. Acceleration, Velocity, and Displacement Time History for the Horizontal Component of the 50-Year Event for Counties Identified by 0.30g-1 in Figure 4.3 (TR-50Y-0.30g-1).
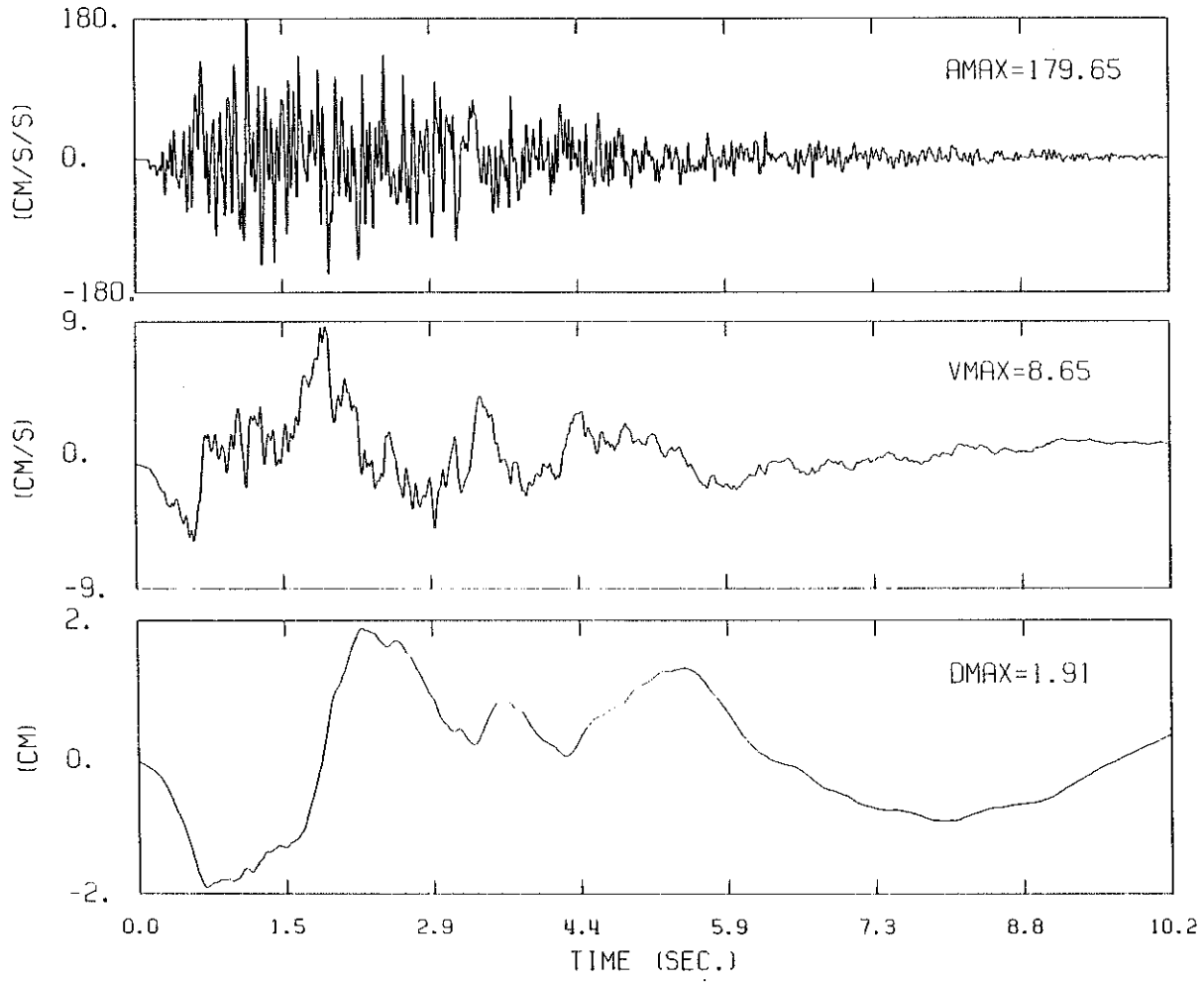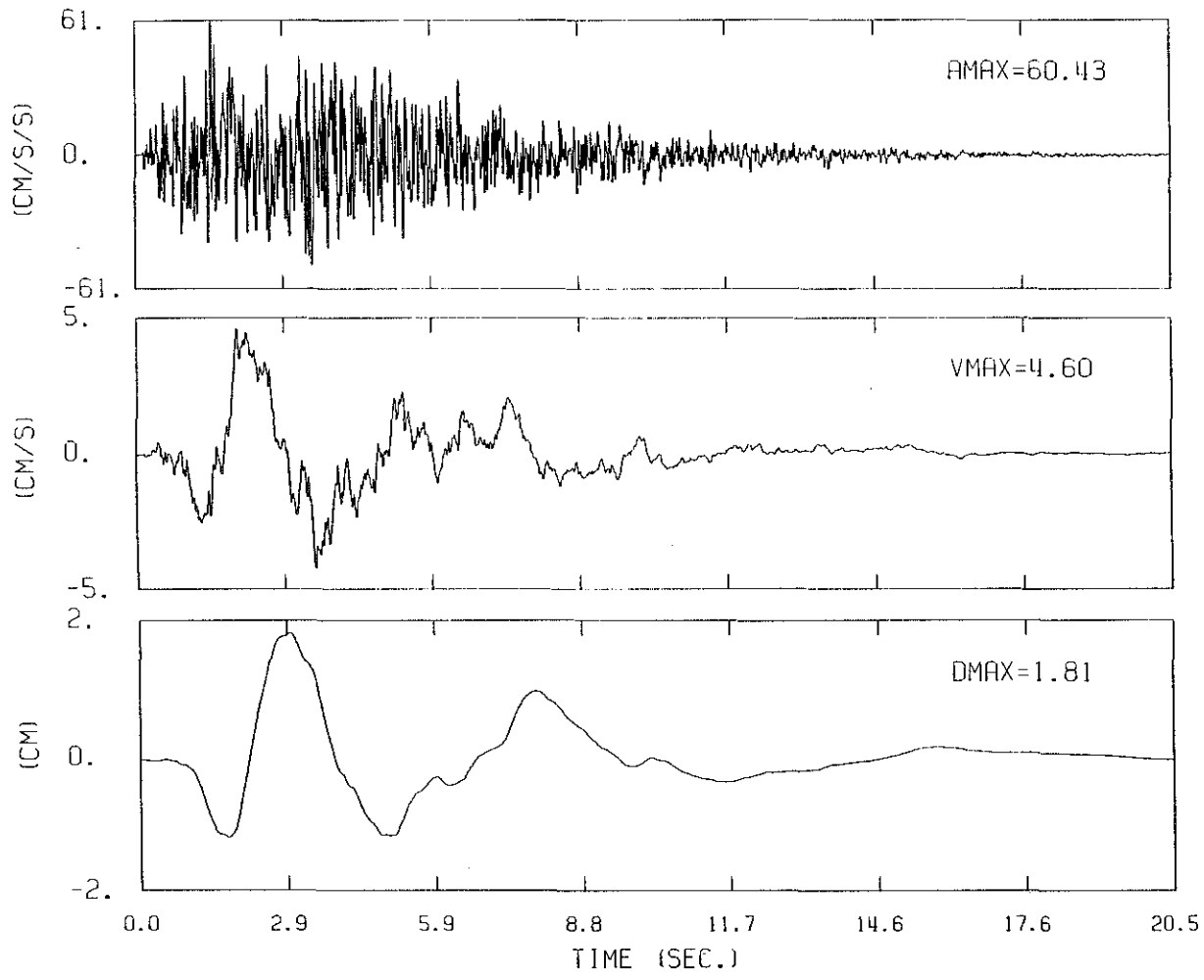
Figure B.2. Acceleration, Velocity, and Displacement Time History for the Vertical Component of the 50-Year Event for Counties Identified by 0.30g-1 in Figure 4.3 (TR-50Y-0.30g-1).
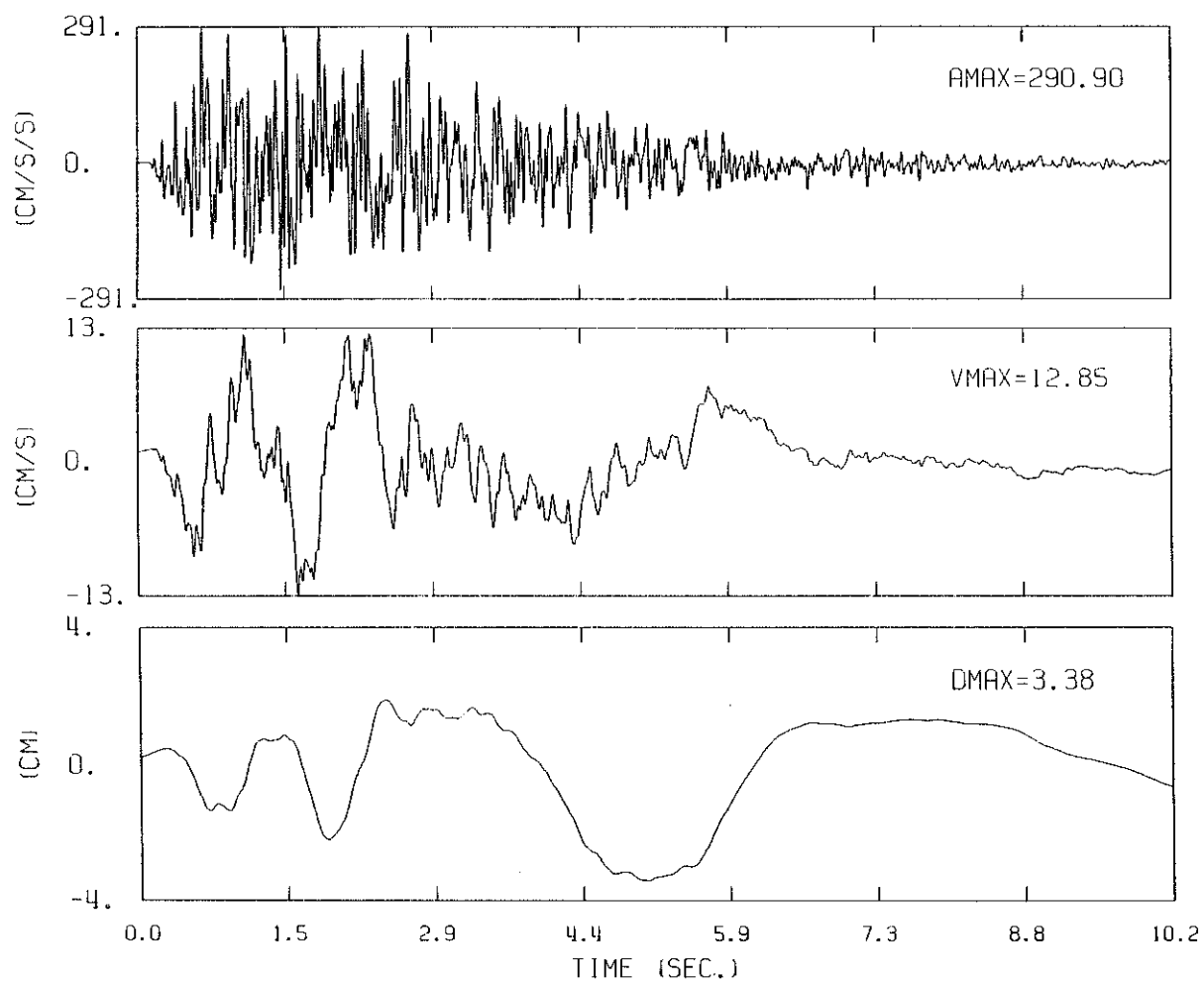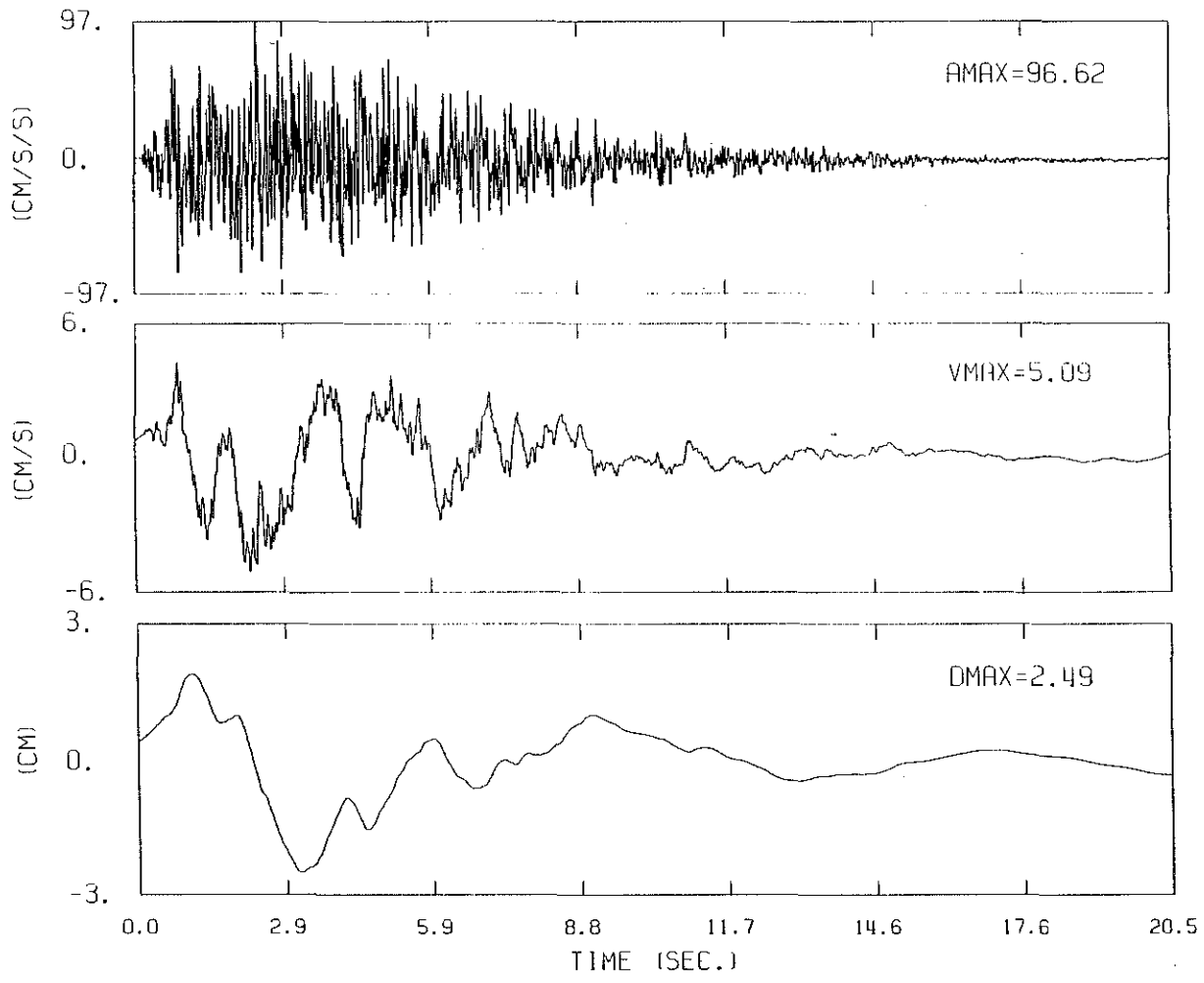
Figure B.3.   Acceleration, Velocity, and Displacement Time History for the Transverse Component of the 50-Year Event for Counties Identified by 0.30g-1 in Figure 4.3 (TR-50Y-0.30g-1).
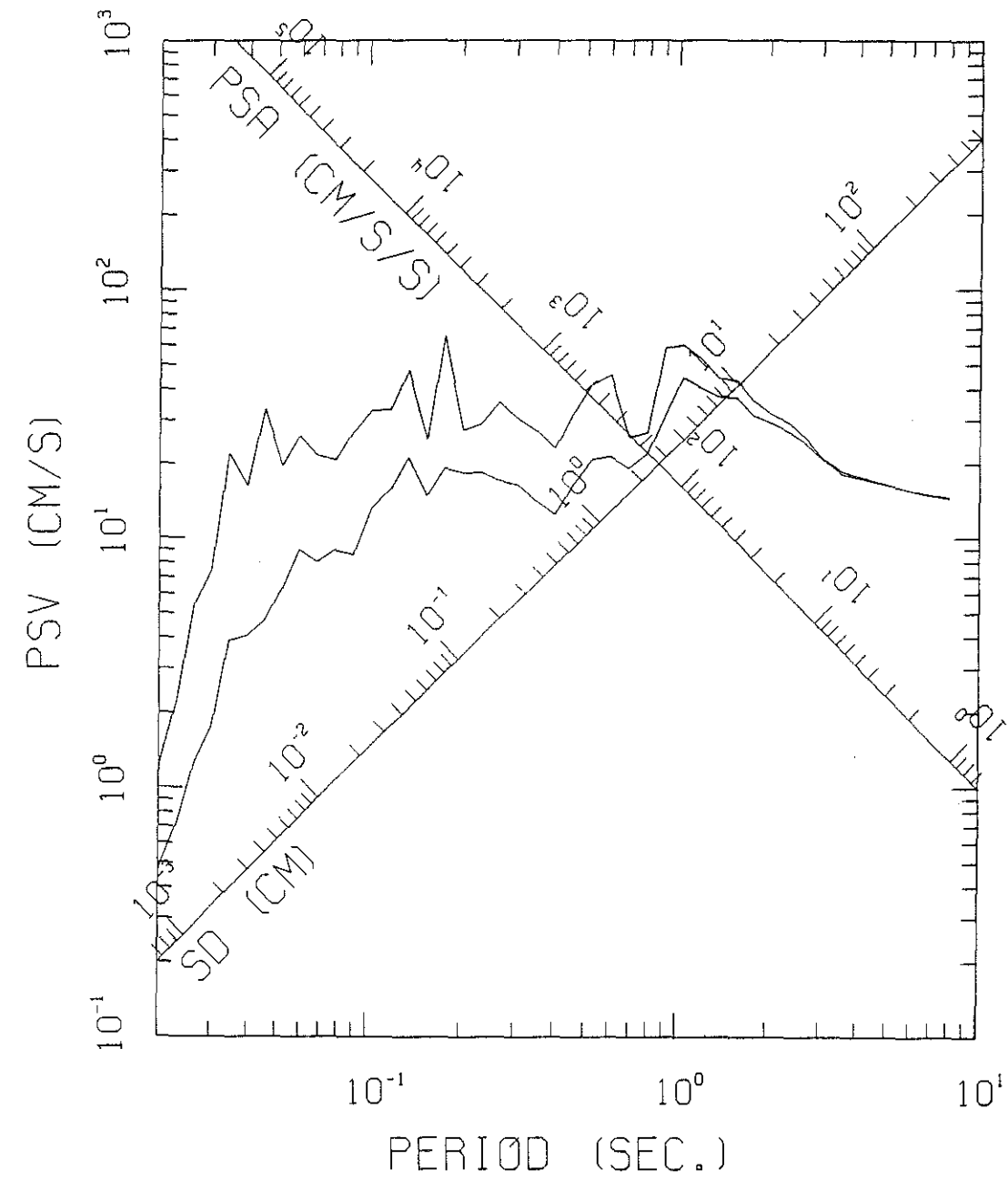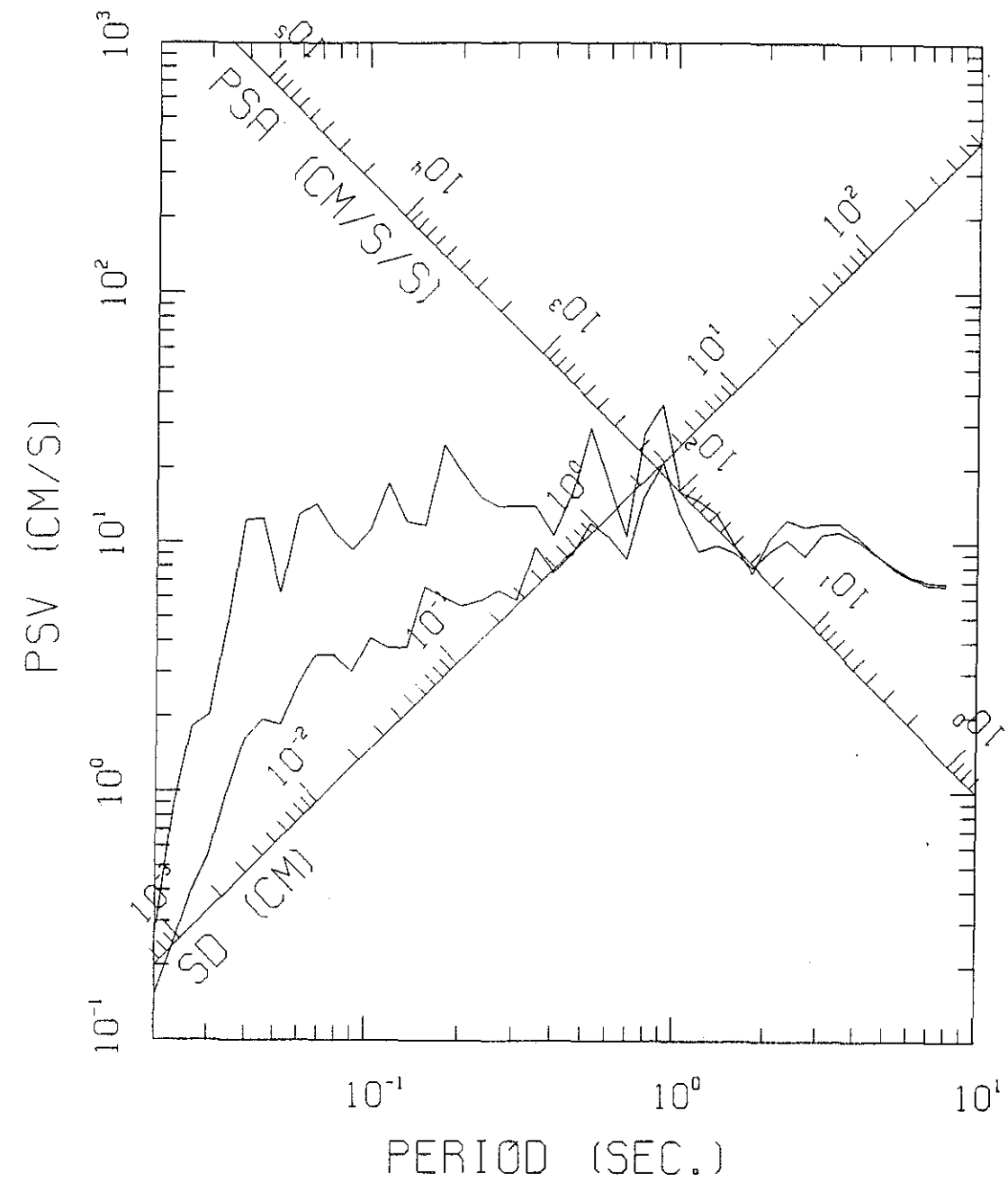
Figure B.4. Response Spectra for the Horizontal Component of the 50-Year Event for Counties Identified by 0.30g-1 in Figure 4.3 (TR-50Y-0.30g-1, Damping Ratio = 0.00 and 0.05).
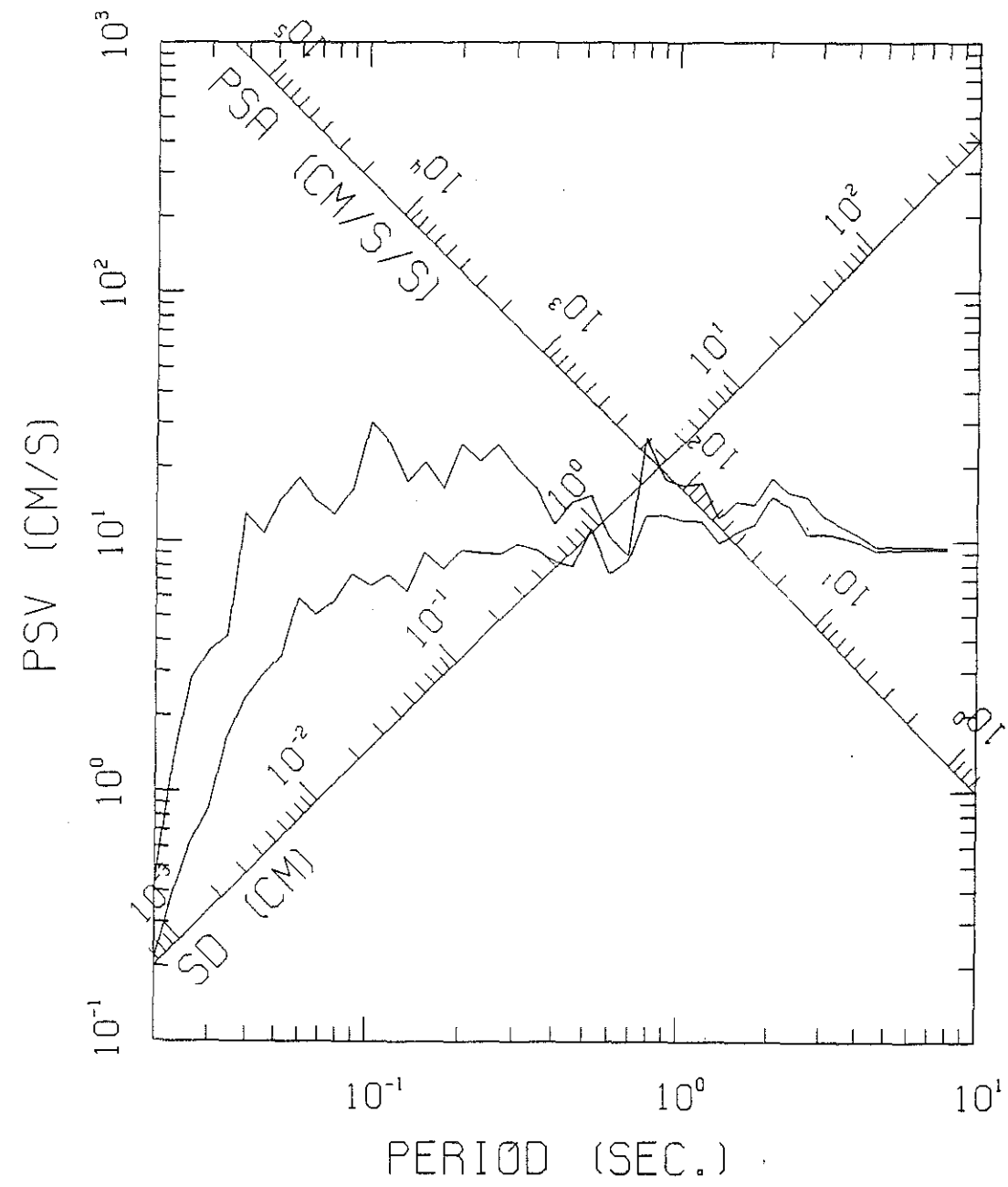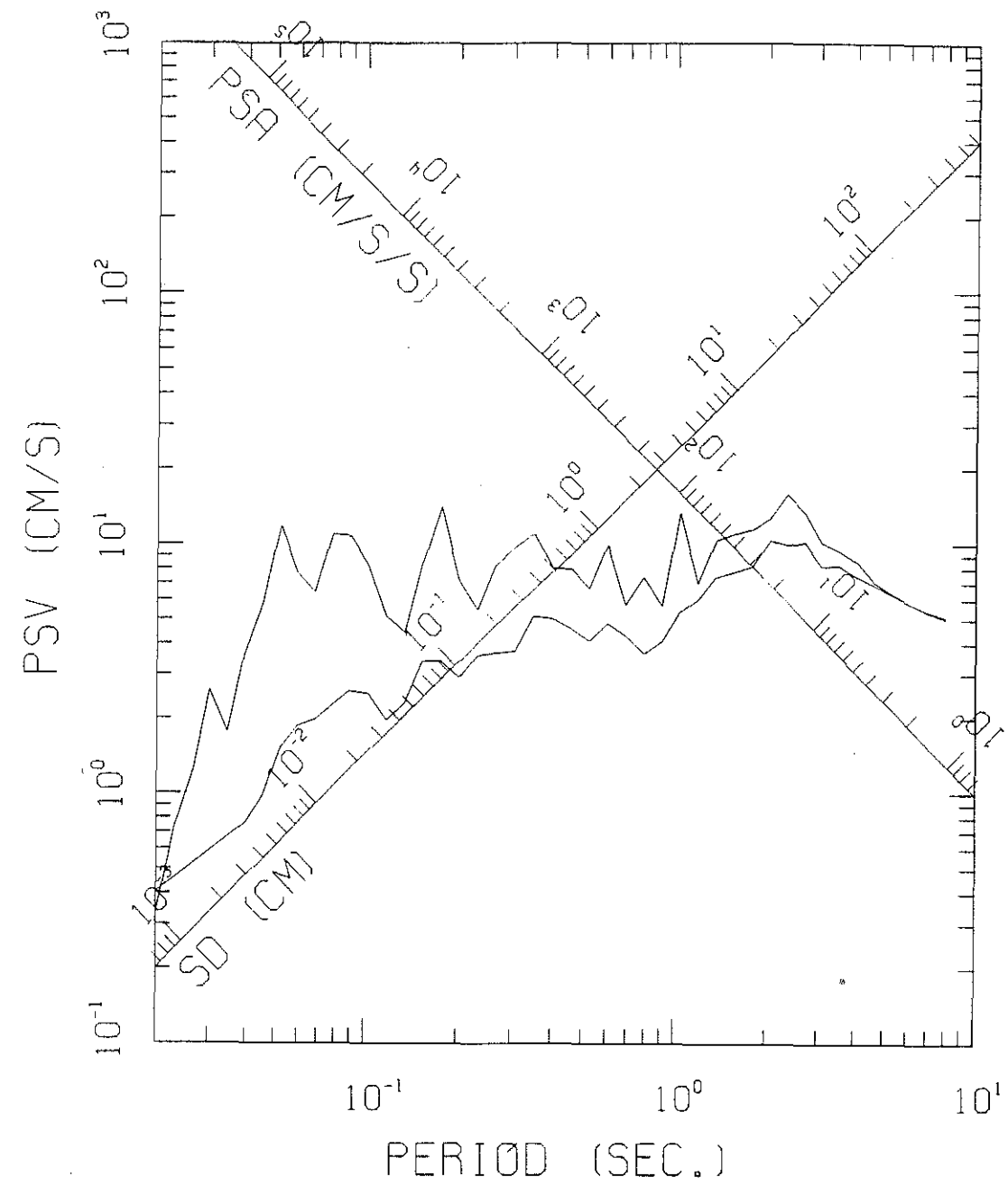
Figure B.5. Response Spectra for the Vertical Component of the 50-Year Event for Counties Identified by 0.30g-1 in Figure 4.3 (TR-50Y-0.30g-1, Damping Ratio = 0.00 and 0.05).
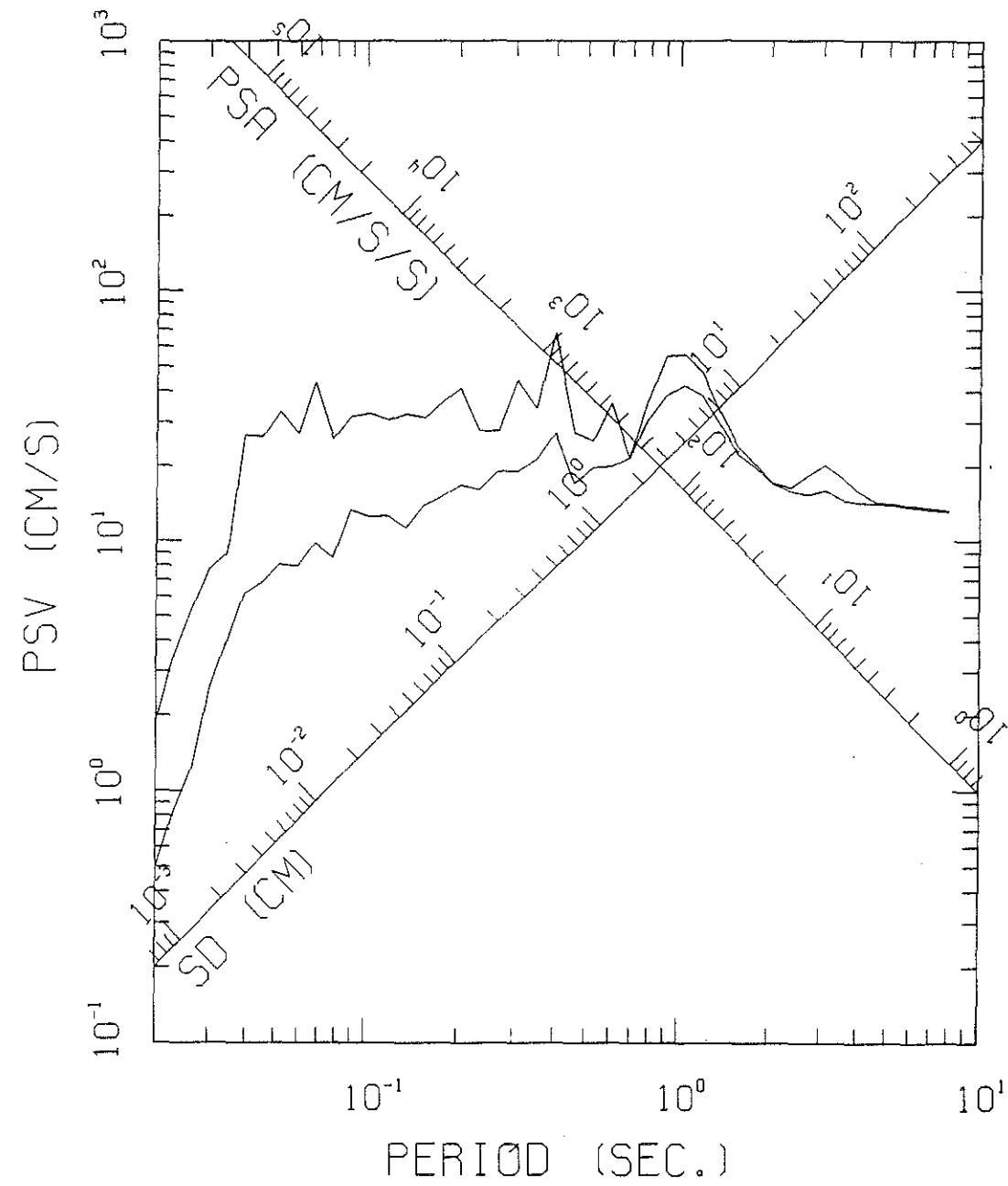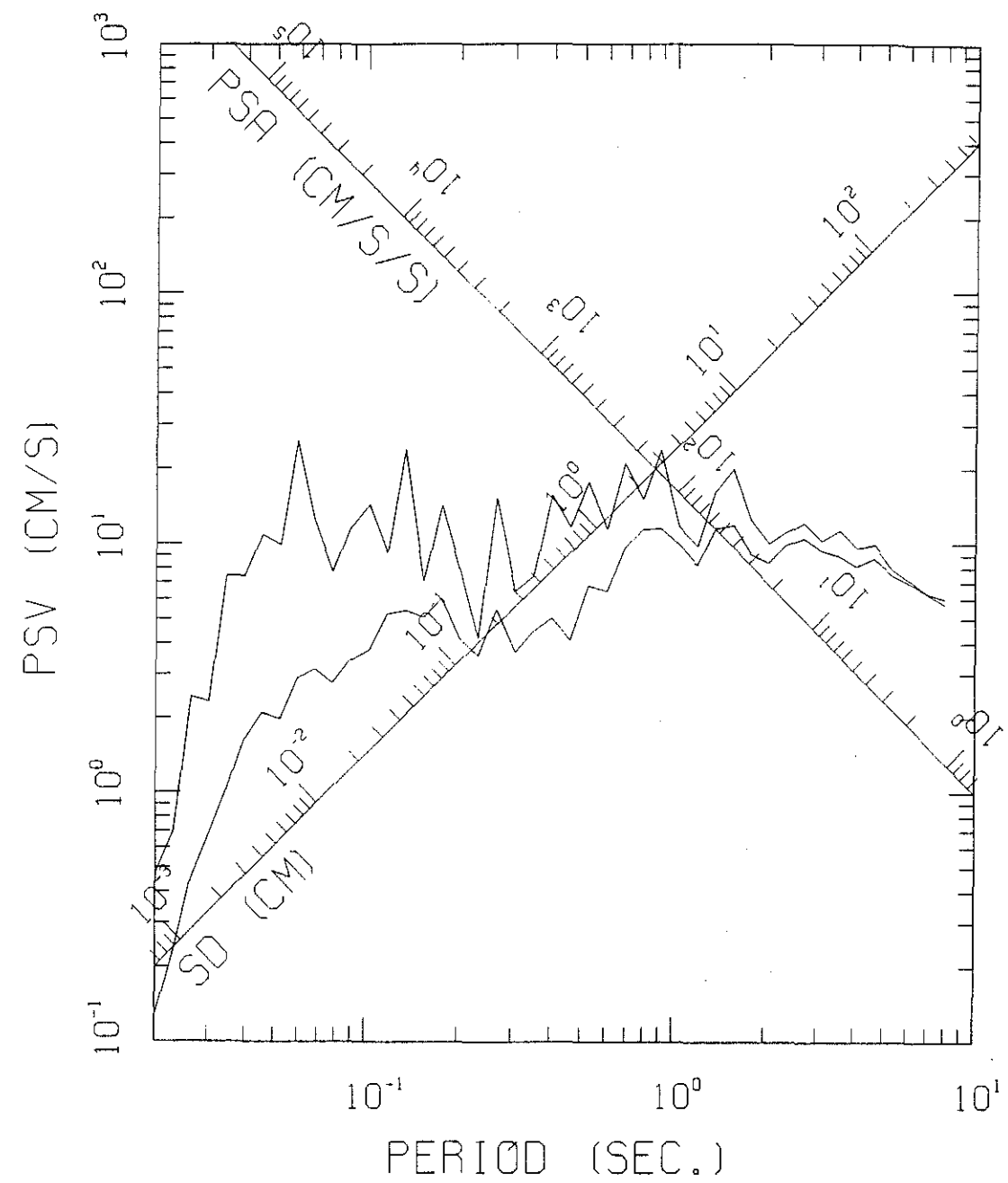
Figure B.6. Response Spectra for the Transverse Component of the 50-Year Event for Counties Identified by 0.30g-1 in Figure 4.3 (TR-50Y-0.30g-1, Damping Ratio = 0.00 and 0.05).
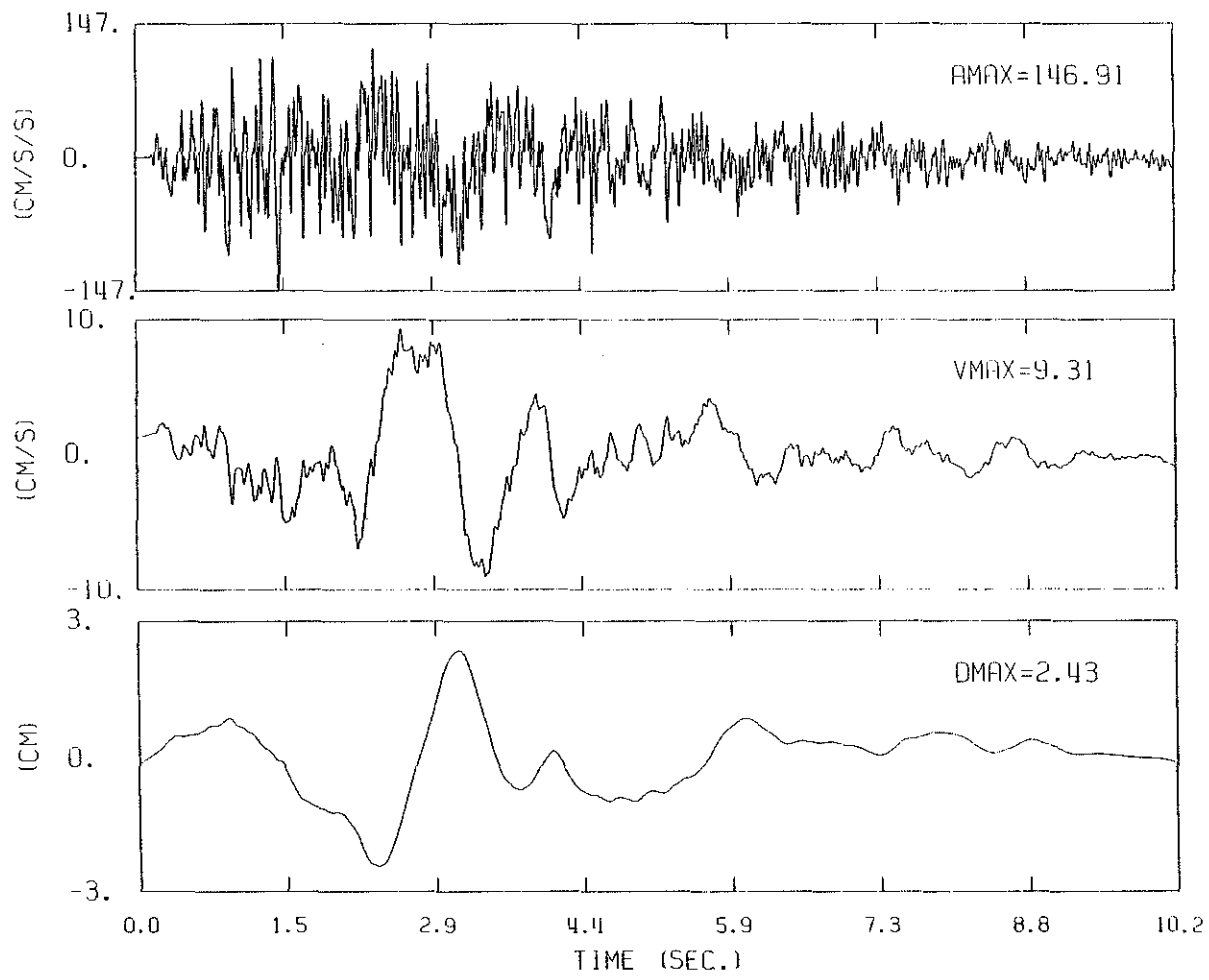
Figure B.7. Acceleration, Velocity, and Displacement Time History for the Horizontal Component of the 50-Year Event for Counties Identified by 0.15g-1 in Figure 4.3 (TR-50Y-0.15g-1).
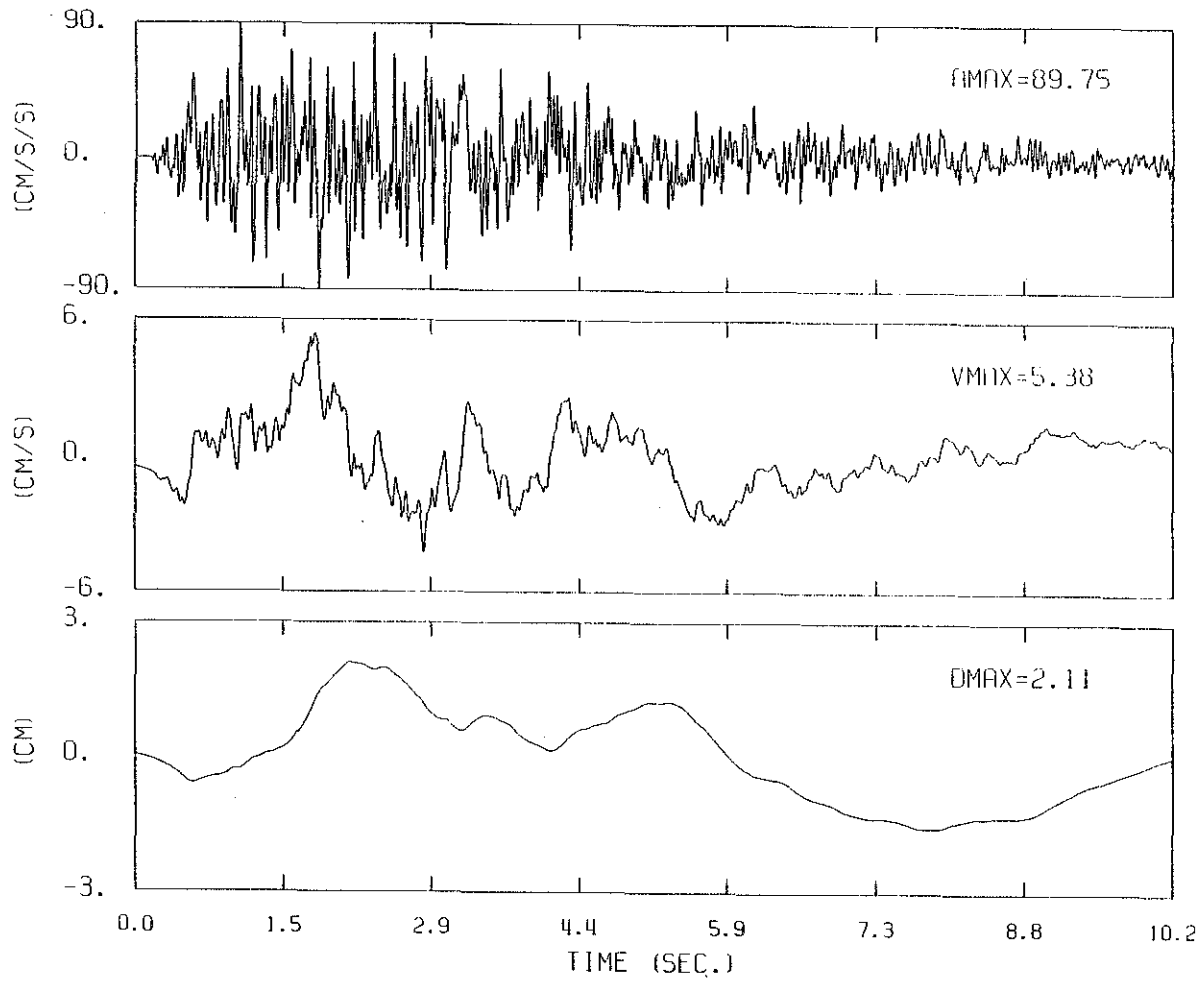
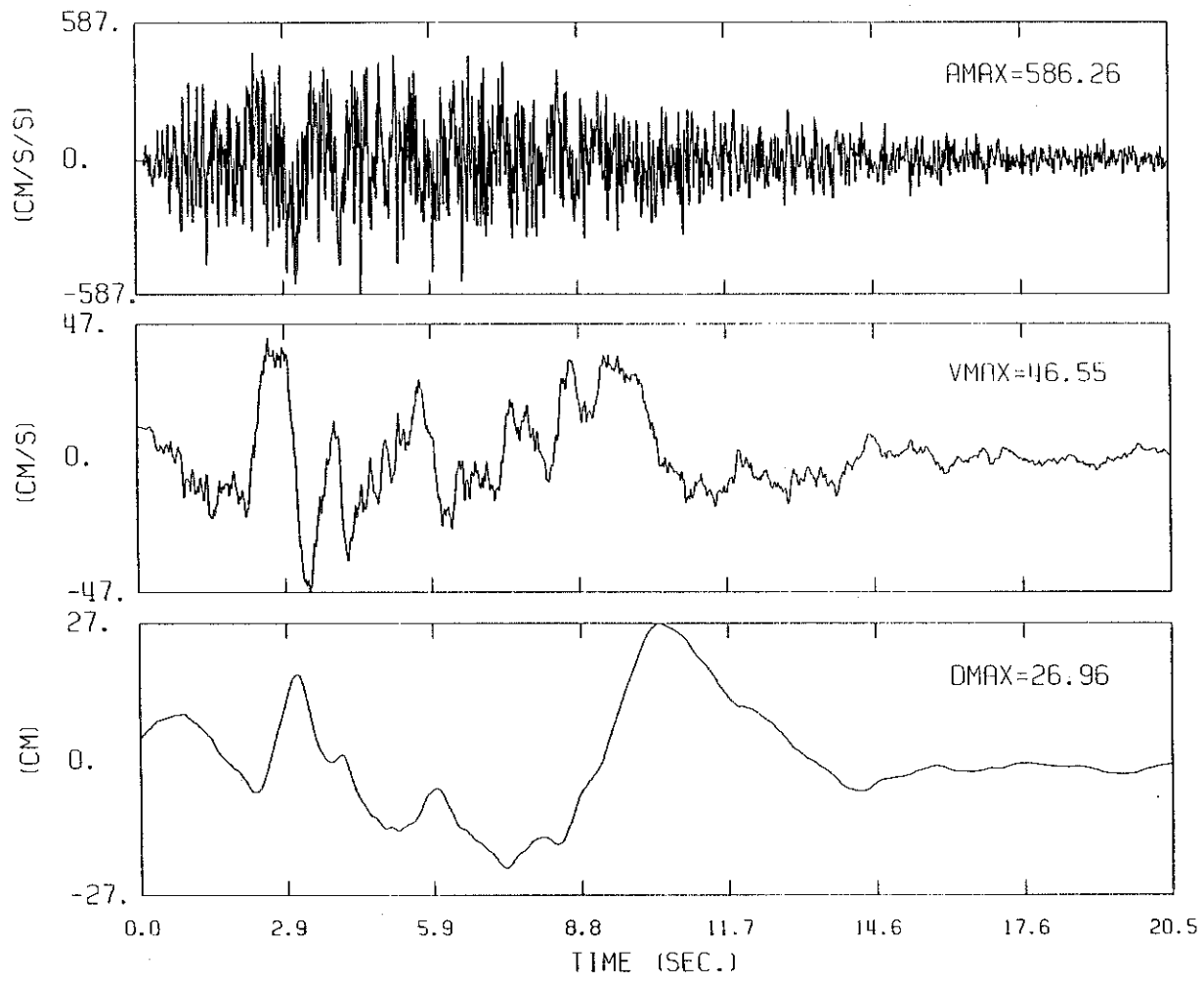**Figure B.8.** Acceleration, Velocity, and Displacement Time History for the Vertical Component of the 50-Year Event for Counties Identified by 0.15g-1 in Figure 4.3 (TR-50Y-0.15g-1).

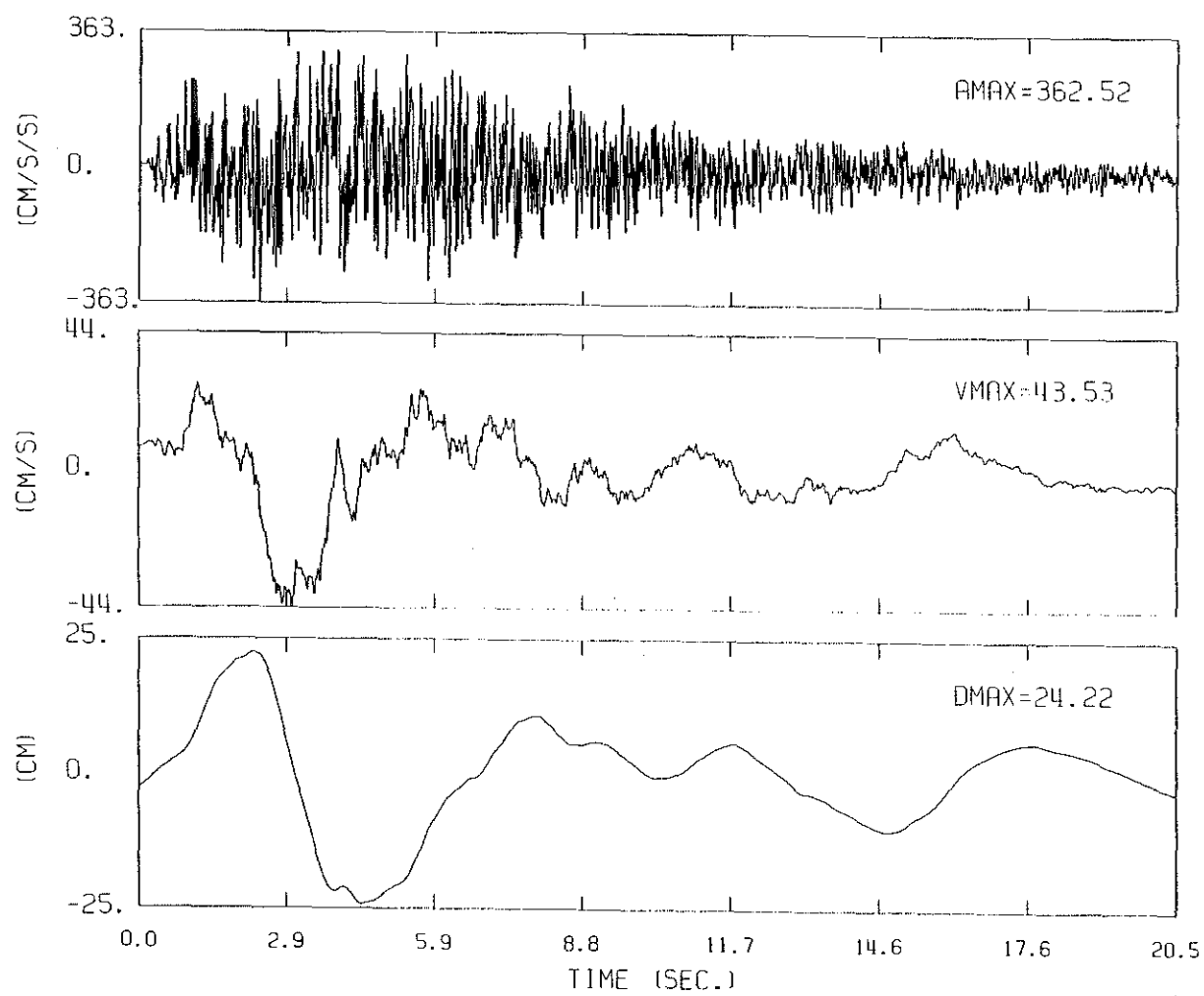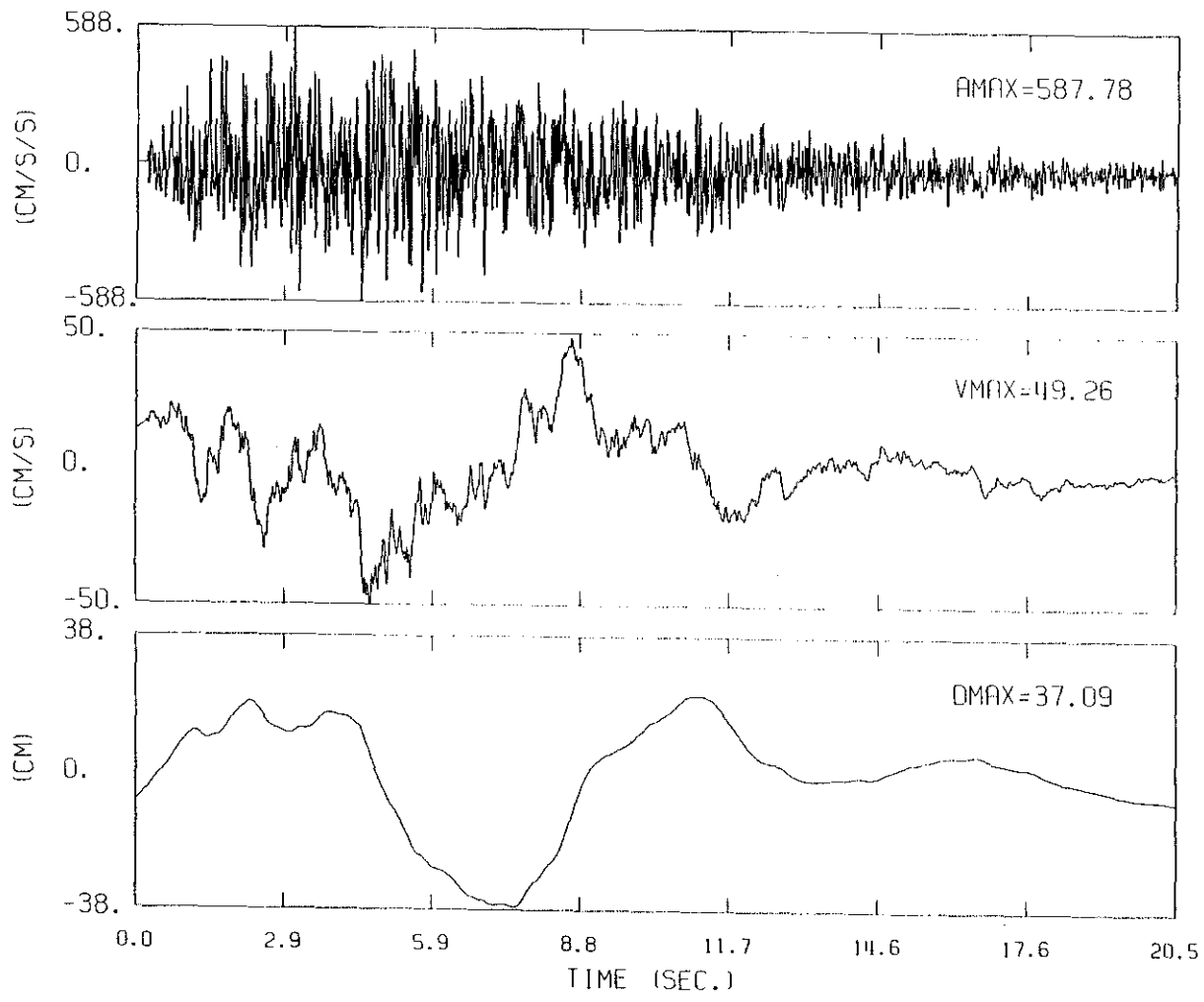AMAX=146.74

VMAX=6.23

DMAX=3.02

TIME (SEC.)
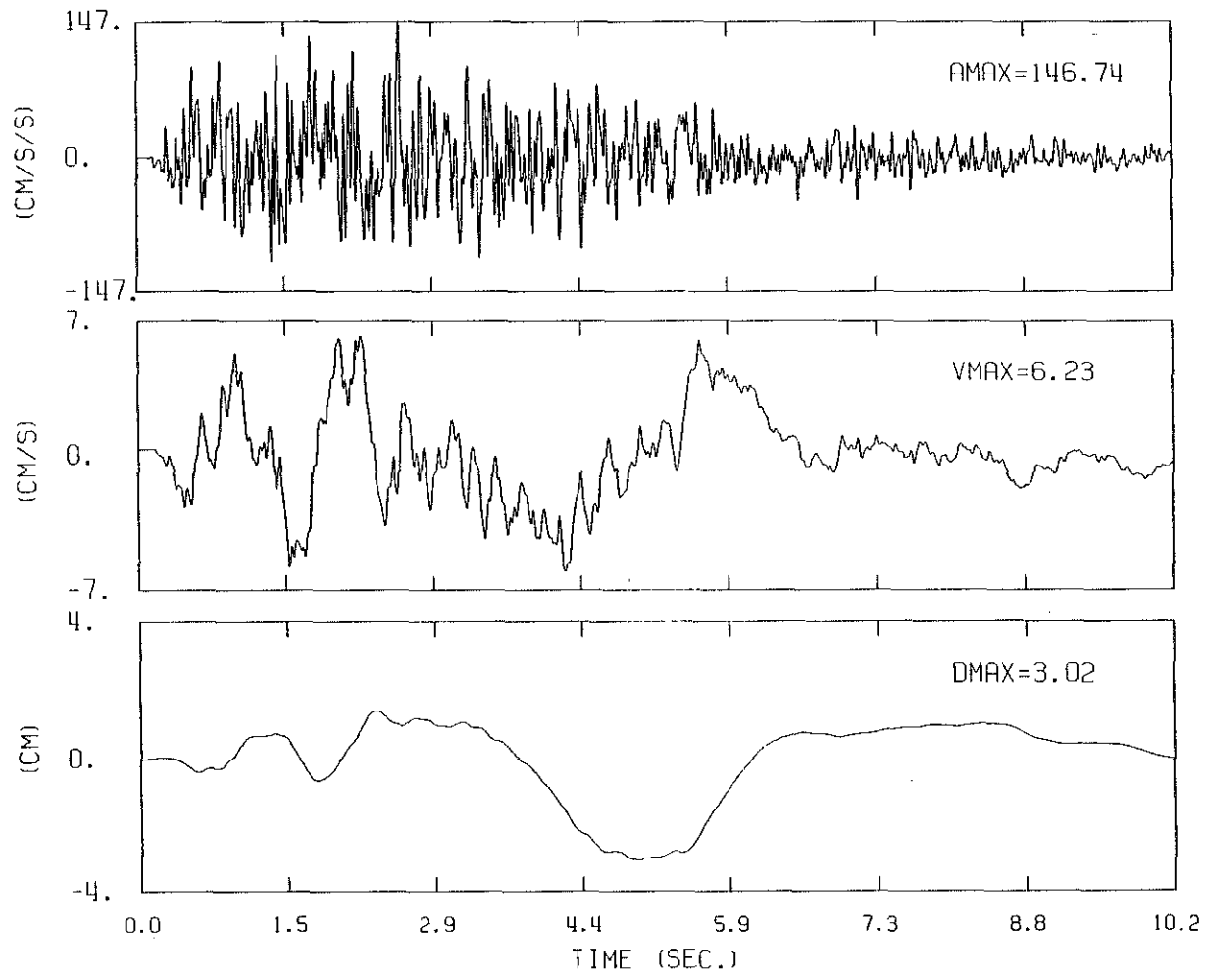
Figure B.9. Acceleration, Velocity, and Displacement Time History for the Transverse Component of the 50-Year Event for Counties Identified by 0.15g-1 in Figure 4.3 (TR-50Y-0.15g-1).
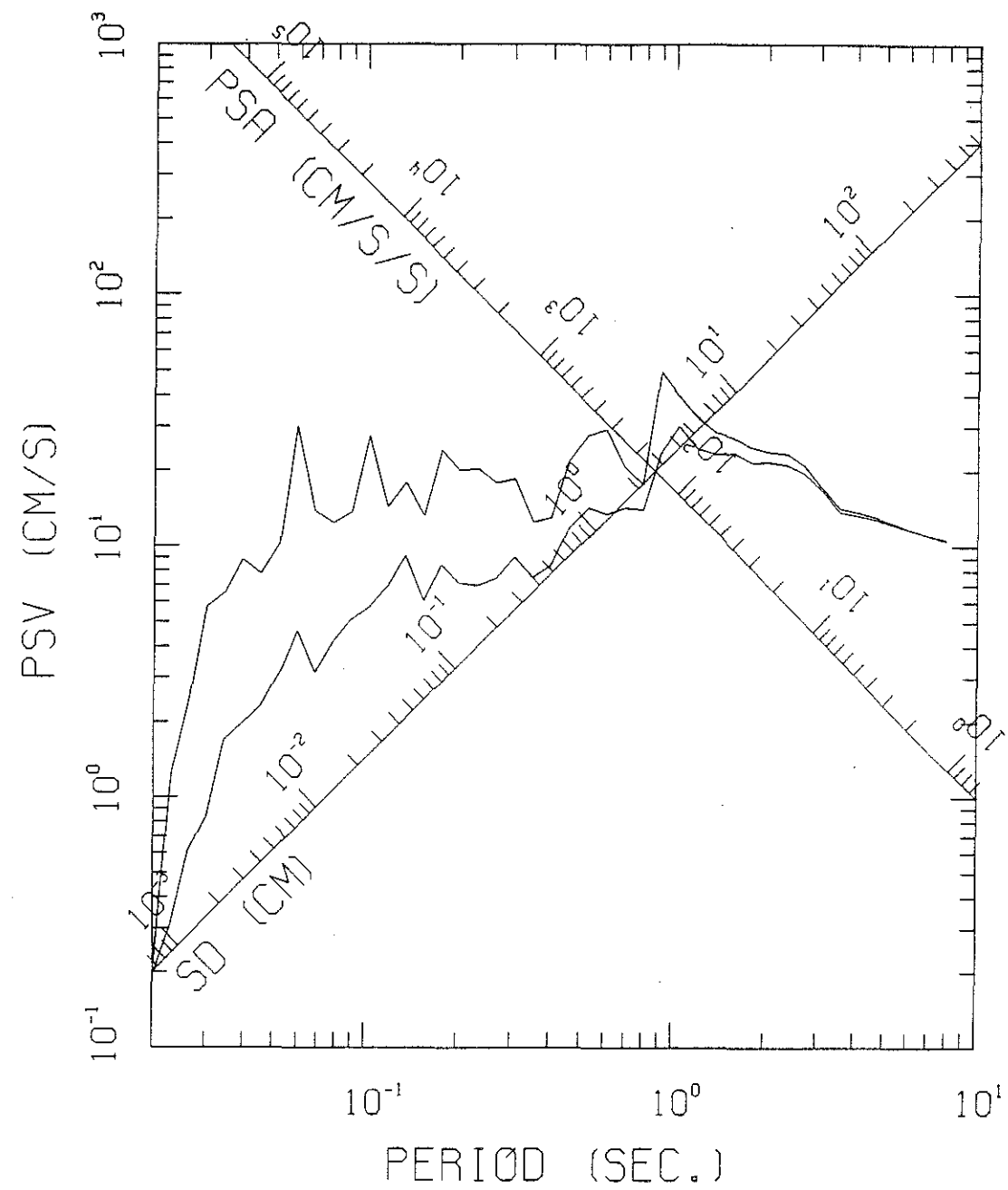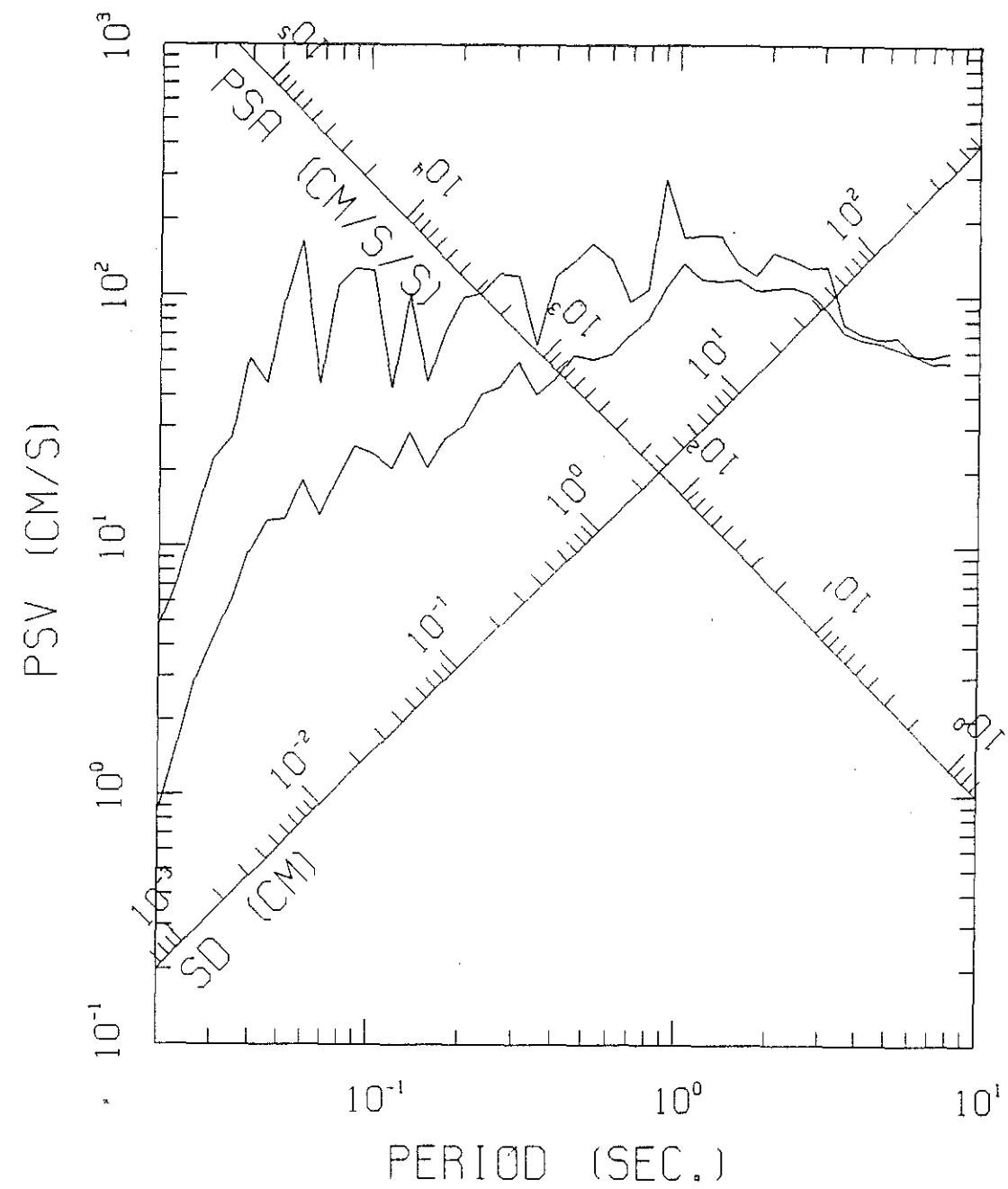
Figure B.10. Response Spectra for the Horizontal Component of the 50-Year Event for Counties Identified by 0.15g-1 in Figure 4.3 (TR-50Y-0.15g-1, Damping Ratio = 0.00 and 0.05).
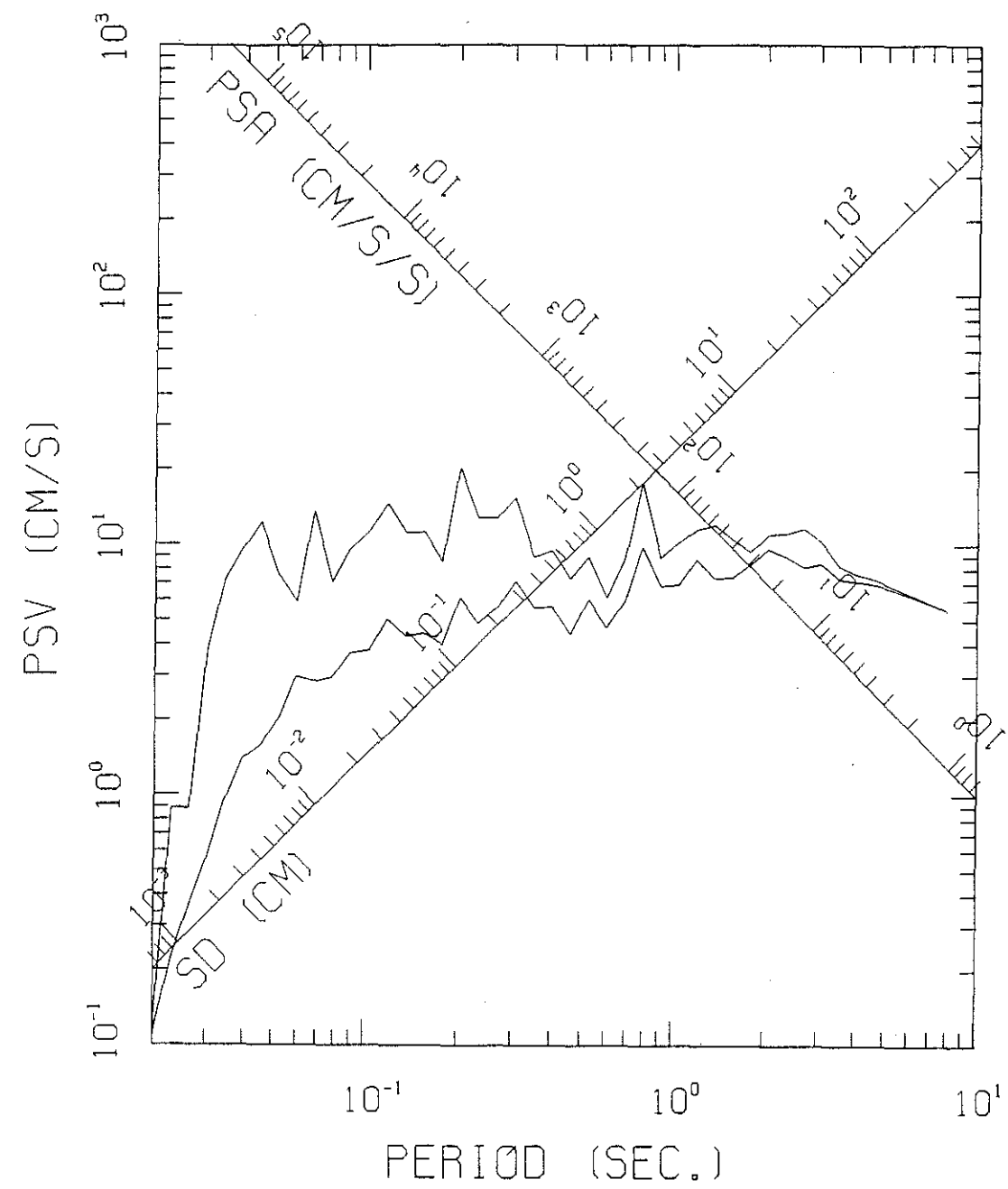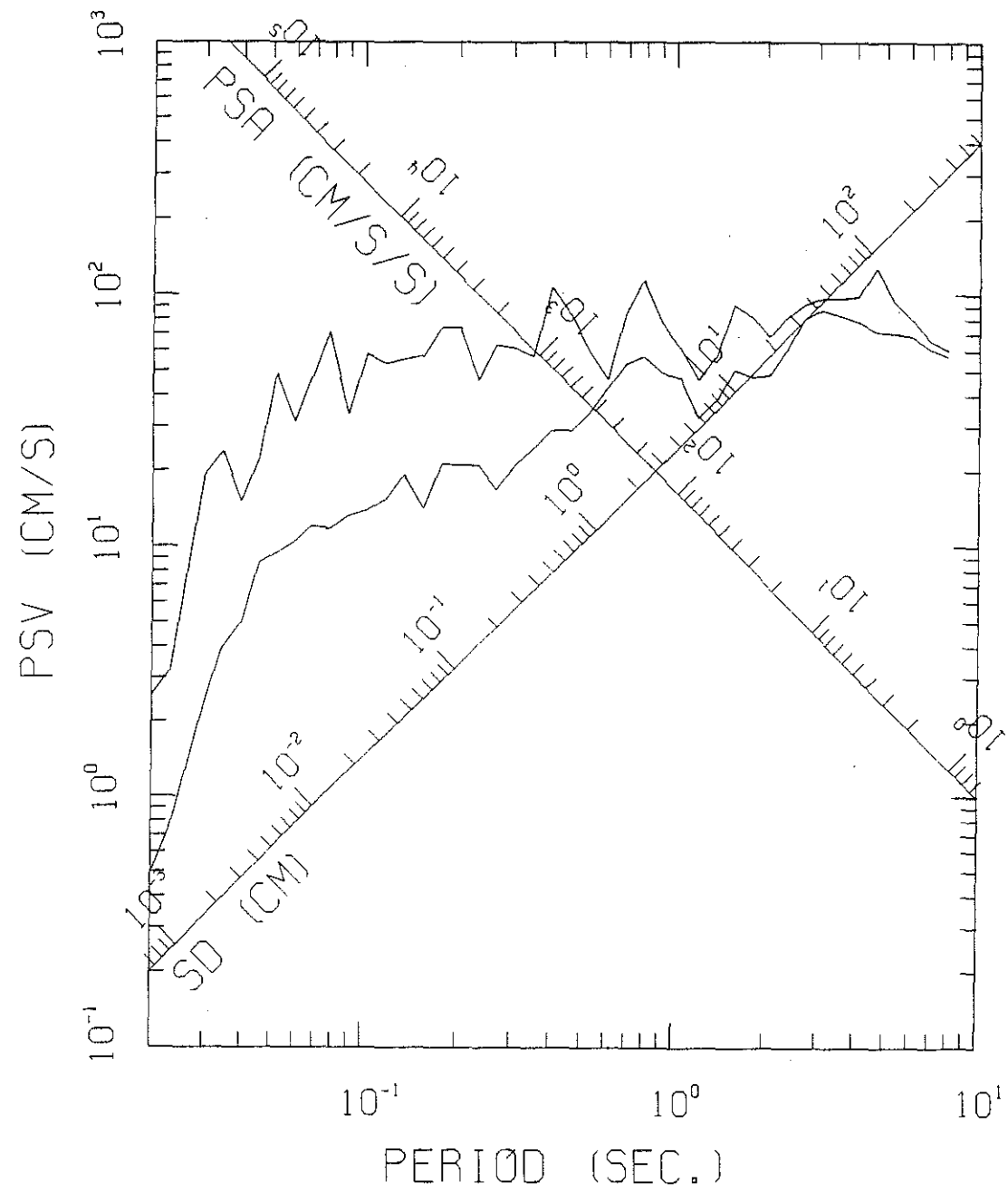
Figure B.11. Response Spectra for the Vertical Component of the 50-Year Event for Counties Identified by 0.15g-1 in Figure 4.3 (TR-50Y-0.15g-1, Damping Ratio = 0.00 and 0.05).
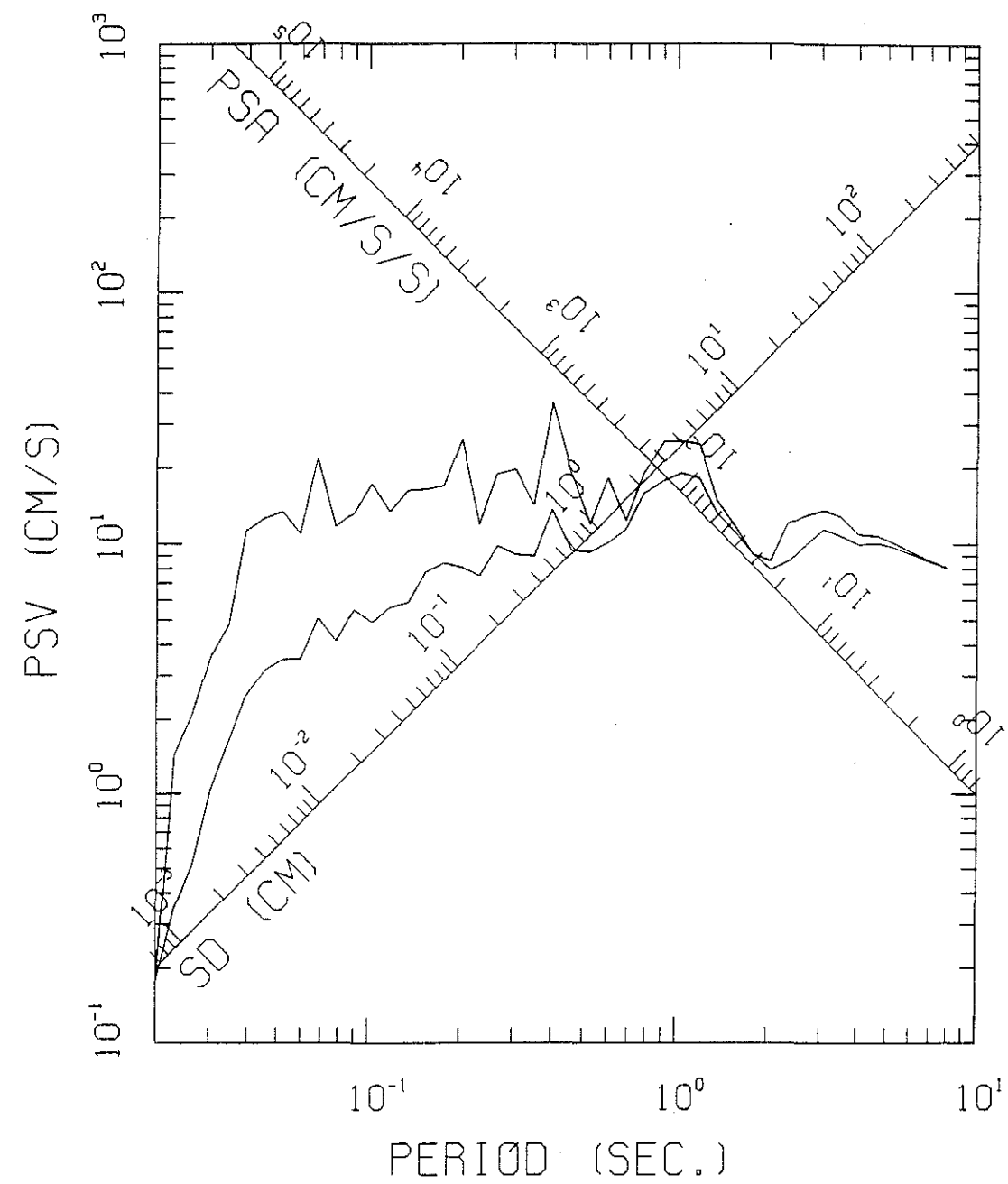
Figure B.12. Response Spectra for the Transverse Component of the 50-Year Event for Counties Identified by 0.15g-1 in Figure 4.3 (TR-50Y-0.15g-1, Damping Ratio = 0.00 and 0.05).
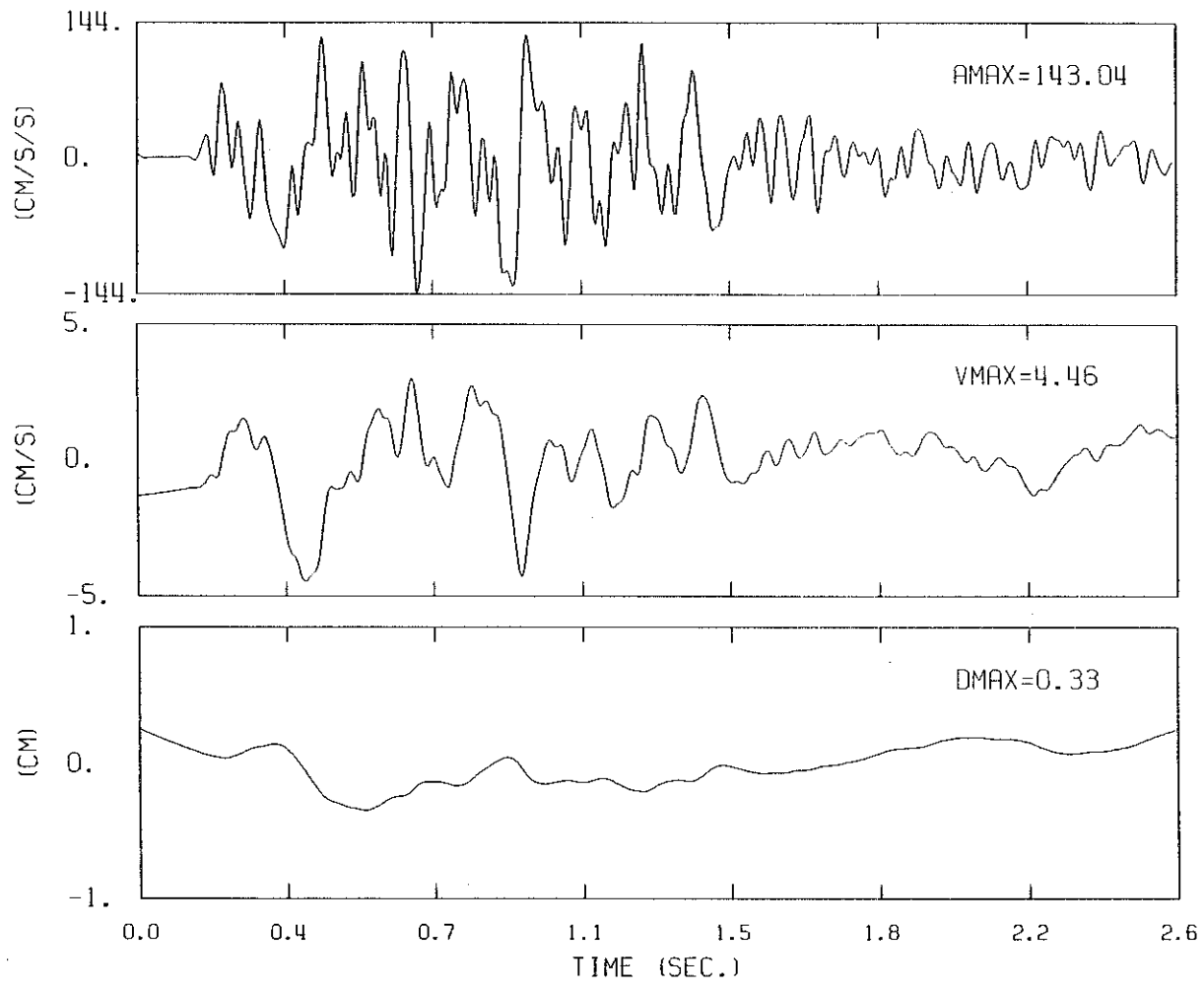
Figure B.13. Acceleration, Velocity, and Displacement Time History for the Horizontal Component of the 50-Year Event for Counties Identified by 0.15g-2 in Figure 4.3 (TR-50Y-0.15g-2).
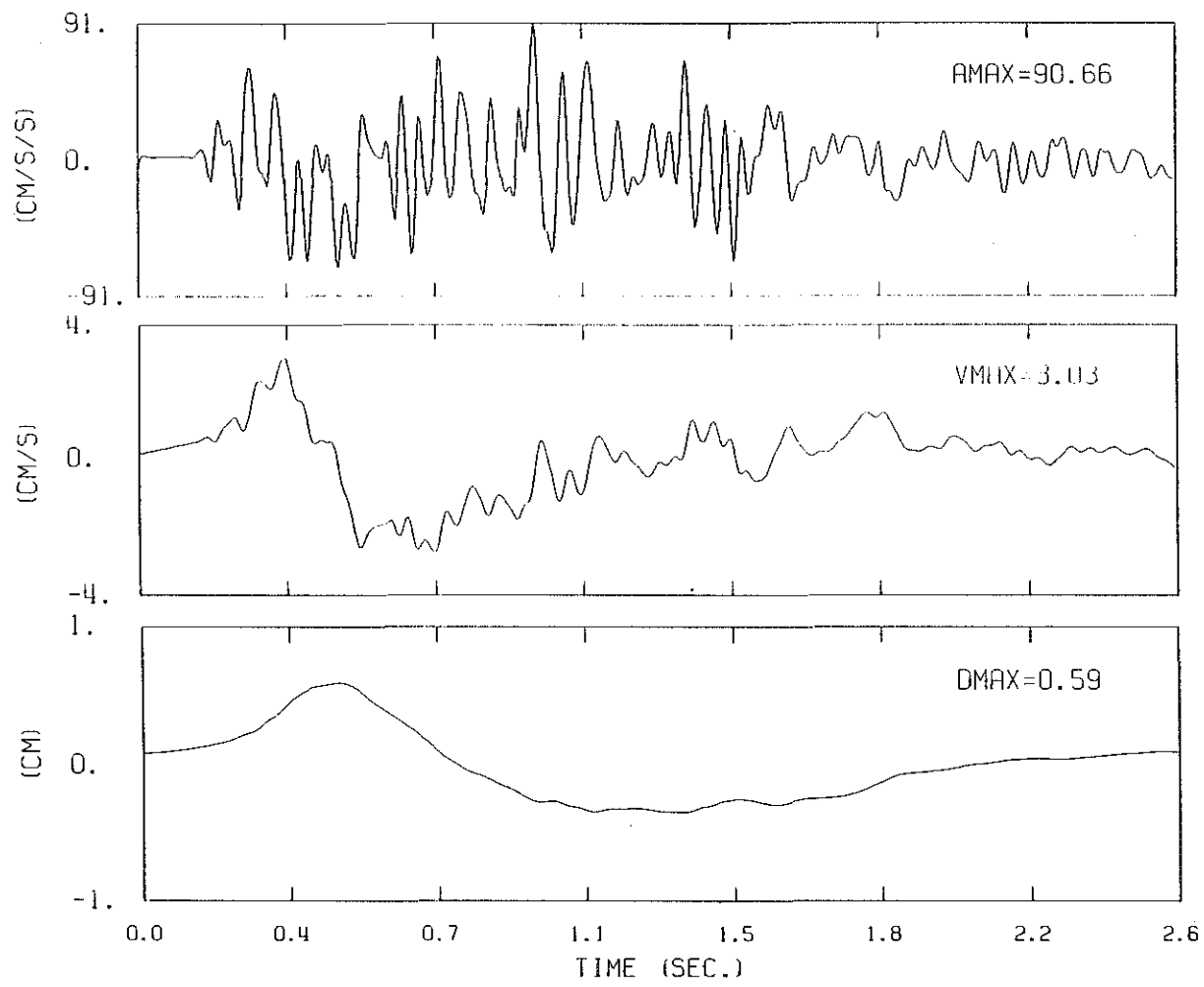
Figure B.14. Acceleration, Velocity, and Displacement Time History for the Vertical Component of the 50-Year Event for Counties Identified by 0.15g-2 in Figure 4.3 (TR-50Y-0.15g-2).
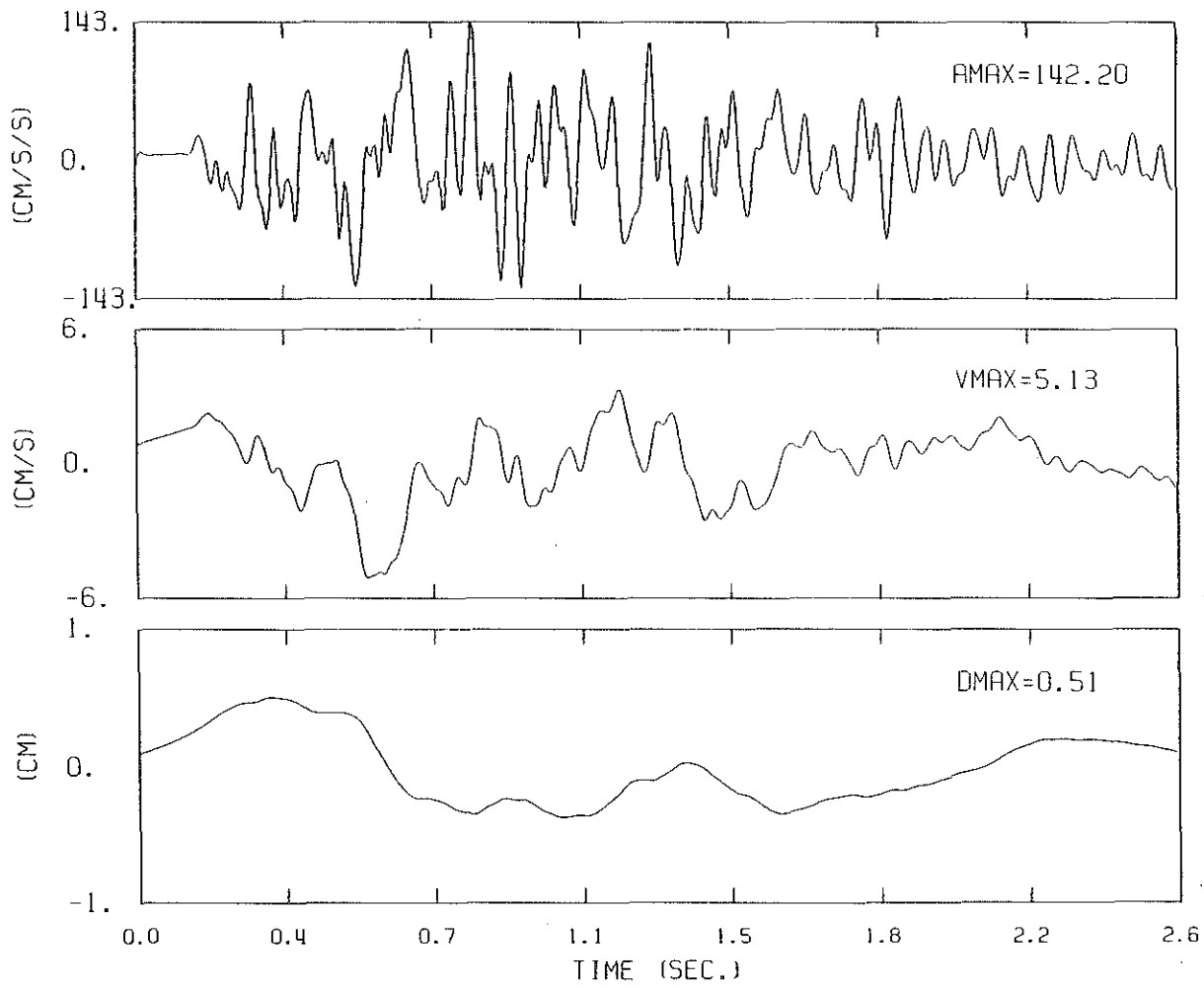
Figure B.15. Acceleration, Velocity, and Displacement Time History for the Transverse Component of the 50-Year Event for Counties Identified by 0.15g-2 in Figure 4.3 (TR-50Y-0.15g-2).
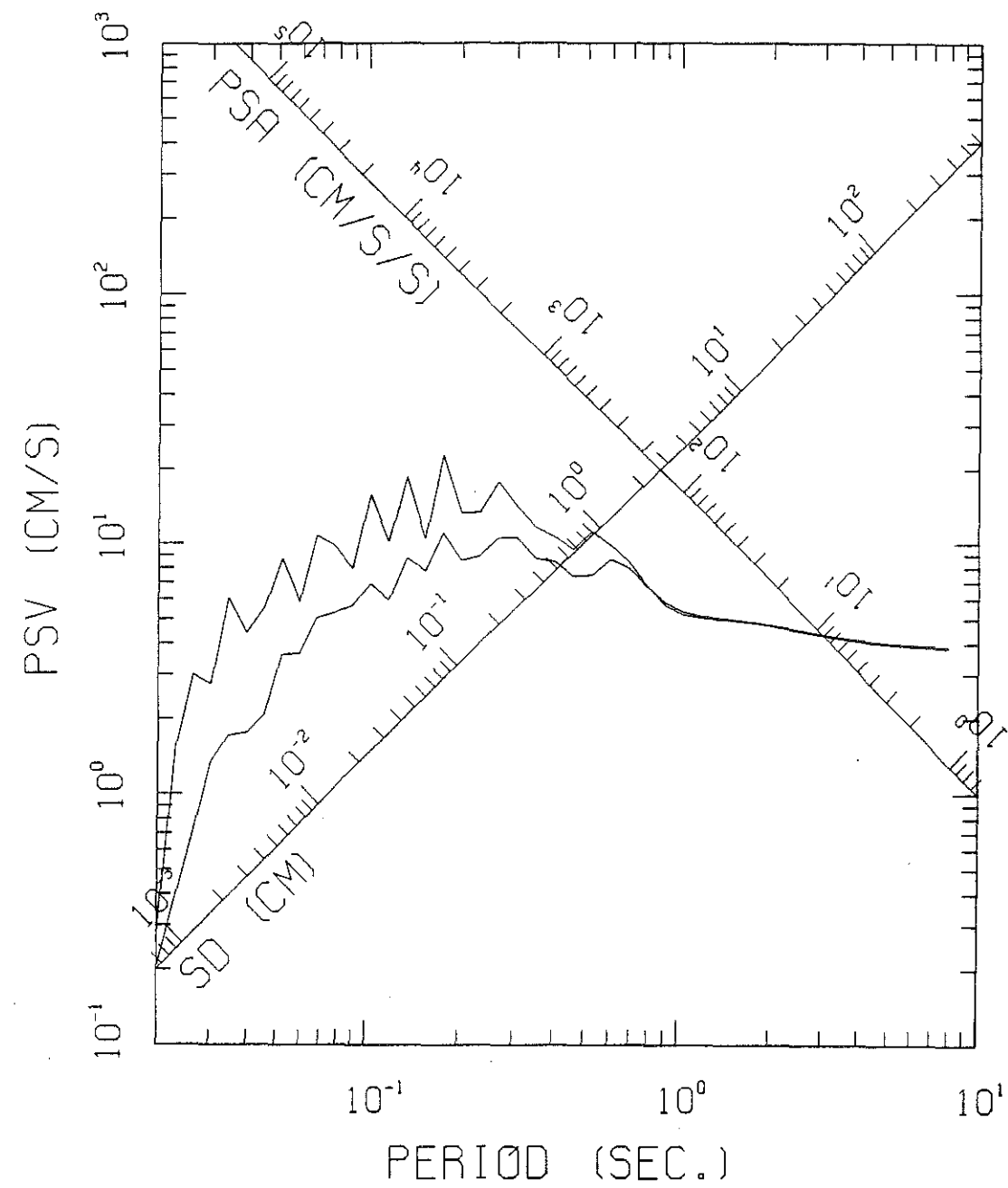
Figure B.16. Response Spectra for the Horizontal Component of the 50-Year Event for Counties Identified by 0.15g-2 in Figure 4.3 (TR-50Y-0.15g-2, Damping Ratio = 0.00 and 0.05).
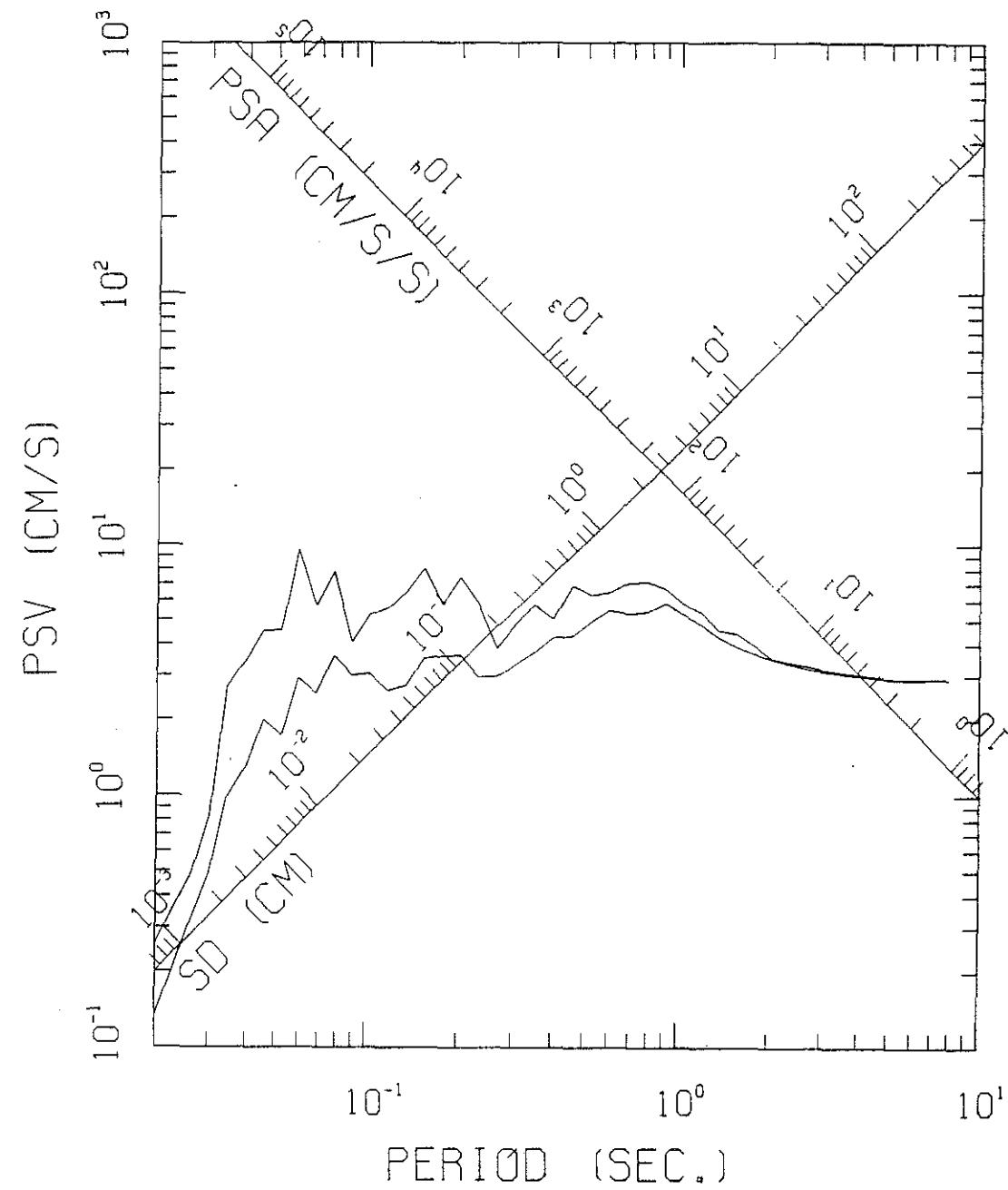
Figure B.17. Response Spectra for the Vertical Component of the 50-Year Event for Counties Identified by 0.15g-2 in Figure 4.3 (TR-50Y-0.15g-2, Damping Ratio = 0.00 and 0.05).
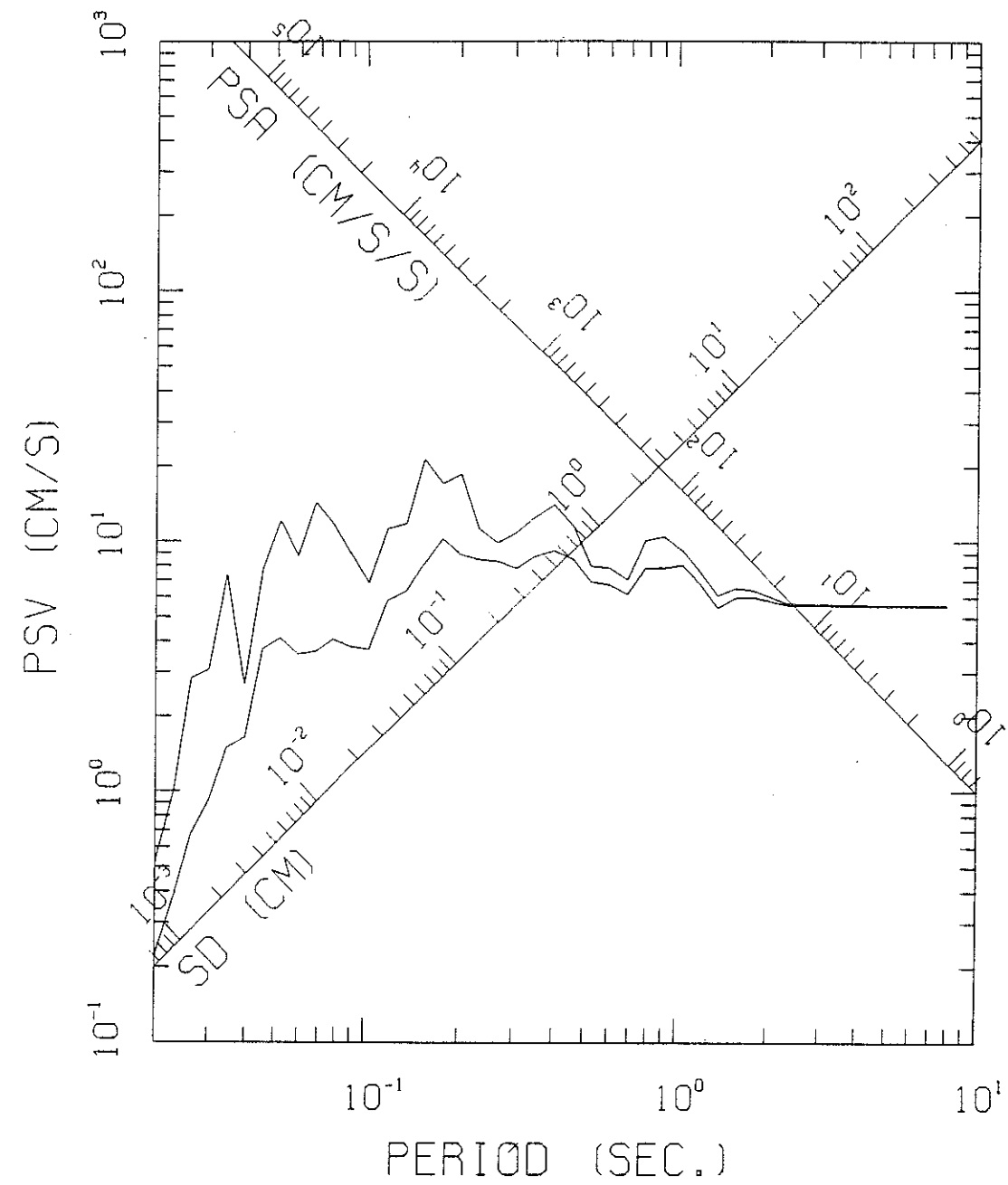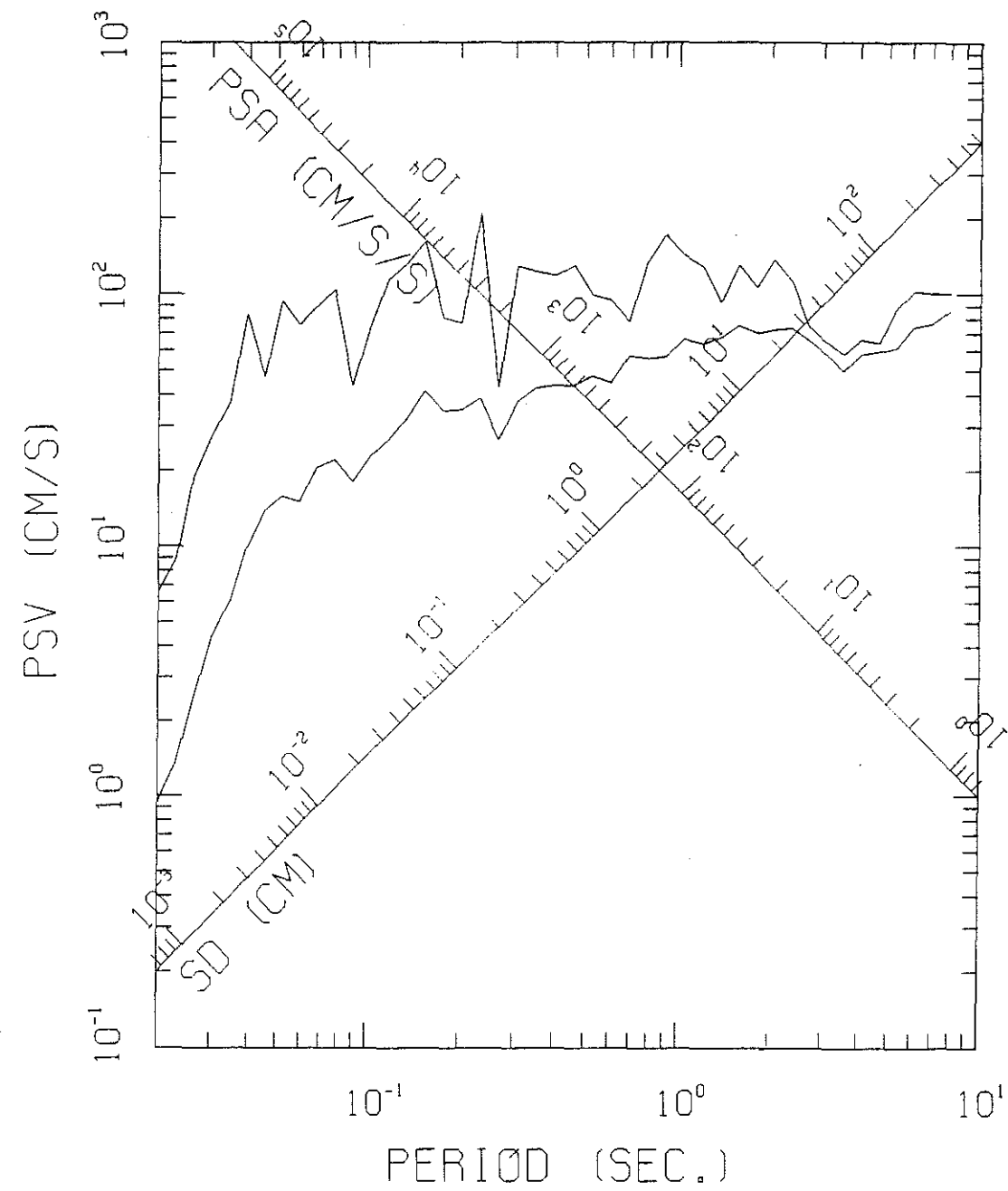
Figure B.18. Response Spectra for the Transverse Component of the 50-Year Event for Counties Identified by 0.15g-2 in Figure 4.3 (TR-50Y-0.15g-2, Damping Ratio = 0.00 and 0.05).
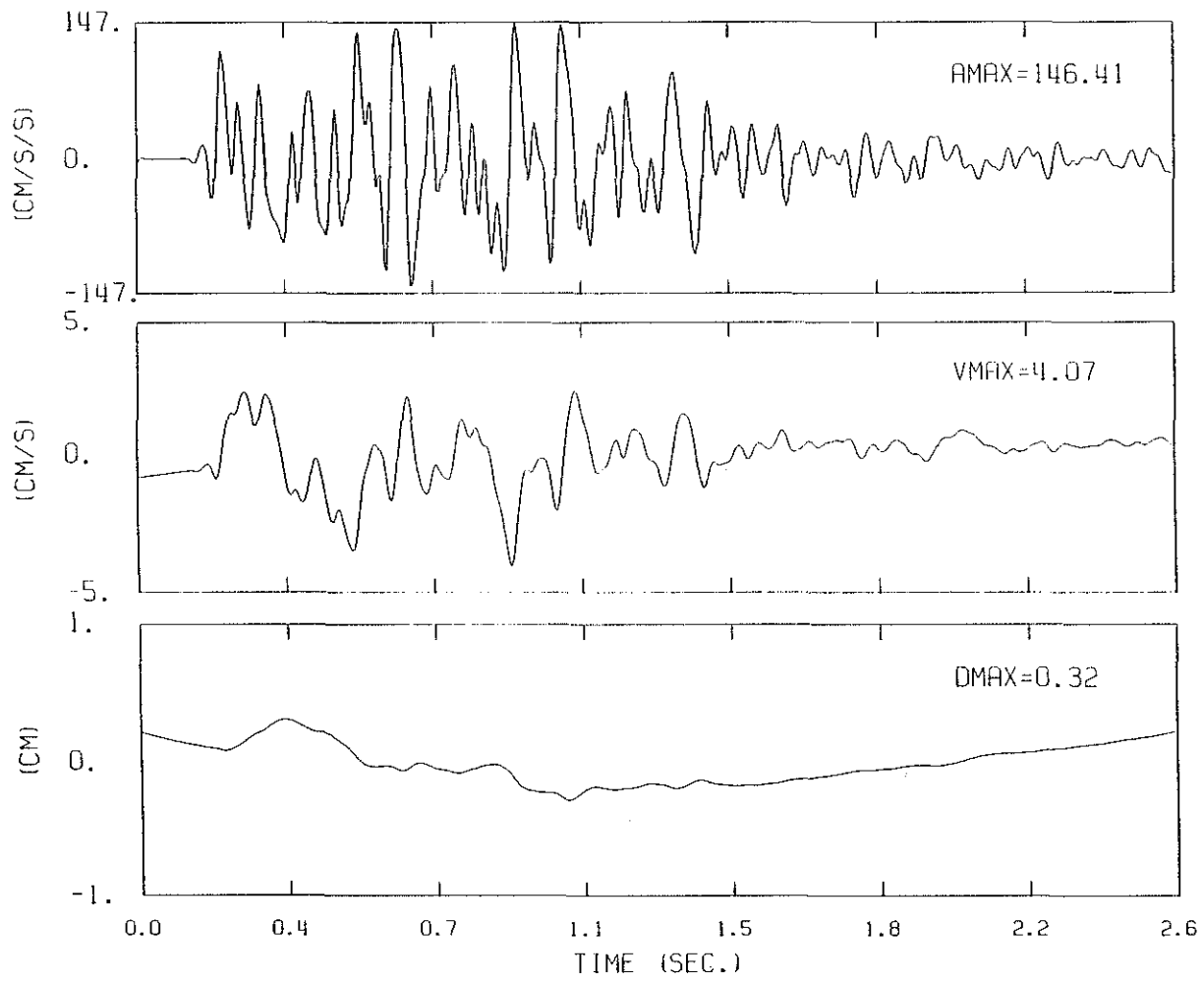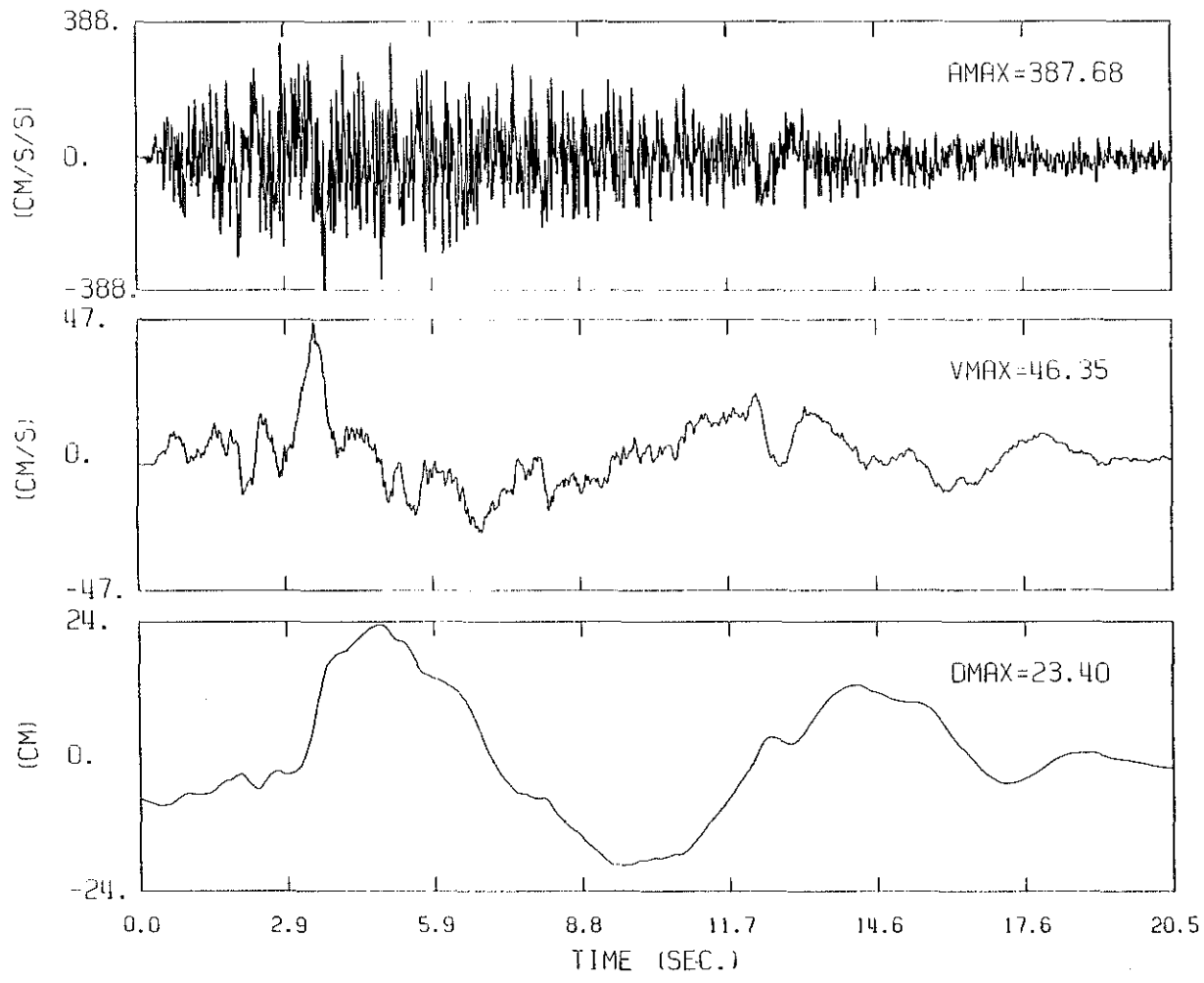
Figure B.19. Acceleration, Velocity, and Displacement Time History for the Horizontal Component of the 50-Year Event for Counties Identified by 0.15g-3 in Figure 4.3 (TR-50Y-0.15g-3).
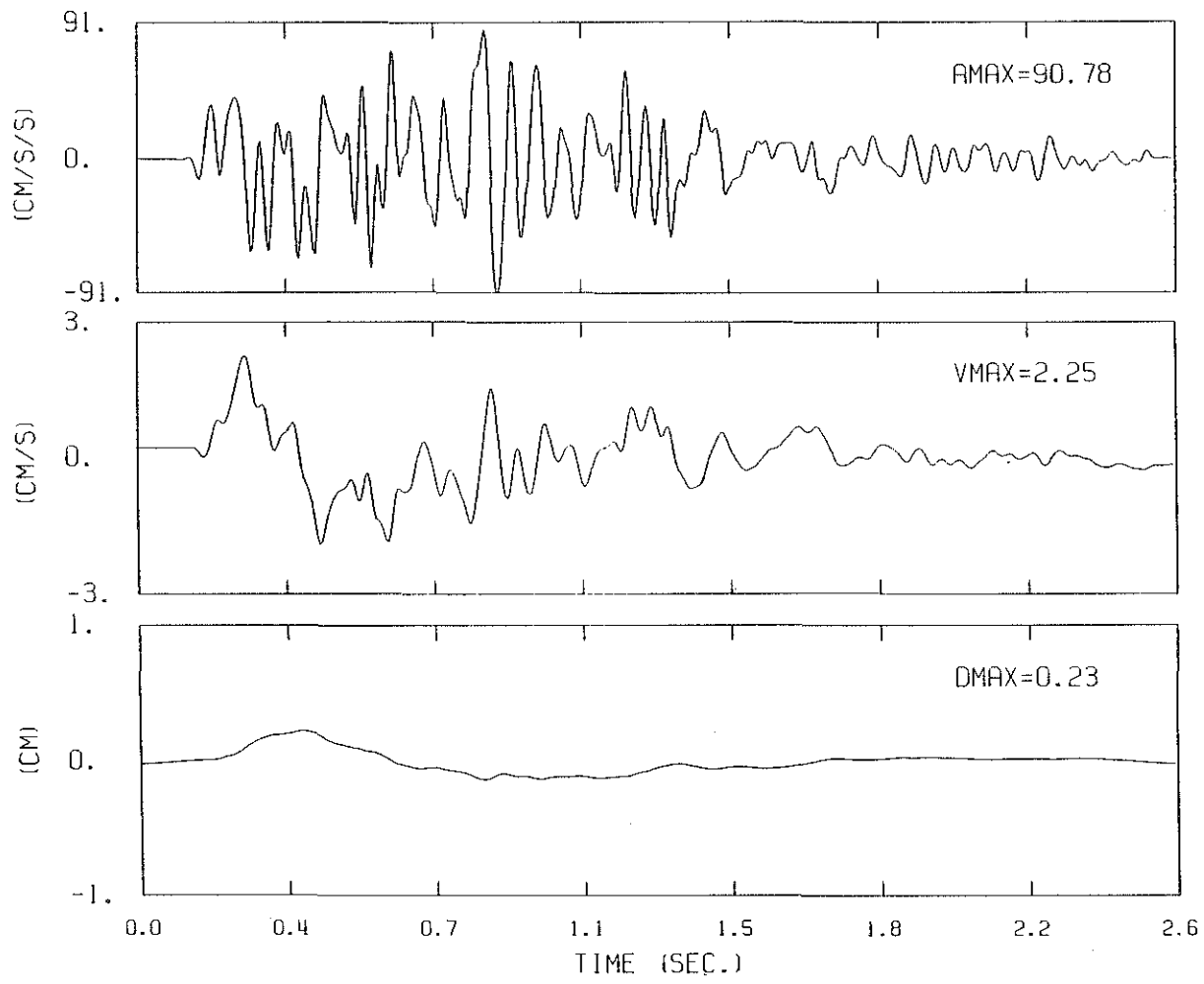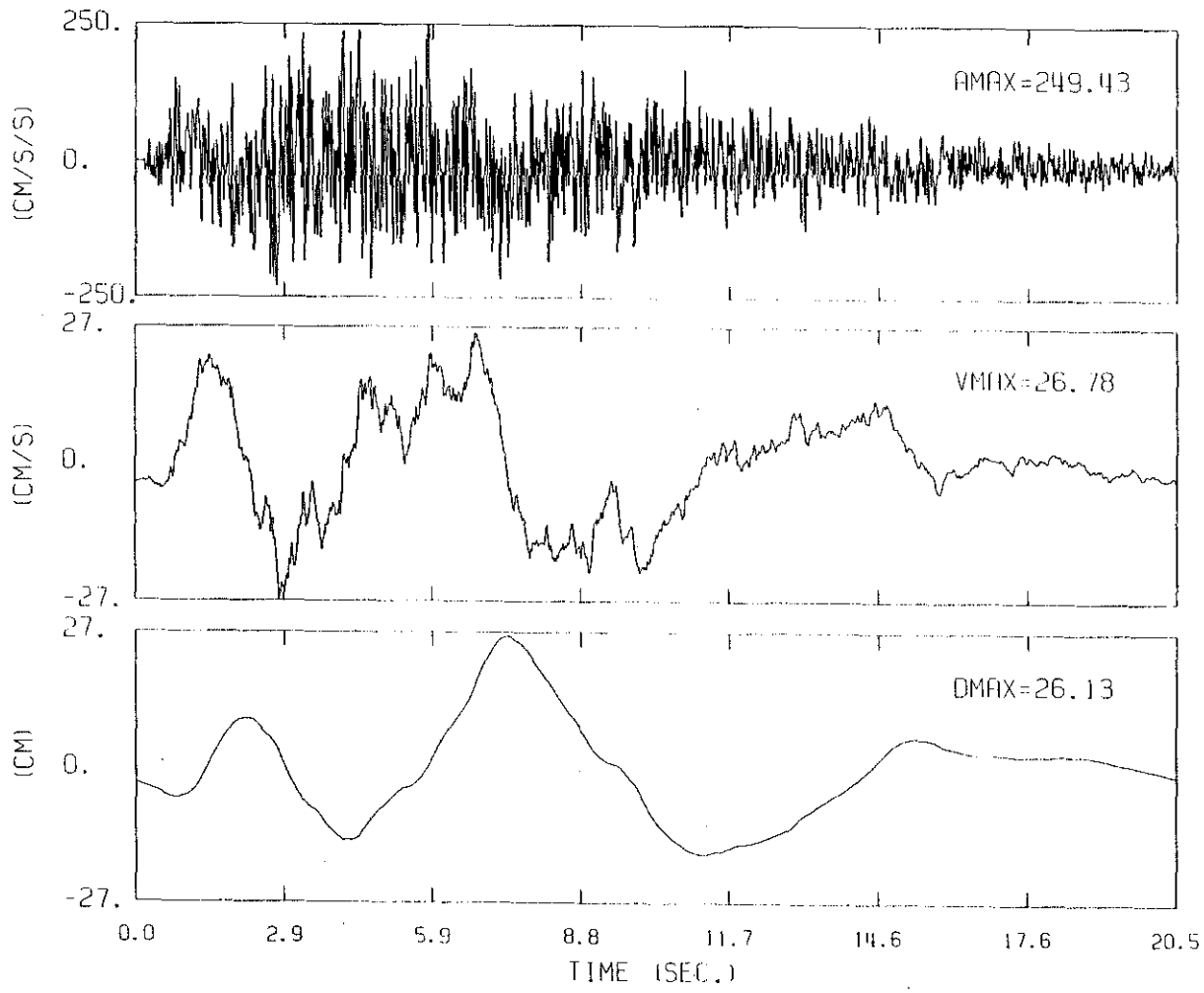
Figure B.20. Acceleration, Velocity, and Displacement Time History for the Vertical Component of the 50-Year Event for Counties Identified by 0.15g-3 in Figure 4.3 (TR-50Y-0.15g-3).
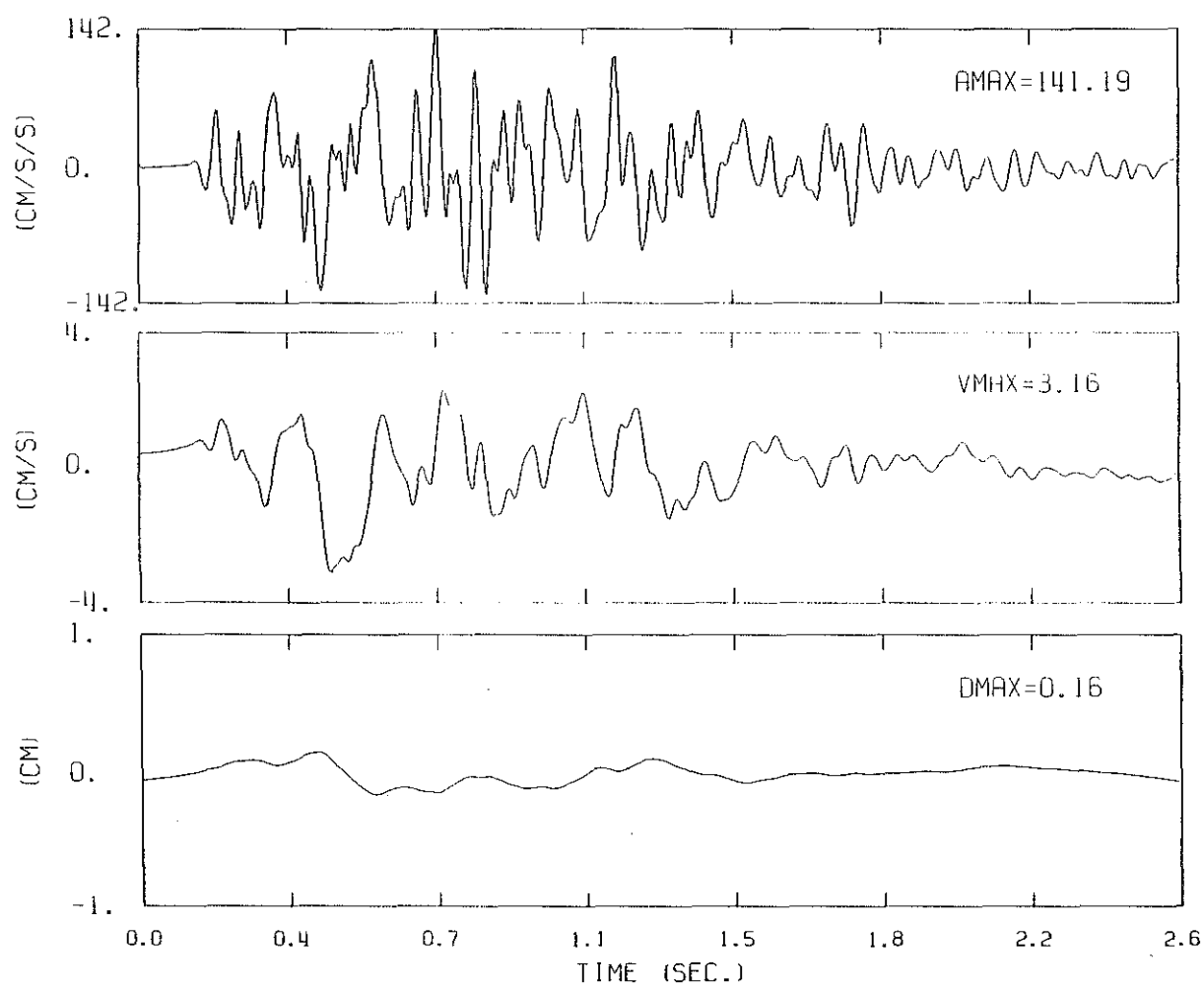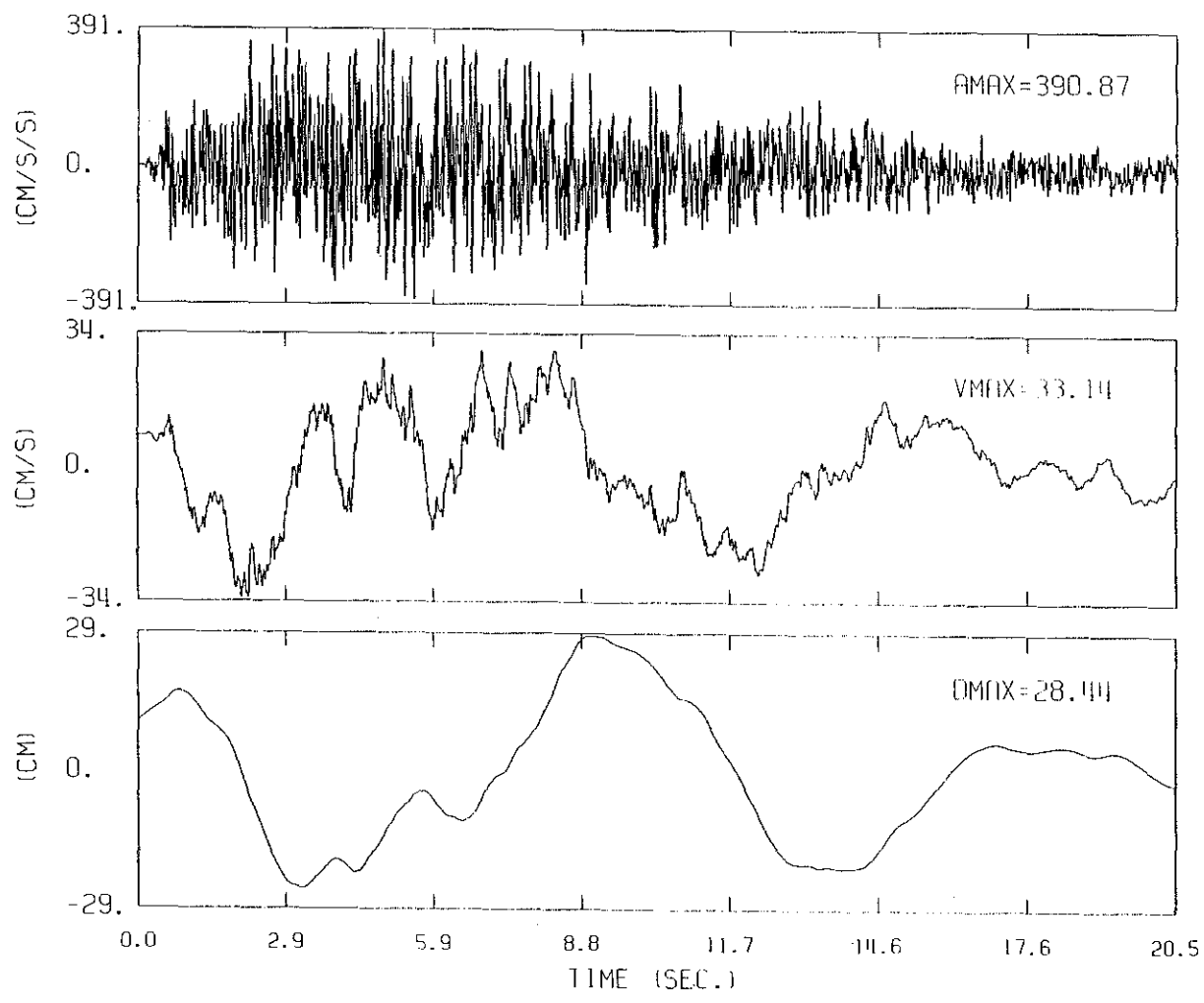
Figure B.21. Acceleration, Velocity, and Displacement Time History for the Transverse Component of the 50-Year Event for Counties Identified by 0.15g-3 in Figure 4.3 (TR-50Y-0.15g-3).
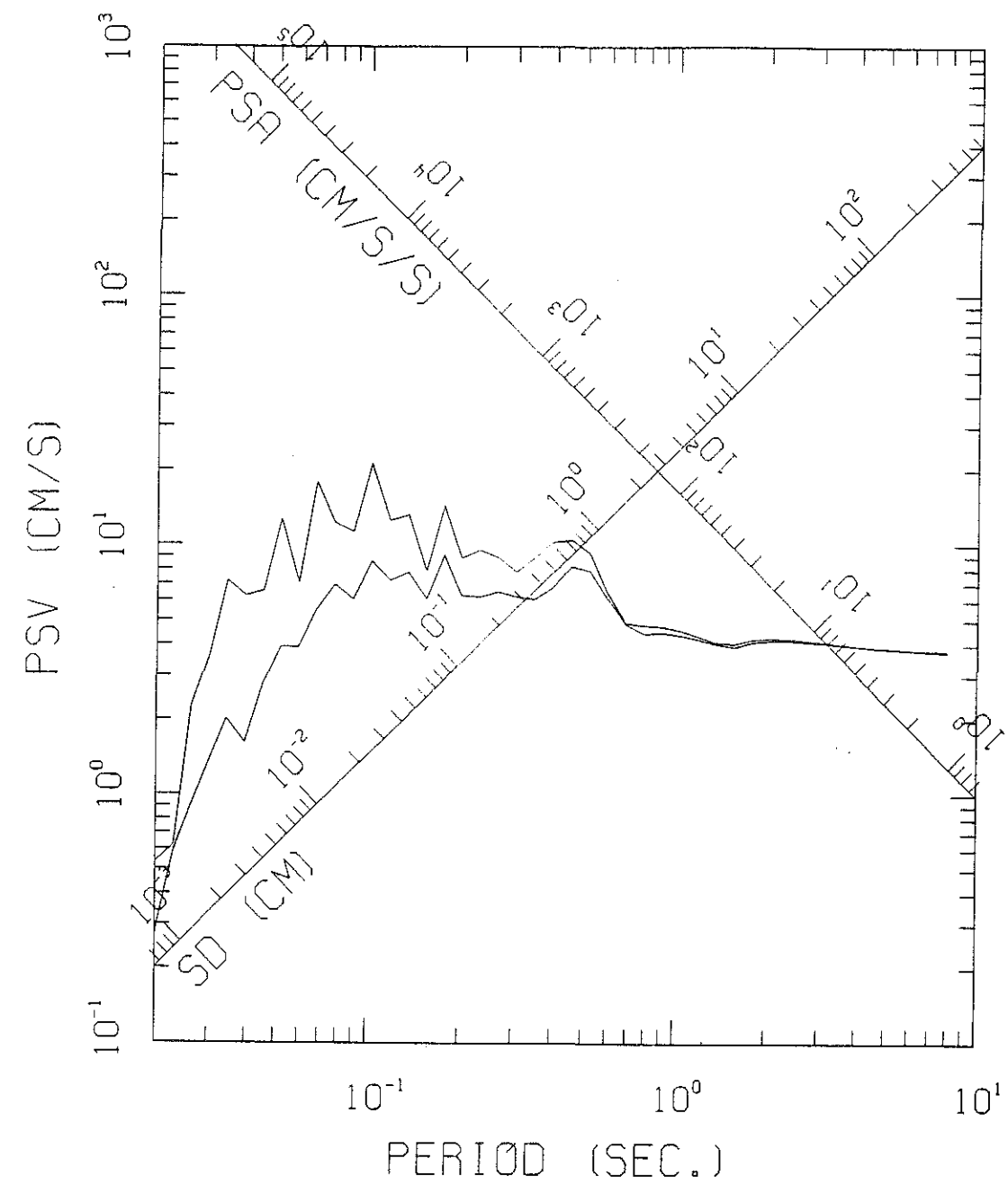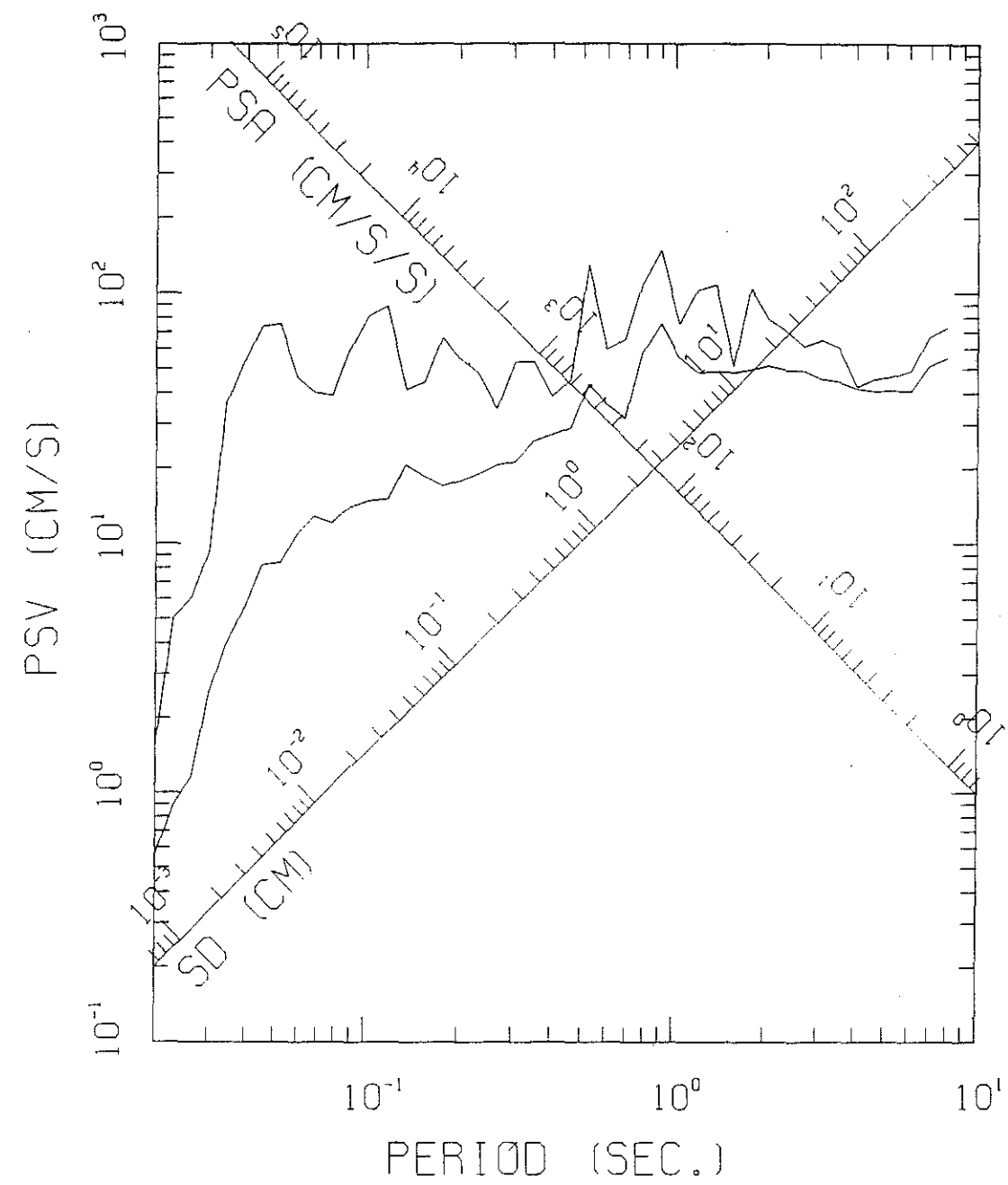
Figure B.22. Response Spectra for the Horizontal Component of the 50-Year Event for Counties Identified by 0.15g-3 in Figure 4.3 (TR-50Y-0.15g-3, Damping Ratio = 0.00 and 0.05).
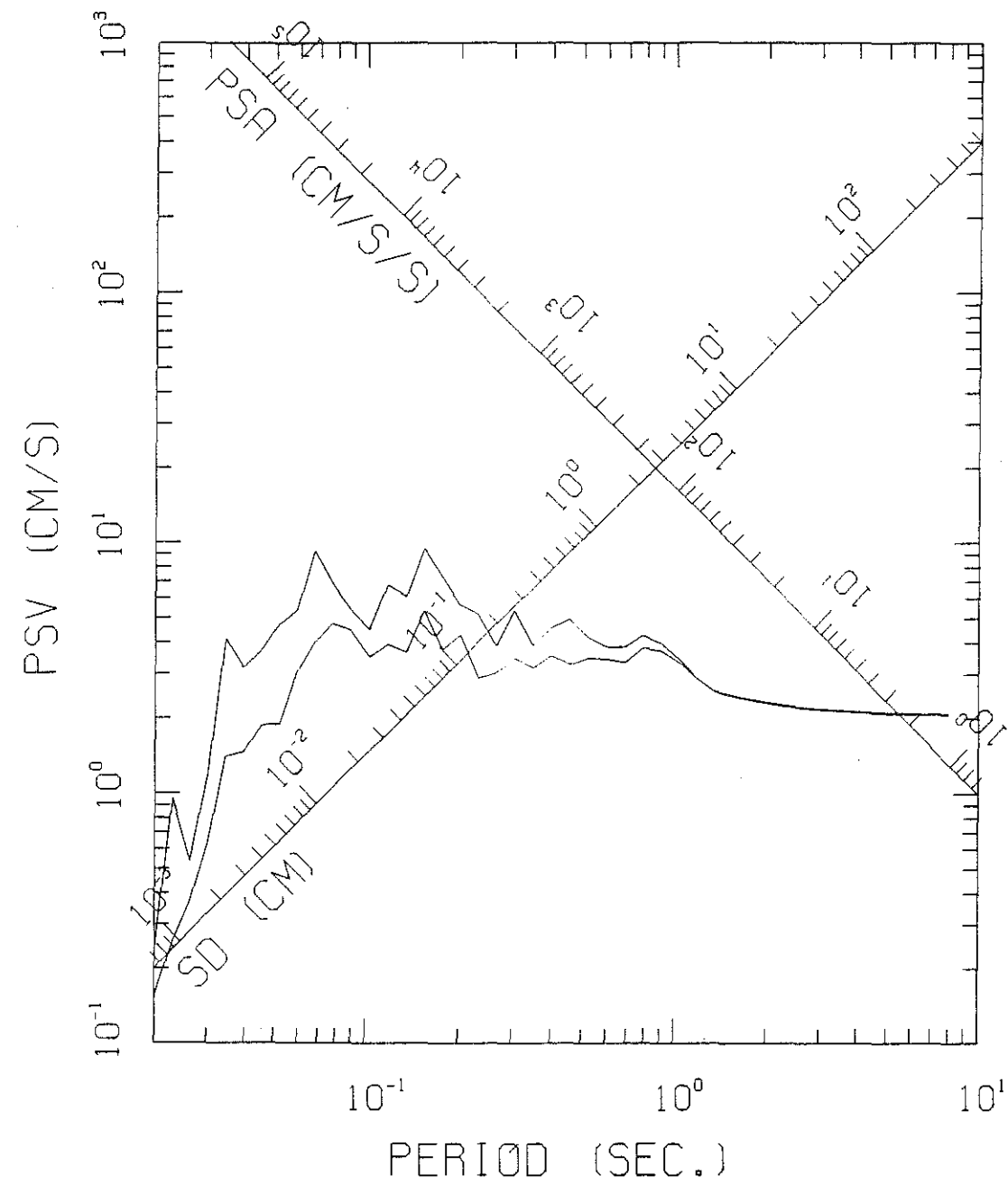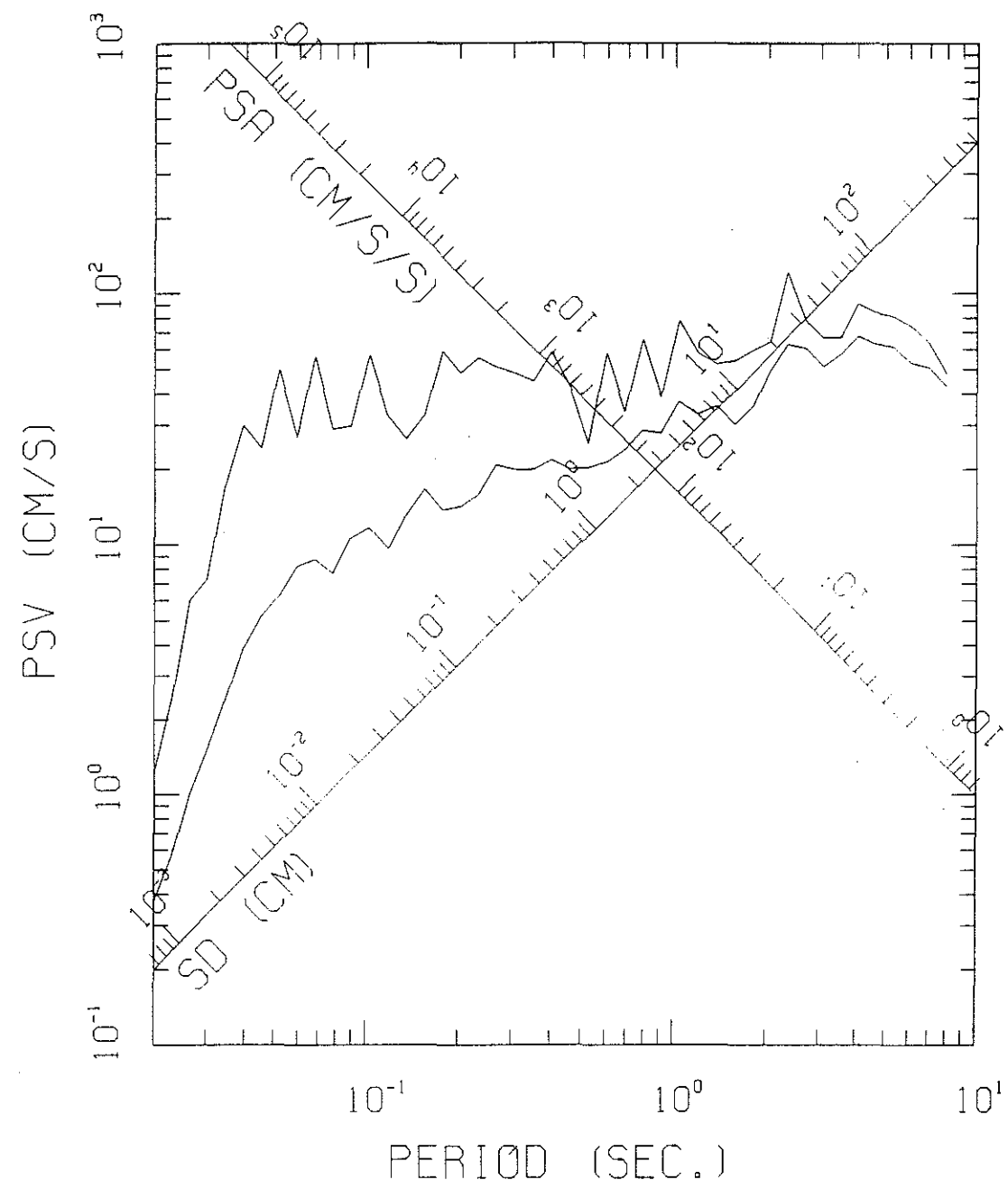
Figure B.23. Response Spectra for the Vertical Component of the 50-Year Event for Counties Identified by 0.15g-3 in Figure 4.3 (TR-50Y-0.15g-3, Damping Ratio = 0.00 and 0.05).
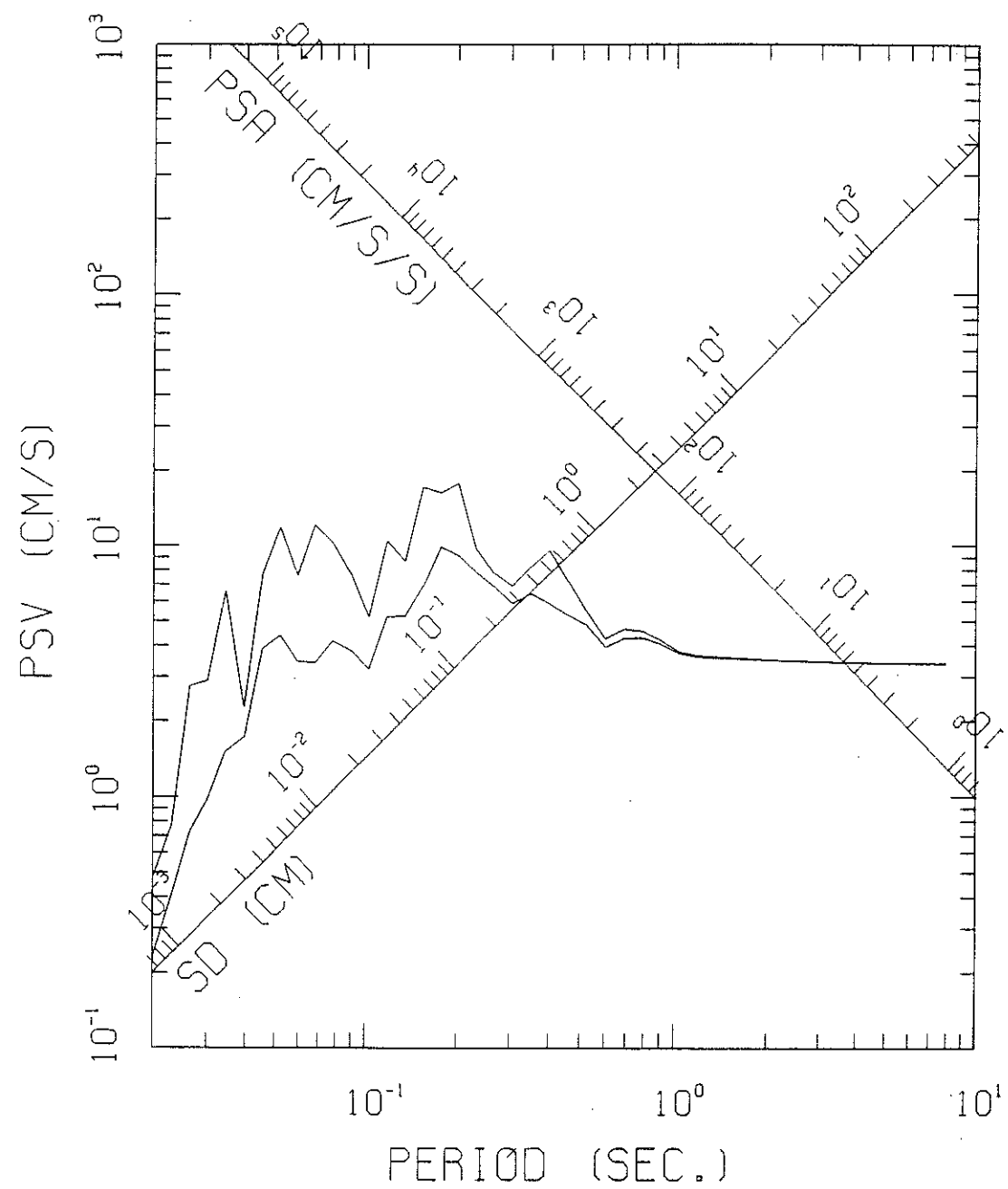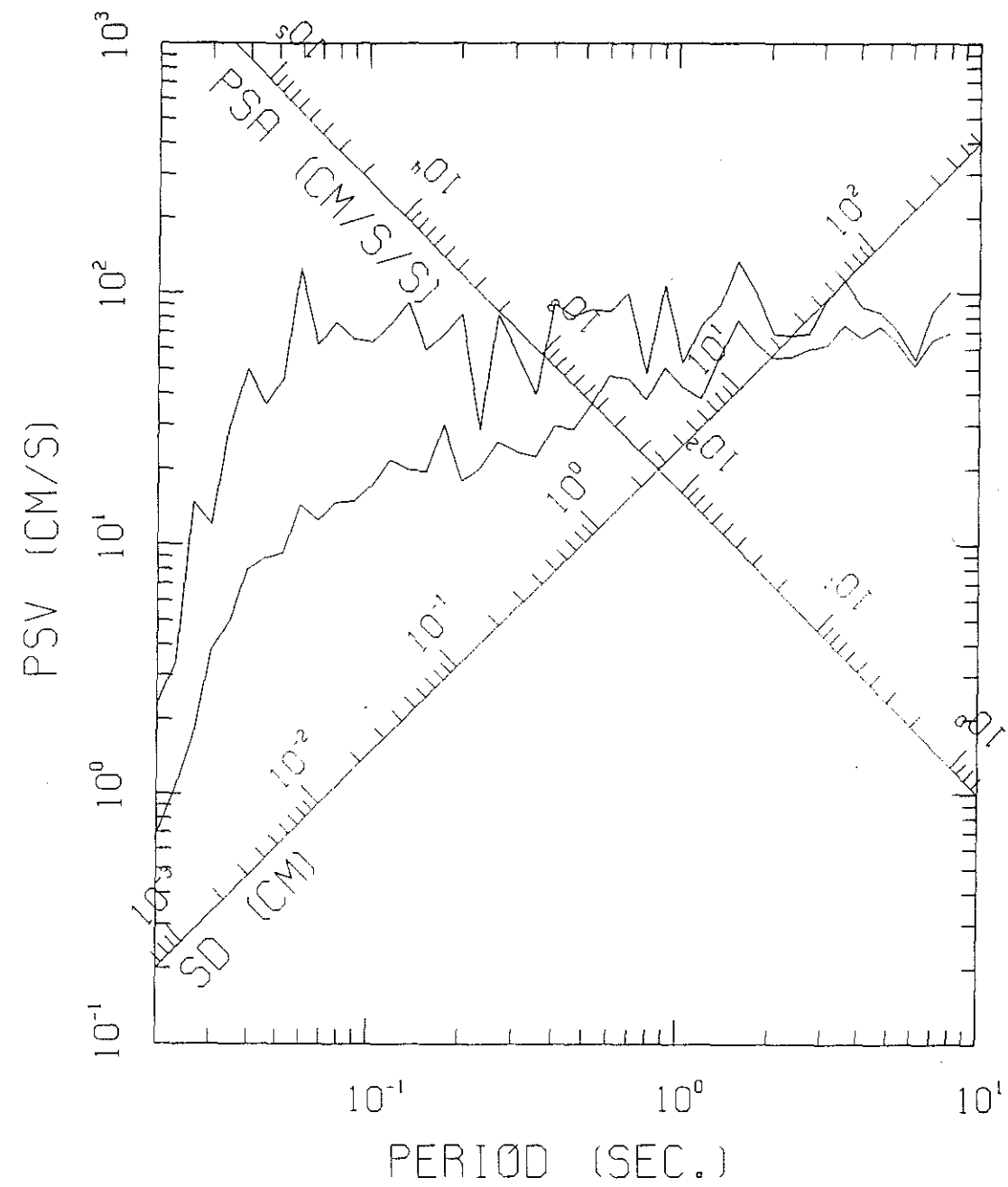
Figure B.24. Response Spectra for the Transverse Component of the 50-Year Event for Counties Identified by 0.15g-3 in Figure 4.3 (TR-50Y-0.15g-3, Damping Ratio = 0.00 and 0.05).
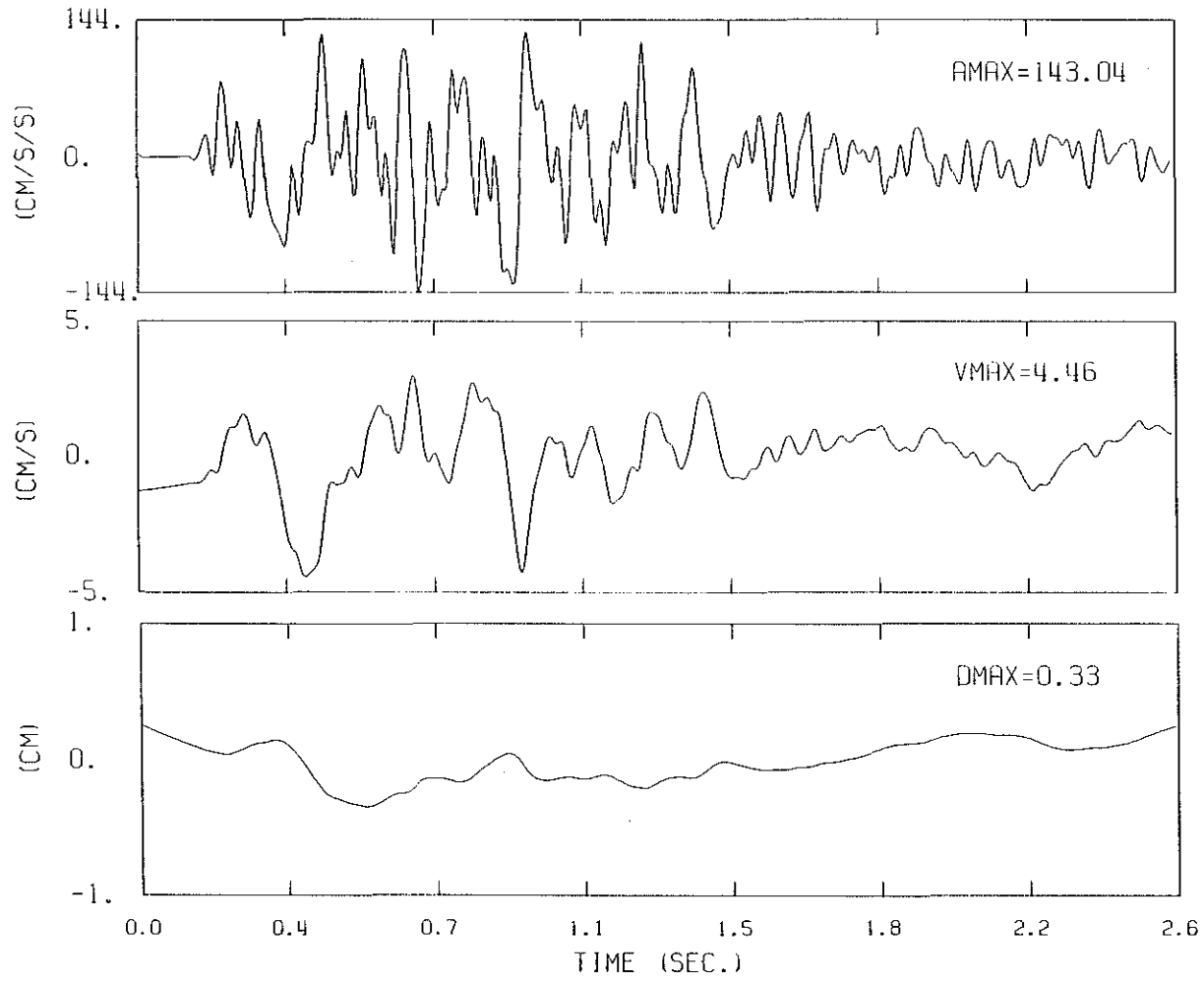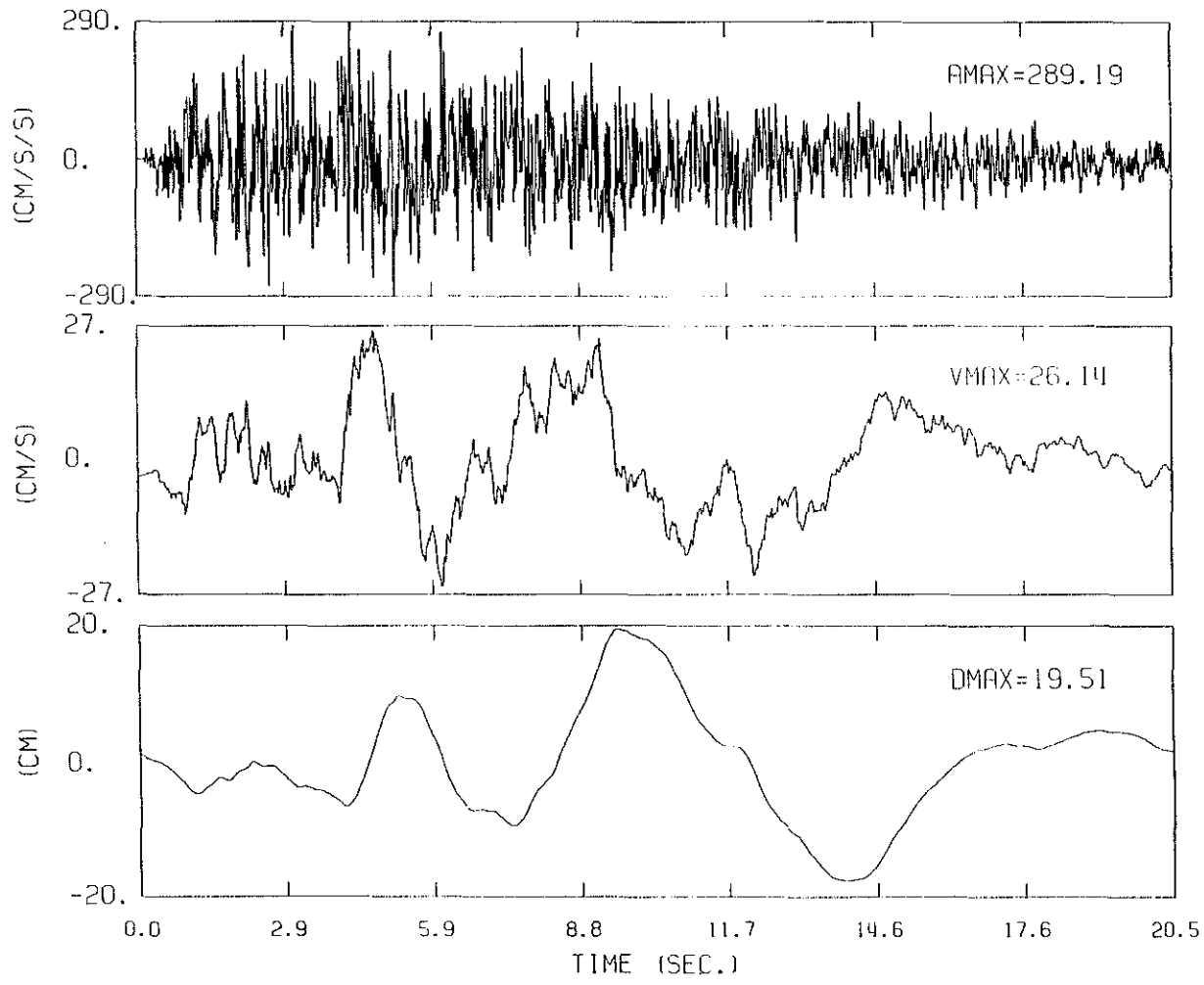
Figure B.25. Acceleration, Velocity, and Displacement Time History for the Horizontal Component of the 50-Year Event for Counties Identified by 0.15g-4 in Figure 4.3 (TR-50Y-0.15g-4).
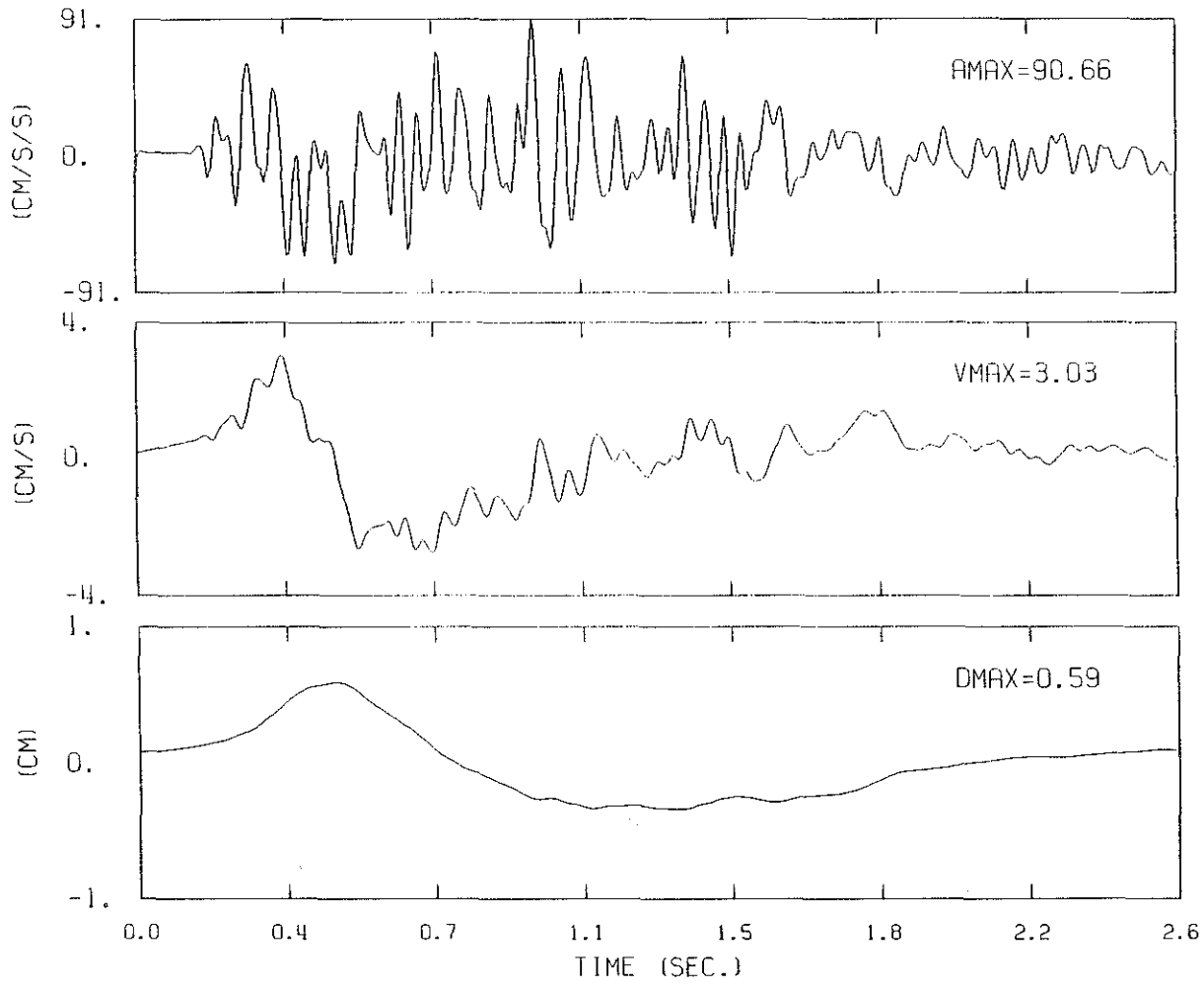
Figure B.26. Acceleration, Velocity, and Displacement Time History for the Vertical Component of the 50-Year Event for Counties Identified by 0.15g-4 in Figure 4.3 (TR-50Y-0.15g-4).
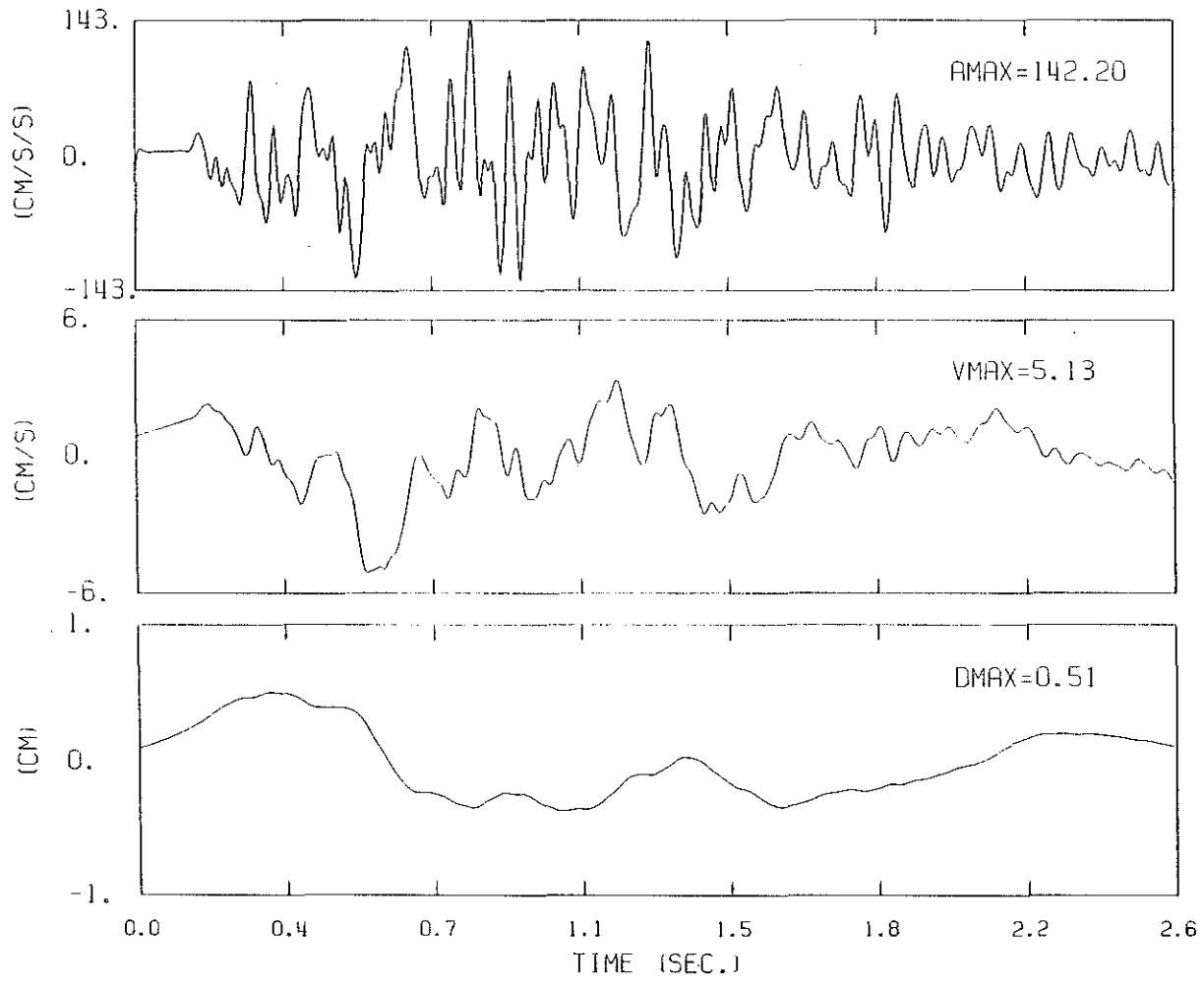
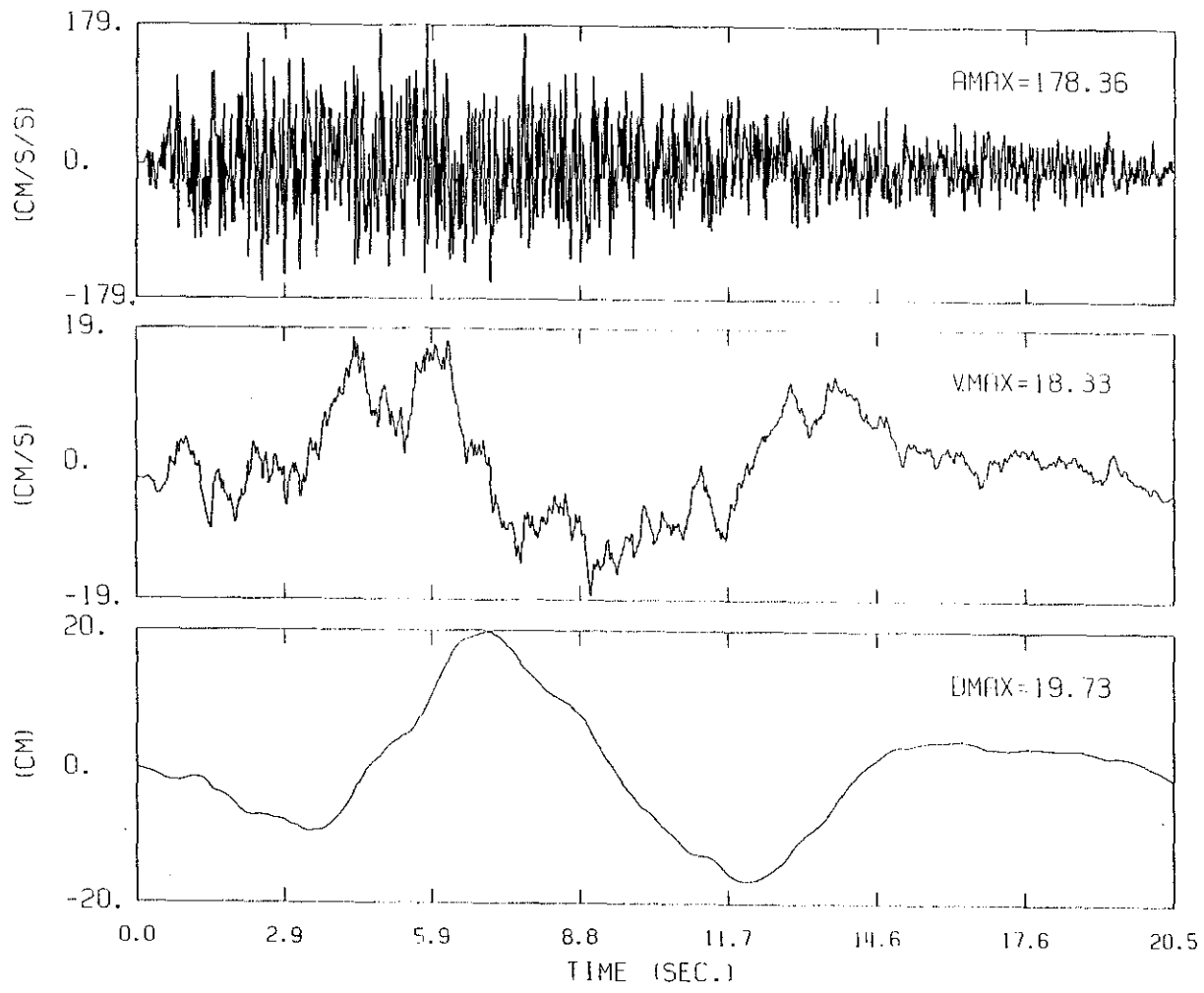**Figure B.27. Acceleration, Velocity, and Displacement Time History for the Transverse Component of the 50-Year Event for Counties Identified by 0.15g-4 in Figure 4.3 (TR-50Y-0.15g-4).**
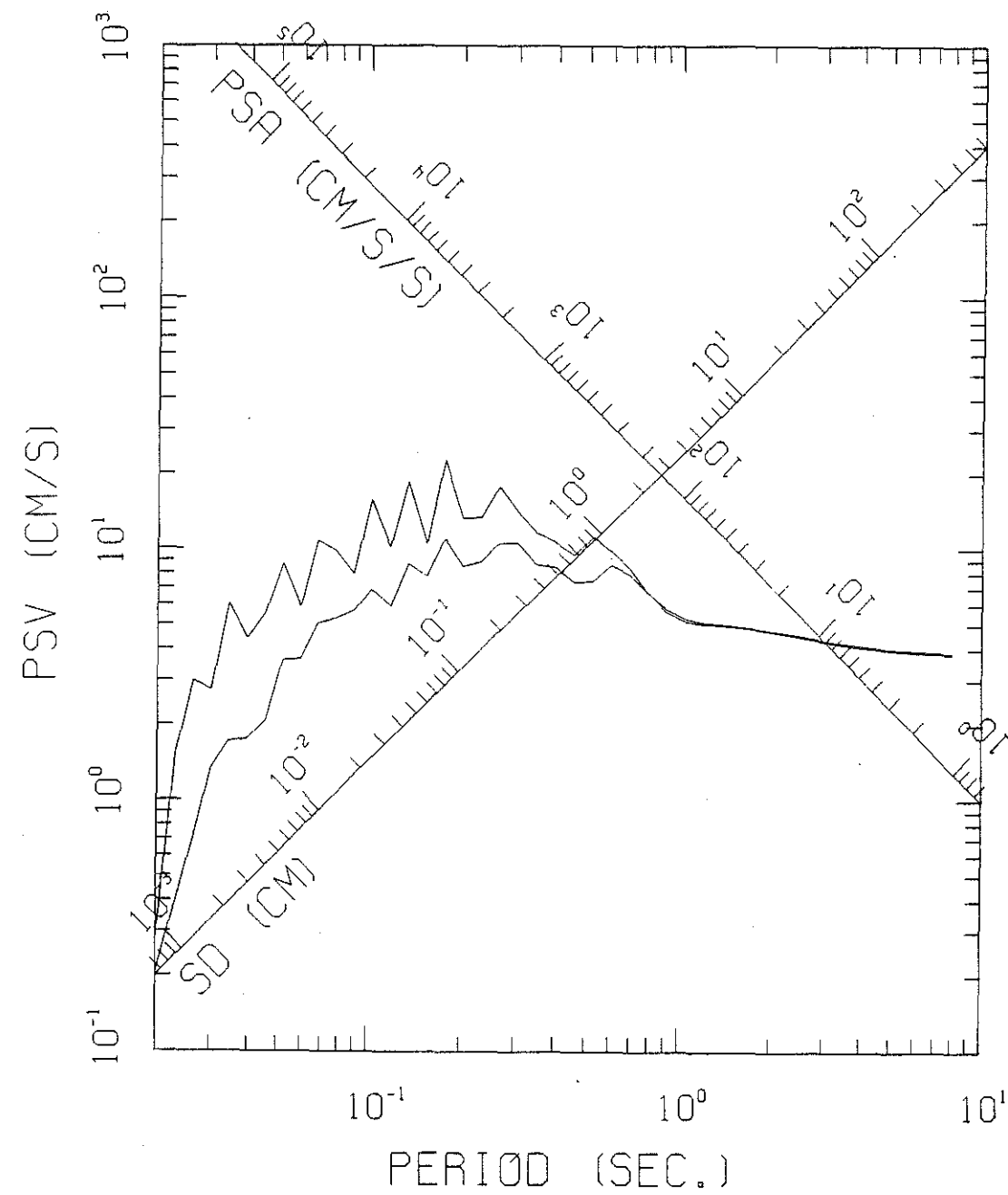
Figure B.28. Response Spectra for the Horizontal Component of the 50-Year Event for Counties Identified by 0.15g-4 in Figure 4.3 (TR-50Y-0.15g-4, Damping Ratio = 0.00 and 0.05).
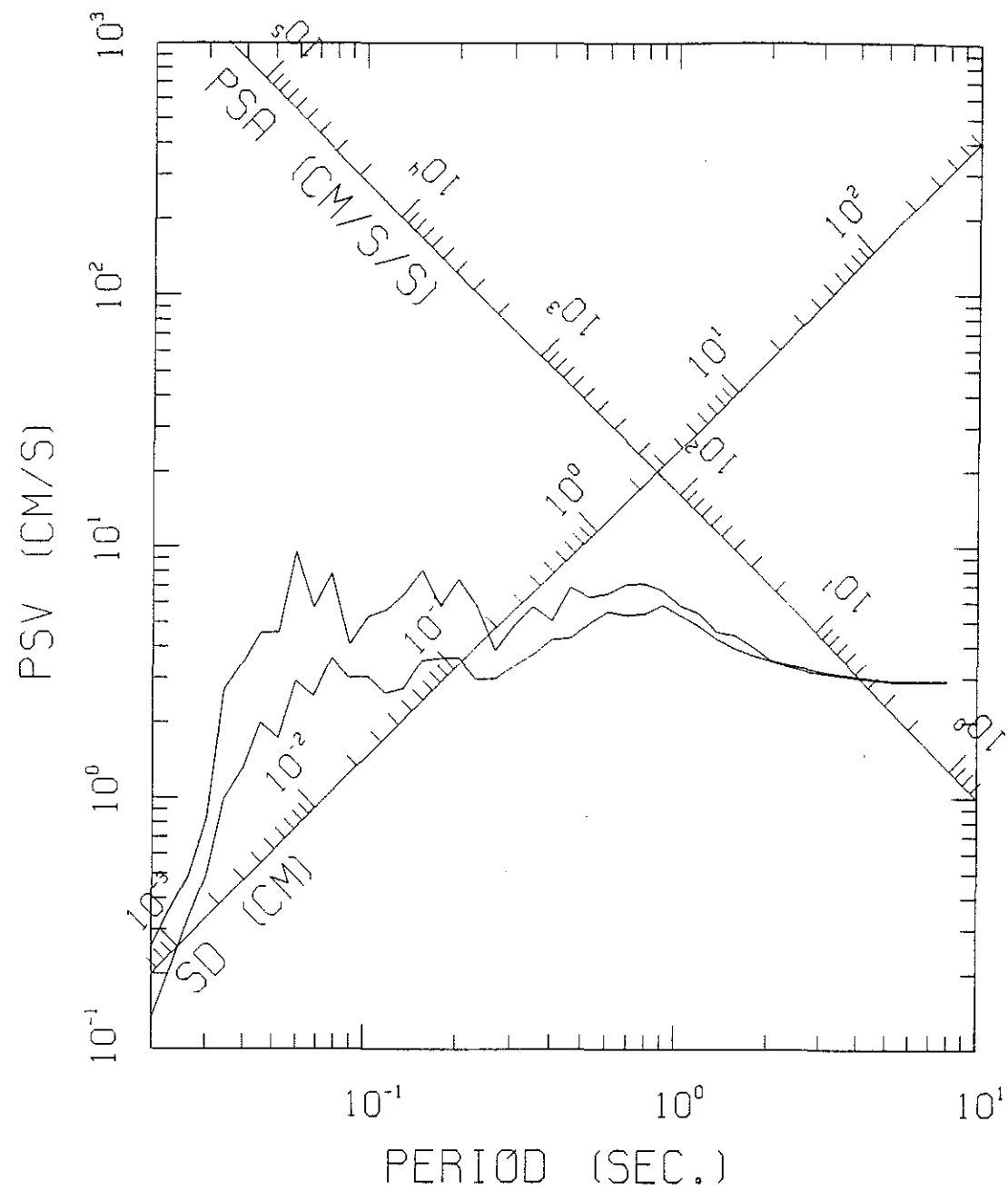
Figure B.29. Response Spectra for the Vertical Component of the 50-Year Event for Counties Identified by 0.15g-4 in Figure 4.3 (TR-50Y-0.15g-4, Damping Ratio = 0.00 and 0.05).
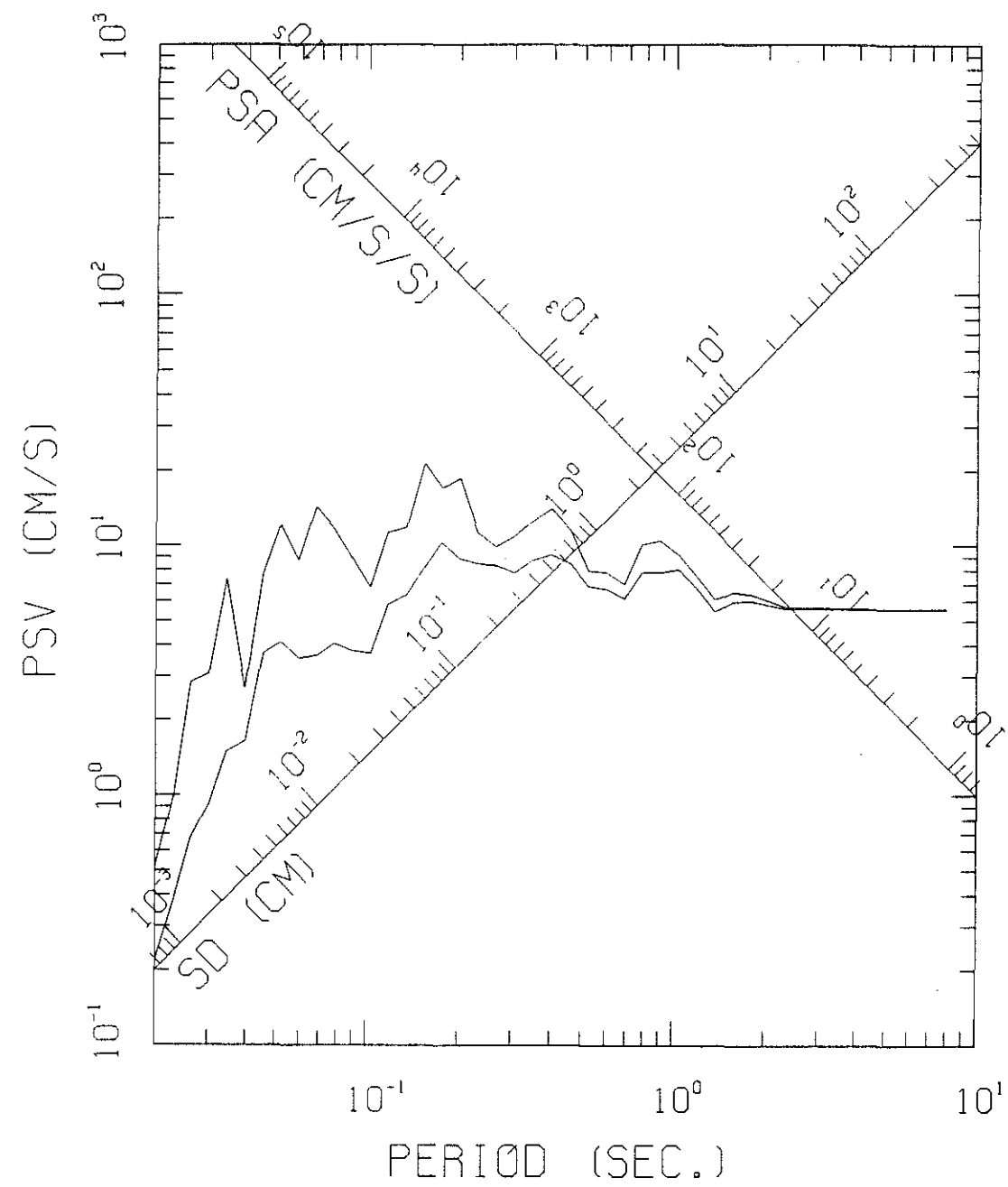
Figure B.30. Response Spectra for the Transverse Component of the 50-Year Event for Counties Identified by 0.15g-4 in Figure 4.3 (TR-50Y-0.15g-4, Damping Ratio = 0.00 and 0.05).
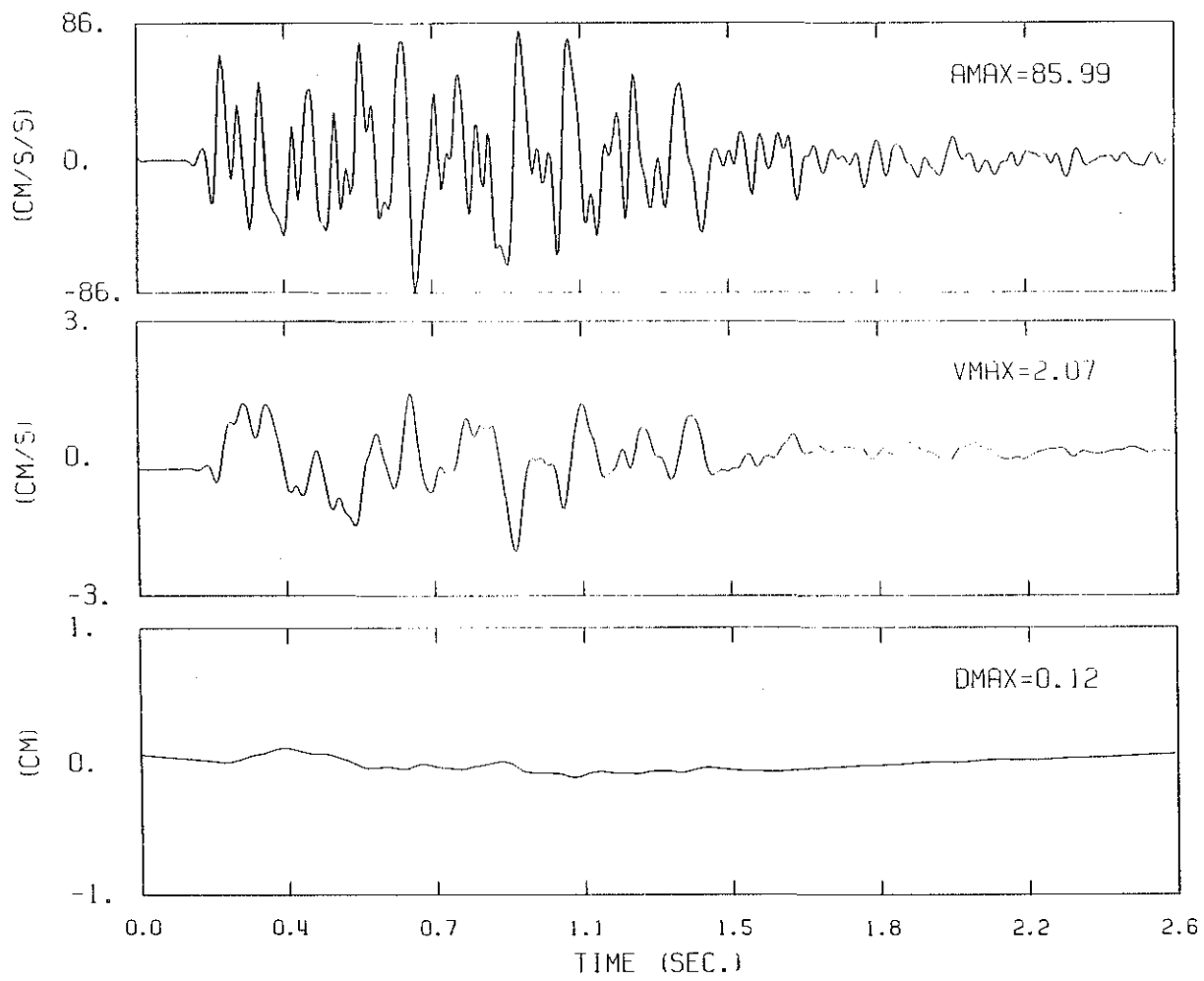
Figure B.31. Acceleration, Velocity, and Displacement Time History for the Horizontal Component of the 50-Year Event for Counties Identified by 0.09g-1 in Figure 4.3 (TR-50Y-0.09g-1).
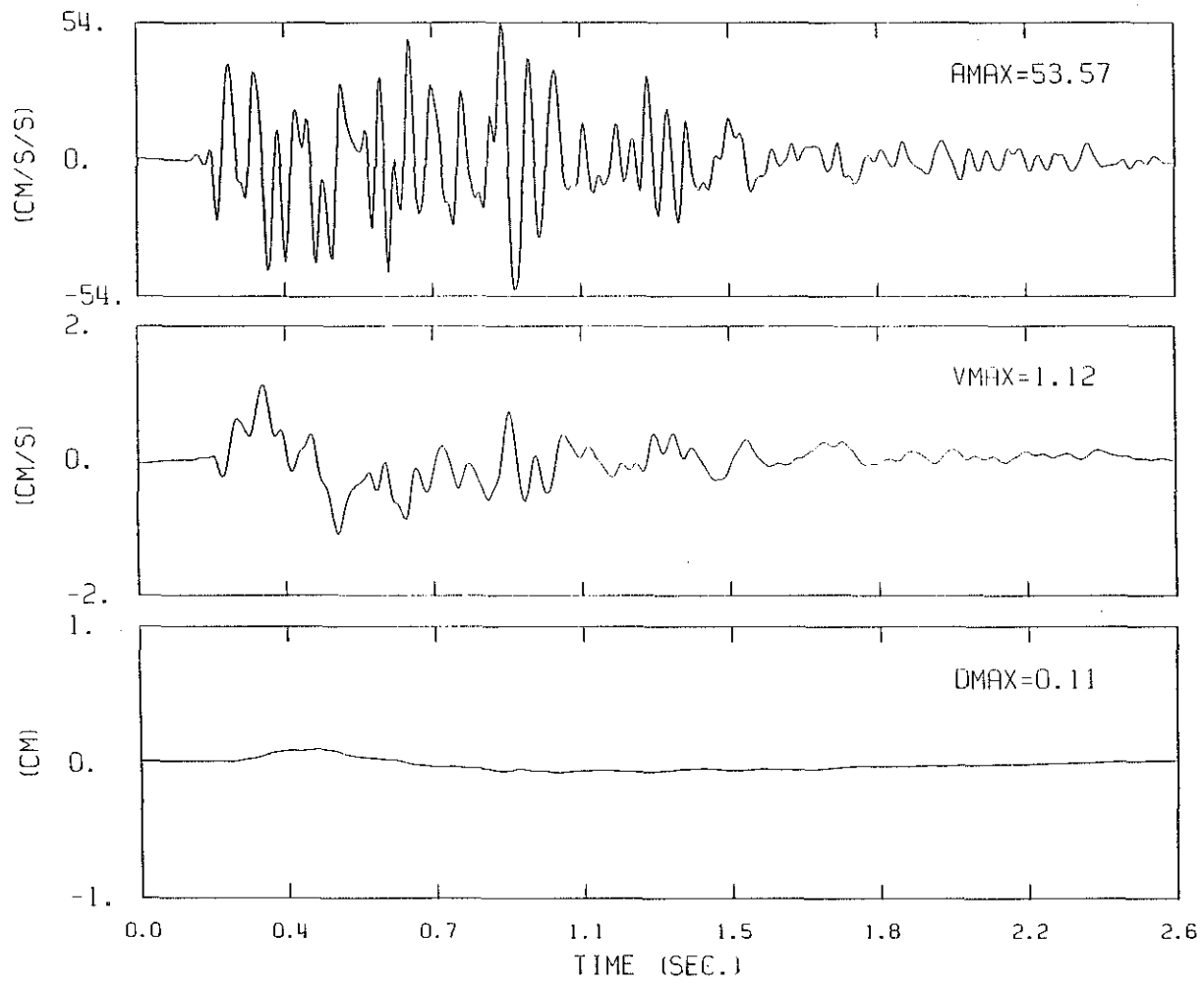
Figure B.32. Acceleration, Velocity, and Displacement Time History for the Vertical Component of the 50-Year Event for Counties Identified by 0.09g-1 in Figure 4.3 (TR-50Y-0.09g-1).
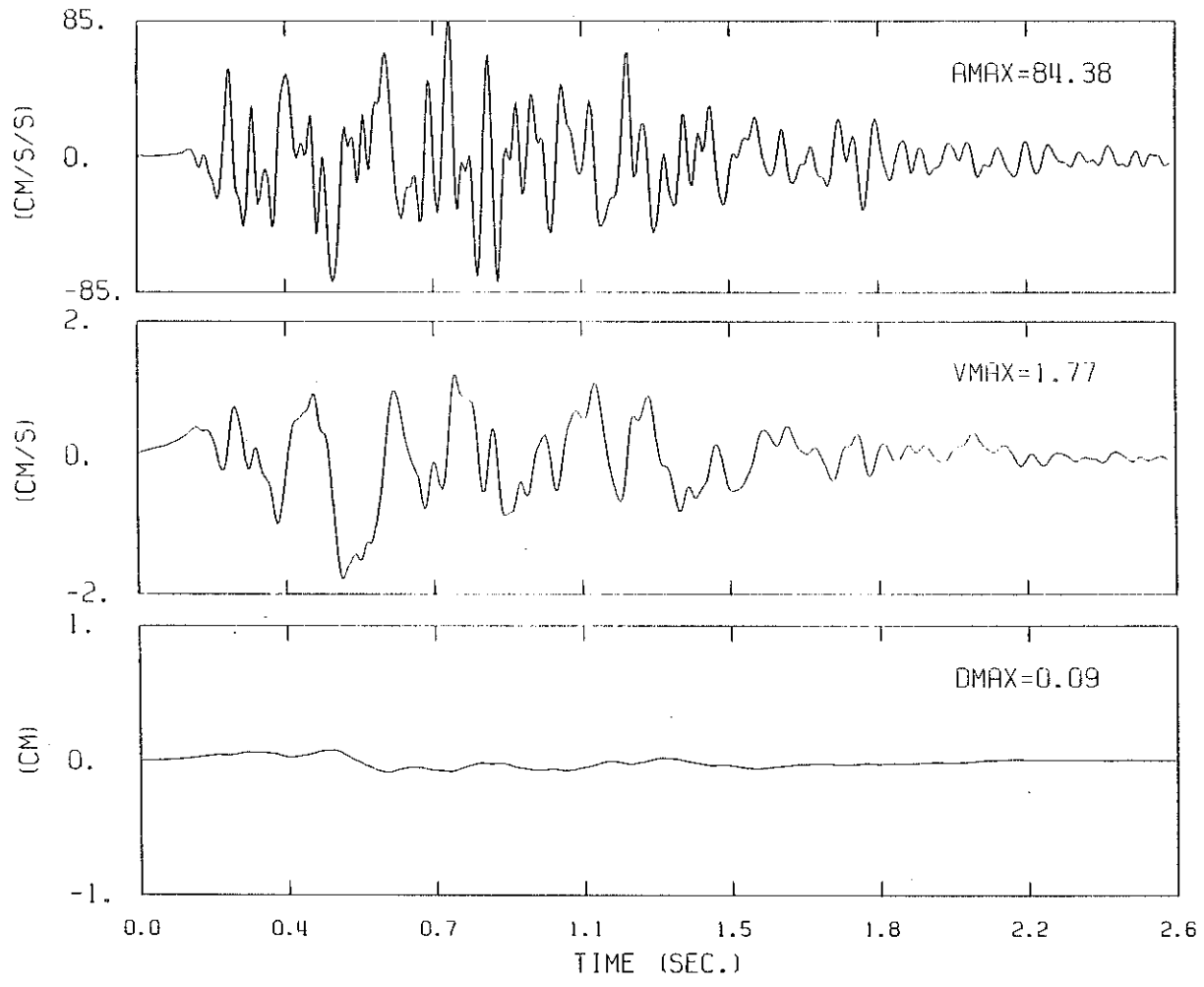
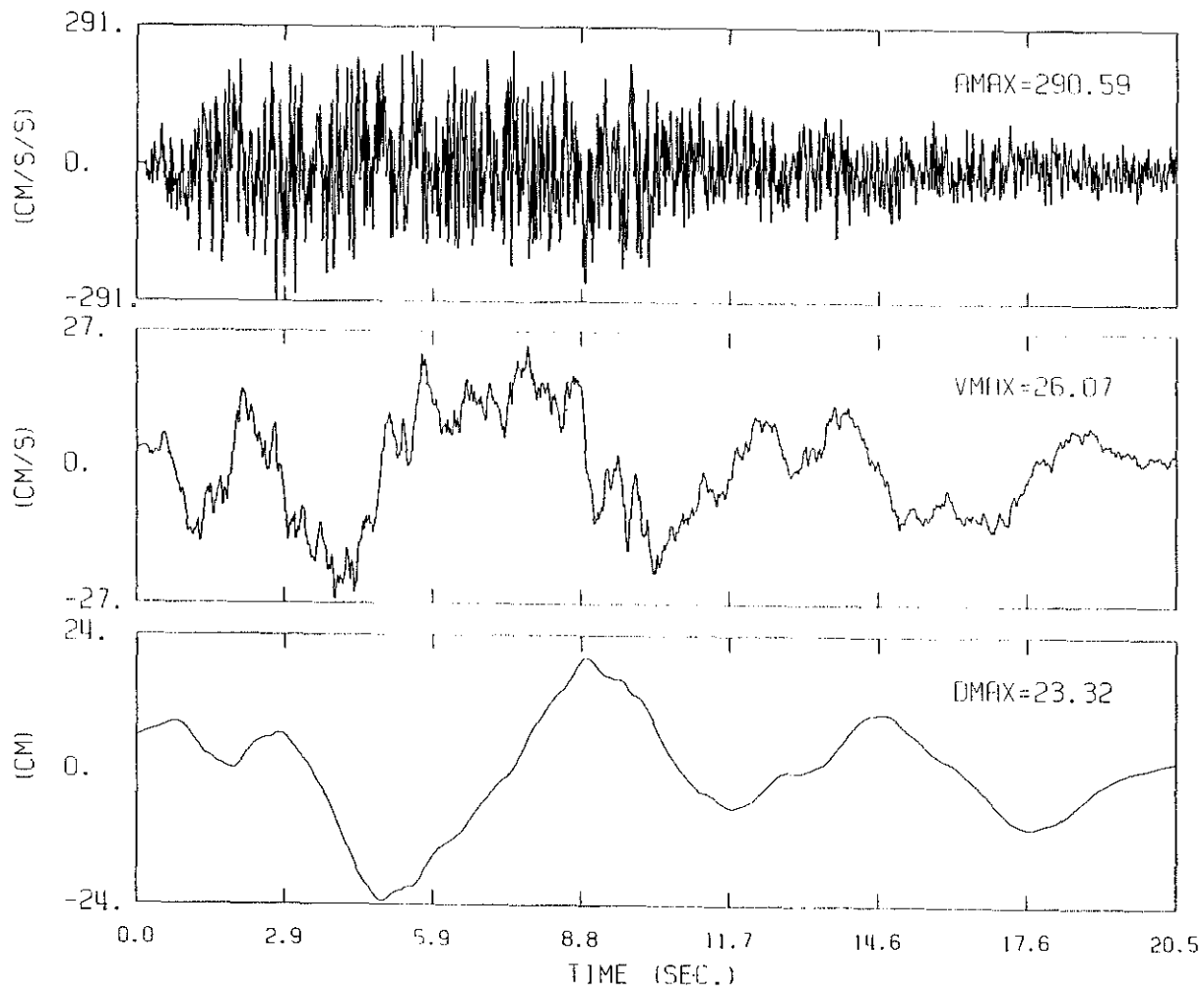**Figure B.33.** Acceleration, Velocity, and Displacement Time History for the Transverse Component of the 50-Year Event for Counties Identified by 0.09g-1 in Figure 4.3 (TR-50Y-0.09g-1).
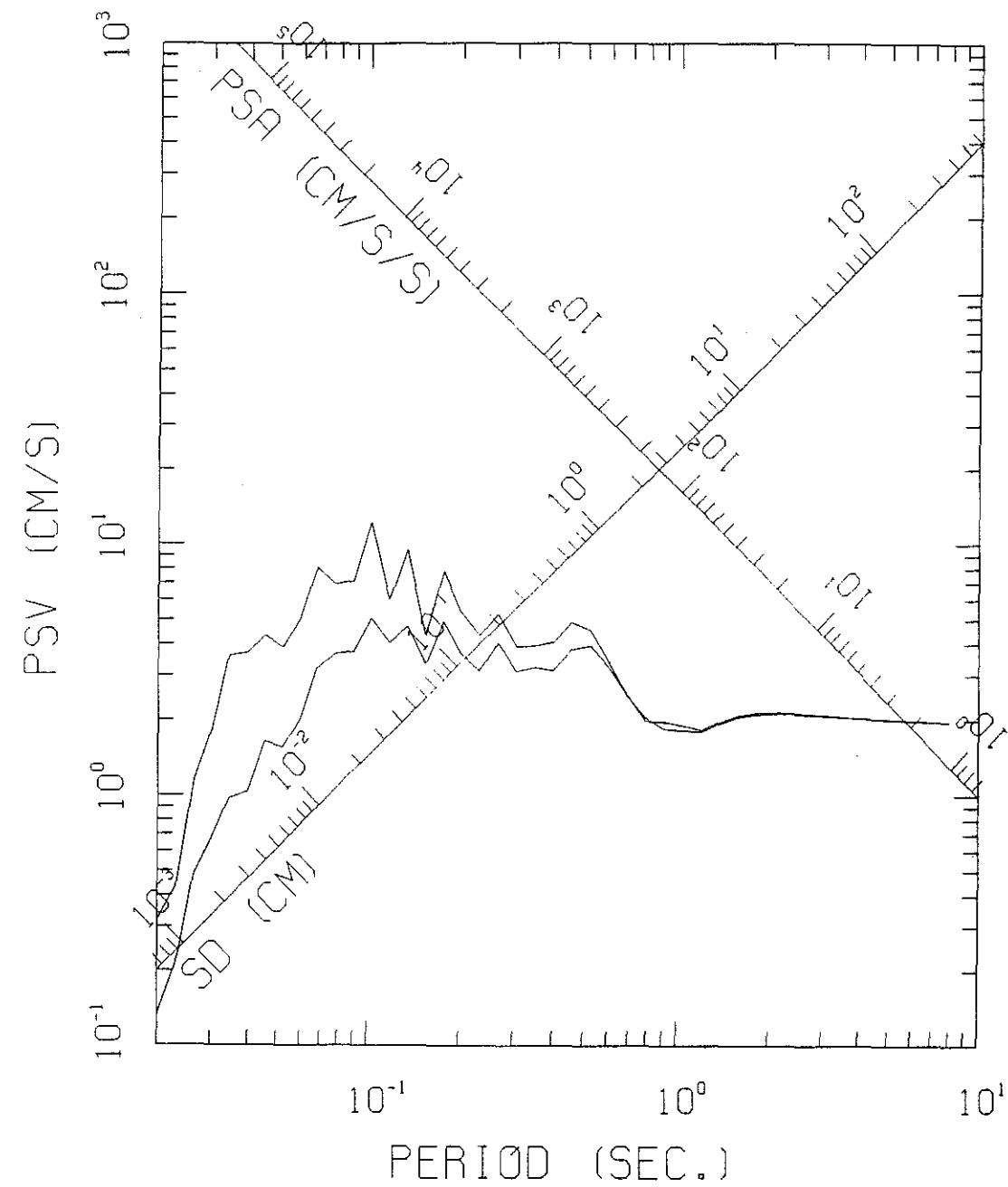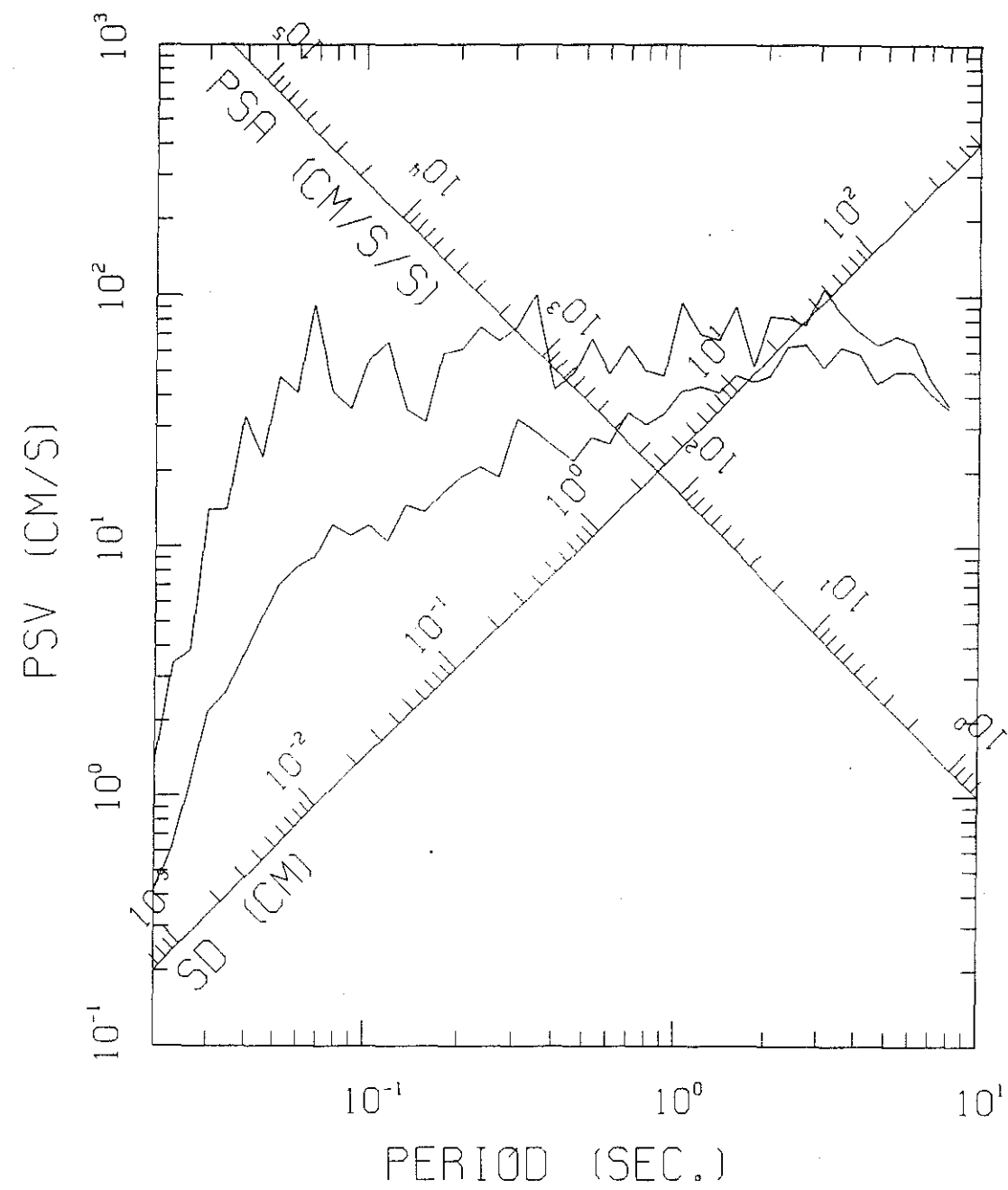
Figure B.34. Response Spectra for the Horizontal Component of the 50-Year Event for Counties Identified by 0.09g-1 in Figure 4.3 (TR-50Y-0.09g-1, Damping Ratio = 0.00 and 0.05).
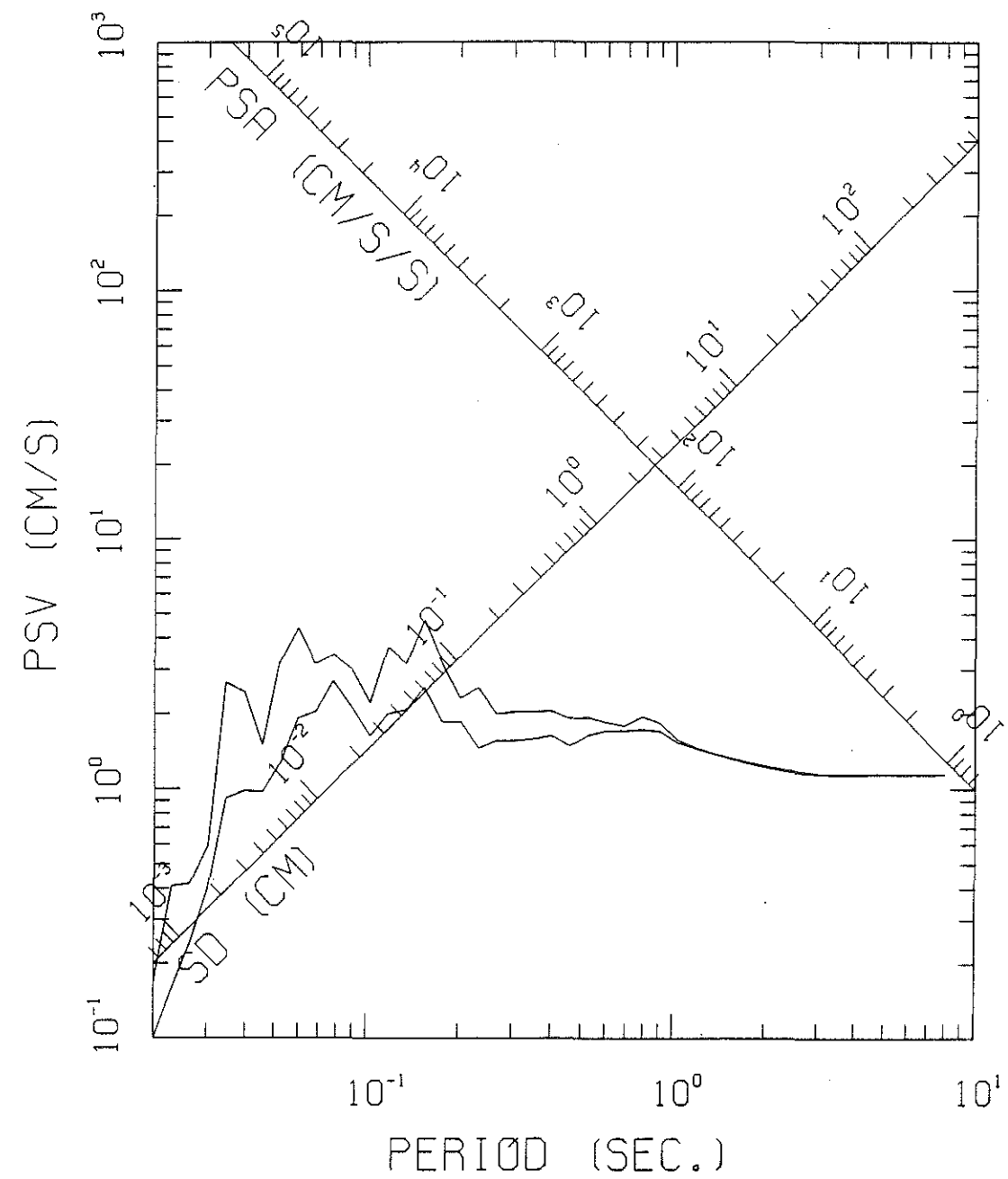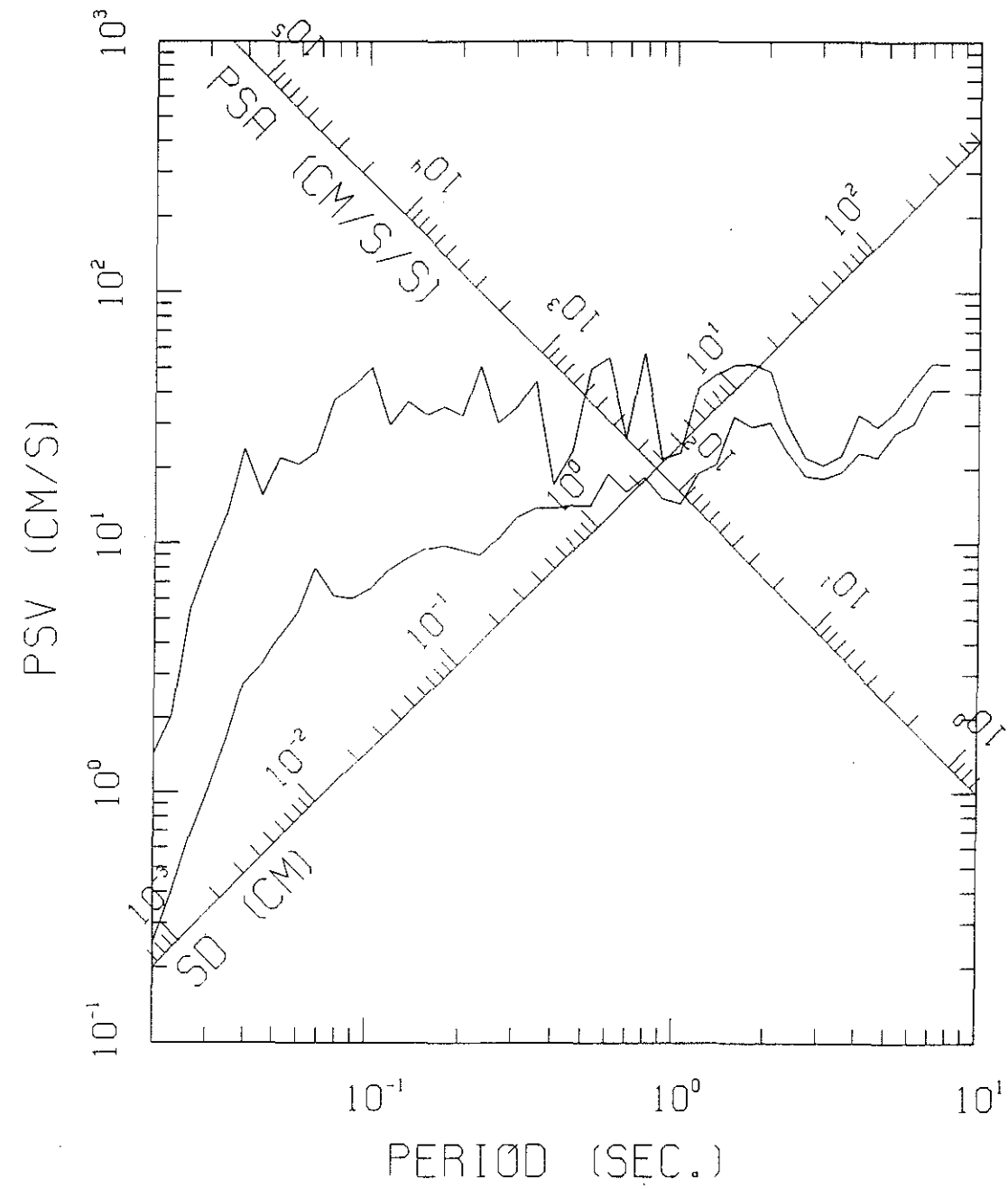
Figure B.35. Response Spectra for the Vertical Component of the 50-Year Event for Counties Identified by 0.09g-1 in Figure 4.3 (TR-50Y-0.09g-1, Damping Ratio = 0.00 and 0.05).
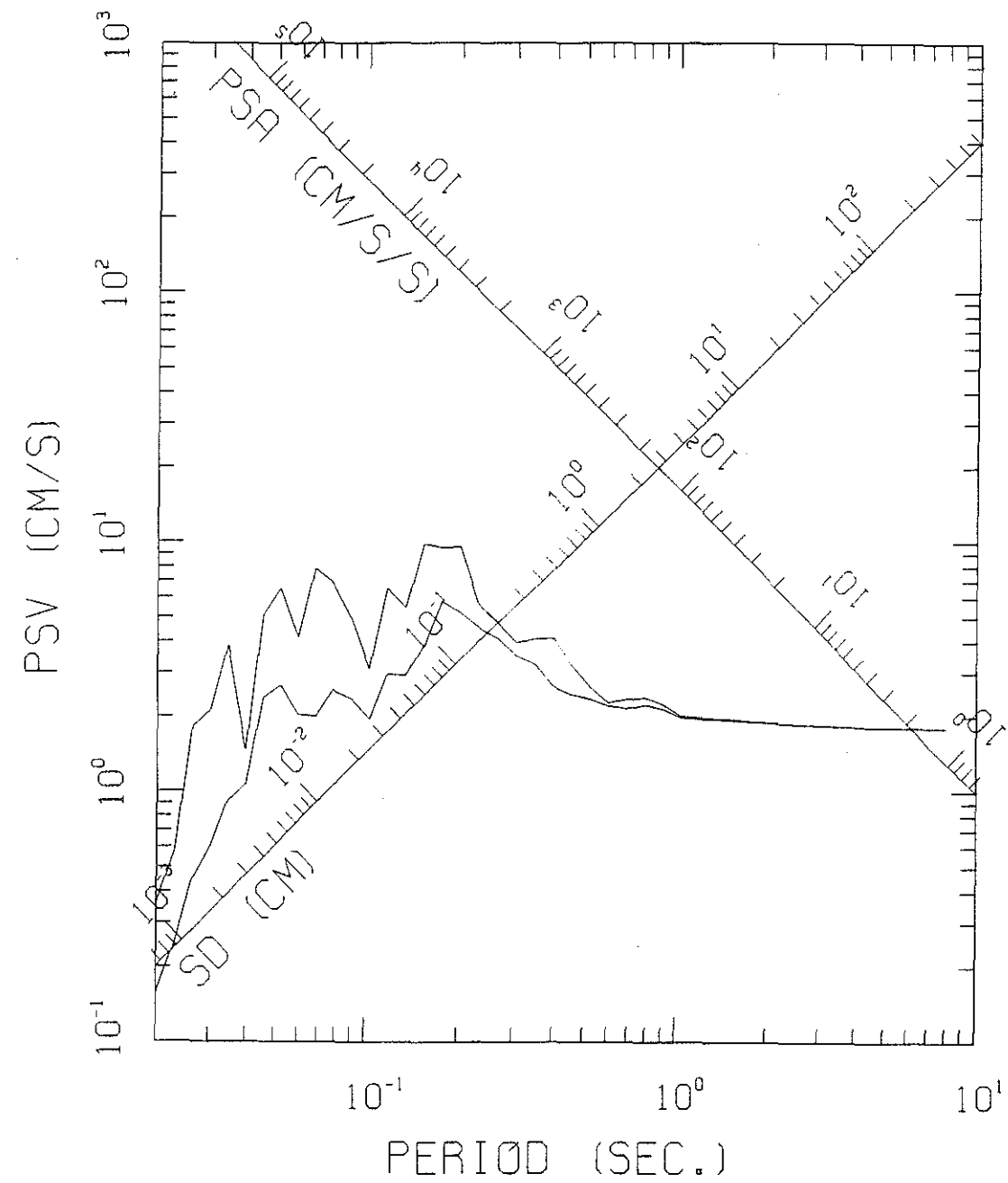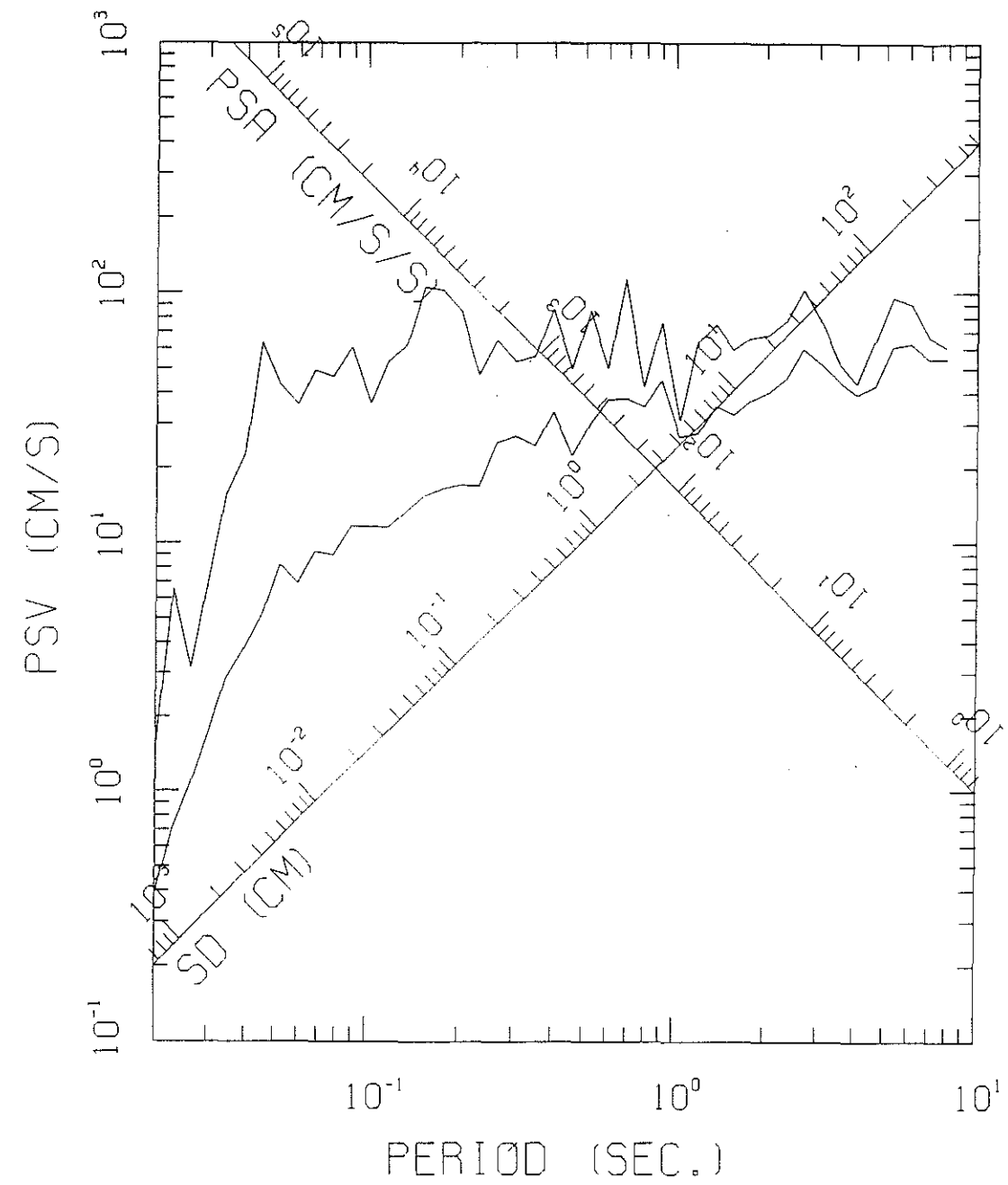
Figure B.36. Response Spectra for the Transverse Component of the 50-Year Event for Counties Identified by 0.09g-1 in Figure 4.3 (TR-50Y-0.09g-1, Damping Ratio = 0.00 and 0.05).
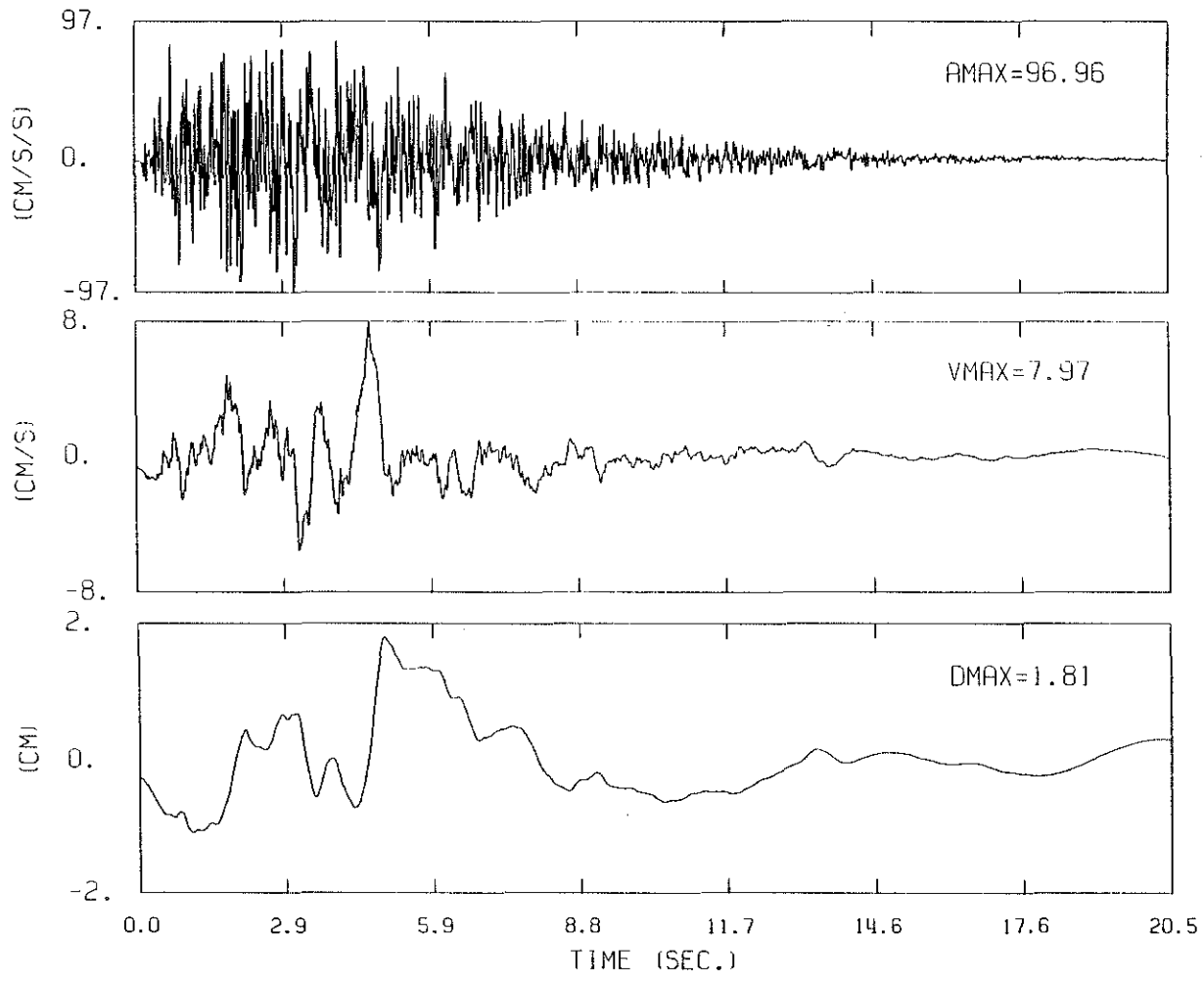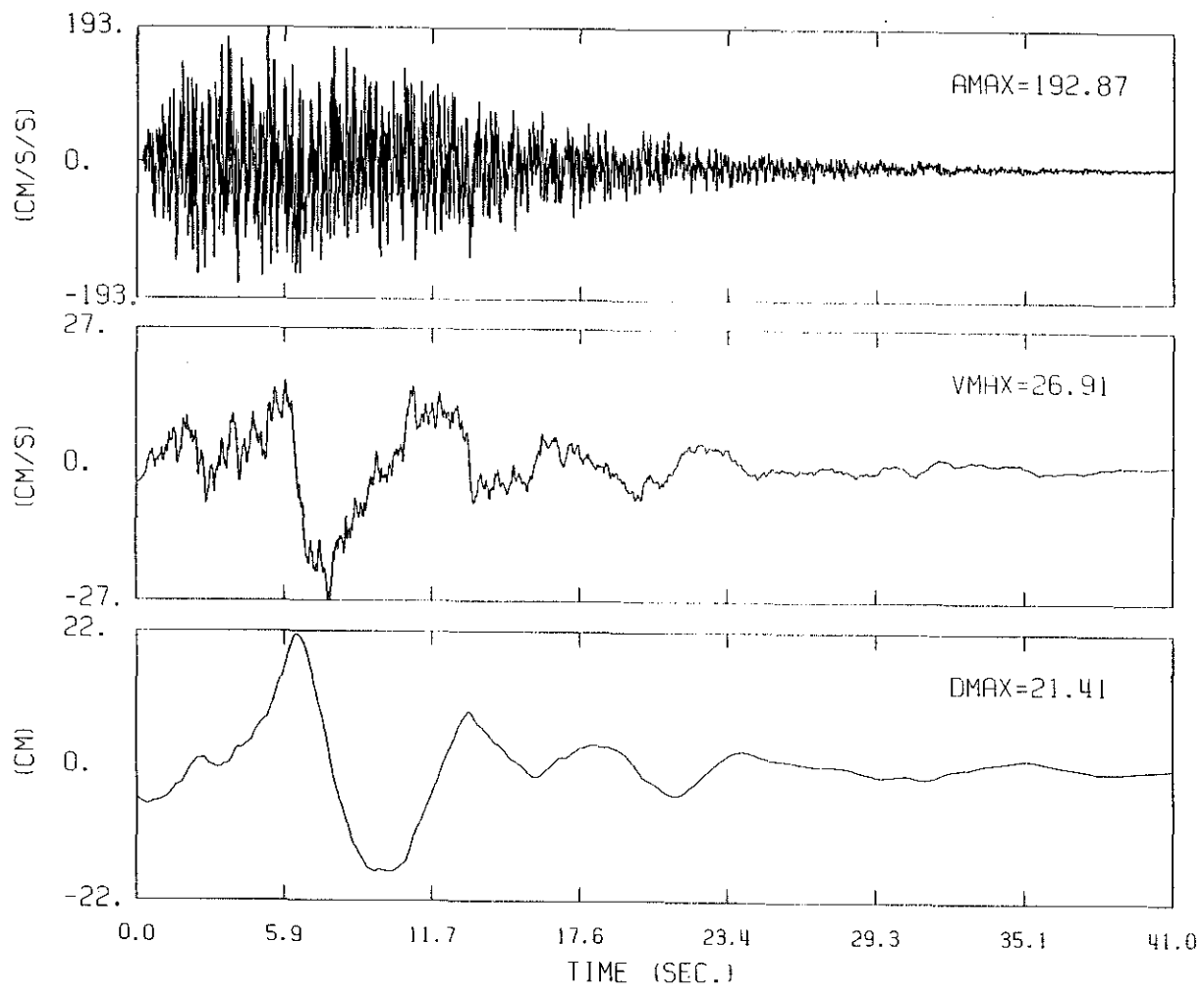
Figure B.37. Acceleration, Velocity, and Displacement Time History for the Horizontal Component of the 50-Year Event for Counties Identified by 0.09g-2 in Figure 4.3 (TR-50Y-0.09g-2).

Figure B.38. Acceleration, Velocity, and Displacement Time History for the Vertical Component of the 50-Year Event for Counties Identified by 0.09g-2 in Figure 4.3 (TR-50Y-0.09g-2).

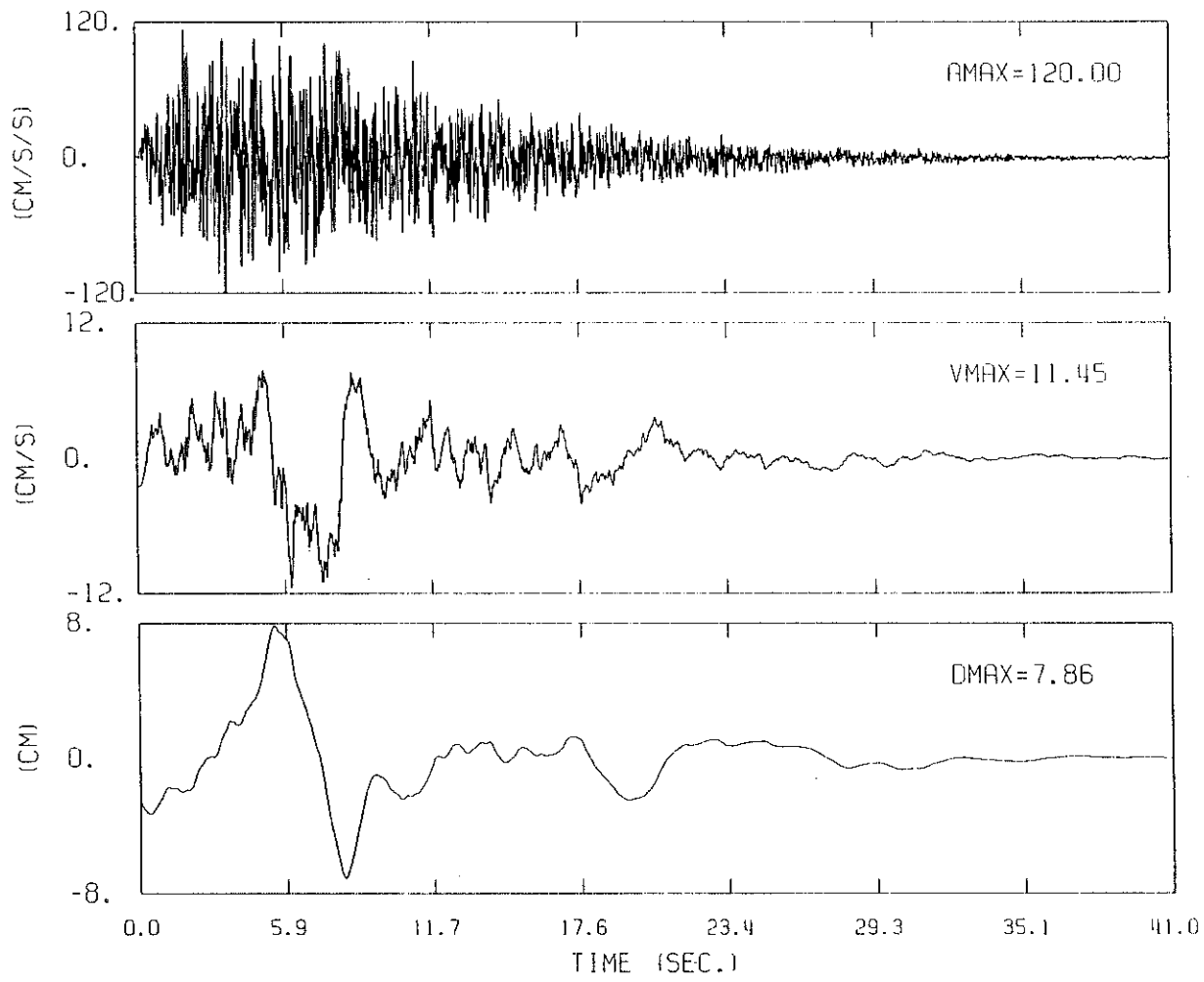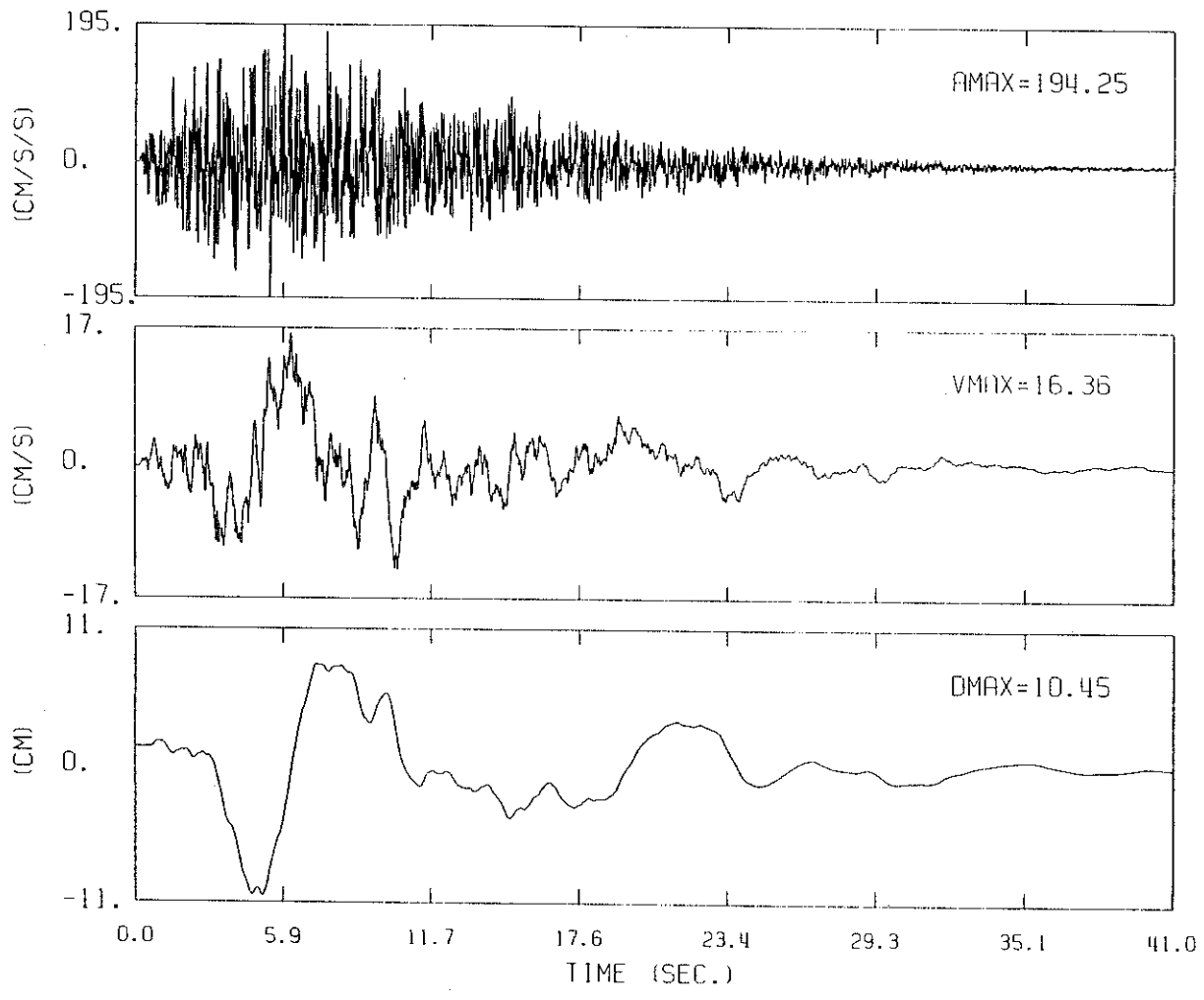Figure B.39. Acceleration, Velocity, and Displacement Time History for the Transverse Component of the 50-Year Event for Counties Identified by 0.09g-2 in Figure 4.3 (TR-50Y-0.09g-2).
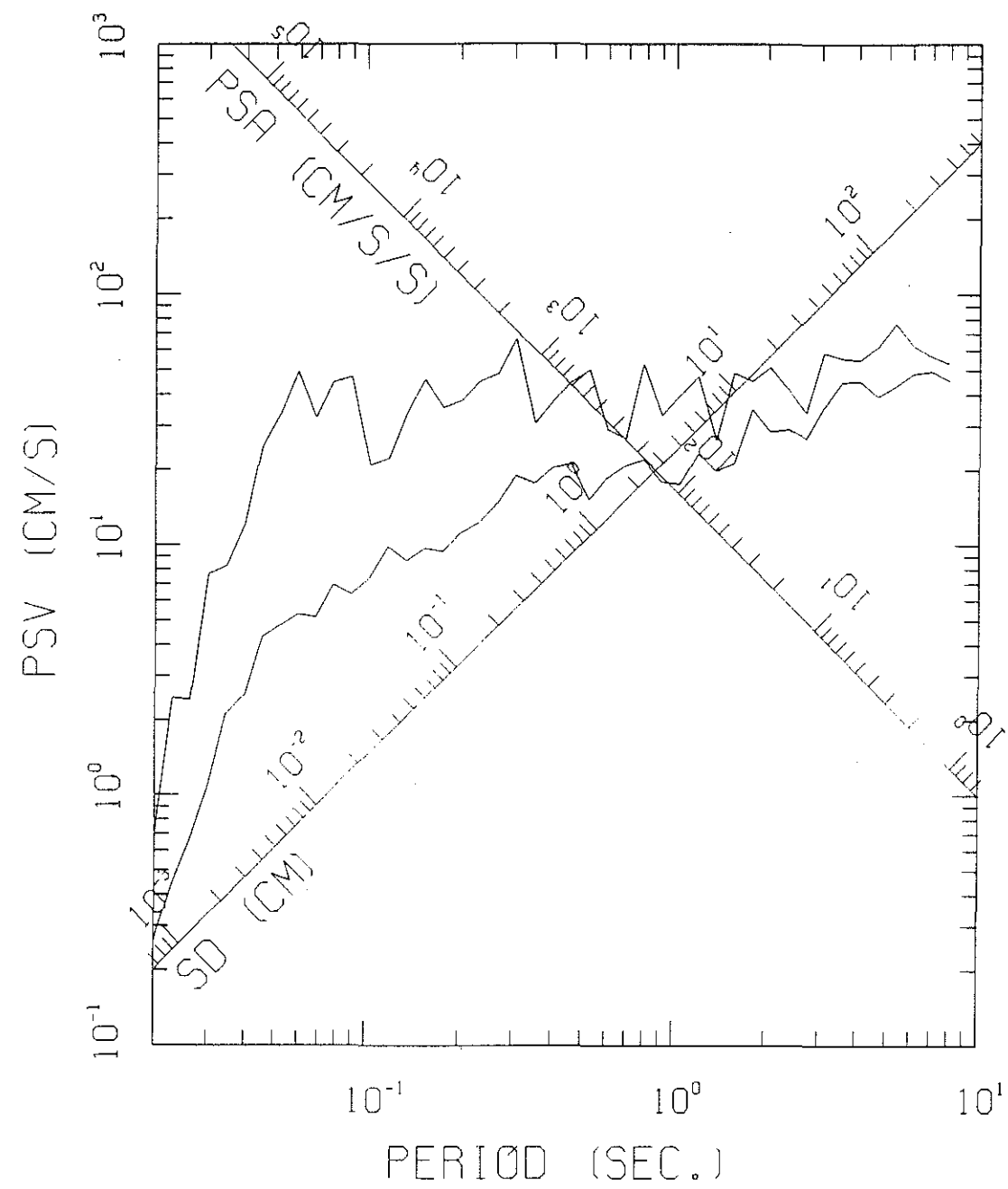
Figure B.40. Response Spectra for the Horizontal Component of the 50-Year Event for Counties Identified by 0.09g-2 in Figure 4.3 (TR-50Y-0.09g-2, Damping Ratio = 0.00 and 0.05).

Figure B.41. Response Spectra for the Vertical Component of the 50-Year Event for Counties Identified by 0.09g-2 in Figure 4.3 (TR-50Y-0.09g-2, Damping Ratio = 0.00 and 0.05).
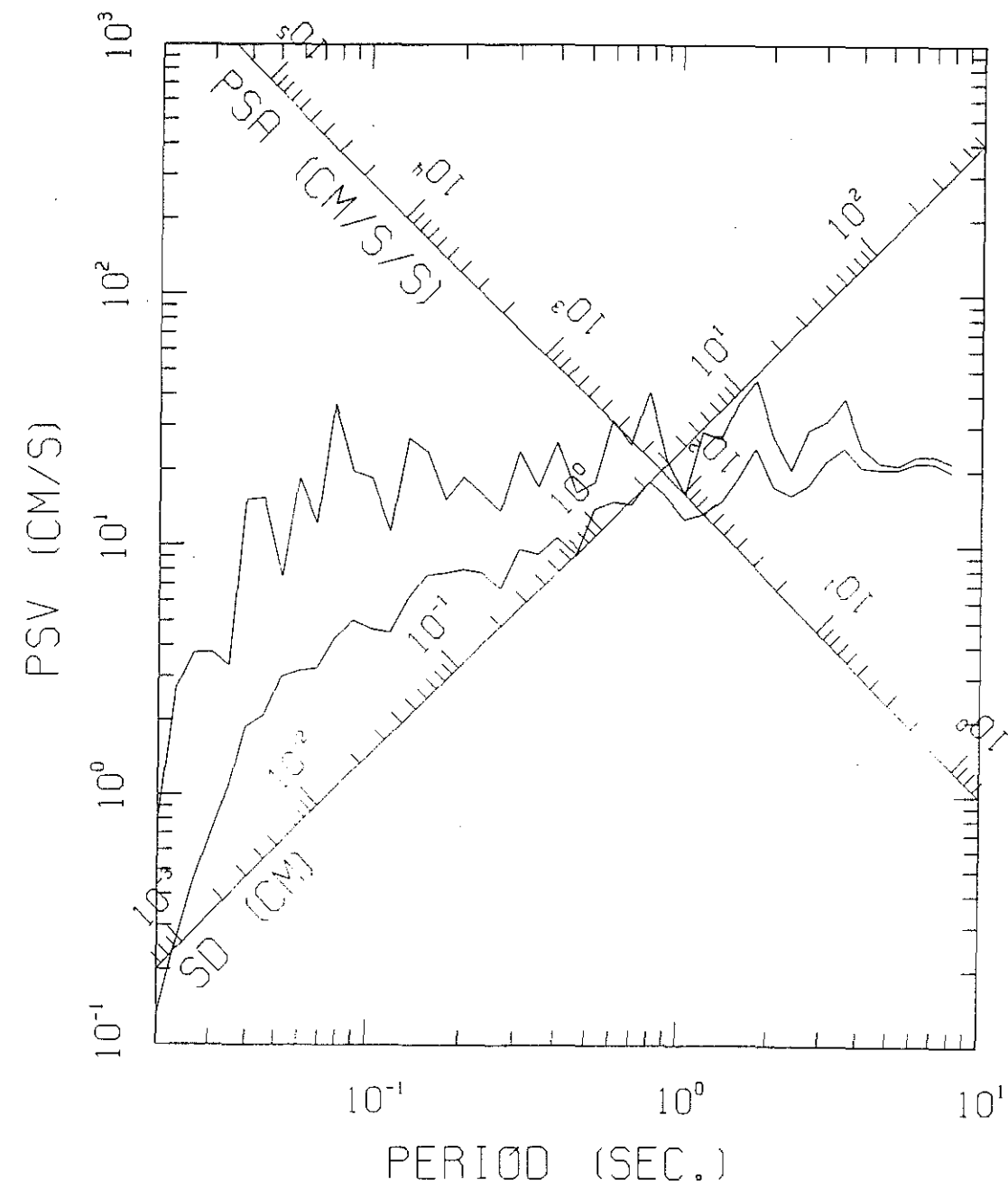
Figure B.42. Response Spectra for the Transverse Component of the 50-Year Event for Counties Identified by 0.09g-2 in Figure 4.3 (TR-50Y-0.09g-2, Damping Ratio = 0.00 and 0.05).

APPENDIX C:
TIME HISTORIES AND RESPONSE SPECTRA
FOR 500-YEAR EVENT

Figure C.1. Acceleration, Velocity, and Displacement Time History for the Horizontal Component of the 500-Year Event for Counties Identified by 0.60g-1 in Figure 4.3 (TR-500Y-0.60g-1).

Figure C.2. Acceleration, Velocity, and Displacement Time History for the Vertical Component of the 500-Year Event for Counties Identified by 0.60g-1 in Figure 4.3 (TR-500Y-0.60g-1).

Figure C.3. Acceleration, Velocity, and Displacement Time History for the Transverse Component of the 500-Year Event for Counties Identified by 0.60g-1 in Figure 4.3 (TR-500Y-0.60g-1).

Figure C.4. Response Spectra for the Horizontal Component of the 500-Year Event for Counties Identified by 0.60g-1 in Figure 4.3 (TR-500Y-0.60g-1, Damping Ratio = 0.00 and 0.05).
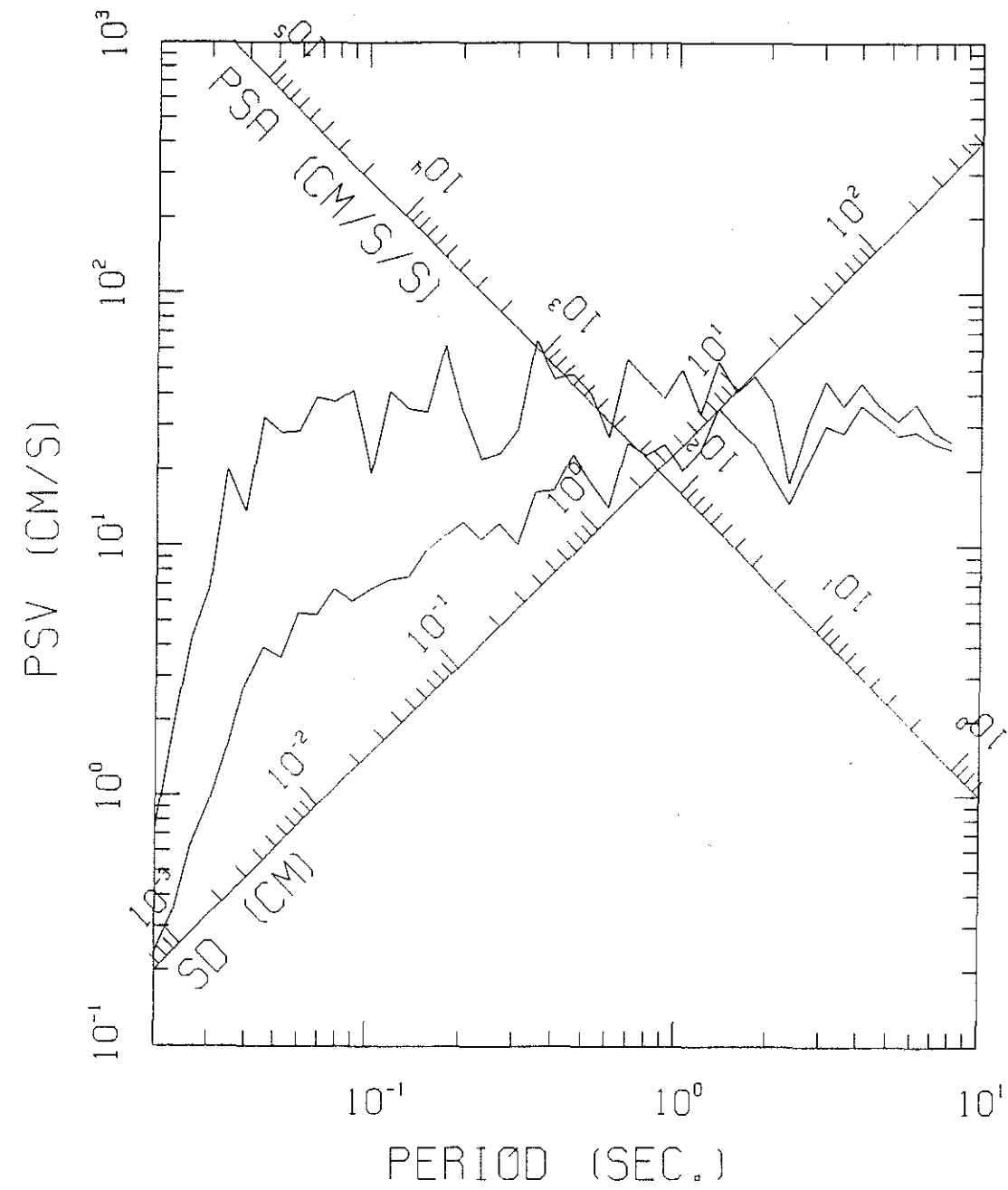
Figure C.5. Response Spectra for the Vertical Component of the 500-Year Event for Counties Identified by 0.60g-1 in Figure 4.3 (TR-500Y-0.60g-1, Damping Ratio = 0.00 and 0.05).

Figure C.6. Response Spectra for the Transverse Component of the 500-Year Event for Counties Identified by 0.60g-1 in Figure 4.3 (TR-500Y-0.60g-1, Damping Ratio = 0.00 and 0.05).
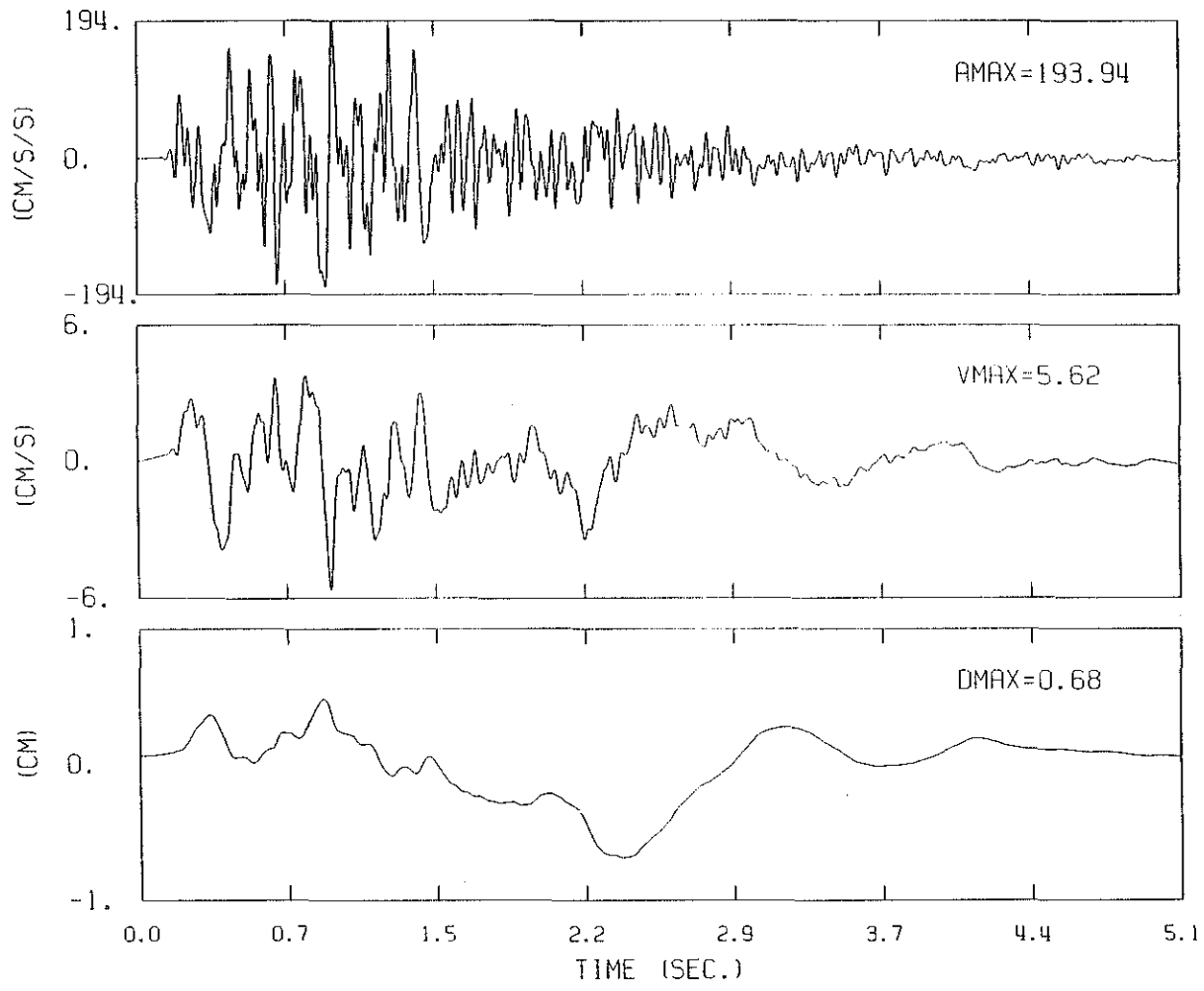
Figure C.7. Acceleration, Velocity, and Displacement Time History for the Horizontal Component of the 500-Year Event for Counties Identified by 0.40g-1 in Figure 4.3 (TR-500Y-0.40g-1).
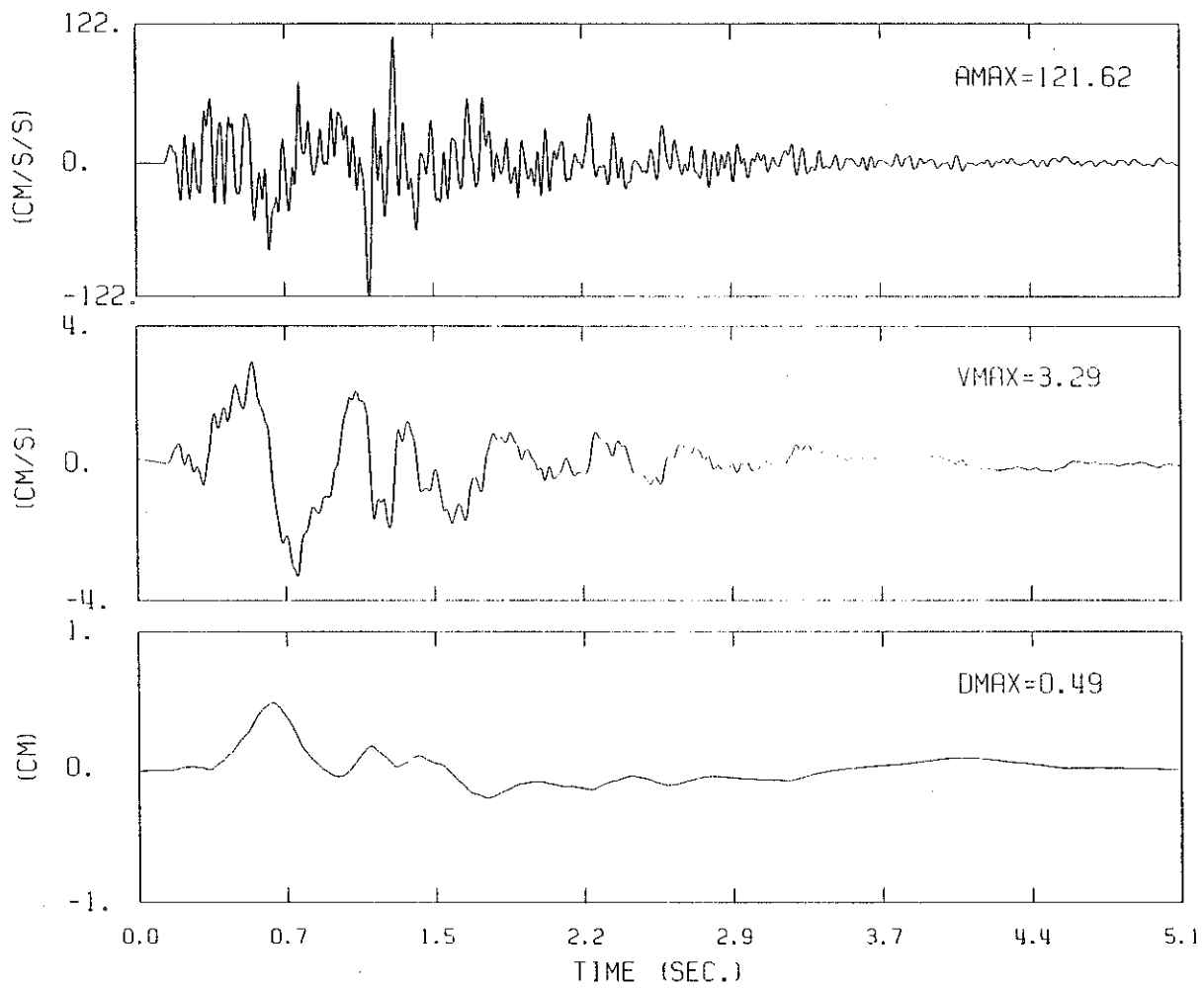
Figure C.8. Acceleration, Velocity, and Displacement Time History for the Vertical Component of the 500-Year Event for Counties Identified by 0.40g-1 in Figure 4.3 (TR-500Y-0.40g-1).
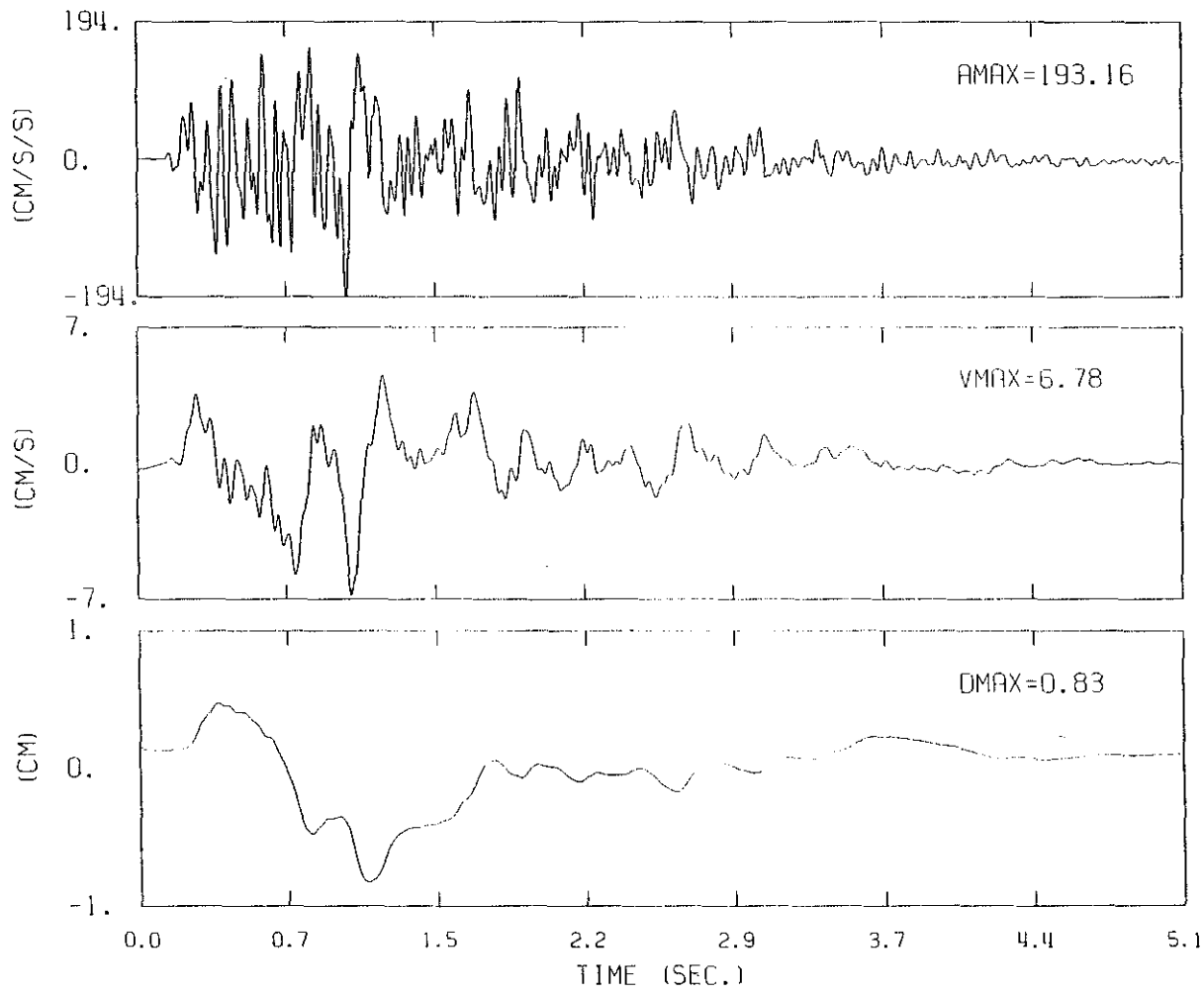
Figure C.9. Acceleration, Velocity, and Displacement Time History for the Transverse Component of the 500-Year Event for Counties Identified by 0.40g-1 in Figure 4.3 (TR-500Y-0.40g-1).
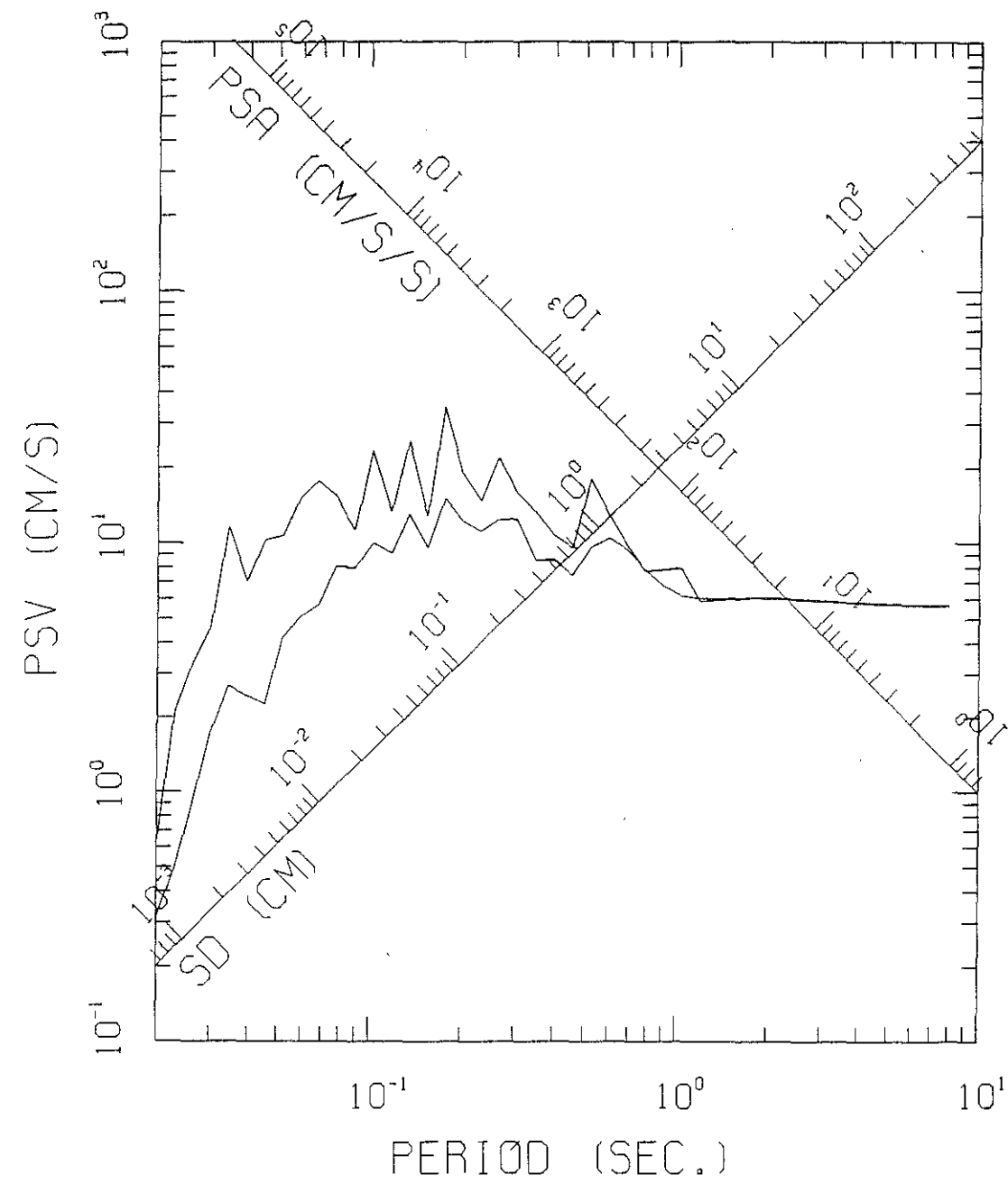
Figure C.10. Response Spectra for the Horizontal Component of the 500-Year Event for Counties Identified by 0.40g-1 in Figure 4.3 (TR-500Y-0.40g-1, Damping Ratio = 0.00 and 0.05).
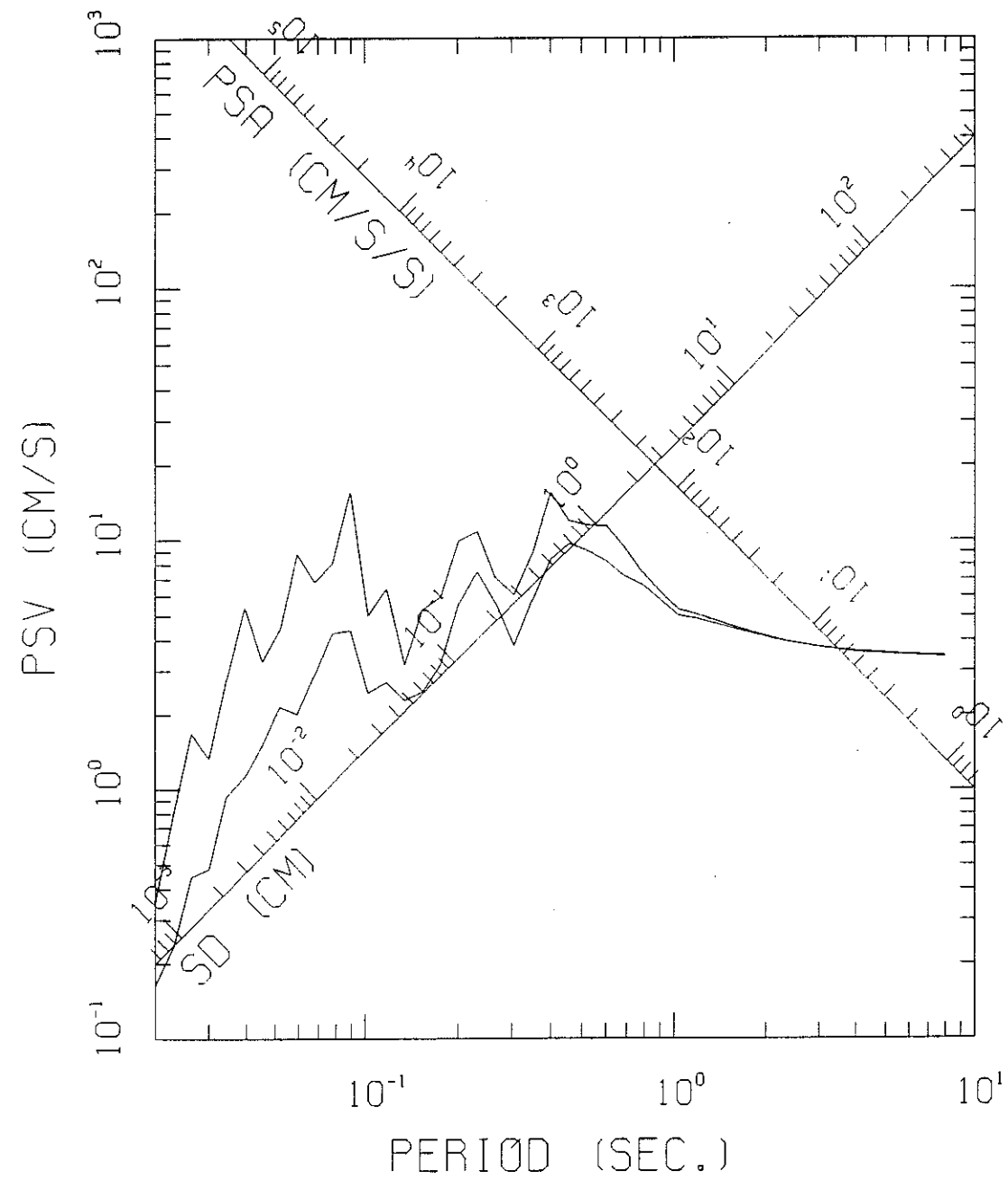
Figure C.11. Response Spectra for the Vertical Component of the 500-Year Event for Counties Identified by 0.40g-1 in Figure 4.3 (TR-500Y-0.40g-1, Damping Ratio = 0.00 and 0.05).
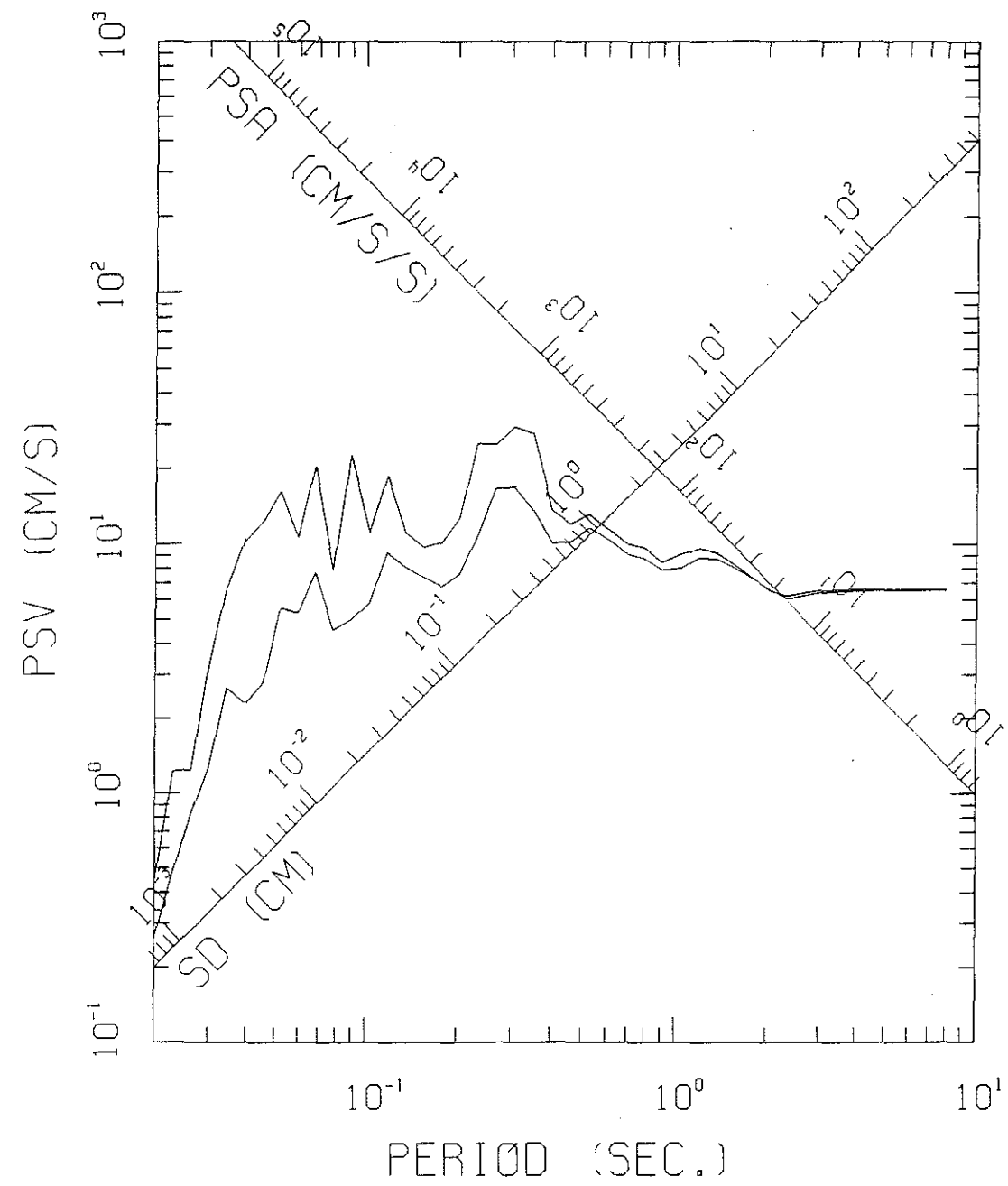
Figure C.12. Response Spectra for the Transverse Component of the 500-Year Event for Counties Identified by 0.40g-1 in Figure 4.3 (TR-500Y-0.40g-1, Damping Ratio = 0.00 and 0.05).
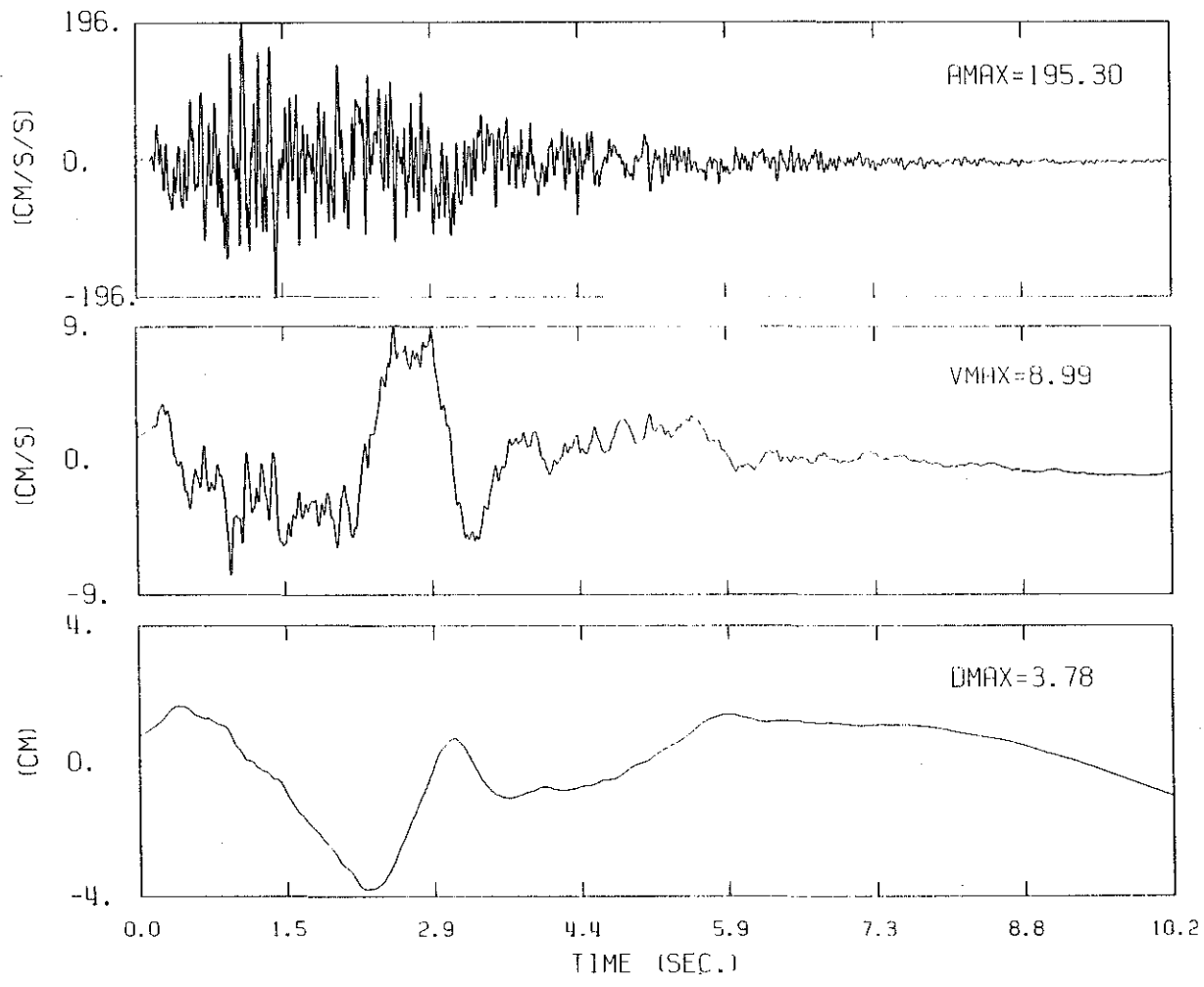
Figure C.13. Acceleration, Velocity, and Displacement Time History for the Horizontal Component of the 500-Year Event for Counties Identified by 0.30g-1 in Figure 4.3 (TR-500Y-0.30g-1).
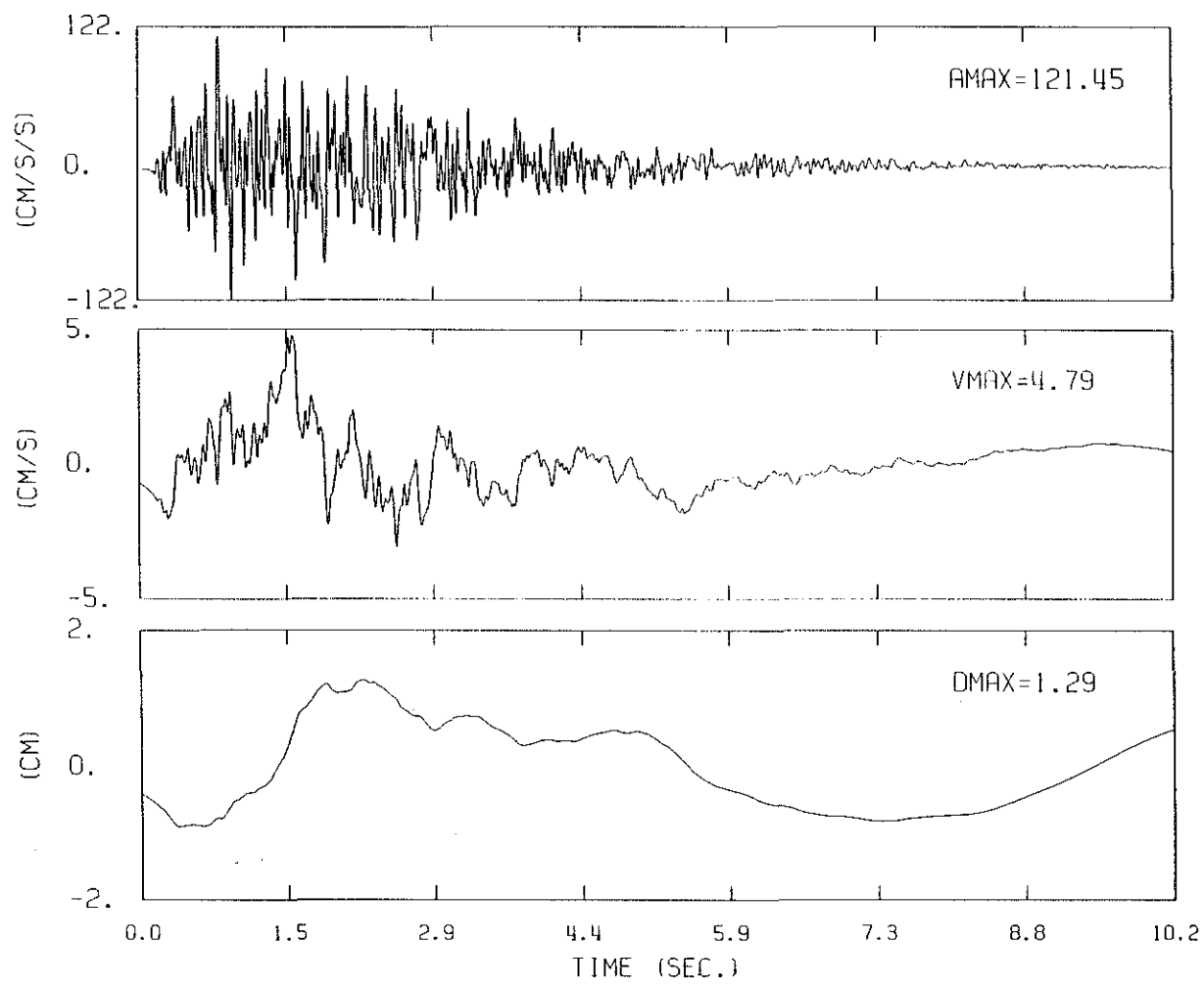
Figure C.14. Acceleration, Velocity, and Displacement Time History for the Vertical Component of the 500-Year Event for Counties Identified by 0.30g-1 in Figure 4.3 (TR-500Y-0.30g-1).

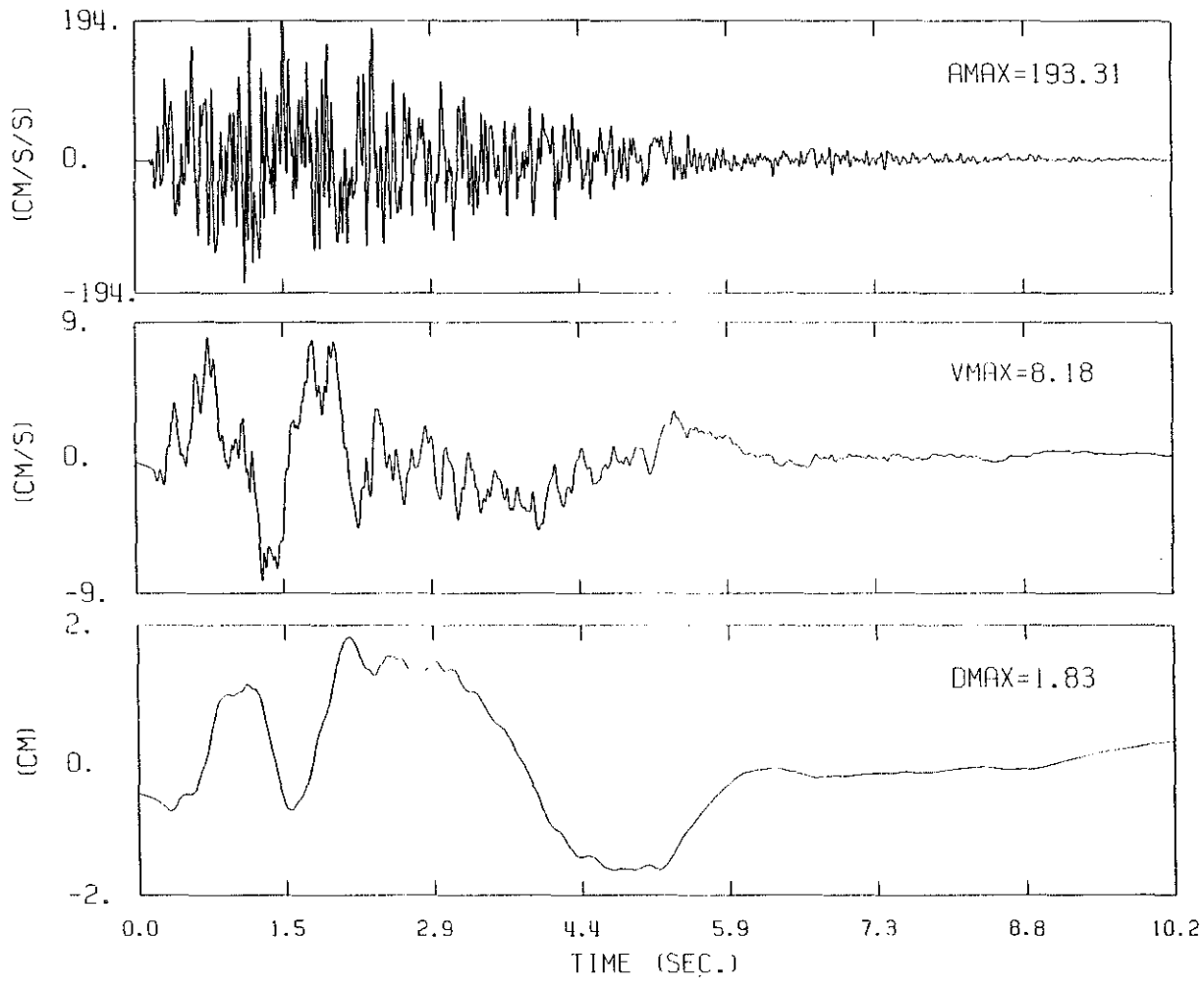**Figure C.15.** Acceleration, Velocity, and Displacement Time History for the Transverse Component of the 500-Year Event for Counties Identified by 0.30g-1 in Figure 4.3 (TR-500Y-0.30g-1).
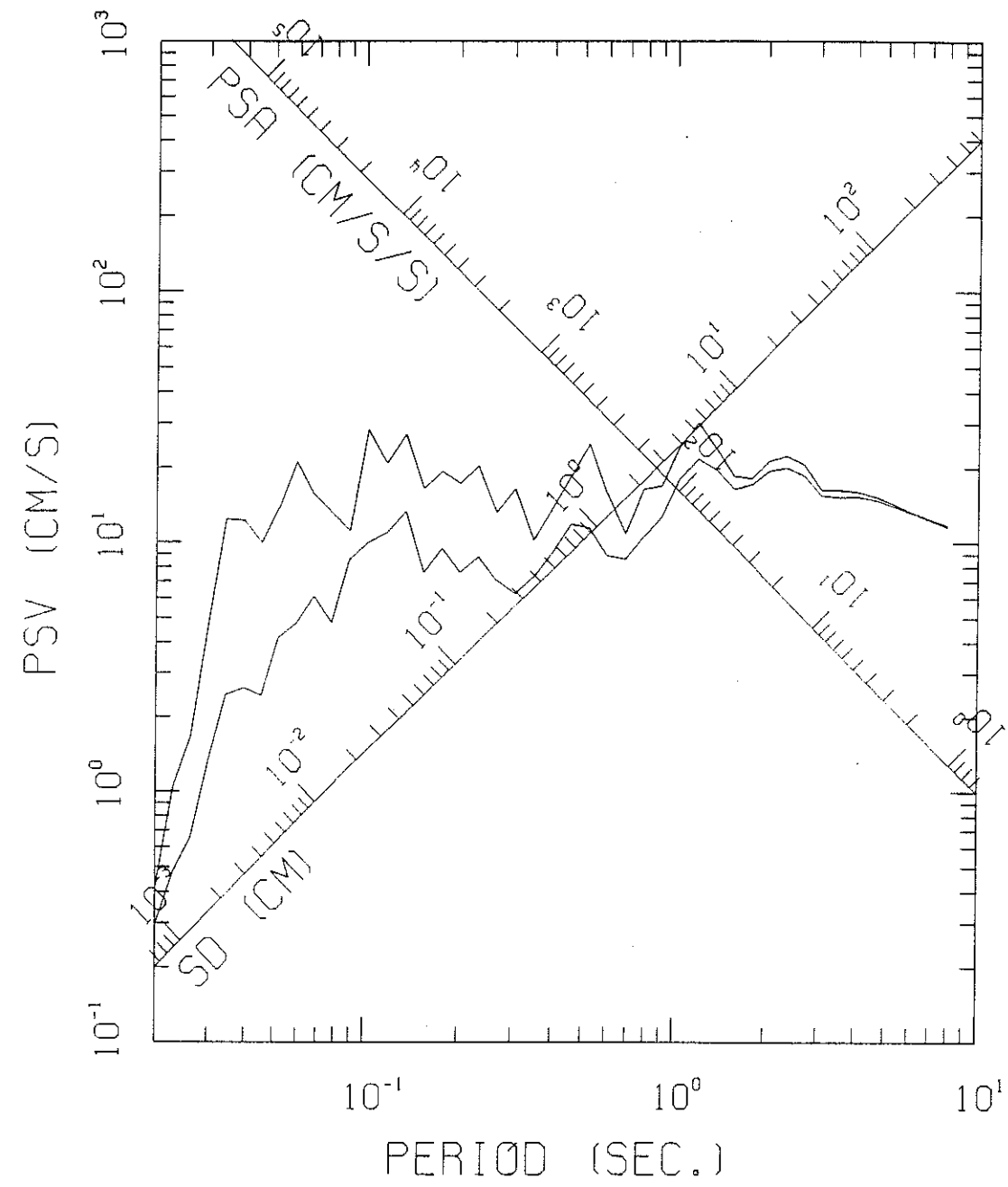
Figure C.16. Response Spectra for the Horizontal Component of the 500-Year Event for Counties Identified by 0.30g-1 in Figure 4.3 (TR-500Y-0.30g-1, Damping Ratio = 0.00 and 0.05).

Figure C.17. Response Spectra for the Vertical Component of the 500-Year Event for Counties Identified by 0.30g-1 in Figure 4.3 (TR-500Y-0.30g-1, Damping Ratio = 0.00 and 0.05).

Figure C.18. Response Spectra for the Transverse Component of the 500-Year Event for Counties Identified by 0.30g-1 in Figure 4.3 (TR-500Y-0.30g-1, Damping Ratio = 0.00 and 0.05).

Figure C.19. Acceleration, Velocity, and Displacement Time History for the Horizontal Component of the 500-Year Event for Counties Identified by 0.19g-1 in Figure 4.3 (TR-500Y-0.19g-1).

Figure C.20. Acceleration, Velocity, and Displacement Time History for the Vertical Component of the 500-Year Event for Counties Identified by 0.19g-1 in Figure 4.3 (TR-500Y-0.19g-1).

Figure C.21. Acceleration, Velocity, and Displacement Time History for the Transverse Component of the 500-Year Event for Counties Identified by 0.19g-1 in Figure 4.3 (TR-500Y-0.19g-1).

Figure C.22. Response Spectra for the Horizontal Component of the 500-Year Event for Counties Identified by 0.19g-1 in Figure 4.3 (TR-500Y-0.19g-1, Damping Ratio = 0.00 and 0.05).
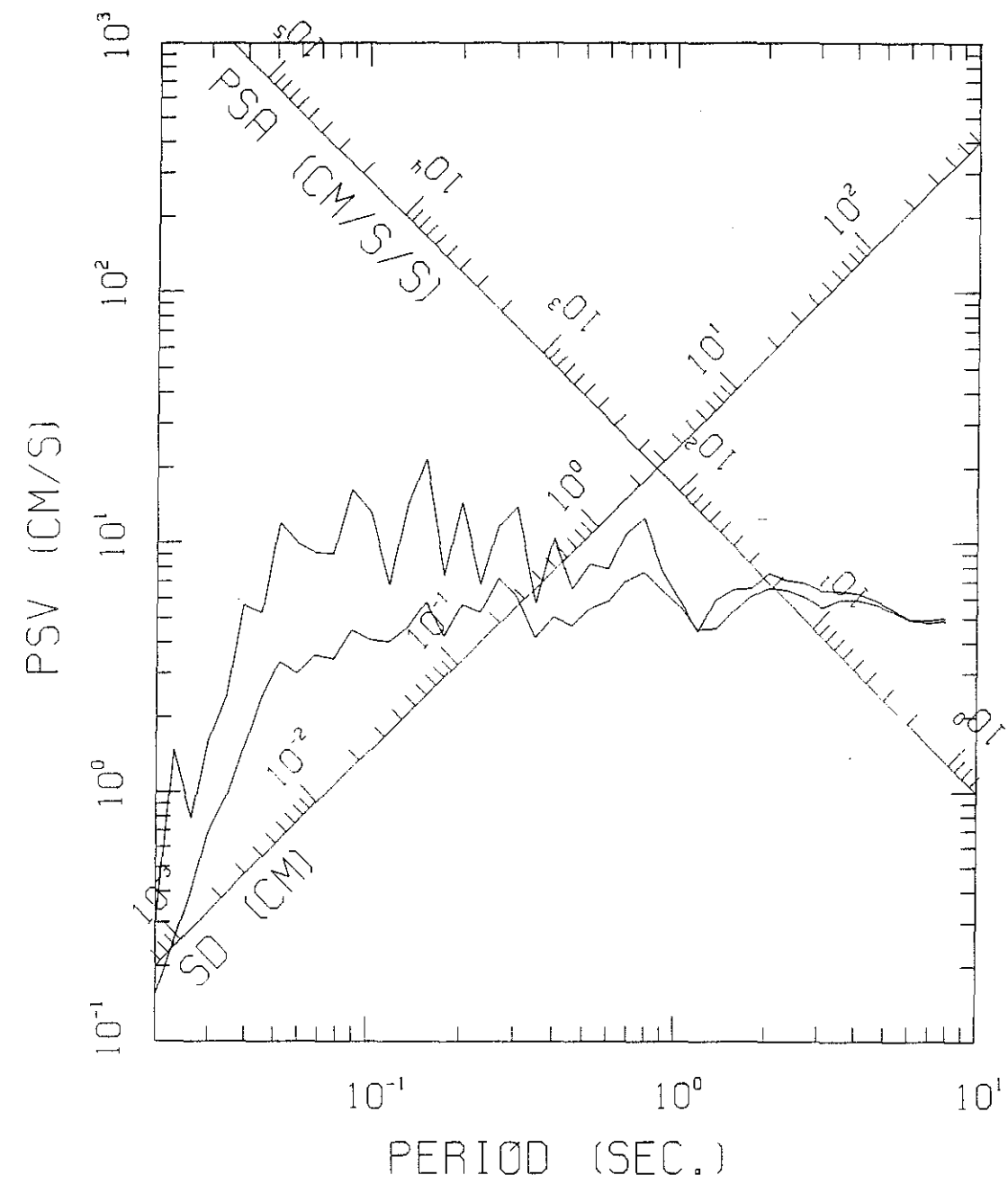
Figure C.23. Response Spectra for the Vertical Component of the 500-Year Event for Counties Identified by 0.19g-1 in Figure 4.3 (TR-500Y-0.19g-1, Damping Ratio = 0.00 and 0.05).
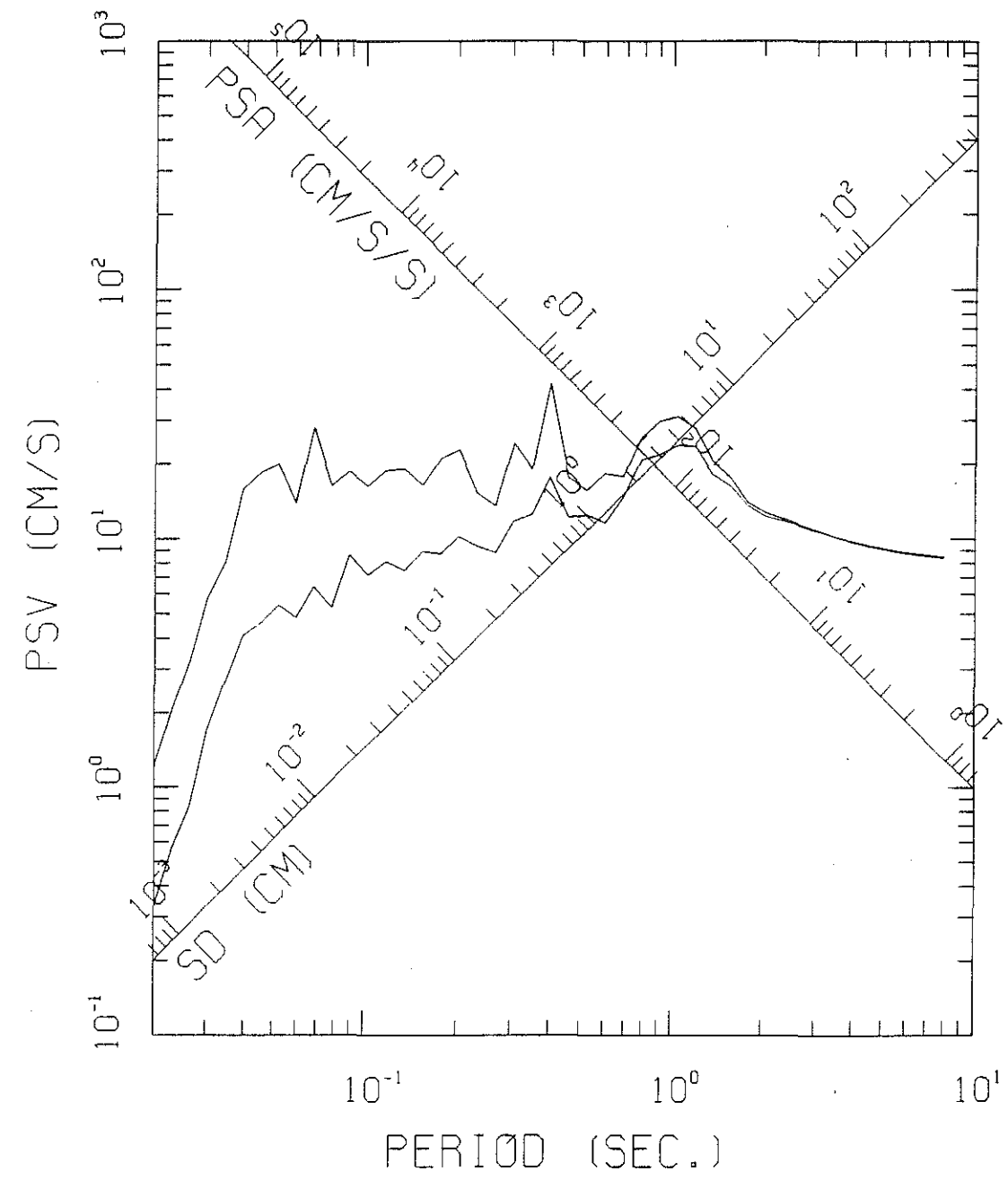
Figure C.24. Response Spectra for the Transverse Component of the 500-Year Event for Counties Identified by 0.19g-1 in Figure 4.3 (TR-500Y-0.19g-1, Damping Ratio = 0.00 and 0.05).
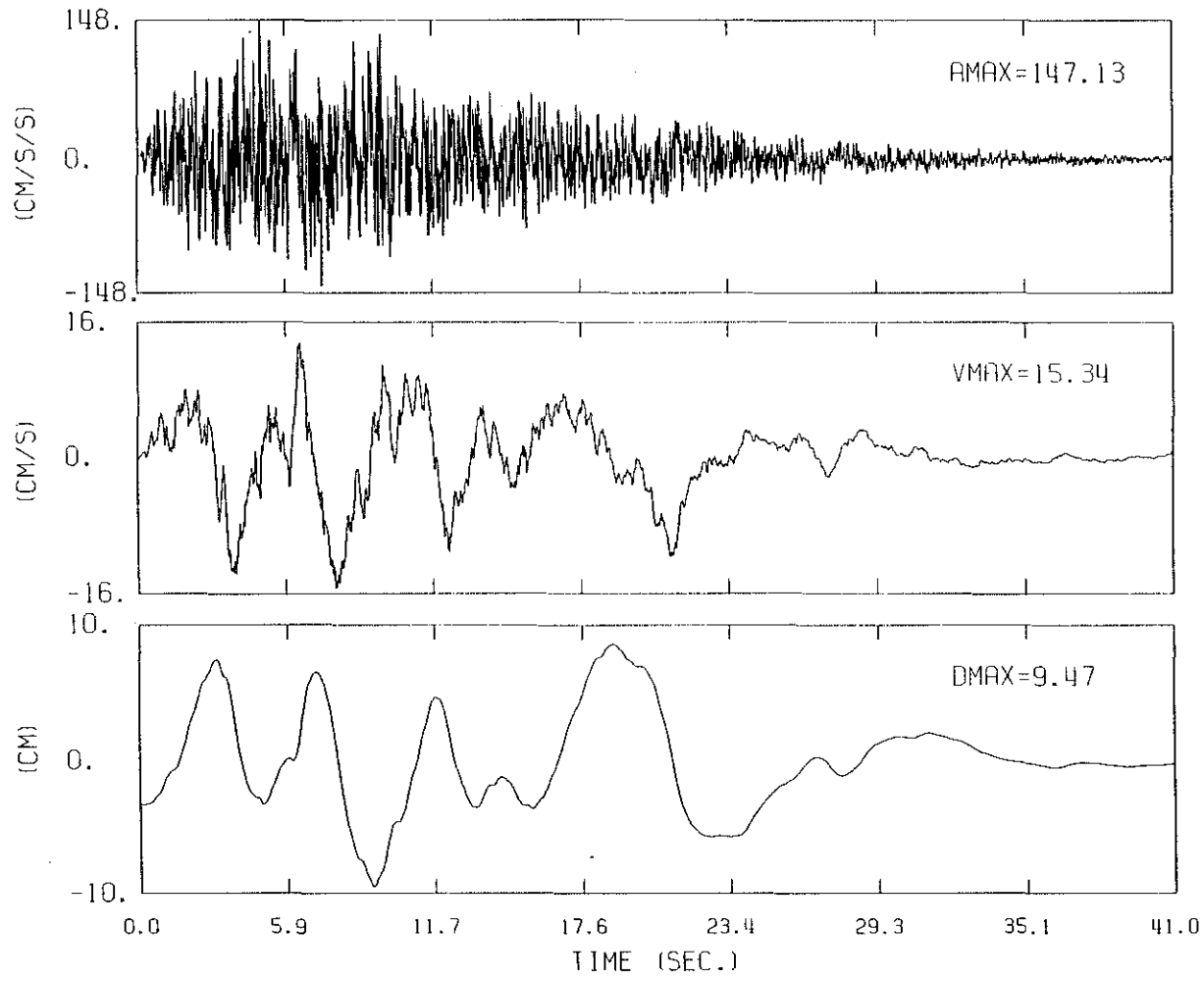
Figure C.25. Acceleration, Velocity, and Displacement Time History for the Horizontal Component of the 500-Year Event for Counties Identified by 0.19g-2 in Figure 4.3 (TR-500Y-0.19g-2).
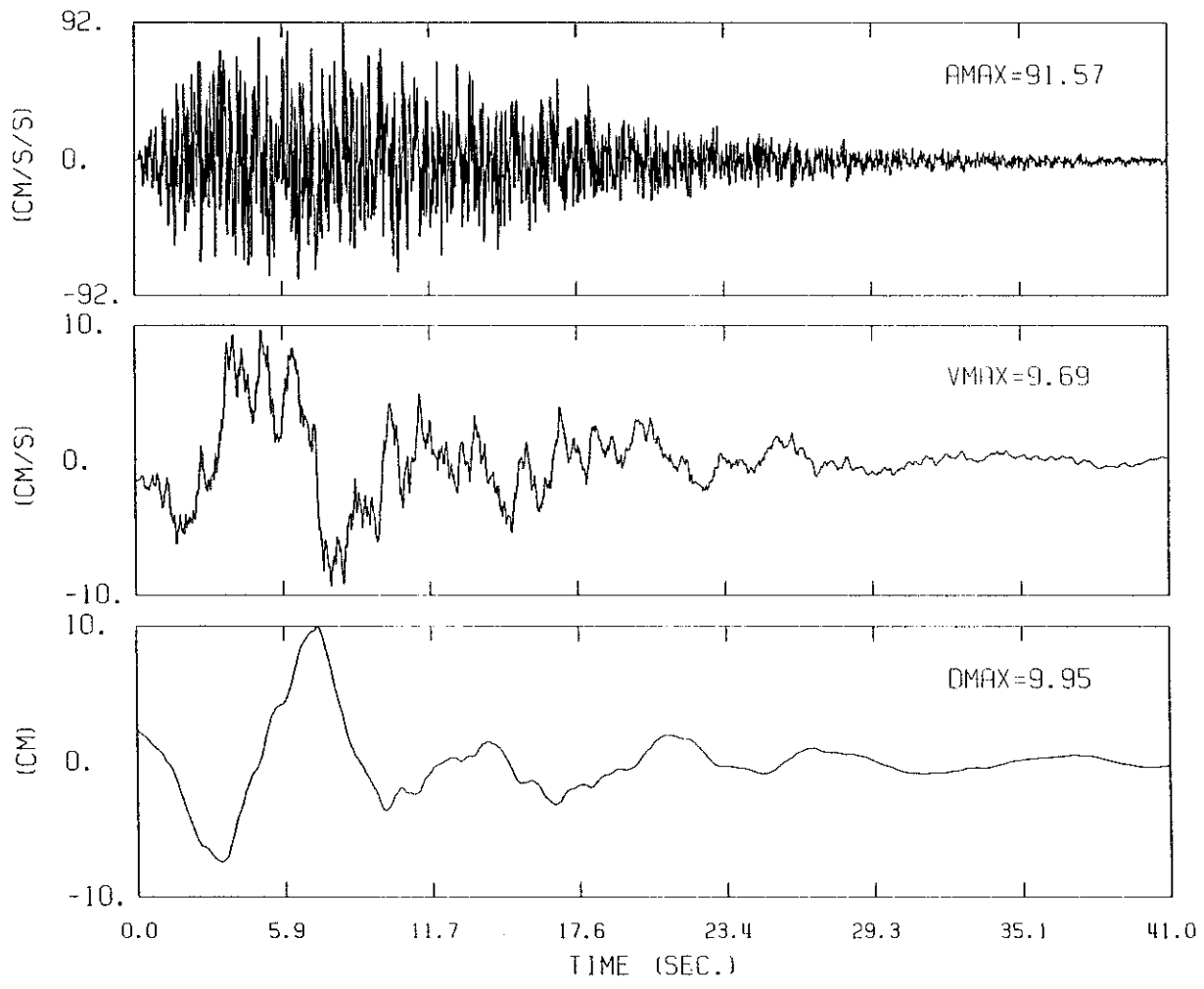
Figure C.26. Acceleration, Velocity, and Displacement Time History for the Vertical Component of the 500-Year Event for Counties Identified by 0.19g-2 in Figure 4.3 (TR-500Y-0.19g-2).
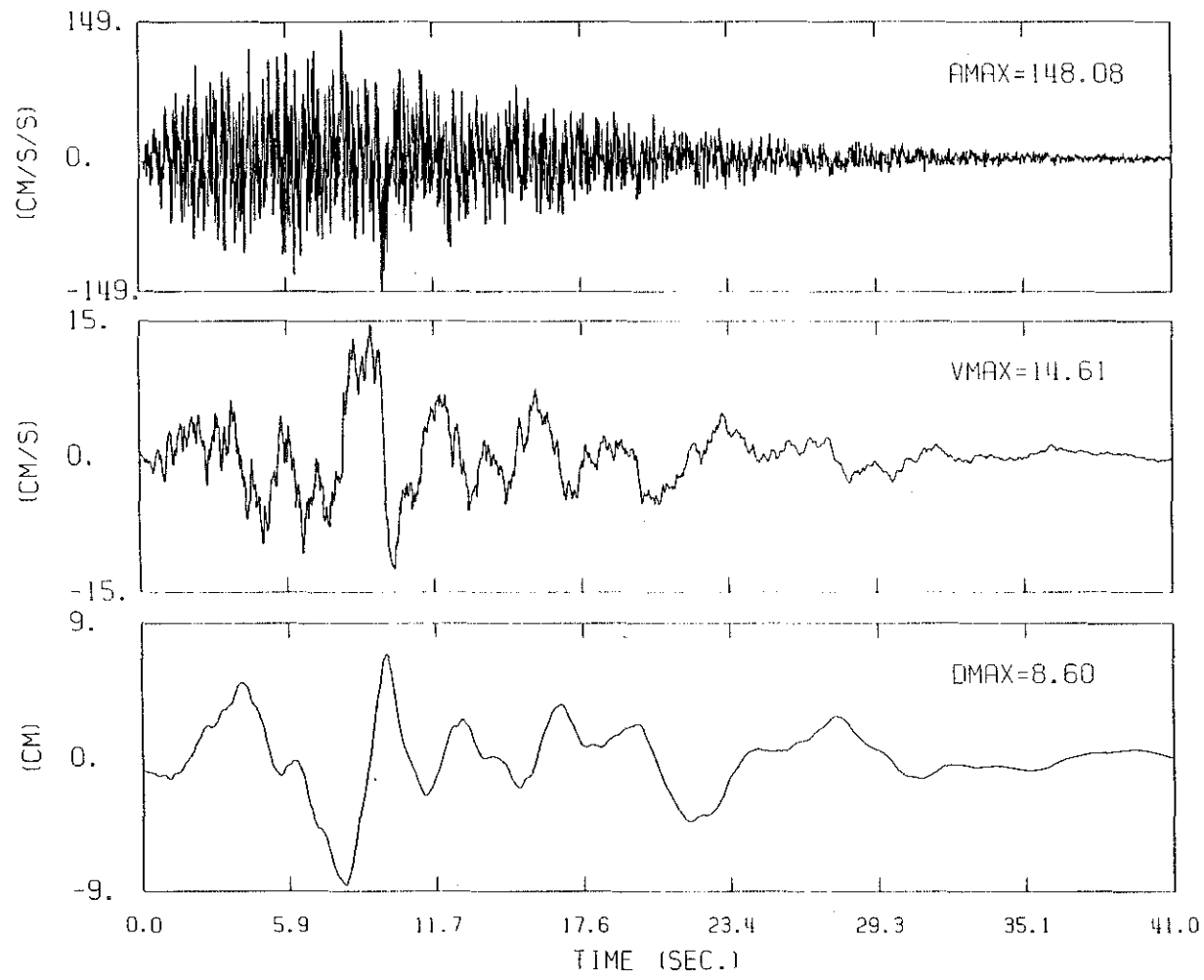
Figure C.27. Acceleration, Velocity, and Displacement Time History for the Transverse Component of the 500-Year Event for Counties Identified by 0.19g-2 in Figure 4.3 (TR-500Y-0.19g-2).
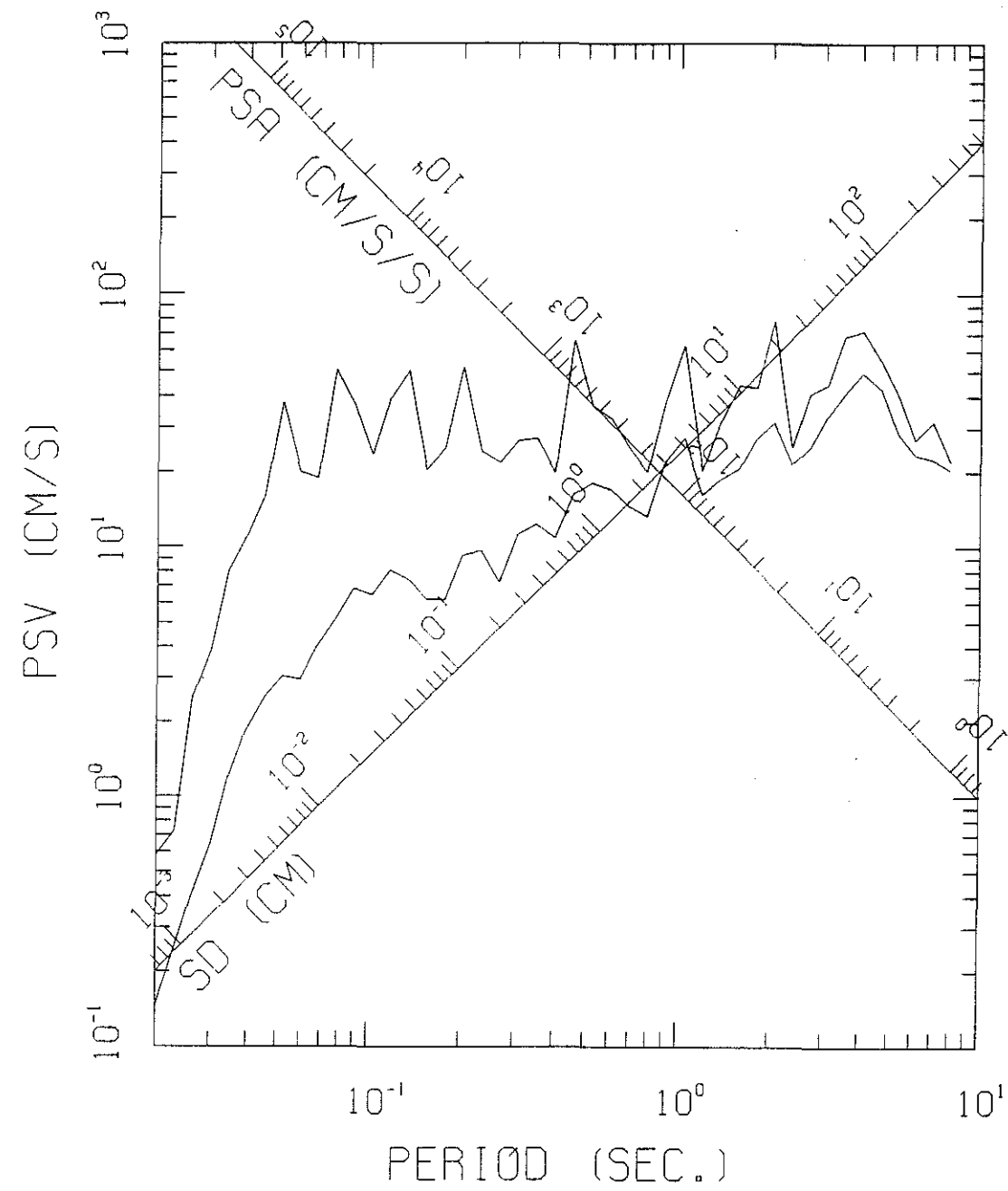
Figure C.28. Response Spectra for the Horizontal Component of the 500-Year Event for Counties Identified by 0.19g-2 in Figure 4.3 (TR-500Y-0.19g-2, Damping Ratio = 0.00 and 0.05).
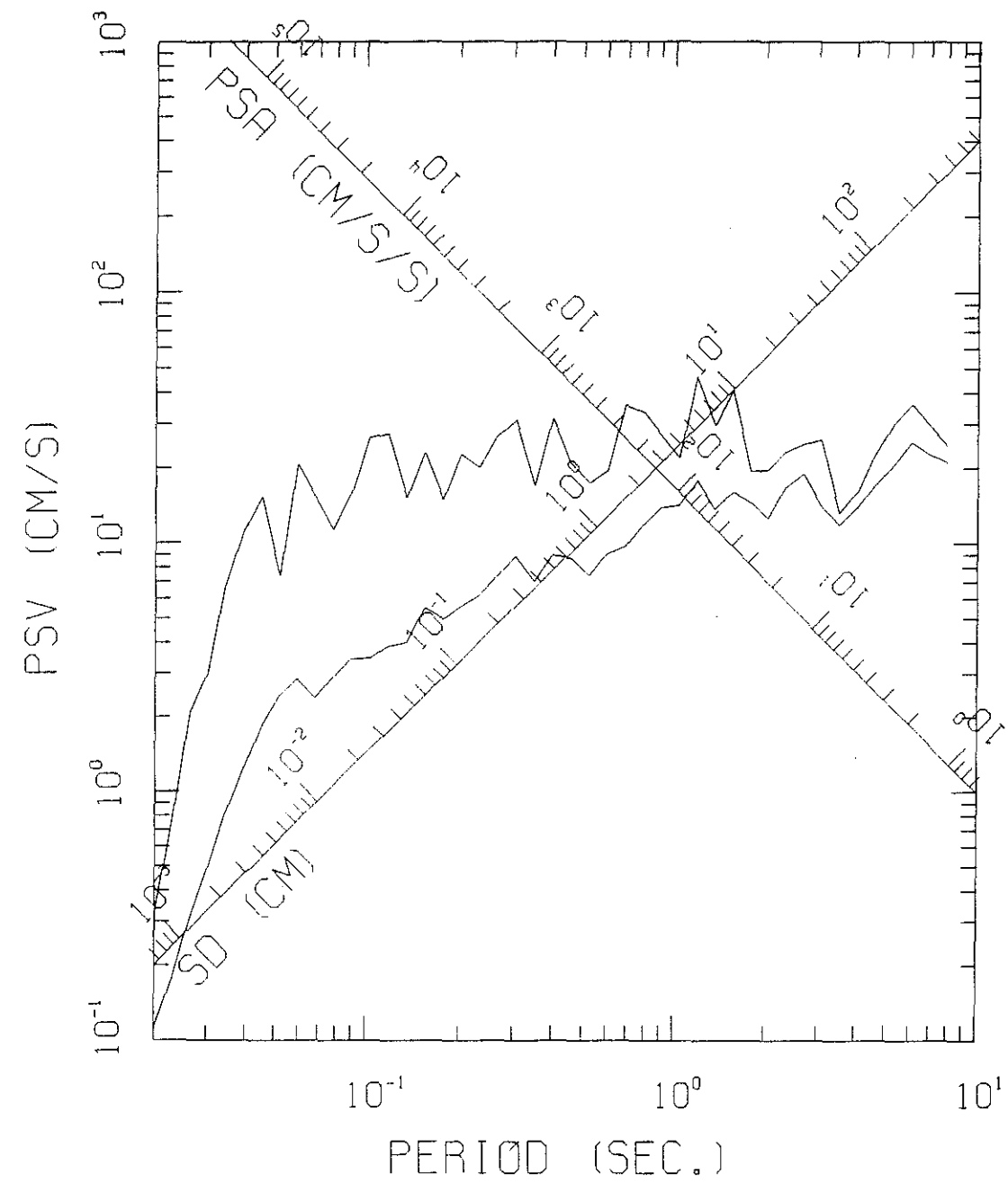
Figure C.29. Response Spectra for the Vertical Component of the 500-Year Event for Counties Identified by 0.19g-2 in Figure 4.3 (TR-500Y-0.19g-2, Damping Ratio = 0.00 and 0.05).
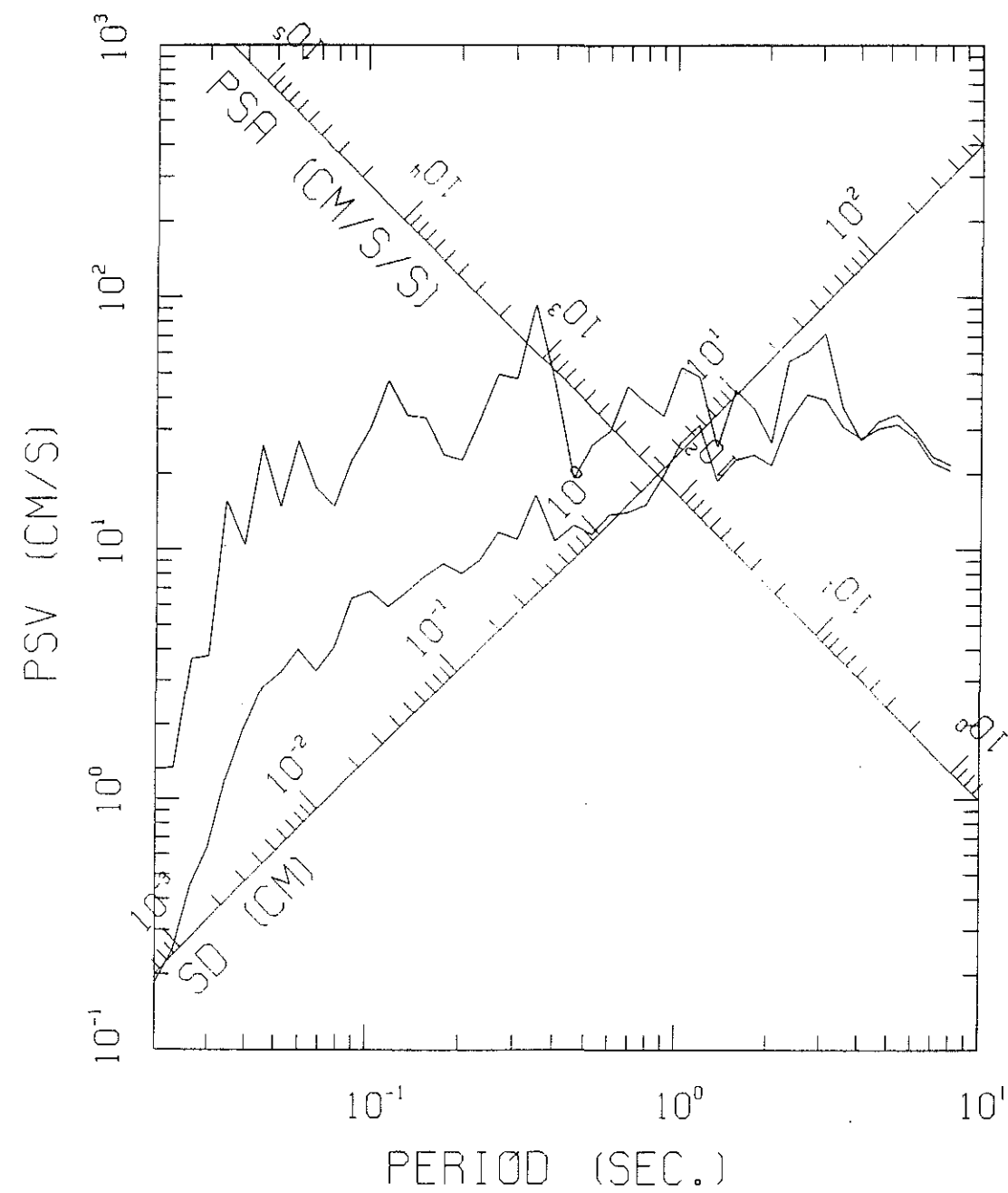
Figure C.30. Response Spectra for the Transverse Component of the 500-Year Event for Counties Identified by 0.19g-2 in Figure 4.3 (TR-500Y-0.19g-2, Damping Ratio = 0.00 and 0.05).

Figure C.31. Acceleration, Velocity, and Displacement Time History for the Horizontal Component of the 500-Year Event for Counties Identified by 0.19g-3 in Figure 4.3 (TR-500Y-0.19g-3).

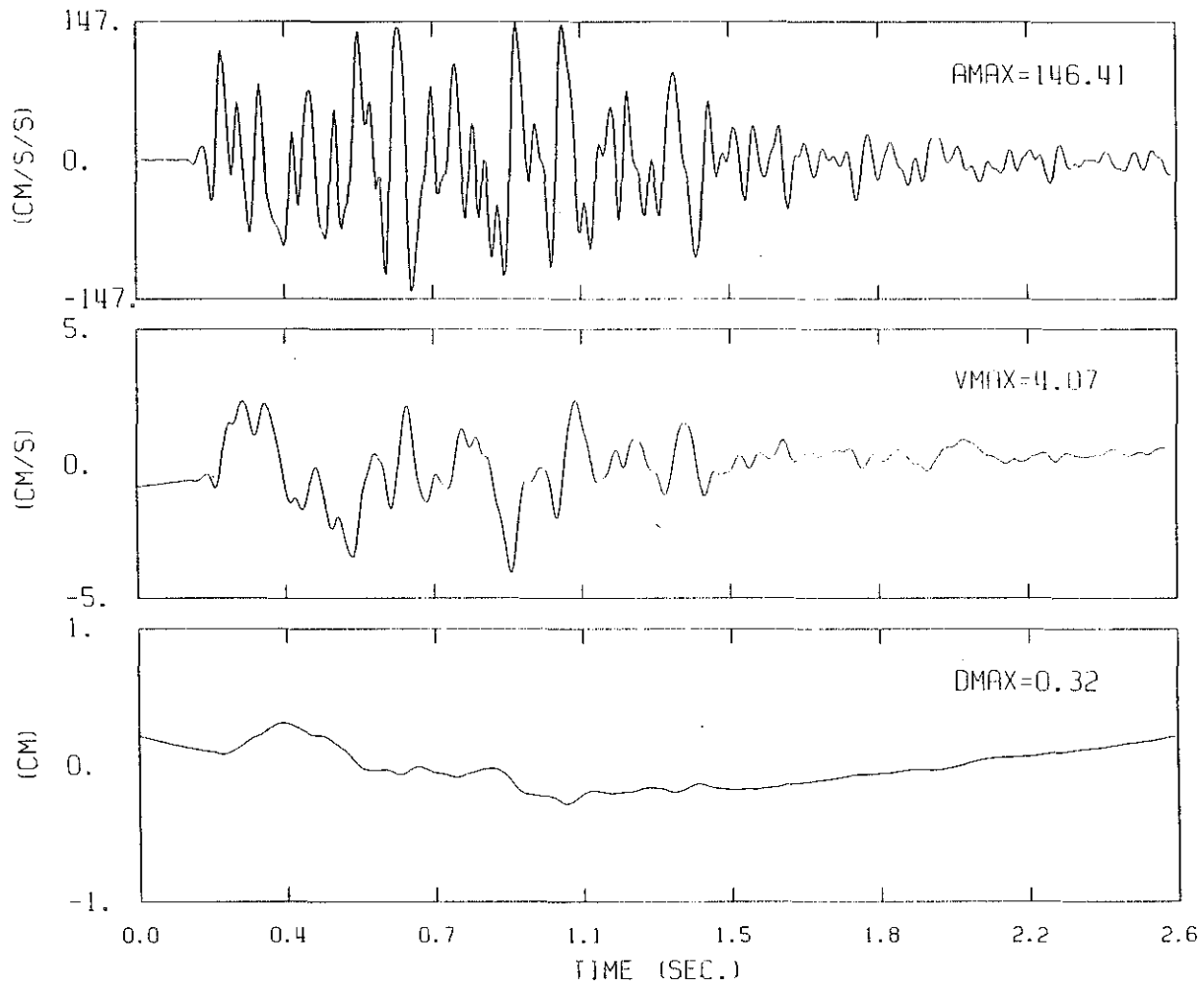**Figure C.32. Acceleration, Velocity, and Displacement Time History for the Vertical Component of the 500-Year Event for Counties Identified by 0.19g-3 in Figure 4.3 (TR-500Y-0.19g-3).**

Figure C.33. Acceleration, Velocity, and Displacement Time History for the Transverse Component of the 500-Year Event for Counties Identified by 0.19g-3 in Figure 4.3 (TR-500Y-0.19g-3).

Figure C.34. Response Spectra for the Horizontal Component of the 500-Year Event for Counties Identified by 0.19g-3 in Figure 4.3 (TR-500Y-0.19g-3, Damping Ratio = 0.00 and 0.05).

Figure C.35. Response Spectra for the Vertical Component of the 500-Year Event for Counties Identified by 0.19g-3 in Figure 4.3 (TR-500Y-0.19g-3, Damping Ratio = 0.00 and 0.05).

Figure C.36. **Response Spectra for the Transverse Component of the 500-Year Event for Counties Identified by 0.19g-3 in Figure 4.3 (TR-500Y-0.19g-3, Damping Ratio = 0.00 and 0.05).**

Figure C.37. Acceleration, Velocity, and Displacement Time History for the Horizontal Component of the 500-Year Event for Counties Identified by 0.15g-1 in Figure 4.3 (TR-500Y-0.15g-1).
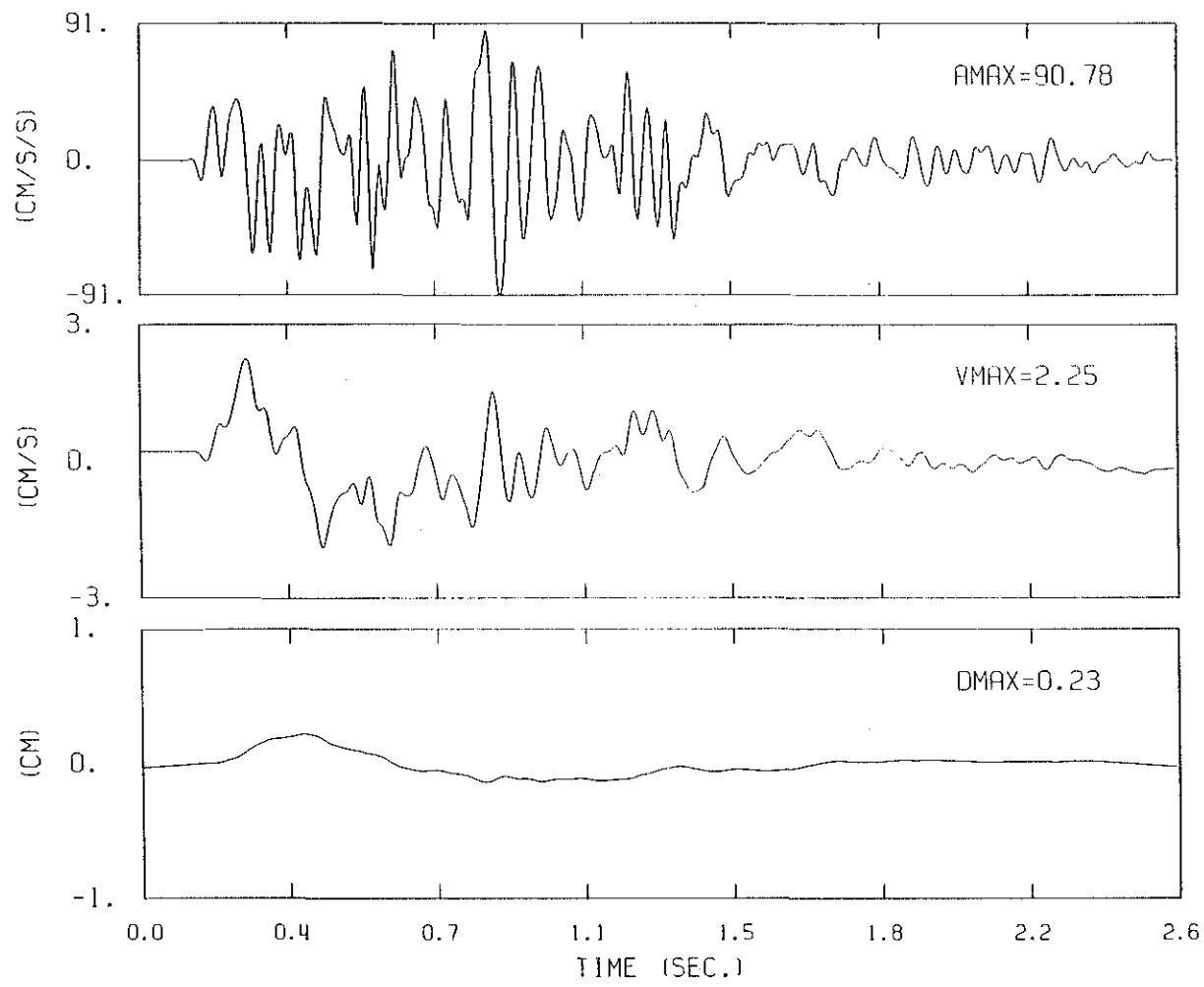
Figure C.38. Acceleration, Velocity, and Displacement Time History for the Vertical Component of the 500-Year Event for Counties Identified by 0.15g-1 in Figure 4.3 (TR-500Y-0.15g-1).
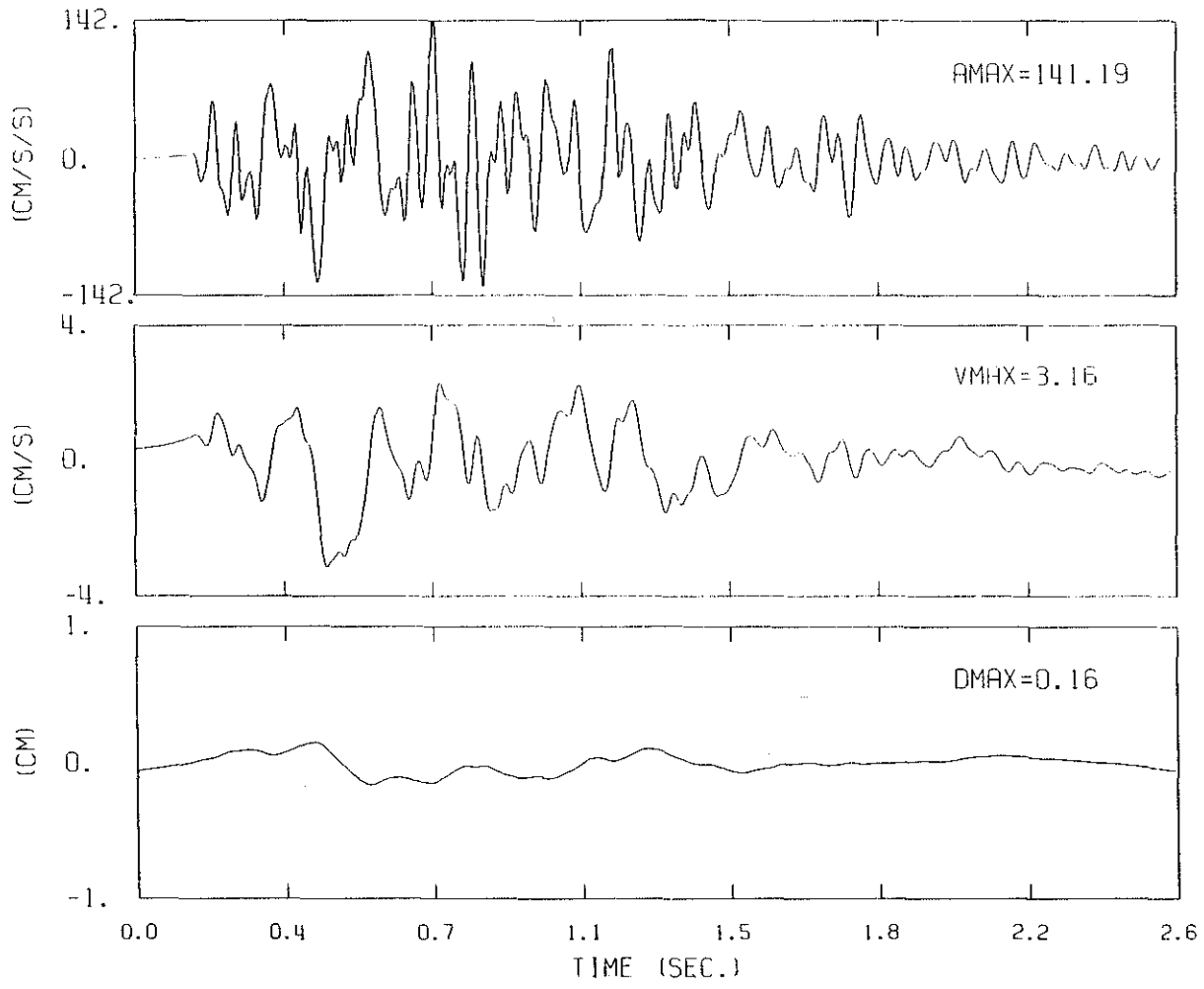
Figure C.39. Acceleration, Velocity, and Displacement Time History for the Transverse Component of the 500-Year Event for Counties Identified by 0.15g-1 in Figure 4.3 (TR-500Y-0.15g-1).
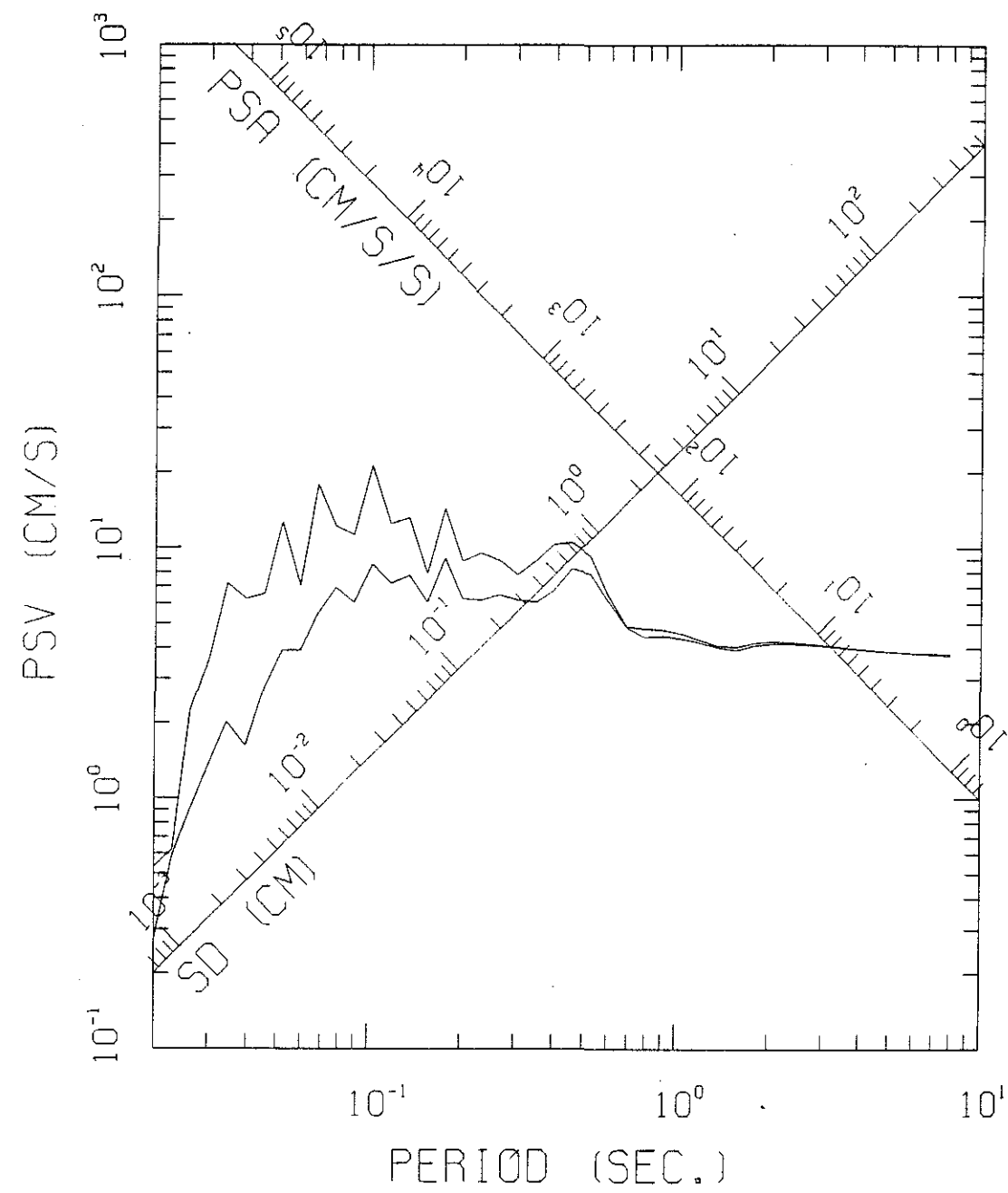
Figure C.40. Response Spectra for the Horizontal Component of the 500-Year Event for Counties Identified by 0.15g-1 in Figure 4.3 (TR-500Y-0.15g-1, Damping Ratio = 0.00 and 0.05).
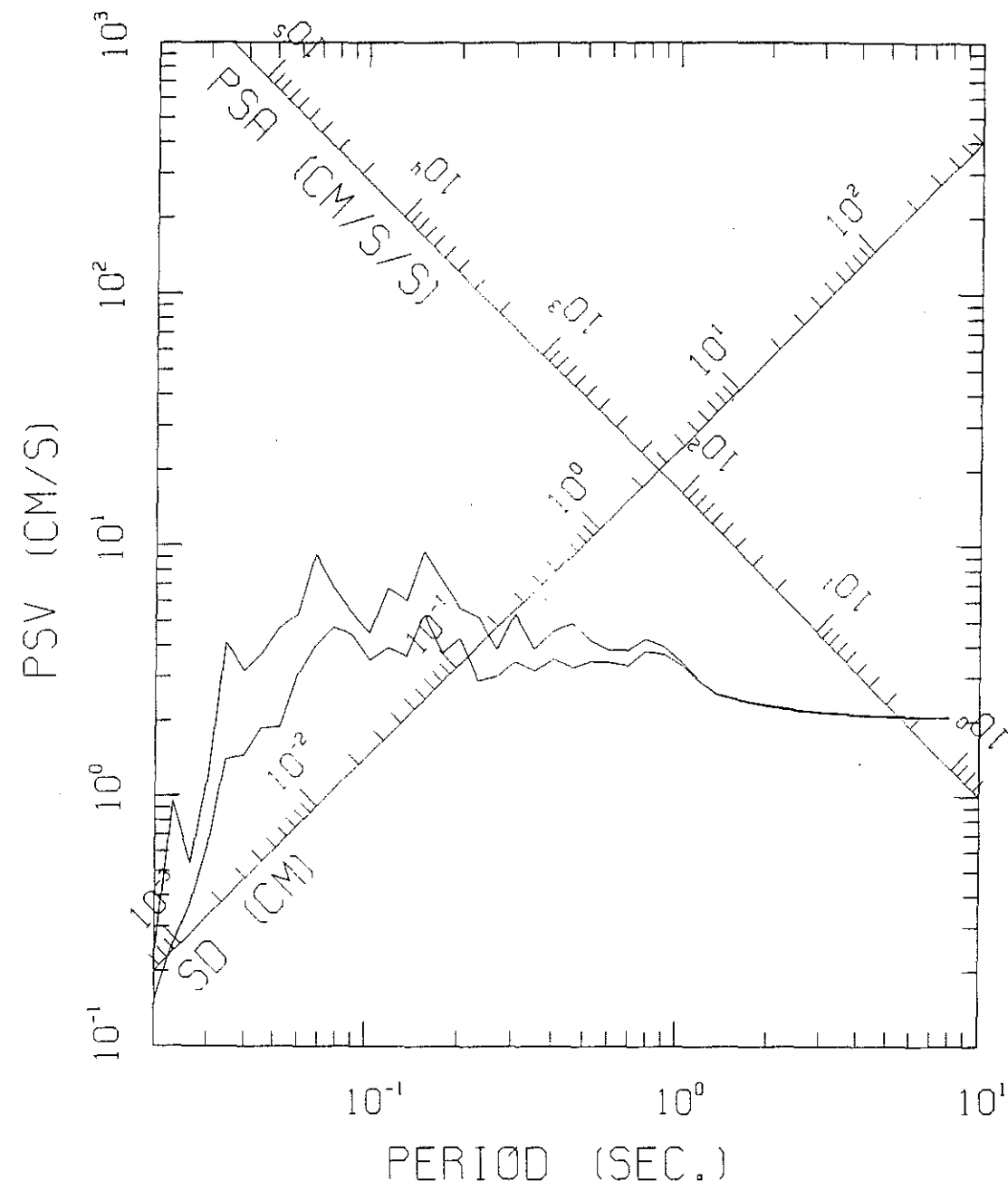
Figure C.41. Response Spectra for the Vertical Component of the 500-Year Event for Counties Identified by 0.15g-1 in Figure 4.3 (TR-500Y-0.15g-1, Damping Ratio = 0.00 and 0.05).
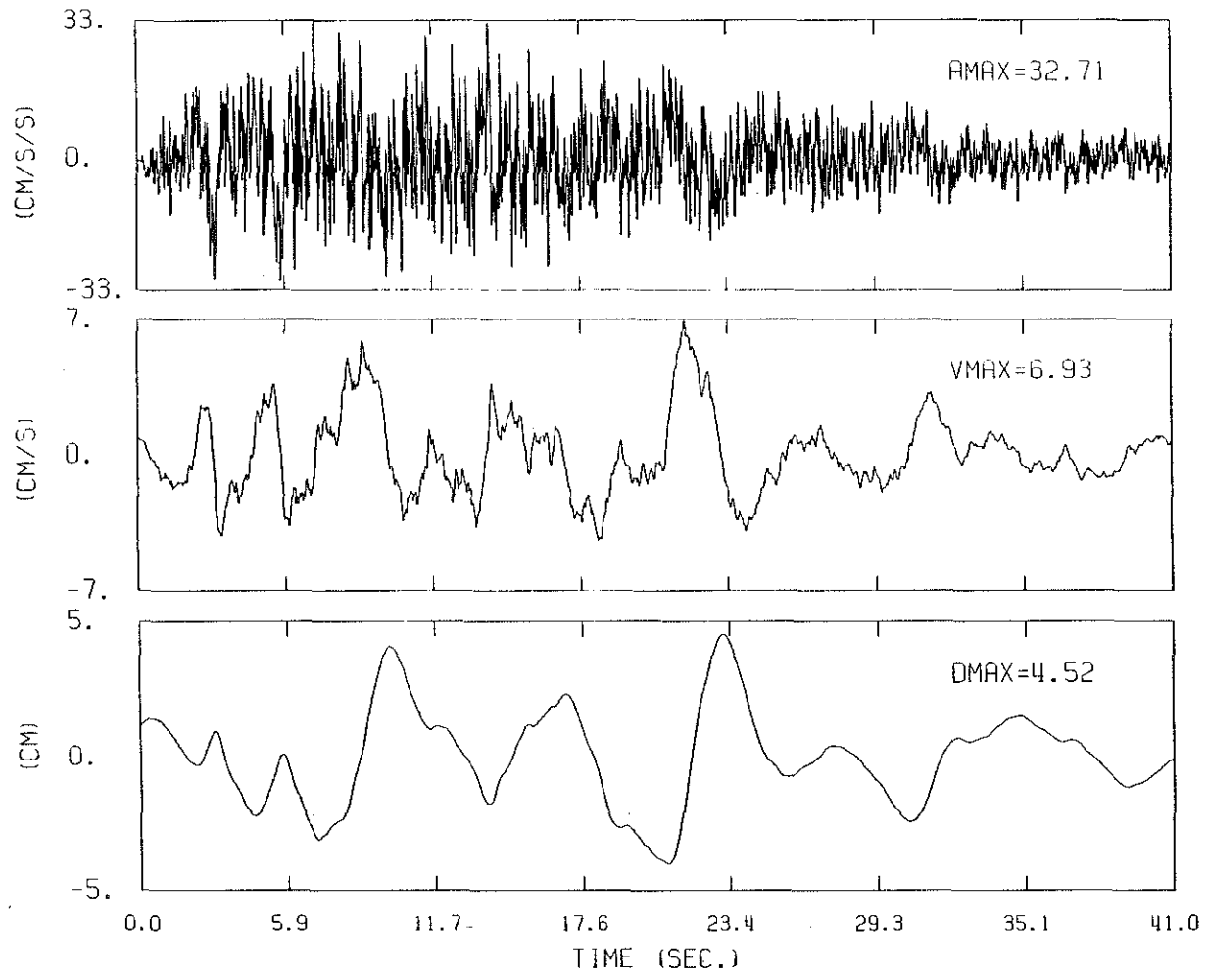
Figure C.42. Response Spectra for the Transverse Component of the 500-Year Event for Counties Identified by 0.15g-1 in Figure 4.3 (TR-500Y-0.15g-1, Damping Ratio = 0.00 and 0.05).

Figure C.43. Acceleration, Velocity, and Displacement Time History for the Horizontal Component of the 500-Year Event for Counties Identified by 0.15g-2 in Figure 4.3 (TR-500Y-0.15g-2).
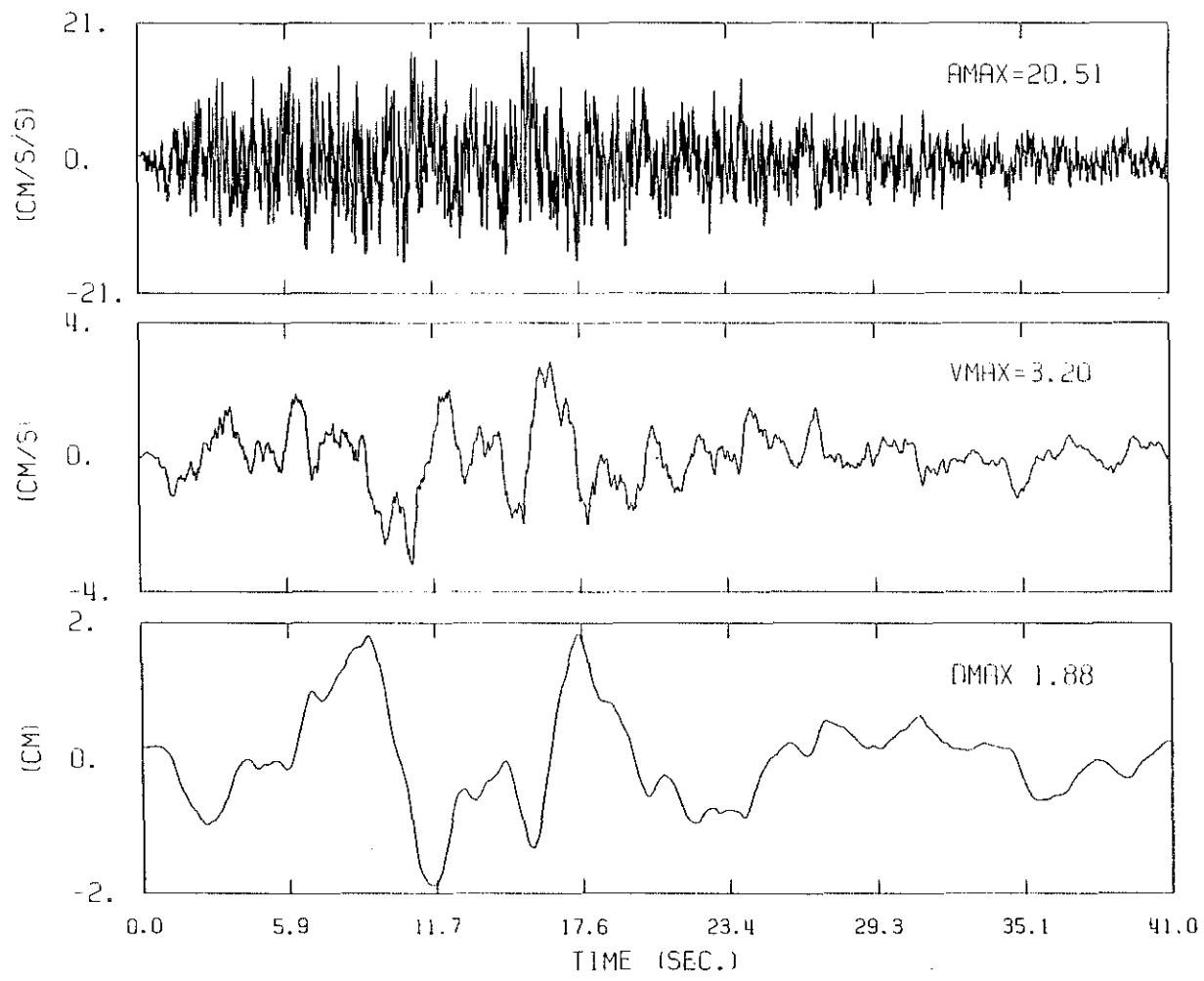
Figure C.44. Acceleration, Velocity, and Displacement Time History for the Vertical Component of the 500-Year Event for Counties Identified by 0.15g-2 in Figure 4.3 (TR-500Y-0.15g-2).
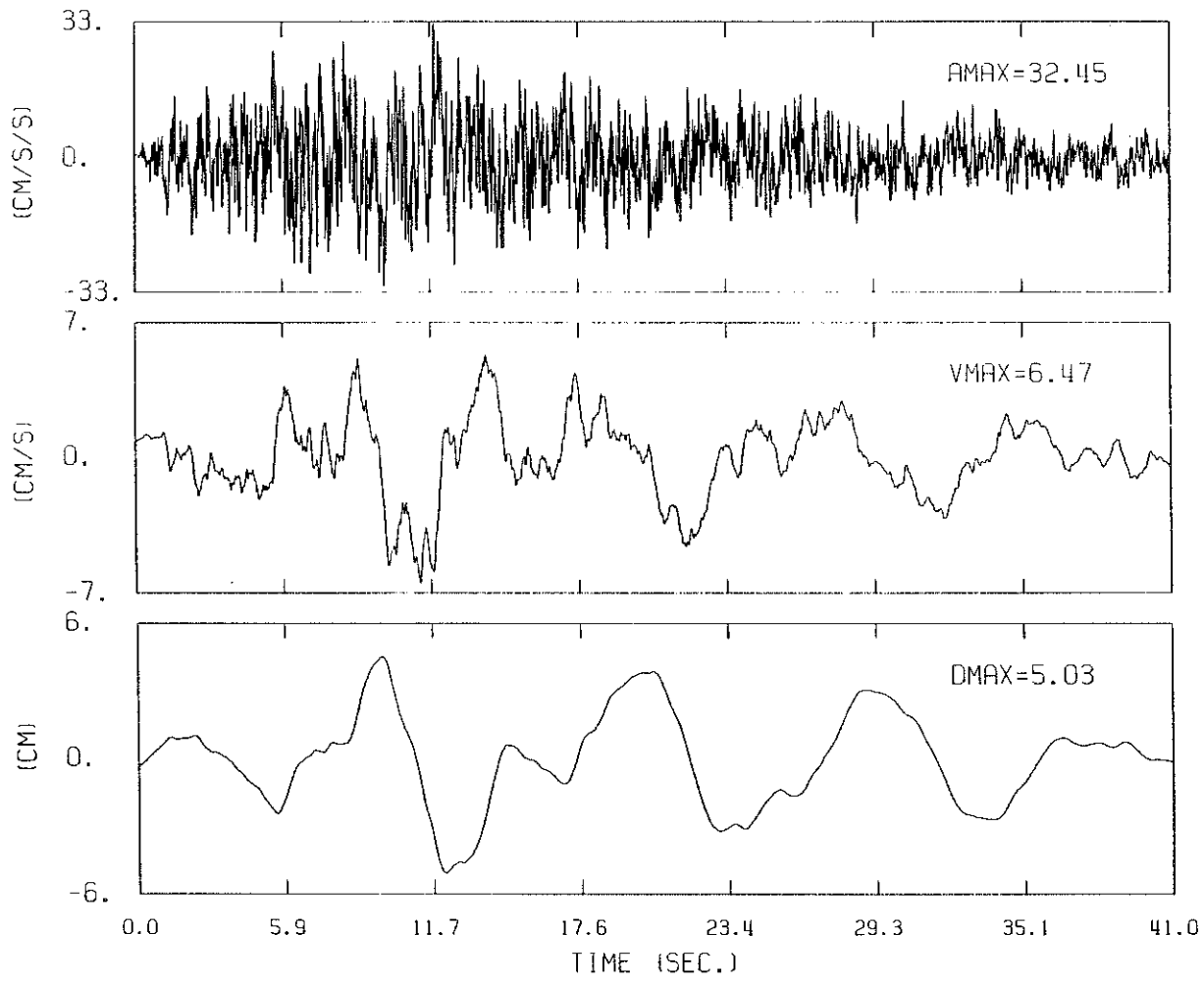
Figure C.45. Acceleration, Velocity, and Displacement Time History for the Transverse Component of the 500-Year Event for Counties Identified by 0.15g-2 in Figure 4.3 (TR-500Y-0.15g-2).
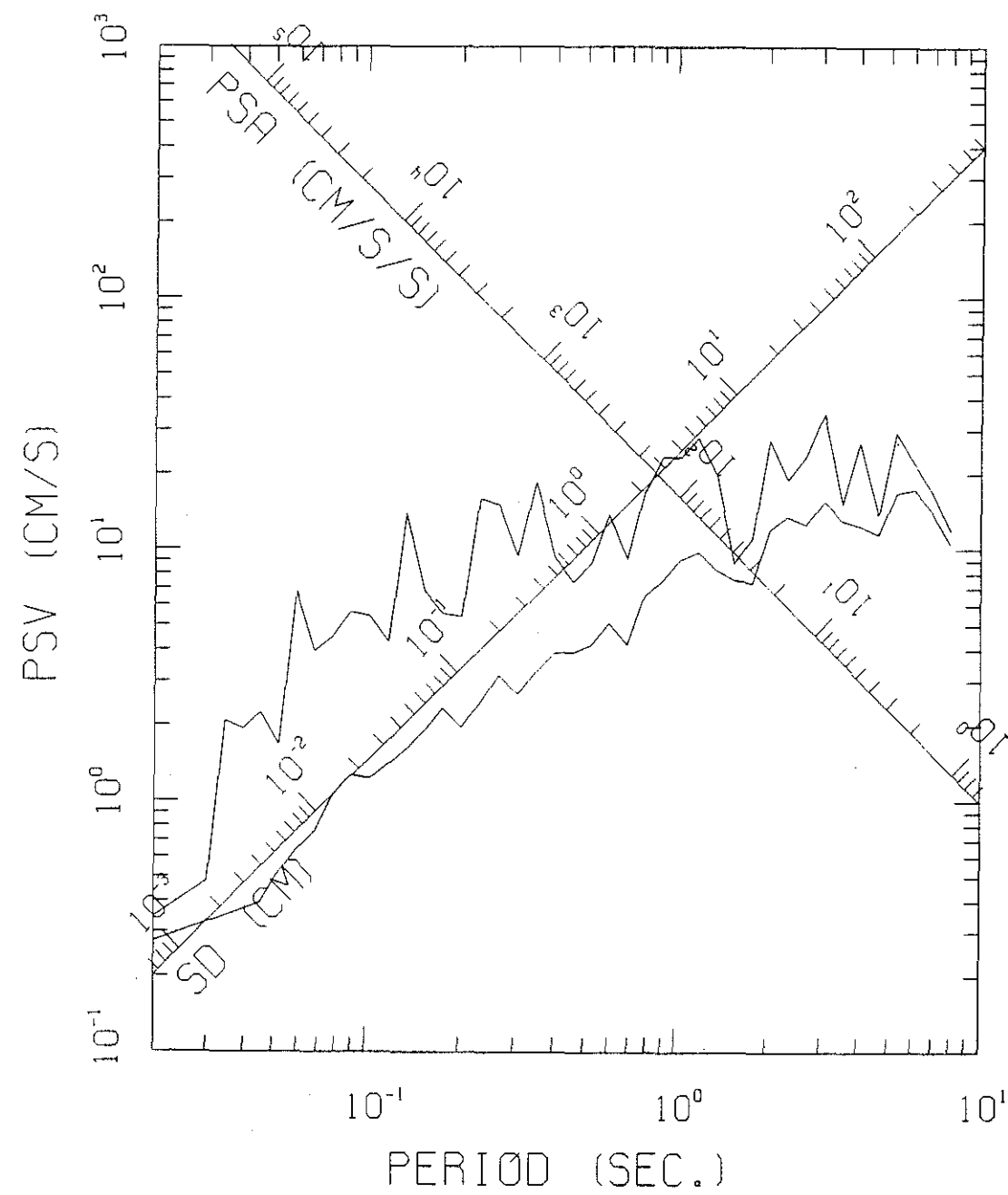
Figure C.46. Response Spectra for the Horizontal Component of the 500-Year Event for Counties Identified by 0.15g-2 in Figure 4.3 (TR-500Y-0.15g-2, Damping Ratio = 0.00 and 0.05).
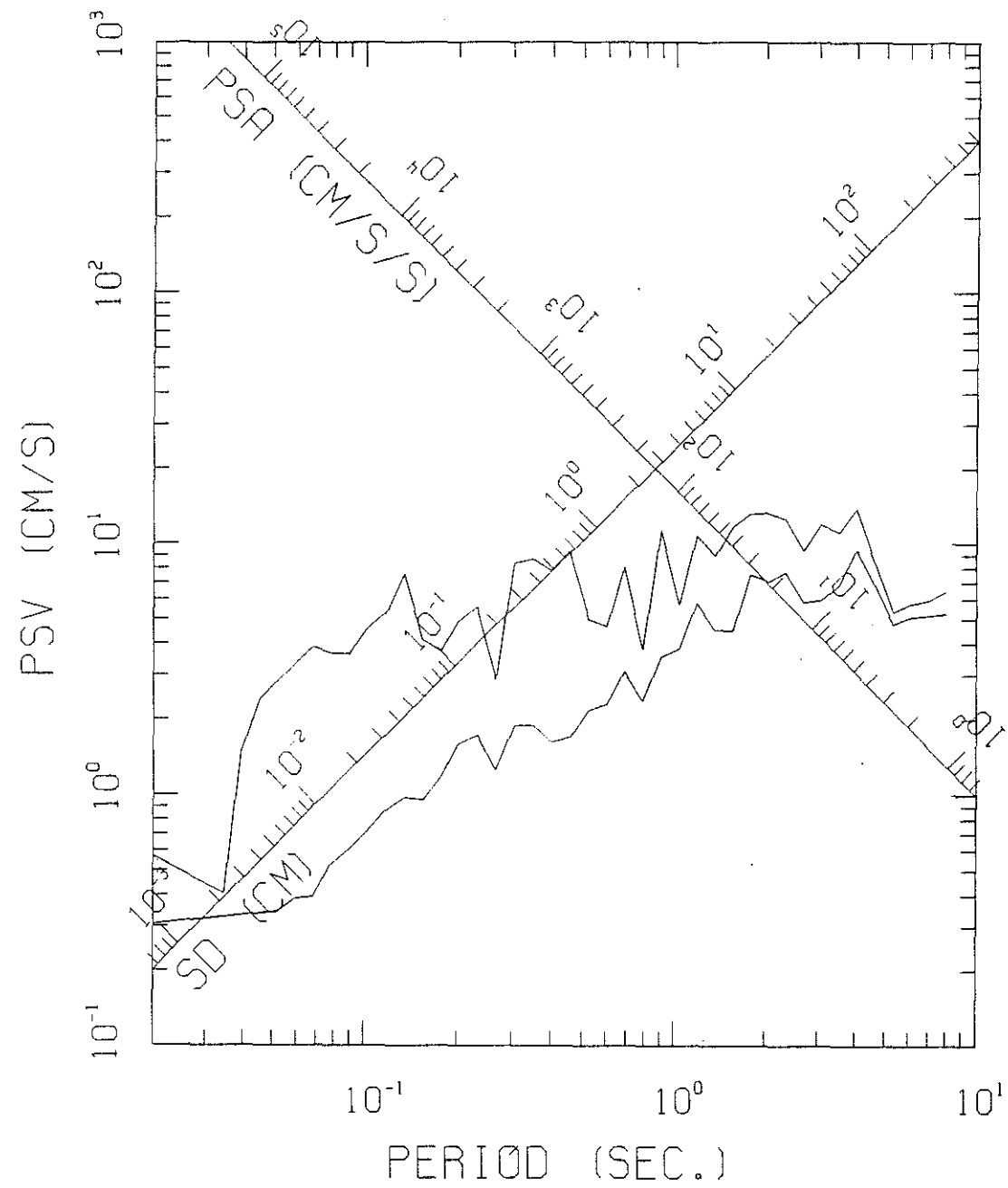
Figure C.47. Response Spectra for the Vertical Component of the 500-Year Event for Counties Identified by 0.15g-2 in Figure 4.3 (TR-500Y-0.15g-2, Damping Ratio = 0.00 and 0.05).
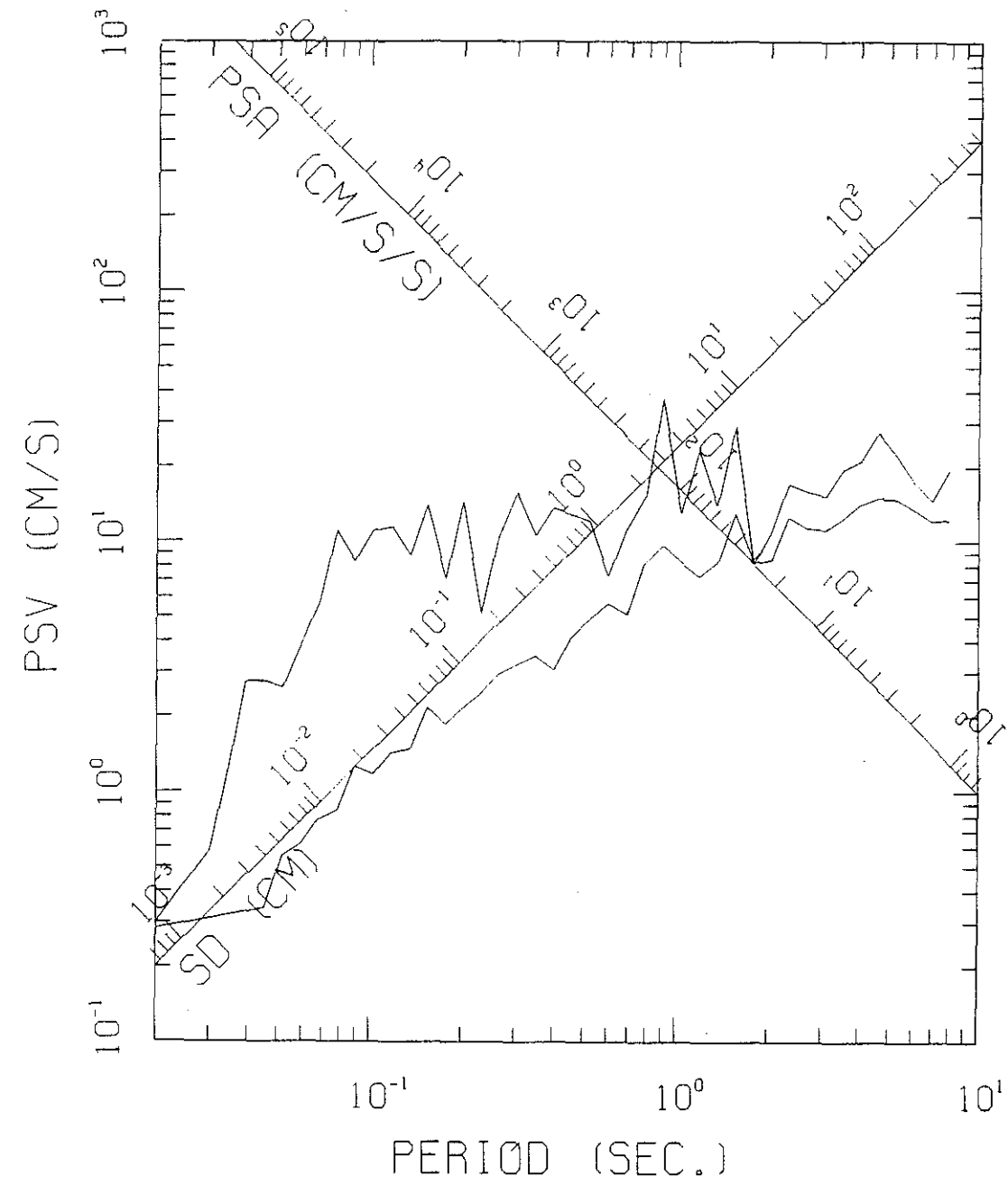
Figure C.48. Response Spectra for the Transverse Component of the 500-Year Event for Counties Identified by 0.15g-2 in Figure 4.3 (TR-500Y-0.15g-2, Damping Ratio = 0.00 and 0.05).

Figure C.49. Acceleration, Velocity, and Displacement Time History for the Horizontal Component of the 500-Year Event for Counties Identified by 0.09g-1 in Figure 4.3 (TR-500Y-0.09g-1).
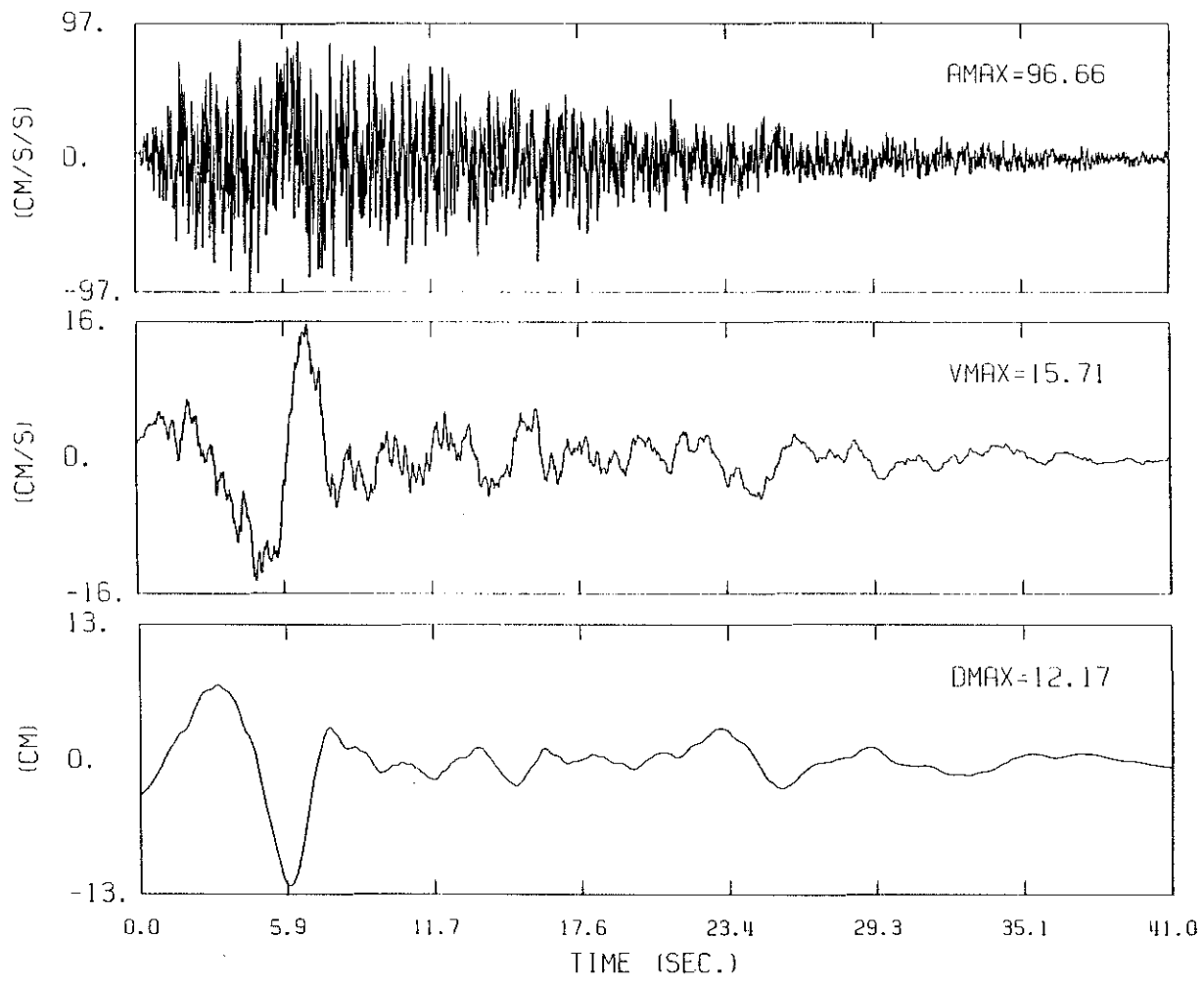
Figure C.50. Acceleration, Velocity, and Displacement Time History for the Vertical Component of the 500-Year Event for Counties Identified by 0.09g-1 in Figure 4.3 (TR-500Y-0.09g-1).

Figure C.51. Acceleration, Velocity, and Displacement Time History for the Transverse Component of the 500-Year Event for Counties Identified by 0.09g-1 in Figure 4.3 (TR-500Y-0.09g-1).

Figure C.52. Response Spectra for the Horizontal Component of the 500-Year Event for Counties Identified by 0.09g-1 in Figure 4.3 (TR-500Y-0.09g-1, Damping Ratio = 0.00 and 0.05).

Figure C.53. Response Spectra for the Vertical Component of the 500-Year Event for Counties Identified by 0.09g-1 in Figure 4.3 (TR-500Y-0.09g-1, Damping Ratio = 0.00 and 0.05).

Figure C.54. Response Spectra for the Transverse Component of the 500-Year Event for Counties Identified by 0.09g-1 in Figure 4.3 (TR-500Y-0.09g-1, Damping Ratio = 0.00 and 0.05).

Figure C.55. Acceleration, Velocity, and Displacement Time History for the Horizontal Component of the 500-Year Event for Counties Identified by 0.09g-2 in Figure 4.3 (TR-500Y-0.09g-2).
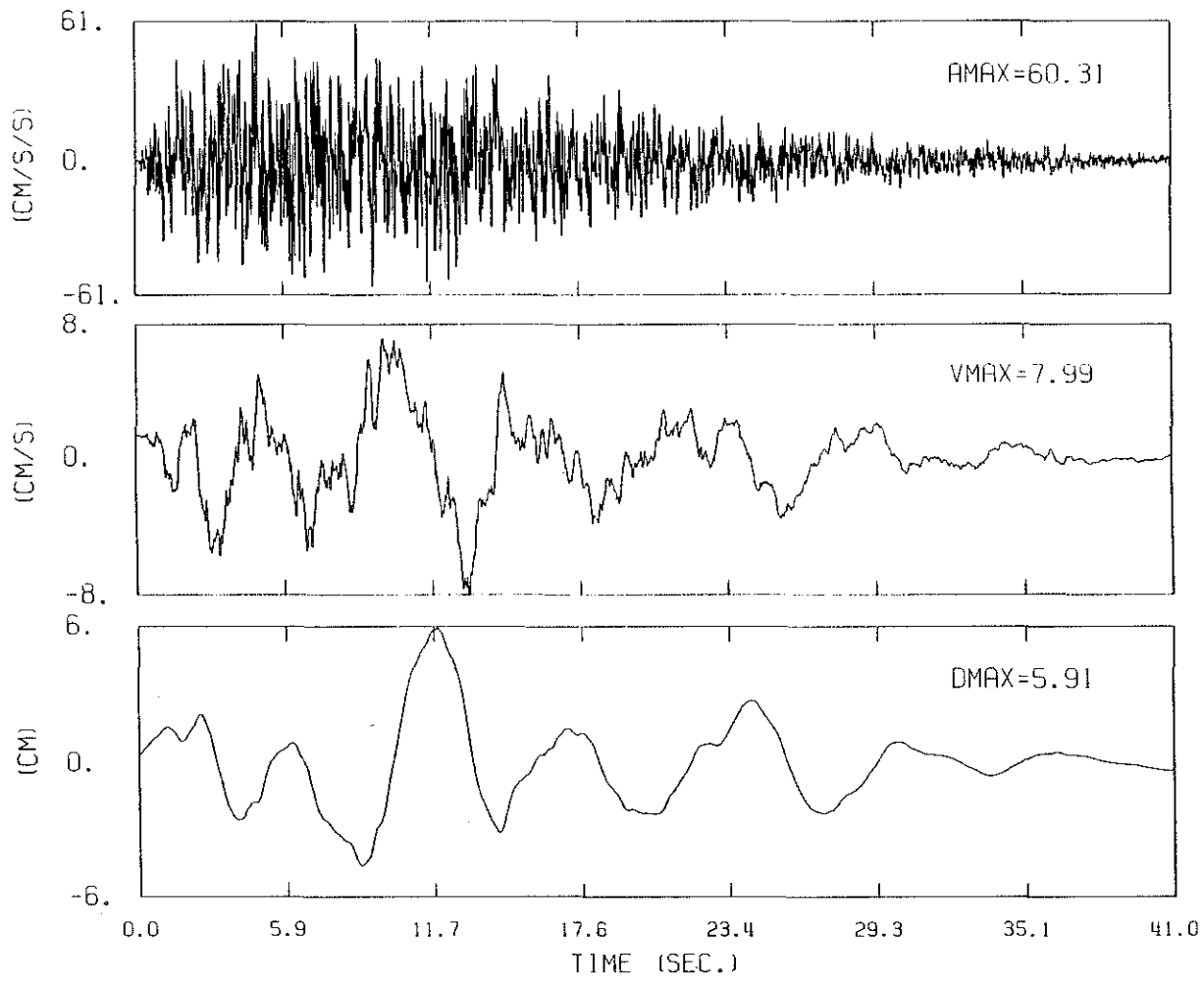
Figure C.56. Acceleration, Velocity, and Displacement Time History for the Vertical Component of the 500-Year Event for Counties Identified by 0.09g-2 in Figure 4.3 (TR-500Y-0.09g-2).
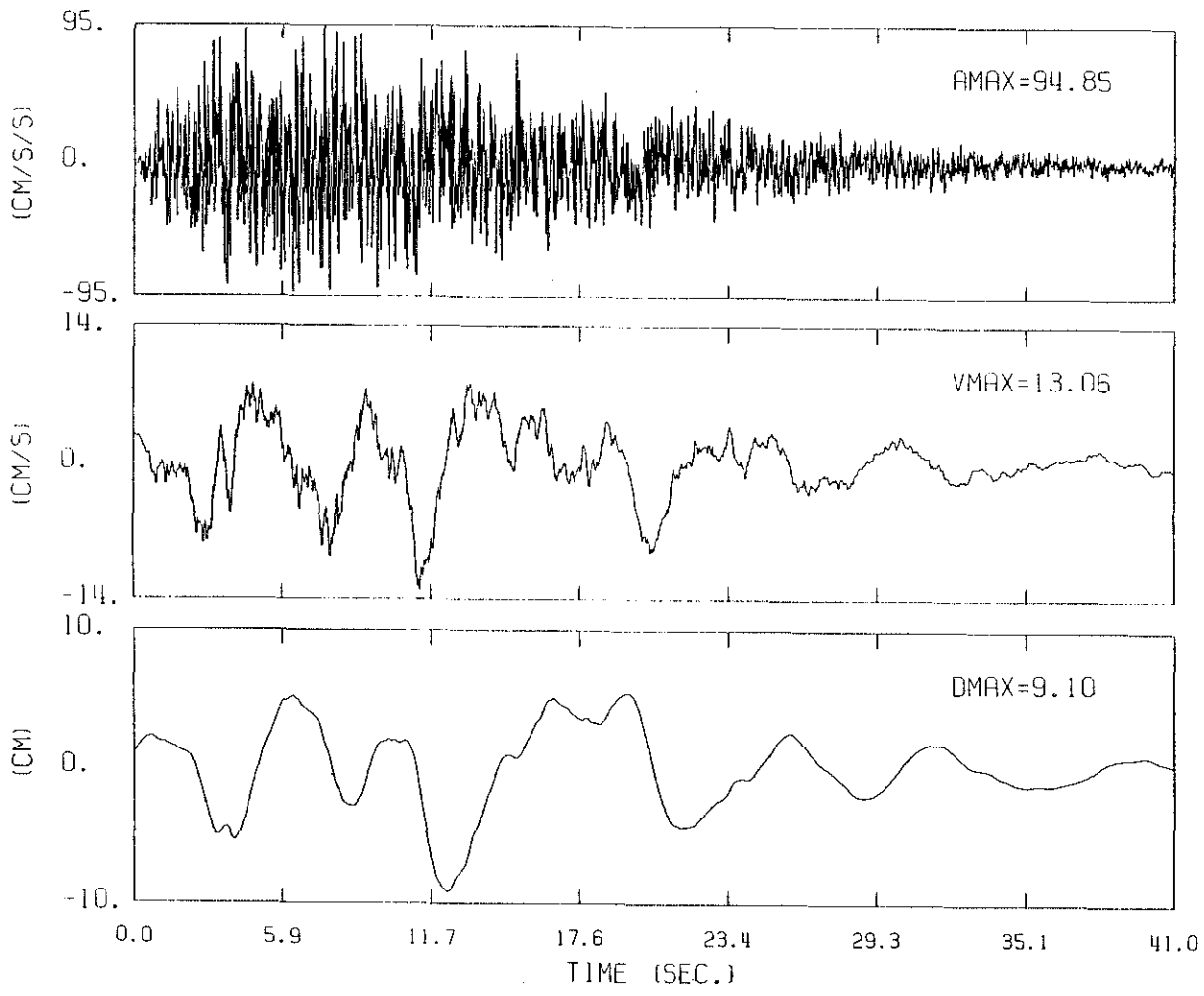
Figure C.57. Acceleration, Velocity, and Displacement Time History for the Transverse Component of the 500-Year Event for Counties Identified by 0.09g-2 in Figure 4.3 (TR-500Y-0.09g-2).
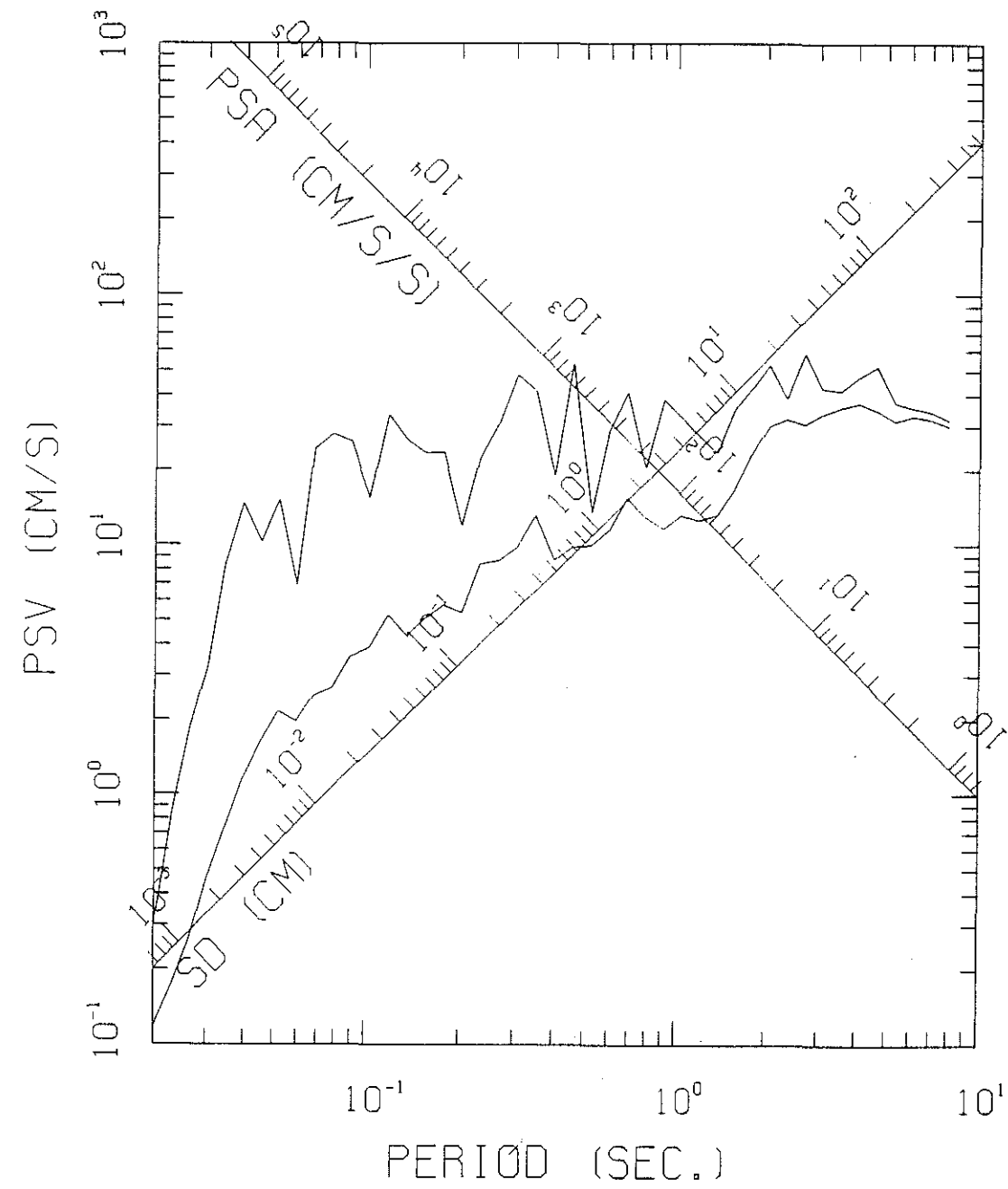
Figure C.58. Response Spectra for the Horizontal Component of the 500-Year Event for Counties Identified by 0.09g-2 in Figure 4.3 (TR-500Y-0.09g-2, Damping Ratio = 0.00 and 0.05).
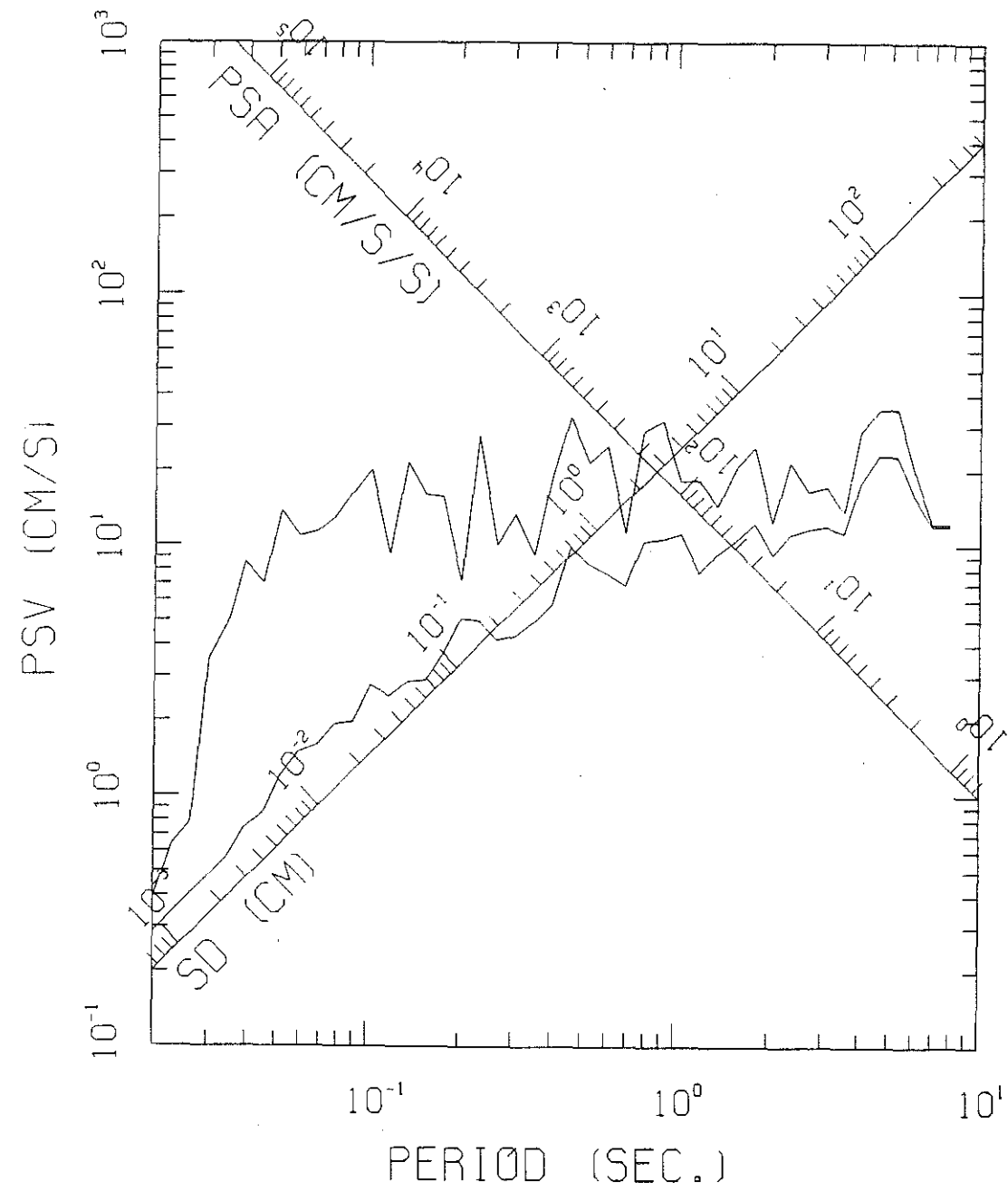
Figure C.59. Response Spectra for the Vertical Component of the 500-Year Event for Counties Identified by 0.09g-2 in Figure 4.3 (TR-500Y-0.09g-2, Damping Ratio = 0.00 and 0.05).
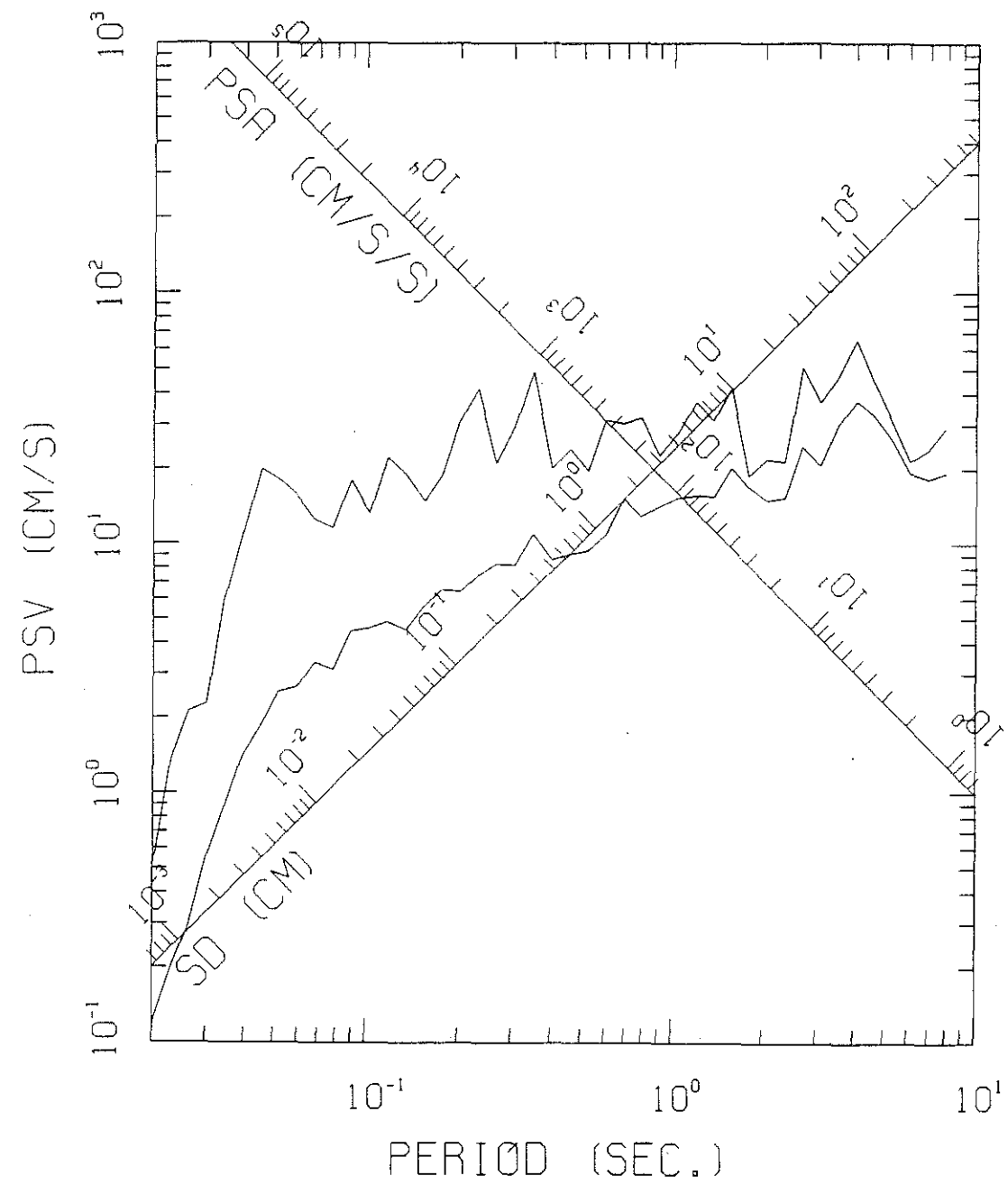
Figure C.60. Response Spectra for the Transverse Component of the 500-Year Event for Counties Identified by 0.09g-2 in Figure 4.3 (TR-500Y-0.09g-2, Damping Ratio = 0.00 and 0.05).
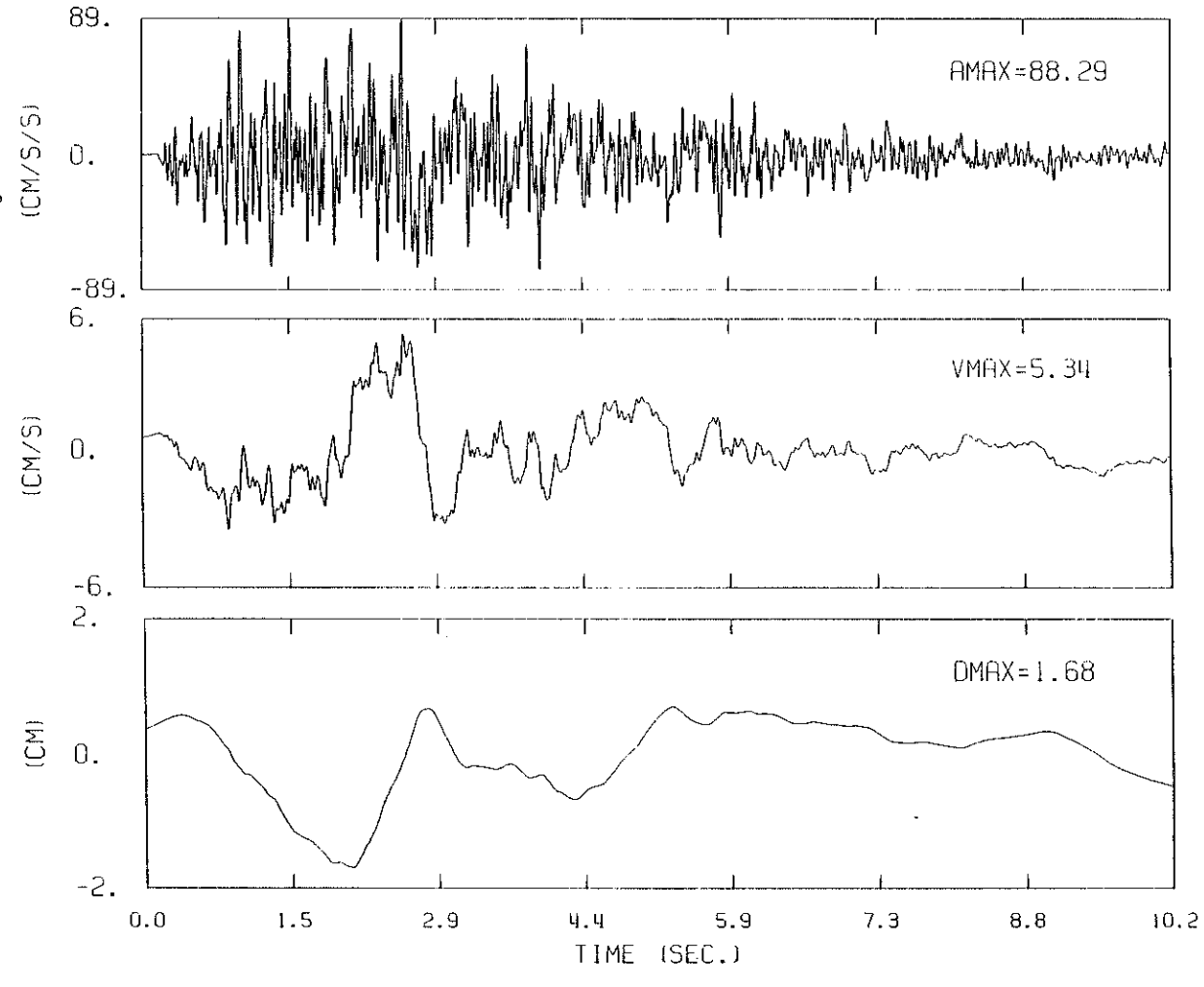
Figure C.61. Acceleration, Velocity, and Displacement Time History for the Horizontal Component of the 500-Year Event for Counties Identified by 0.09g-3 in Figure 4.3 (TR-500Y-0.09g-3).
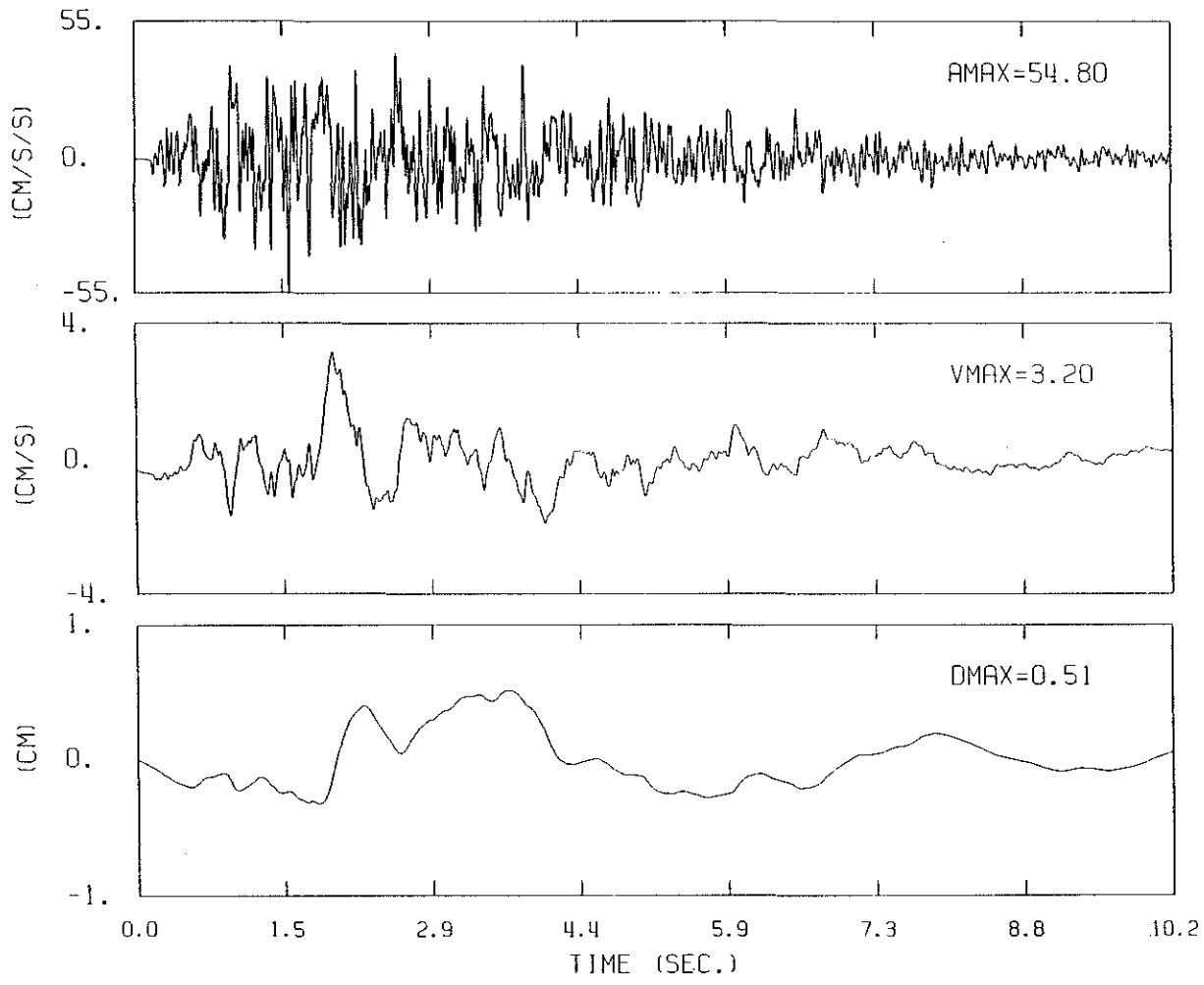
Figure C.62. Acceleration, Velocity, and Displacement Time History for the Vertical Component of the 500-Year Event for Counties Identified by 0.09g-3 in Figure 4.3 (TR-500Y-0.09g-3).
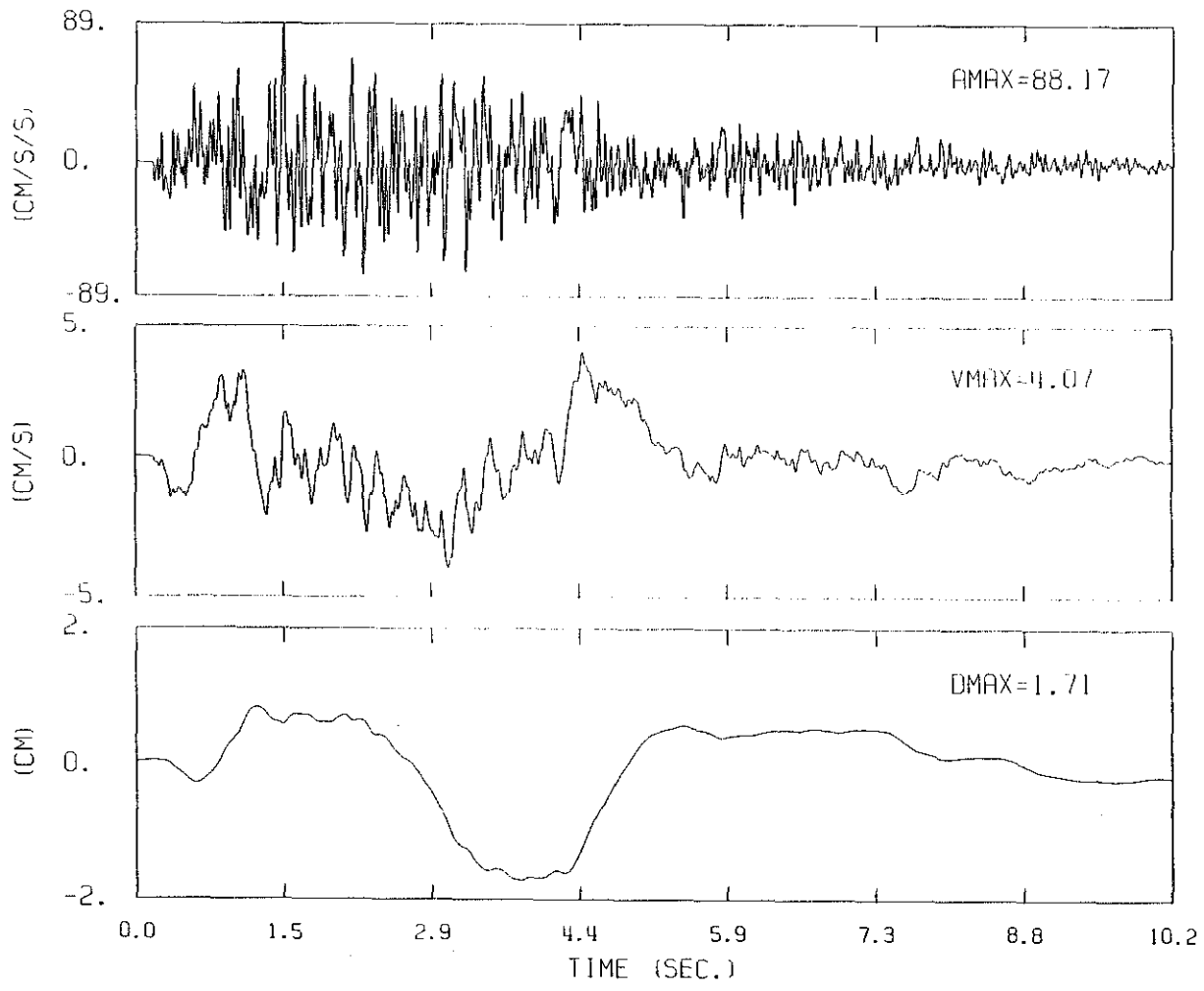
Figure C.63. Acceleration, Velocity, and Displacement Time History for the Transverse Component of the 500-Year Event for Counties Identified by 0.09g-3 in Figure 4.3 (TR-500Y-0.09g-3).
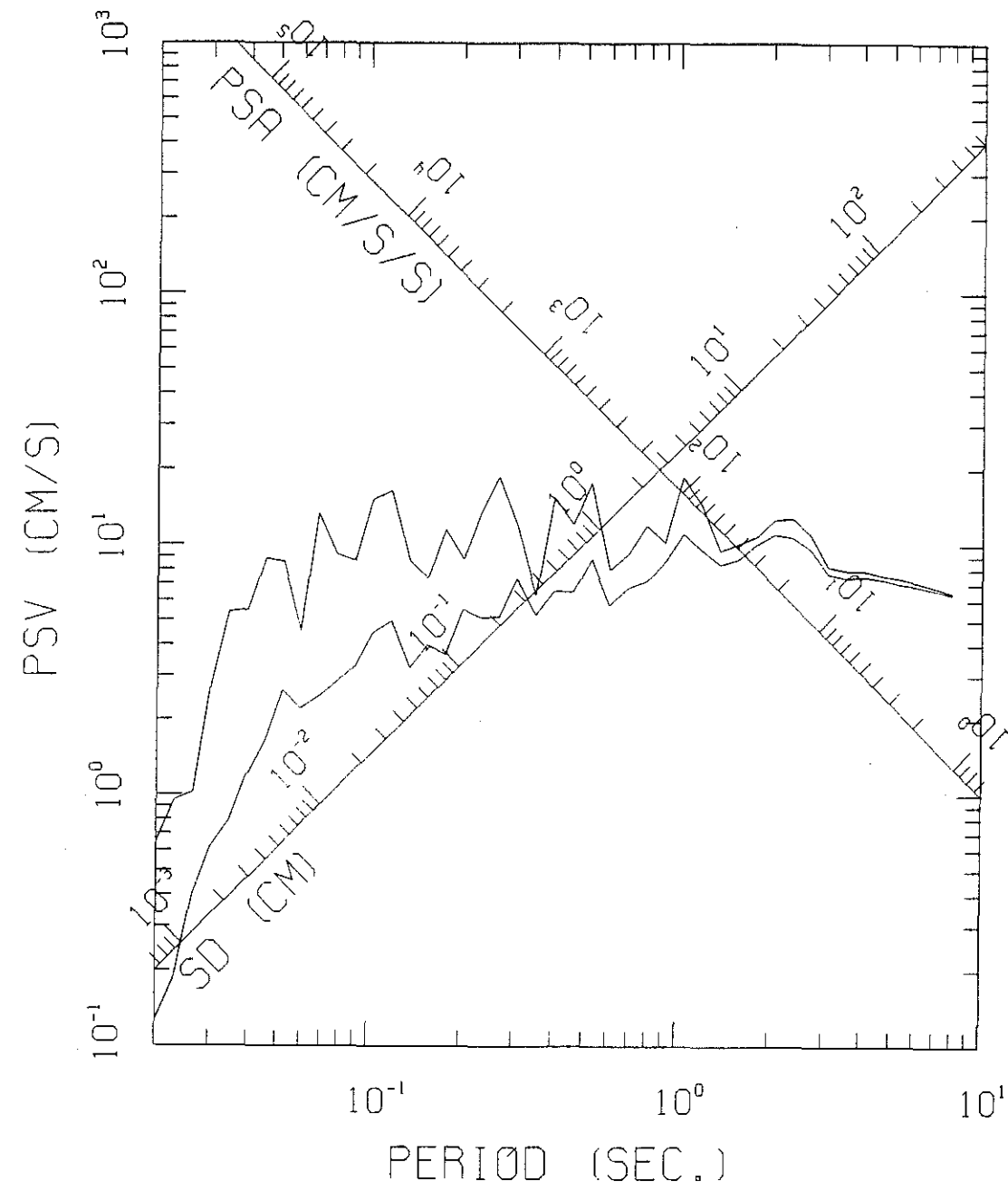
Figure C.64. Response Spectra for the Horizontal Component of the 500-Year Event for Counties Identified by 0.09g-3 in Figure 4.3 (TR-500Y-0.09g-3, Damping Ratio = 0.00 and 0.05).
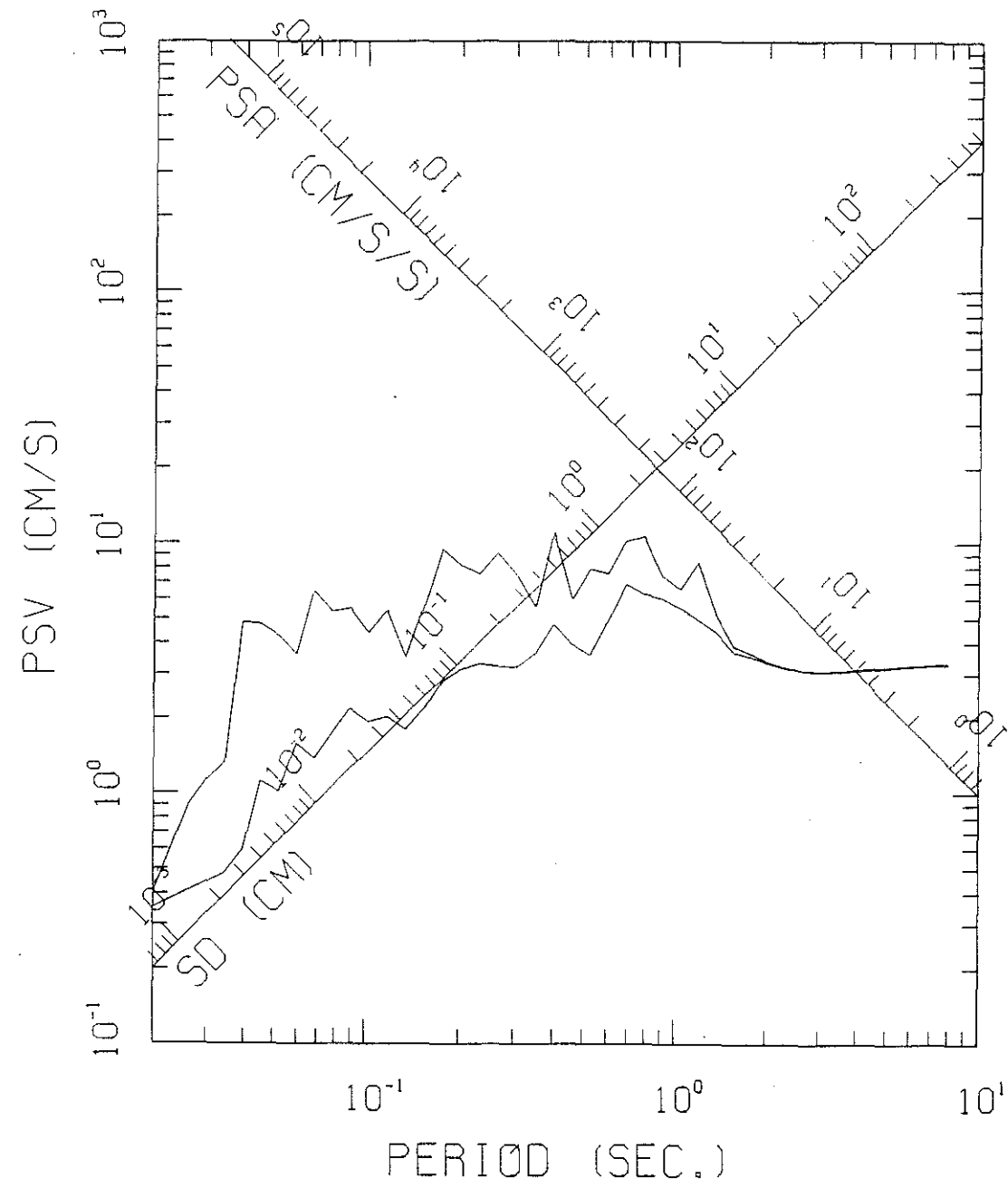
Figure C.65. Response Spectra for the Vertical Component of the 500-Year Event for Counties Identified by 0.09g-3 in Figure 4.3 (TR-500Y-0.09g-3, Damping Ratio = 0.00 and 0.05).

Figure C.66. Response Spectra for the Transverse Component of the 500-Year Event for Counties Identified by 0.09g-3 in Figure 4.3 (TR-500Y-0.09g-3, Damping Ratio = 0.00 and 0.05).
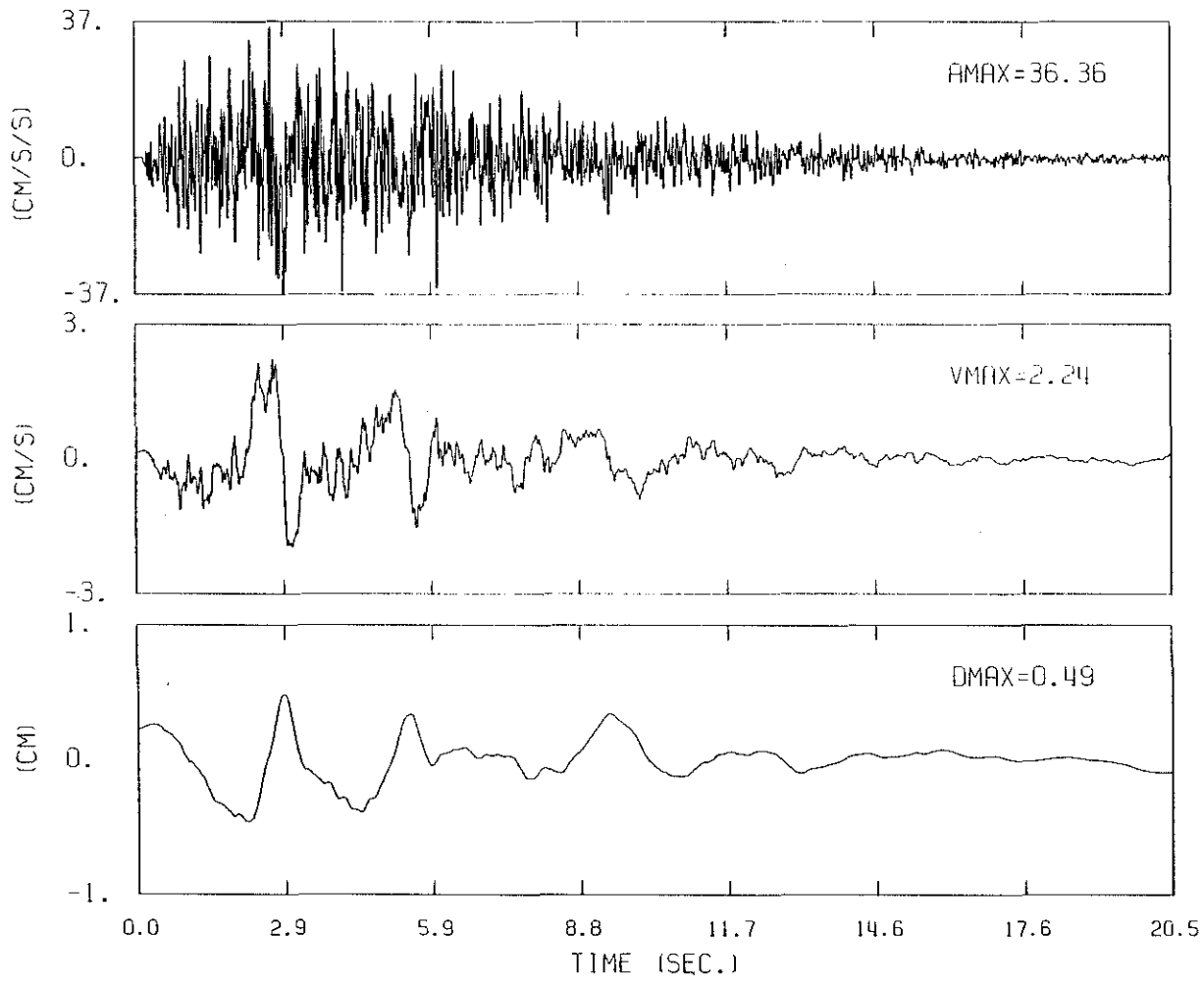
Figure C.67. Acceleration, Velocity, and Displacement Time History for the Horizontal Component of the 500-Year Event for Counties Identified by 0.09g-4 in Figure 4.3 (TR-500Y-0.09g-4).
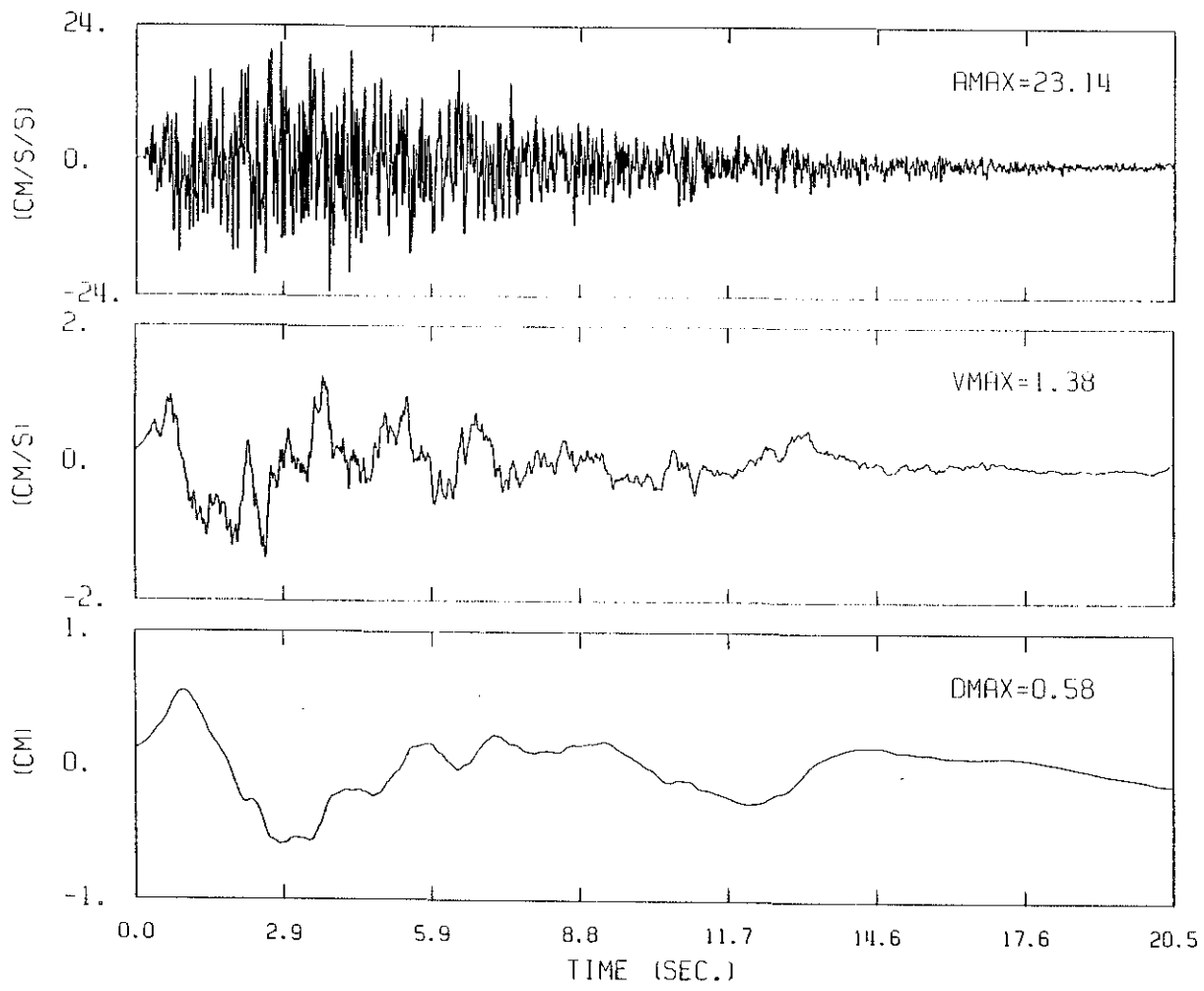
Figure C.68. Acceleration, Velocity, and Displacement Time History for the Vertical Component of the 500-Year Event for Counties Identified by 0.09g-4 in Figure 4.3 (TR-500Y-0.09g-4).
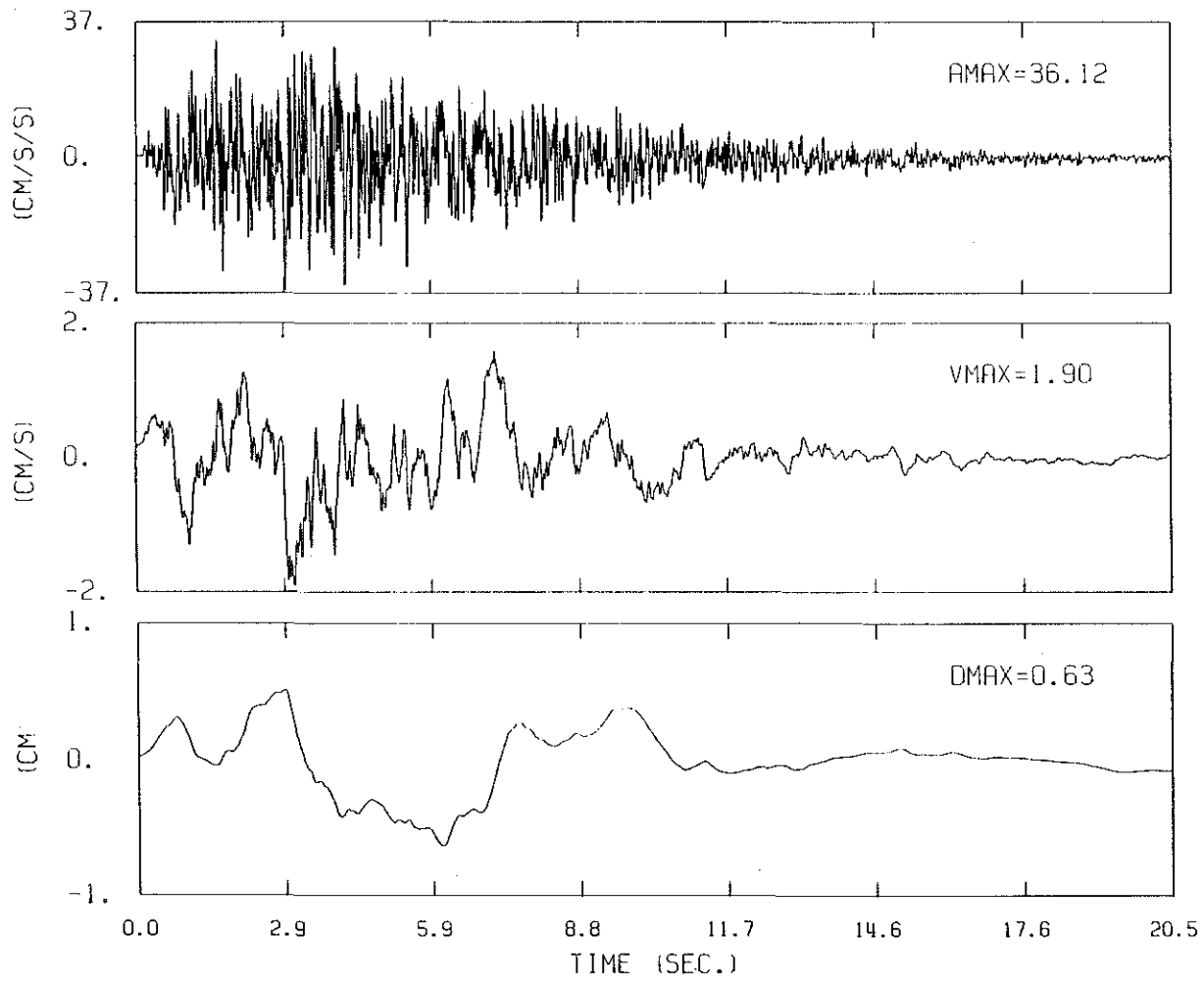
Figure C.69. Acceleration, Velocity, and Displacement Time History for the Transverse Component of the 500-Year Event for Counties Identified by 0.09g-4 in Figure 4.3 (TR-500Y-0.09g-4).

Figure C.70. Response Spectra for the Horizontal Component of the 500-Year Event for Counties Identified by 0.09g-4 in Figure 4.3 (TR-500Y-0.09g-4, Damping Ratio = 0.00 and 0.05).

Figure C.71. Response Spectra for the Vertical Component of the 500-Year Event for Counties Identified by 0.09g-4 in Figure 4.3 (TR-500Y-0.09g-4, Damping Ratio = 0.00 and 0.05).
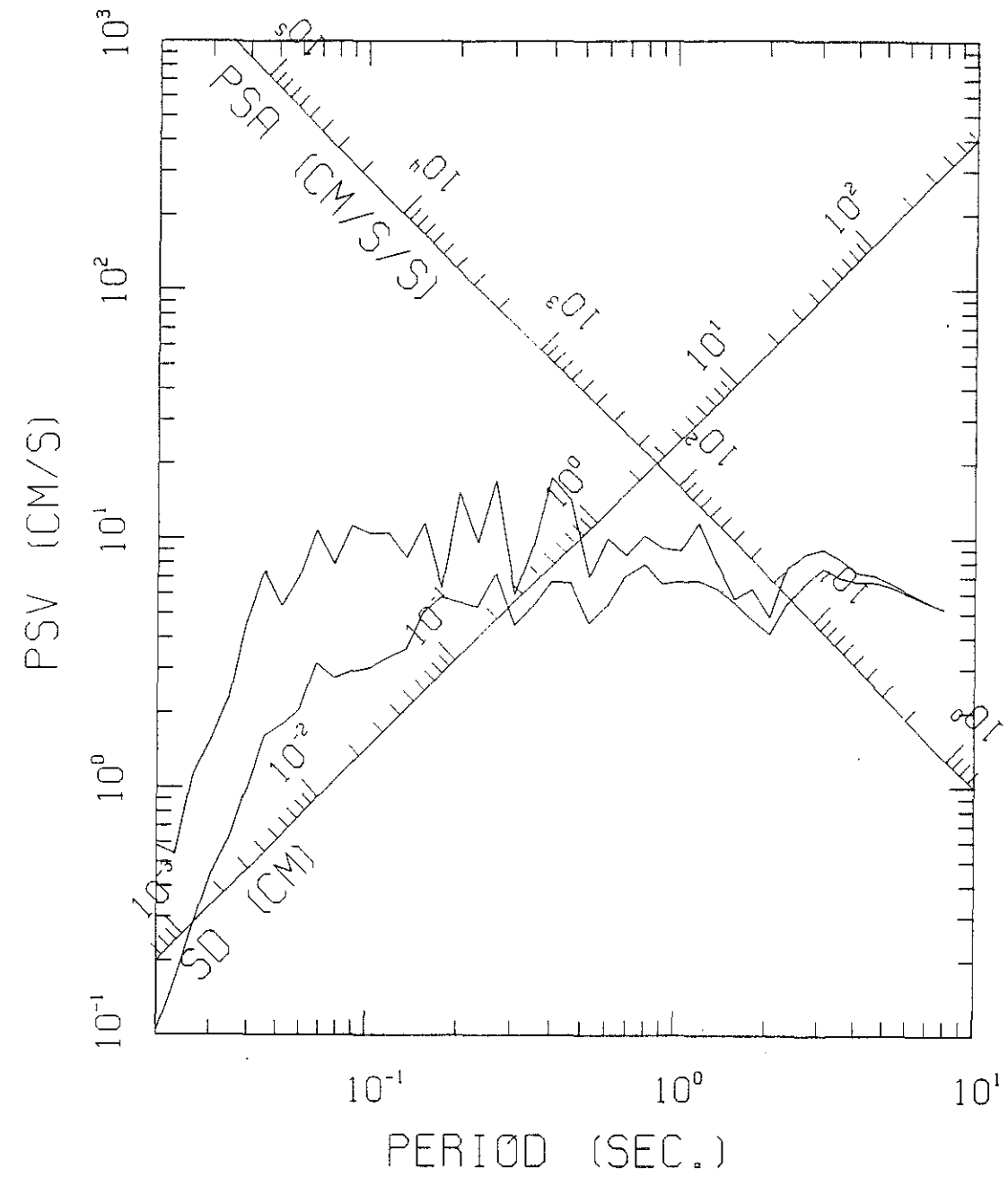
Figure C.72. Response Spectra for the Transverse Component of the 500-Year Event for Counties Identified by 0.09g-4 in Figure 4.3 (TR-500Y-0.09g-4, Damping Ratio = 0.00 and 0.05).
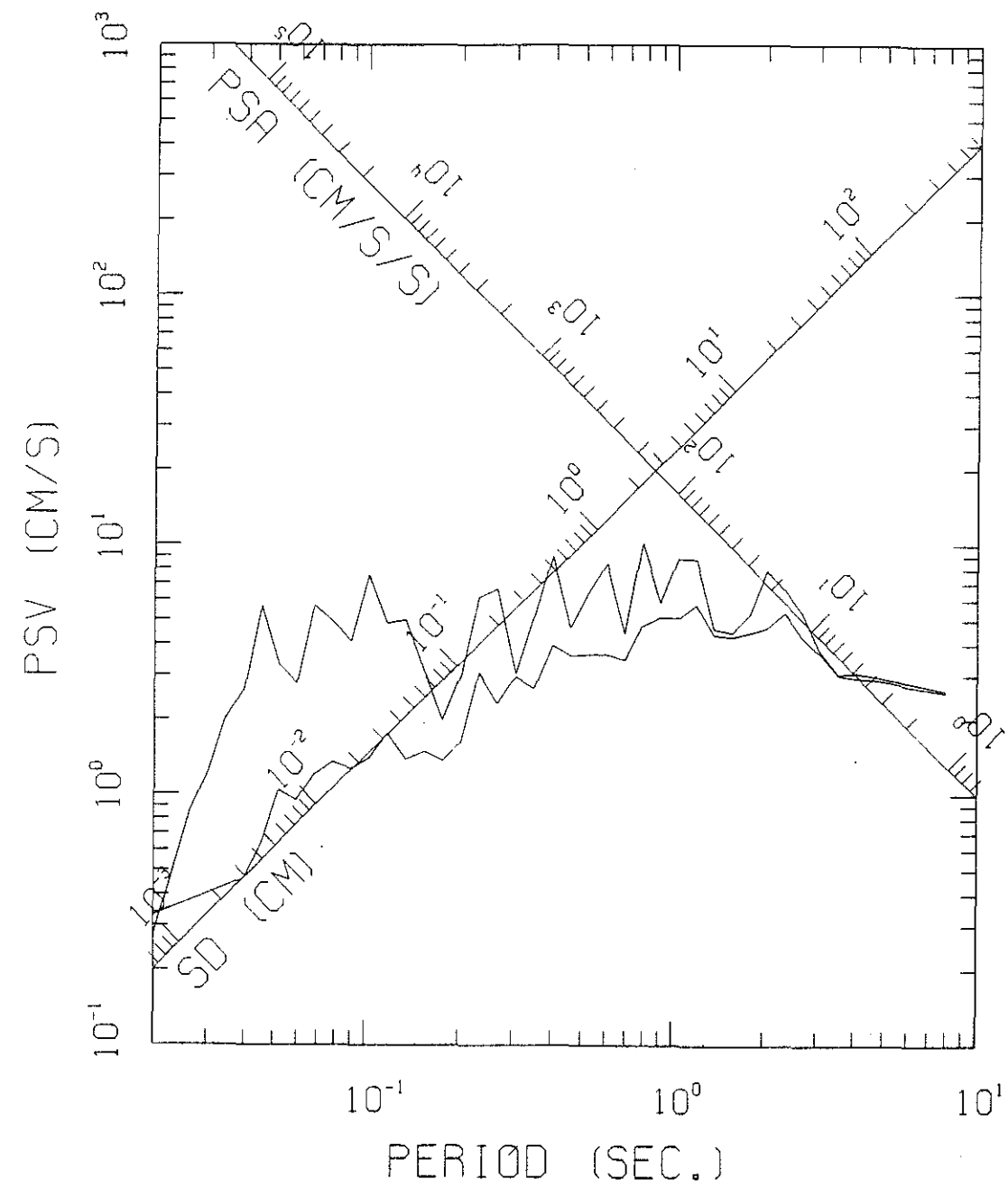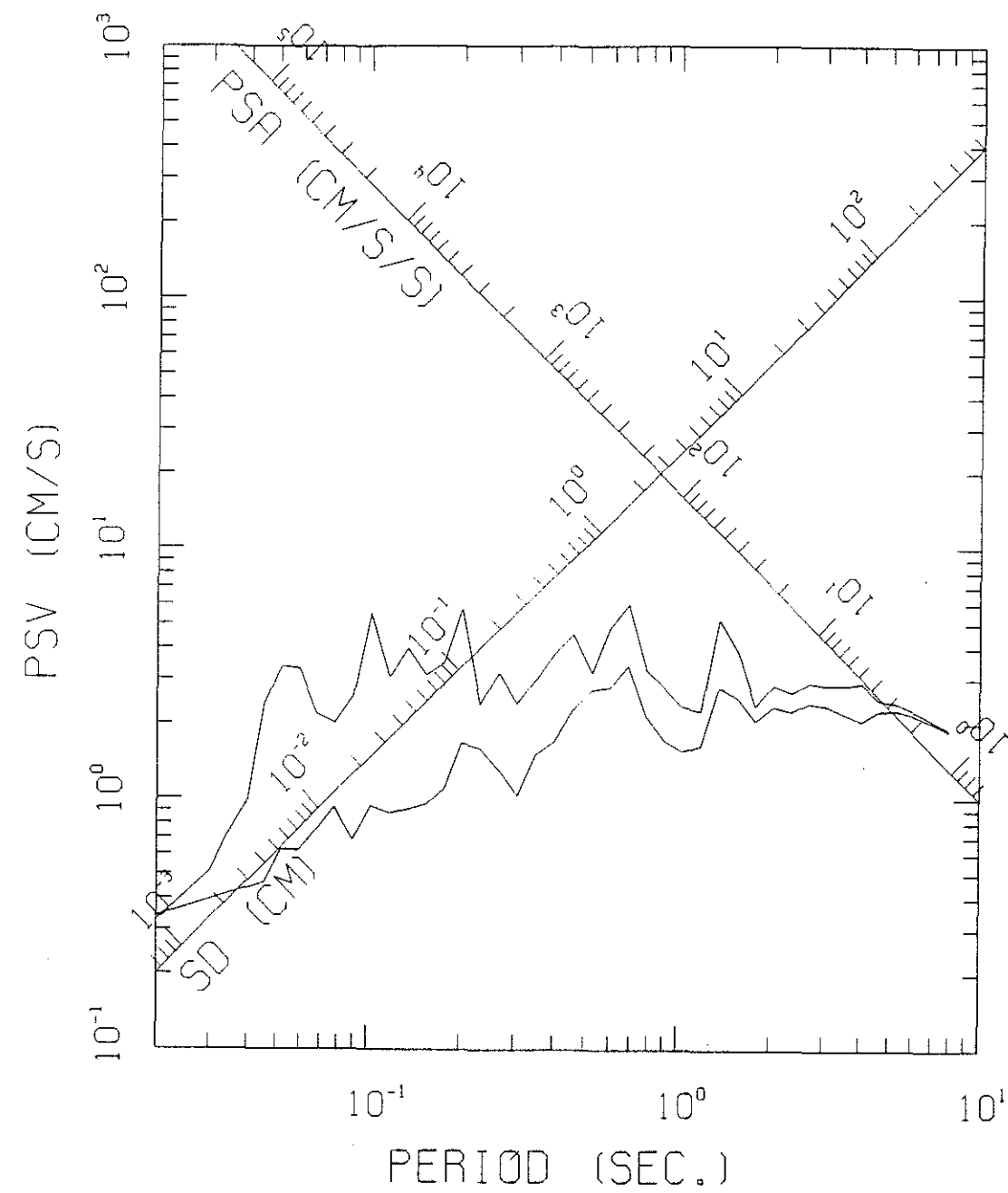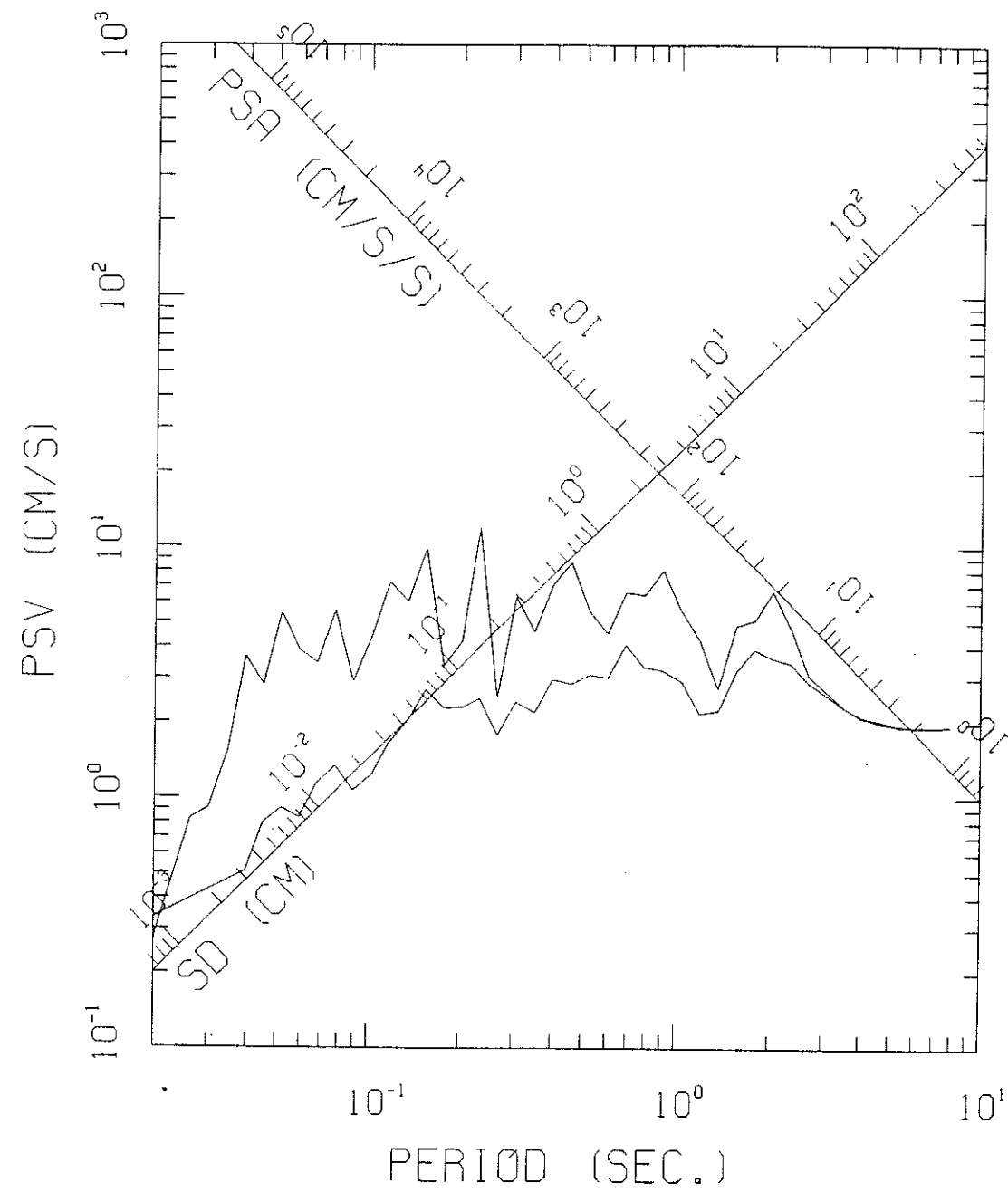
Appendix D: References

Algermissen, S.T., D.M. Perkins, P.C. Thenhaus, S.L. Hanson, and B.L. Bender (1982). Probabilistic estimates of maximum acceleration and velocity in rock in the contiguous United States, *U.S. Geological Survey Open-File Report* 82-1033, 99 p., 6 plates.

Barstow, N.L., K.G. Brill, O.W. Nuttli, and P.W. Pomeroy (1980). An approach to seismic zonation for siting nuclear electric power generating facilities in the eastern United States, *Technical Report NUREG/CR-1577, U.S. Nuclear Regulatory Commission*, 143 p., 5 appendices, 4 plates.

Bernreuter, D.L., J.B. Savy, R.W. Mensing, and J.C. Chen (1988). Seismic hazard characterization of 69 plant sites east of the Rocky Mountains, *Technical Report NUREG/CR5250, U.S. Nuclear Regulatory Commission*, 129 p.

Berry, D. (1908). The Illinois earthquakes of 1811 and 1812, *Transactions of the Illinois State Historical Society for the year 1905* 12, 74-78.

Bollinger, G.A. (1992). Specification of source zones, recurrence rates, focal depths, and maximum magnitudes for earthquakes affecting the Savannah River site in South Carolina, *U.S. Geological Survey Bulletin* 2017, 57 p.

Bollinger, G.A., F.C. Davison, M.S. Sibol, and J.B. Birch (1989). Magnitude recurrence relations for the southeastern United States and its subdivisions, *Journal of Geophysical Research* 94, 2857-2873.

Bollinger, G.A., M.S. Sibol, and M.C. Chapman (1992). Maximum magnitude estimation for an intraplate setting- Example: The Giles County, Virginia, Seismic Zone, *Seismological Research Letters* 63, 139-152.

Bollinger, G.A., and R.L. Wheeler (1988). The Giles County, Virginia, Seismic Zone - Seismological results and geological interpretations, *U.S. Geological Survey Professional Paper* 1355, 85 p.

Boore, D.M. (1983). Stochastic simulation of high-frequency ground motions based on seismological models of radiated spectra, *Bulletin of the Seismological Society of America* 73, 1865-1894.

Brune, J.N. (1970). Tectonic stress and spectra of seismic shear waves from earthquakes, *Journal of Geophysical Research* 75, 4997-5009.

Brune, J.N. (1971). Correction, *Journal of Geophysical Research* 76, 5002.

Chiu, J.M., A.C. Johnston, and Y.T. Yang (1992). Imaging the active faults of the central New Madrid Seismic Zone using PANDA array data, *Seismological Research Letters* 63, 375-393.

EPRI (1986). Seismic hazard methodology for the central and eastern United States, *Technical Report NP-4726-A*, Electric Power Institute, July 1986. Revised, 1988, vol. 1 through 11.

Hamburger, M.W., and J. Rupp (1988). The June 1987 southeastern Illinois earthquake: Possible tectonism associated with the La Salle Anticlinal Belt, *Seismological Research Letters* 59, 151-158.

Hass, L., M. Ellis, and A. Rydelek (1992). Minimum Magnitude of Completeness and Rates of Seismicity in the New Madrid Region, *Seismological Research Letters* 63, 395-405.

Heigold, P.C., and D.R. Kolata (1993). Proterozoic crustal boundary in the southern part of the Illinois Basin, *Tectonophysics* 217, 307-319.

Herrmann, R.B. (1979). Surface wave focal mechanisms for eastern North American earthquakes with tectonic implications, *Journal of Geophysical Research* 84, 3543-3552.

Herrmann, R.B. (1985). An extension of random vibration theory estimates of strong ground motions to large earthquakes, *Bulletin of the Seismological Society of America* 75, 1447-1453.

Hildenbrand, T.G., V.E. Langenheim, and P.C. Heigold (1994). Geophysical setting of the Northern Reelfoot Rift and Southern Illinois Basin region, *Proceedings of the Illinois Basin Energy and Mineral Resources Workshop*, Evansville, September 12-13, 18-20.

Holzer, T.L., (1994). Loma Prieta damage largely attributed to enhanced ground shaking,

EOS, Transactions of the American Geophysical Union 75, 299-301.

Idriss, I.M. and J.I. Sun (1992). User's manual for SHAKE91, a computer program for conducting equivalent linear seismic response analyses of horizontally layered soil deposits; program modified based on the original SHAKE program published in December 1972 by Schnabel, Lysmer and Seed.

Johnston, A.C. and S.J. Nava (1990). Seismic hazard assessment in the central United States, in *Neotectonics in Earthquake Evaluation*, Krinitzsky, E.L., and D.B. Slemmons, eds., *Reviews in Engineering Geology* 8, Geological Society of America, Boulder, Colorado, 47-58.

Naeim, F., and J.C. Anderson (1993). Classification and evaluation of earthquake records for design, the 1993 NEHRP Professional Fellowship Report, *Earthquake Engineering Research Institute*, 288 p.

Nuttli, O.W. (1973a). The Mississippi Valley earthquakes of 1811-1812: Intensities, ground motion, and magnitudes, *Bulletin of the Seismological Society of America* 63, 1189-1207.

Nuttli, O.W. (1973b). Seismic-wave attenuation and magnitude relations for eastern North America, *Journal of Geophysical Research* 78, 876-885.

Nuttli, O.W. (1981). On the problem of estimating the maximum magnitude earthquake, *U.S. Geological Survey Open-File Report* 81-437, 111-123.

Nuttli, O.W., and R.B. Herrmann (1978). State-of-the-art for assessing earthquake hazards in the United States; Report 12, Credible earthquakes for the central United States, *U.S. Army Corps of Engineers Miscellaneous Paper S-73-1*, 99 pp.

Nuttli, O.W.,. and R.B. Herrmann (1984). Ground motion of Mississippi Valley earthquakes, *Journal of Technical Topics in Civil Engineering* 100, 54-69.

Obermeier, S.F., P.J. Munson, C.A. Munson, J.R. Martin, A.D. Frankel, T.L. Youd, and E.C. Pond (1992). Liquefaction evidence for strong Holocene earthquake(s) in the Wabash Valley of Indiana-Illinois, *Seismological Research Letters* 63, 321-335.

O'Connor, J.M., and B.R. Ellingwood (1992). Site-dependent models of earthquake ground motion, *Earthquake Engineering and Structural Dynamics* 21, 573-589.

Powell, C.A., G.A. Bollinger, M.C. Chapman, M.S. Sibol, A.C. Johnston, and R.L.

Wheeler (1994). A seismotectonic model for the 300-kilometer-long Eastern Tennessee Seismic Zone, *Science* 264, 686-688.

Reiter, L. (1990). *Earthquake Hazard Analysis: Issues and Insights*, Columbia University Press, New York, 254 p.

Shin, T.C., and R.B. Herrmann (1987). Lg attenuation and source studies using 1982 Miramichi data, *Bulletin of the Seismological Society of America* 77, 384-397.

Stauder, W., and O.W. Nuttli (1970). Seismic studies: south central Illinois earthquake of November 9, 1968, *Bulletin of the Seismological Society of America* 60, 973-981.

Stewart, J.P., S.W. Chang, J.D. Bray, R.B. Seed, N. Sitar, and M.F. Riemer (1995). A report on geotechnical aspects of the January 17, 1994, Northridge earthquake, *Seismological Research Letters* 66(3), 7-19.

Stover, C.W., and Coffman, J.L. (1993). Seismicity of the United States, 1568-1989 (Revised), *U.S. Geological Survey Professional Paper* 1527, 418 p.

Street, R. (1979). An instrumental $m_{b,Lg}$ magnitude of the 1897 Giles County, Virginia, earthquake, *Earthquake Notes* 50(2), 21-24.

Street, R. (1980). The southern Illinois earthquake of September 27, 1891, *Bulletin of the Seismological Society of America* 70, 915-920.

Street, R. (1982). Ground-motion values obtained for the July 27, 1980, Sharpsburg, Kentucky, earthquake, *Bulletin of the Seismological Society of America* 72, 1295-1307.

Street, R., and R.F. Green (1984). The historical seismicity of the central United States: 1811-1928, *U.S. Geological Survey Report, Contract No. 14-08-001-21251*.

Street, R., and O.W. Nuttli (1990). The great central Mississippi Valley earthquakes of 1811-1812, *Kentucky Geological Survey, Special Publication 14, Series XI*, University of Kentucky, Lexington, 15 p.

Street, R., K. Taylor, D. Jones, J. Harris, G. Steiner, A. Zekulin, and D. Zhang (1993). The 4.6 $m_{b,Lg}$ northeastern Kentucky earthquake of September 7, 1988, *Seismological Research Letters* 64, 187-200.

Street, R., E. Woolery, Z. Wang, and J. Harris (1995). A short note on shear-wave

velocities and other site conditions at selected strong-motion stations in the New Madrid Seismic Zone, *Seismological Research Letters* 66(1), 56-63.

Taylor, K.B., R.B. Herrmann, M.W. Hamburger, G.L. Pavlis, A. Johnston, C. Langer, and C. Lam (1989). The southern Illinois earthquake of 10 June 1987, *Seismological Research Letters* 60, 101-110.

Torro, G.R., W.J. Silva, R.K. McGuire, and R.B. Herrmann (1992). Probabilistic Seismic Hazard Mapping of the Mississippi Embayment, *Seismological Research Letters* 63, 449-475.

Wheeler, R.L. (1995). Earthquakes and the cratonward limit of Iapetan faulting in eastern North America, *Geology* 23, 105-108.

Wood, H.O., and F. Neumann (1931). Modified Mercalli intensity scale of 1931, *Bulletin of the Seismological Society of America* 21, 277-283.

Zoback, M.L., and M.D. Zoback (1981). State of stress and intra-plate earthquakes in the U.S., *Science* 213, 96-104.